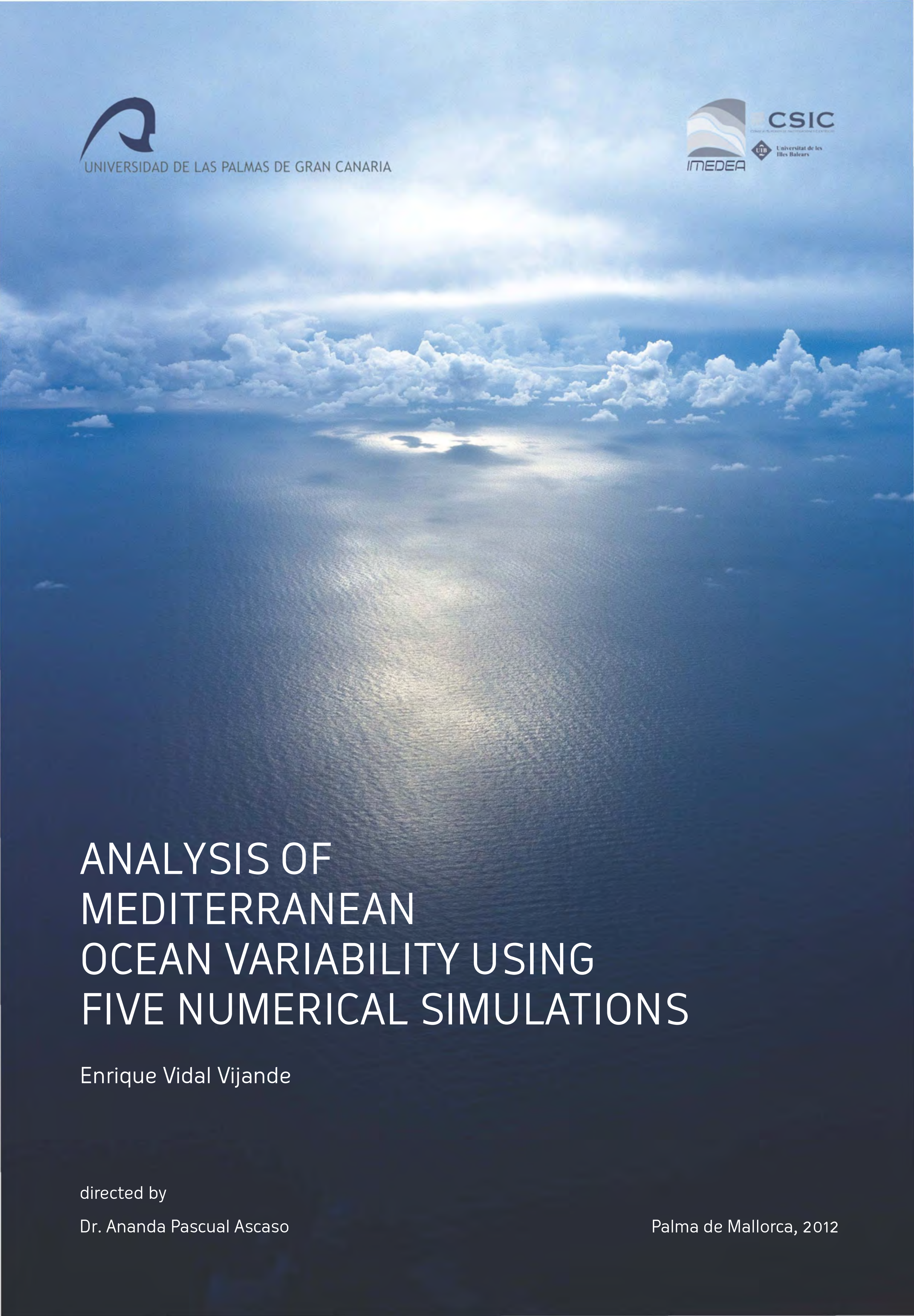

UNIVERSIDAD DE LAS PALMAS DE GRAN CANARIA

CSIC

Universitat de les Illes Balears

IMEDEA

ANALYSIS OF MEDITERRANEAN OCEAN VARIABILITY USING FIVE NUMERICAL SIMULATIONS

Enrique Vidal Vijande

directed by

Dr. Ananda Pascual Ascaso

Palma de Mallorca, 2012

D SALVADOR GALVÁN HERRERA, SECRETARIO DEL DEPARTAMENTO DE FÍSICA DE LA UNIVERSIDAD DE LAS PALMAS DE GRAN CANARIA,

CERTIFICA,

Que el Consejo de Doctores del Departamento en su sesión de fecha .... tomó el acuerdo de dar el consentimiento para su tramitación, a la tesis doctoral titulada "ANALYSIS OF MEDITERRANEAN OCEAN VARIABILITY USING FIVE NUMERICAL SIMULATIONS" presentada por el doctorando ENRIQUE VIDAL VIJANDE y dirigida por la Doctora Dª ANANDA PASCUAL ASCASO.

Y para que así conste, y a efectos de lo previsto en el Artº 73.2 del Reglamento de Estudios de Doctorado de esta Universidad, firmo la presente en Las Palmas de Gran Canaria,

a.......................de...de dos mil doce

UNIVERSIDAD DE LAS PALMAS DE GRAN CANARIA
Departamento de Física

PROGRAMA DE DOCTORADO EN OCEANOGRAFÍA

BIENIO 2007 - 2009

TÍTULO DE LA TESIS

Analysis of Mediterranean Ocean Variability using Five Numerical Simulations

[ANALISIS DE LA VARIABILIDAD OCEÁNICA DEL MEDITERRANEO UTILIZANDO CINCO SIMULACIONES NUMÉRICAS]

Tesis doctoral presentada por Enrique Vidal Vijande para obtener el grado de Doctor por la Universidad de Las Palmas de Gran Canaria. Dirigida por la Doctora Dª Ananda Pascual Ascaso, científico titular del CSIC en el IMEDEA(CSIC-UIB)

Enrique Vidal Vijande

Dra. Dª Ananda Pascual Ascaso

Palma de Mallorca, Abril 2012

Acknowledgements

Mi mayor agradecimiento es, sin lugar a duda, para Ananda Pascual, por haber sido una fantástica directora de tesis y haberme guiado y apoyado durante estos años. Gracias por su enorme implicación, su amistad y por haber creado un ambiente de trabajo enriquecedor y estimulante. También agradezco profundamente su apoyo a mis iniciativas y proyectos personales. Ha sido para mi una verdadera mentora.

Mis más sinceros agradecimientos a Joaquín Tintoré por haberme dado la oportunidad de empezar a trabajar en el IMEDEA, y luego por aceptar ser mi director de tesis durante el primer año, y por su apoyo continuado a lo largo de estos años.

Agradezco también la concesión de la beca pre-doctoral I3P del CSIC, la cual me ha permitido realizar esta tesis, y al proyecto EU-MyOcean FP7 por financiar mi asistencia a diversos congresos. Gracias a Alejandro Orfila por su apoyo y ayuda en escribir el proyecto de tesis que me permitió la concesión de la beca pre-doctoral, además de sus valiosos consejos.

I deeply acknowledge the hospitality and generosity of Bernard Barnier during my stay in Grenoble, and also for providing access to the various ORCA simulations used throughout this thesis. We had very interesting discussions, and provided me with valuable insights into the inner workings of ocean models. I would also like to thank Jean-Marc Molines for all his technical assistance with the ORCA model data.

I would like to thank Nicolas Ferry for providing the GLORYS1V1 data.

I would like to thank Samuel Somot for providing the NEMOMED8 data.

I would also like to thank Bruno Buongiorno Nardelli for his hospitality and friendship during my stay in Rome, for teaching me how to use EOFs for oceanographic data, and also for all the photographic conversations.

Del Instituto de Ciencias del Mar de Barcelona, mis agradecimientos a Josep Luis Pelegrí por aceptar ser mi tutor durante los cursos de doctorado y por toda su ayuda y generosidad. De la Universidad de Las Palmas de Gran Canaria, gracias a Ángel Rodríguez Santana y al equipo de Tercer Ciclo por su ayuda en los tramites para el depósito y lectura de esta tesis.

Gracias a mis padres Gerardo y María y a mi hermano Carlos por su incesante apoyo y ánimo, que me ha permitido llegar hasta aquí. Esta tesis no hubiese sido posible sin ellos.

A Laura, por estar siempre a mi lado, por haberme dado toda tu energía y apoyo, y mantener mi cabeza centrada en los momentos complicados, sobre todo en los últimos meses.

Abstract

The oceans play a fundamental role on the slow evolution of climate and all life on earth, and must therefore be studied and understood. The increase in oceanographic research and available measurements over the past half century have greatly increased our knowledge about the ocean's behaviour and variability, and highlighted its complexity and ubiquity over a wide range of space and time scales. However observational datasets still remain too short, too superficial or too dispersed in time and space to allow detailed studies of many of the physical processes governing the ocean's variability. In order to continue advancing our understanding of how the oceans work, it is crucial to complement observational data with ocean numerical modelling studies.

Throughout this thesis, we explore different aspects of the variability and circulation of the Mediterranean Sea, where many of the oceanic processes found throughout the worlds oceans can be studied in a reduced scale. We perform a comprehensive analysis through the validation of a series of ocean numerical models comparing them with observational datasets.

The first part is an initial approach at the analysis in the Mediterranean Sea of a $1/4^o$ global ocean simulation (ORCA025-G70). We focus on basin scale mean temperature (T) and salinity (S) temporal evolution at different depth layers by comparing to the MEDAR database, mean sea surface height temporal evolution and trends by comparing with altimetry, and transport through the Strait of Gibraltar and the Black Sea by comparing to the available literature. The results show that T variability at surface is well reproduced, but trends in intermediate and deep layers are positively biased. Poor results are obtained for S interannual variability, mainly due to the sea surface salinity (SSS) relaxation. Sea surface height interannual variability and seasonal cycle are well reproduced but climatological trends are too positive due to an imbalance in the freshwater fluxes from the atmospheric forcing. Water transport through the main straits is within the range of observed values.

The second part is a continuation of the analysis with global models, this time focusing on the Western Mediterranean (WMED) and adding two more simulations, one with higher vertical resolution and improved atmospheric forcing (ORCA025-G85) and one with data assimilation (GLORYS). The results show that the combination of a higher vertical resolution and better time continuity of the atmospheric forcing in G85 offer better T trend results at intermediate and deep layers with respect to G70. On the other hand, G85 has a much weaker SSS restoring and displays unrealistic negative S trends. Two exceptional deep convection events in the Gulf of Lions are reproduced by G85 due to the extremity of the atmospheric conditions, while weaker convection events are not reproduced due to the coarse resolution of both the model and atmospheric forcing. GLORYS has a better T and S performance than the ORCA hindcasts. Temporal evolution of sea level interannual variability is well reproduced in all simulations, but the ORCA hindcasts, which do not maintain a water balance show exaggerated positive trends, especially G85 that has a weaker SSS restoring. Through EOF analysis, the simulations recreate the surface circulation variability patterns correctly within their resolution limits. Transports through the main straits appears to be

correct when contrasted against the available literature.

In the third and final part of this thesis we use two high resolution simulations, ORCA12 ($1/12^o$) and NEMOMED8 ($1/8^o$) focusing on the WMED. For the standard T and S analysis, the results of both simulations show an improvement in T, especially trends at intermediate and deep layers. In S, ORCA12 gives similar results to the previous simulations, however NEMOMED8 shows a marked improvement due to a better water balance and lack of SSS restoring. When reproducing deep convection in the Gulf of Lions, NEMOMED8 correlates well with observations, however ORCA12 creates a very warm and stable intermediate layer preventing most deep convection events from reaching beyond intermediate layers. The analysis of mean geostrophic currents revealed correct overall circulation scheme but each simulation had slight discrepancies with observations. When decomposing the circulation signal using EOFs, the temporal and spatial patterns of NEMOMED8 are consistent with observations, however ORCA12 had an overly smooth and stable circulation pattern. Overall, NEMOMED8 is found to be a mature and reliable simulation although some room for improvement remains. ORCA12 is an interesting push forward in terms of global high resolution modelling, but being a first iteration, much improvement is expected in following simulations.

Resumen

Los océanos desempeñan un papel fundamental en la lenta evolución del clima y de toda la vida en la Tierra, y por lo tanto deben ser estudiados y comprendidos. El aumento de la investigación oceanográfica y los datos disponibles en el último medio siglo han mejorado considerablemente nuestros conocimientos sobre el comportamiento del océano y su variabilidad, resaltando su complejidad en un amplio rango de escalas espaciales y temporales. Sin embargo, las observaciones disponibles siguen siendo demasiado cortas, demasiado superficiales o demasiado dispersas en el tiempo y el espacio para permitir estudios detallados de muchos de los procesos físicos que gobiernan la variabilidad del océano. Con el fin de seguir avanzando en nuestra comprensión los océanos, es fundamental complementar los datos observacionales con los estudios de modelización numérica.

A lo largo de esta tesis, se exploran diferentes aspectos de la variabilidad y la circulación del Mar Mediterráneo, una cuenca en la que muchos de los procesos oceánicos que tienen lugar en el océano global se puede estudiar a una escala reducida. Para ello, llevamos a cabo un análisis exhaustivo a través de la validación de una serie de modelos numéricos oceánicos comparándolos con datos observacionales.

La primera parte es una primera aproximación al análisis en el mar Mediterráneo de una simulación global de $1/4\ ^o$ (ORCA025-G70). Nos centramos en: temperatura y salinidad promedio a escala de cuenca y su evolución temporal a diferentes profundidades mediante la comparación con la base de datos MEDAR; evolución temporal y tendencias del nivel del mar mediante la comparación con altimetría, y, finalmente, el transporte a través del Estrecho de Gibraltar y el Mar Negro, mediante la comparación con las publicaciones disponibles. Los resultados muestran que la variabilidad de temperatura en superficie se reproduce bien, pero la tendencia en las capas intermedias y profundas están sesgadas positivamente. En salinidad se no se obtienen resultados satisfactorios en cuanto a la variabilidad interanual, y es debido principalmente a la relajación de salinidad en superficie. La variabilidad interanual y el ciclo estacional del nivel del mar se reproducen correctamente, pero las tendencias climatológicas son excesivamen positivas debido a un desequilibrio en los flujos de agua dulce del forzamiento atmosférico. El transporte del agua a través de los estrechos principales se encuentra dentro del rango de valores observados.

La segunda parte es una continuación del análisis con modelos globales, esta vez centrándose en el Mediterráneo Occidental (WMED) y la adición de dos simulaciones más similares a G70, una con una mayor resolución vertical y la mejora del forzamiento atmosférico (ORCA025-G85) y una con los asimilación de datos (GLORYS). Los resultados muestran que la combinación de una mayor resolución vertical y una mejor continuidad en el tiempo del forzamiento atmosférico en G85 ofrecen mejores resultados en la tendencia de temperatura en las capas intermedias y profundas con respecto a G70. Por otro lado, G85 tiene una relajación en salinidad mucho más débil que G70 y muestra tendencias negativas irrealistas en salinidad. Dos acontecimientos excepcionales de convección profunda en el Golfo de León son reproducidos debido a la extremidad de las condiciones atmosféricas G85, mientras que los eventos de convección más débiles no se reproducen debido a la baja resolución tanto del modelo

como del forzamiento atmosférico. La temperatura y salinidad de GLORYS muestran un mejor comportamiento que las simulaciones ORCA. La evolución temporal de la variabilidad interanual del nivel del mar se reproduce bien en todas las simulaciones, pero en las ORCA, que no mantienen el balance hídrico muestran tendencias positivas exageradas, sobre todo G85 que tiene un una relajación en salinidad más débil. A través del análisis EOF, las simulaciones recrean razonablemente bien (dentro de los límites de su resolución) las características de los patrones de circulación superficial. Los transportes a través de los estrechos principales parecen correctos cuando se comparan con las publicaciones disponibles.

En la tercera y última parte de esta tesis se utilizan dos simulaciones de alta resolución, ORCA12 ($1/12^o$) y NEMOMED8 ($1/8^o$) centrándonos en el Mediterráneo Occidental. Para el análisis estándar de temperatura y salinidad, los resultados de ambas simulaciones muestran una mejora en temperatura, especialmente las tendencias de las capas intermedias y profundas. En salinidad, ORCA12 da resultados similares a las simulaciones anteriores, sin embargo NEMOMED8 muestra una notable mejora debido a un mejor balance hídrico y la ausencia de relajación en salinidad. Al reproducir la convección profunda en el Golfo de León, NEMOMED8 se correlaciona bien con las observaciones, sin embargo ORCA12 crea una capa intermedia muy cálida y estable que bloquea la convección más allá de las capas intermedias. El análisis de las corrientes geostróficas promedio muestra un esquema de circulación general correcto, pero cada simulación tiene pequeñas discrepancias con respecto a las observaciones. Al descomponer la señal de la circulación utilizando EOFs, los patrones temporales y espaciales de NEMOMED8 son consecuentes con las observaciones, sin embargo ORCA12 muestra un patrón de circulación excesivamente suave y estable. En general, NEMOMED8 demuestra que es una simulación madura y fiable a pesar de que sigue habiendo cierto margen de mejora. ORCA12 es un avance muy interesante en cuanto a simulaciones globales de alta resolución, pero al ser una primera iteración, es de esperar que los resultados mejoren notablemente en las próximas versiones.

Contents

Chapter 1

Introduction

Oceanography is the branch of science that studies the world ocean. It is a global term that includes all aspects and processes that drive and occur in the ocean; marine organisms and their ecosystem dynamics, marine geology, chemistry and biochemistry, physical processes and ocean dynamics. As a field of science, oceanography is relatively young with just over a century of history, and most of the advances in oceanography have occurred in the last 50-60 years, a trend rapidly accelerating towards the end of the twentieth century. In this time, physical oceanography has evolved from a field that was primarily concerned with the exploration of the World Ocean, to a focus on much more detailed questions involving mechanisms underlying the ocean circulation and its role in climate.

Due to the central role that the oceans play in many of the matters that affect mankind (climate, resources, demographics, politics, etc.), interest in the study of the oceans has greatly increased over the last 50 years. Until recently, our comprehension of the ocean's variability has been limited by the lack of historical observations. Over the last decades, the quality of oceanic observations has strongly increased, especially during the World Ocean Circulation Experiment (WOCE) and more recently with the help of modern telemetering technology. This modern technology, lead by the advent of satellite remote sensing (altimetry, infrared, microwave and ocean colour) as well as the generalised use of long-term mooring arrays, long endurance Lagrangian drifters and the more recent smart autonomous vehicles (gliders, AUVs, etc) are transforming the way we observe and understand the oceans. Despite this increase in available data, there are still many regions of the oceans that have very few if any *in situ* observations, primarily in the southern hemisphere. Even with global satellite coverage, these sensors rely on electromagnetic energy which cannot penetrate deep or propagate far inside the ocean. Therefore most measurements are limited to the ocean surface. Numerical models, which have experienced a phenomenal growth in both performance and complexity with the exponential increase of processing power in modern computers, help to complete the picture by tying in all the observations and knowledge about the oceans for the creation of three-dimensional forecasts and hindcasts, potentially allowing the study of ocean processes with a level of detail currently impossible with observations alone.

Oceanography has become especially relevant in recent years, as climate change has become an enormous source of interest for both the scientific community and the general public. Earth's climate is in constant change, and while its main variability comes from natural processes, the term *climate change* is generally used when referring to changes in our climate which have been identified since the early part of the 20th century. The observed changes in recent years and those which are predicted over the next century are thought to be mainly as a result of human behaviour rather than due to natural changes in the ocean and atmosphere, however this is still a matter of debate and much study.

With its heat capacity, which is a thousand times larger than that of the atmosphere, the ocean plays a fundamental role in the slow evolution of climate in our planet, moderating mean temperatures and long-term weather making life possible. Oceans are also huge reservoirs of atmospheric gases such as CO_2, absorbing and locking it away for long periods of time (up to 1000 years), dampening to a certain extent the effect of increased CO_2 levels on climate. Due to this vital role, and in order to understand and predict climate change, we must first understand the ocean processes that affect and control it.

1.1 Ocean Variability

The widespread use of modern telemetry and monitoring systems that provide a global vision of the ocean (with varying degrees of temporal, spatial and vertical resolution) have highlighted the complexity and ubiquity of the ocean's variability over a wide range of space and time scales. The length scales of the ocean structures (figure 1.1) can range from a few kilometres (e.g. coastal filaments) to basin scale structures (e.g. the Gulf stream), including intermediate structures of the order of 10-100 km (e.g. mesoscale eddies). The temporal scales of variability of these structures can go from days to seasons, or even decades. The presence in the ocean of all these structures, having different scales of variability and interaction between them, makes the real ocean a very complex system. This complexity is induced by several physical mechanisms, of which one of the main components is the atmospheric forcing (namely, the wind stress and the heat and freshwater fluxes), which directly influences the ocean surface. In a simplified view, the seasonal cycle of the heat flux over the ocean causes a seasonal fluctuation of sea surface temperature, while the seasonal change in the speed and direction of the mean winds changes the intensity and directions of the mean ocean currents and gyres. In addition, the average atmospheric forcing shows considerable year to year variability (e.g. severe vs mild winters), as well as several synoptic atmospheric events (e.g. localized strong gusts of wind, storms, etc.), and have a large impact on the local scale (ocean currents, temperature, salinity, etc). These processes altogether alter the seasonal cycle giving rise to an interannual variability of the ocean.

The ocean can be considered, for a large range of flow features, a quasi-inviscid, stratified fluid under the influence of the earth's rotation and where dynamical instabilities of the mean flow can appear separately from the direct action of the atmospheric forcing (chapter 13, Gill (1982)). These dynamical instabilities (both baroclinic or barotropic) can grow and generate mesoscale eddies and sharp ocean fronts with an associated mesoscale variability. The natural scale associated with mesoscale variability in the ocean is the Rossby radius of deformation or internal radius of deformation, which is basically the horizontal length scale at which the rotational effects become as important as buoyancy effects. In many cases, the mesoscale eddies appear and evolve independently of the external atmospheric forcing, as well as potentially interact with the mean currents and the bottom topography producing long term responses in the ocean circulation giving rise to an internal interannual variability of the ocean.

In the context of interannual variability, with this complex system comprised of so many interlinked processes, it becomes very difficult to discern between the natural variability of the system and the alterations caused by human activity. Despite significant progress, observational datasets remain too short, too superficial (satellites) or too dispersed in time and space (drifters

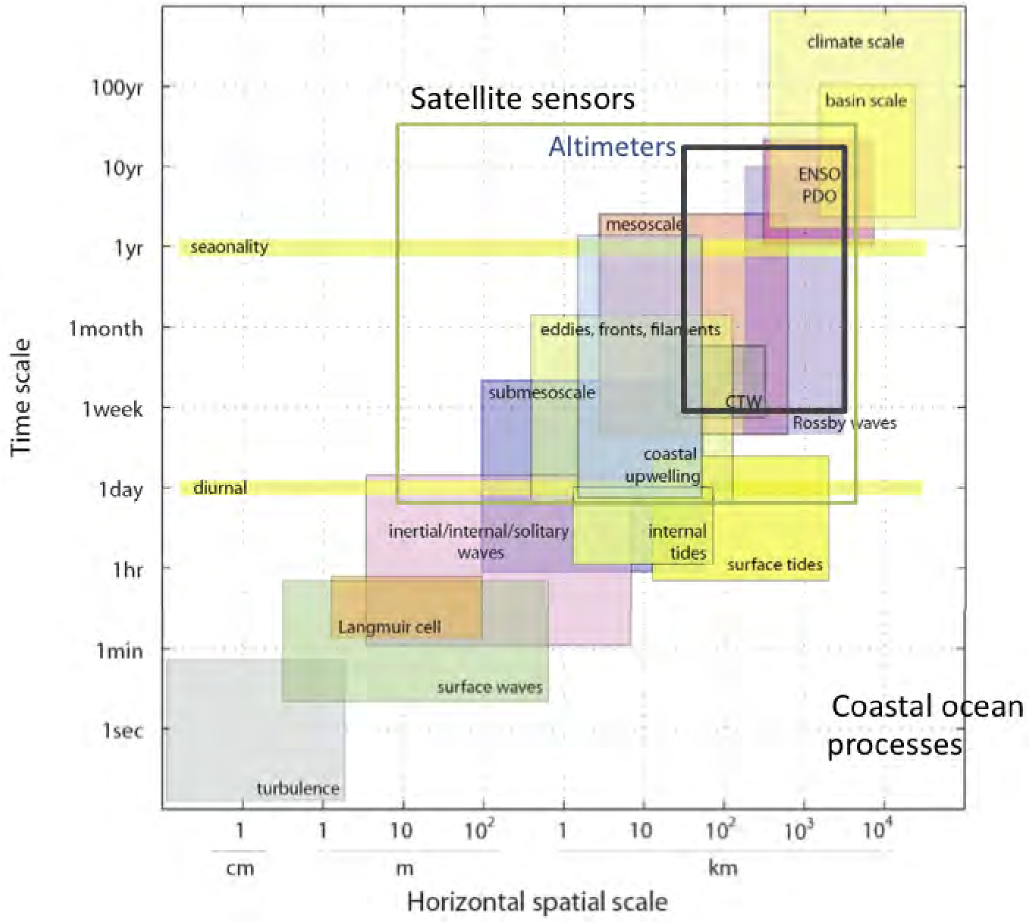

Figure 1.1: Spatial and temporal scales of the ocean (based on Chelton et al. (2001)

and moorings) to allow detailed studies of the above physical processes across their full range of scales (Penduff et al., 2006) (figure 1.2 shows the availability of *in situ* observations since 1958). In order to study the relative importance of each of the mechanisms playing a role on the ocean variability (the external forcing or the internal ocean variability), it is crucial to complement all the information from in-situ data with data from numerical modelling studies.

1.2 Ocean Numerical Modelling

In a general sense, *ocean circulation numerical modelling* involves numerical techniques to calculate approximate solutions of the complex, non-linear, multi-dimensional partial differential equations governing the ocean dynamics.

Ocean models have proved to be a powerful tool to study the ocean dynamics and its variability, specially due to the increase in the computational power achieved during the last two decades.

Recent numerical hindcast simulations provide the continuous and complete evolution of the ocean for the simulation period but require careful quantitative assessments and model-observation mismatch evaluations to guide dynamical studies and further model improvements (Penduff et al., 2007).

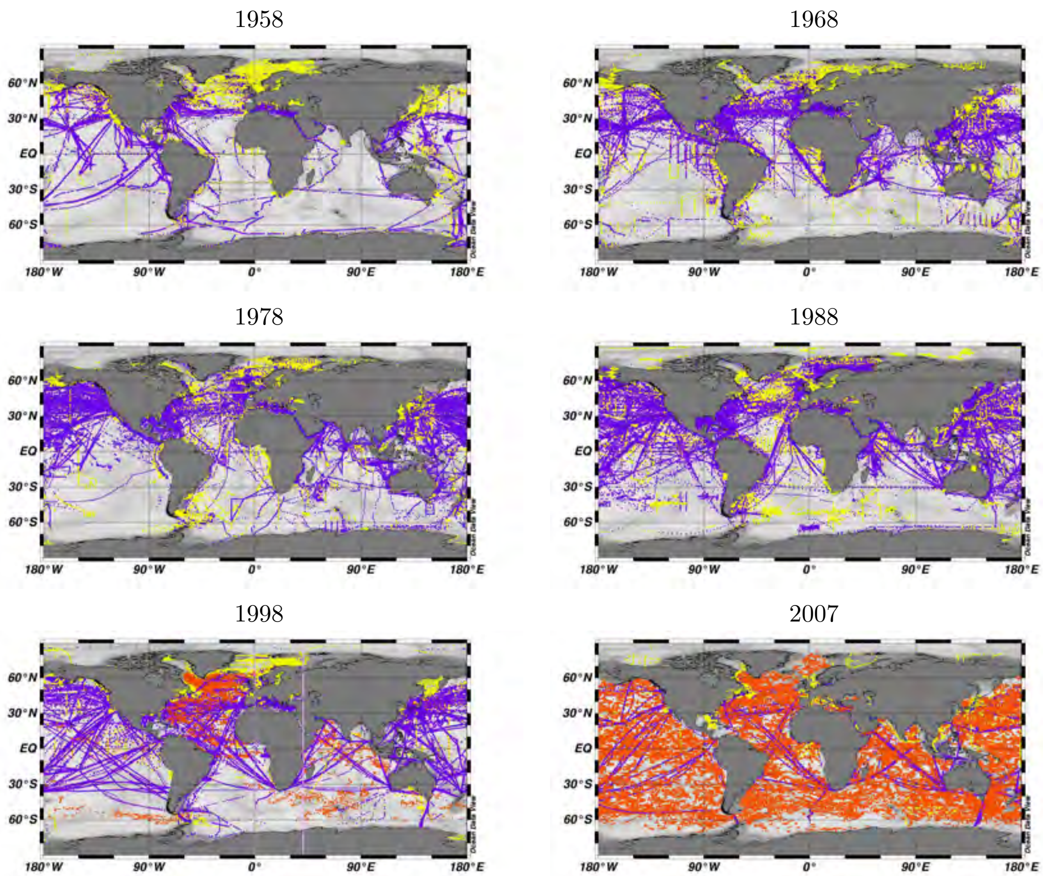

Figure 1.2: Spatial coverage during the years 1958, 1968, 1978, 1998, and 2007 of *in situ* measurements from different instruments: bathythermographs=MBT, XBT (in violet), TESAC (in yellow) and ARGO Floats (in orange) (from Juza (2011)).

Because ocean models are completely flexible in their configuration, and can be designed in many different ways to study the various ocean processes, it is important to understand firstly, what exactly their function is going to be, and secondly their limitations in terms of what scales can be represented or resolved by the model, what scales need to parametrized, and finally what scales are being imperfectly represented. The ocean circulation is a complicated function of the density structure of the water masses composing the ocean basins, the radiative fluxes at its surface, and the atmospheric forcing imposed at the surface. This forcing contains a variety of temporal (ranging from hourly to beyond decadal variations) and spatial scales (ranging from kilometre to basin scales).

Due to this extraordinary complexity, and because of computational limitations, ocean models must compromise their configurations in terms of resolution, area covered, equation approximations/simplification and other parametrizations. As such there are many types of ocean models and Kantha and Clayson (2000) present a comprehensive review.

For this thesis where we are interested in the three-dimensional ocean variability, the models must be baroclinic, global or regional, have sufficient resolution to resolve the features to be studied, maintain a free-surface formulation (for sea level and mass addition as features to be studied) and be linked to the atmosphere either via external atmospheric forcing or coupled atmospheric models.

One of the typical simplifications used in large-scale ocean circulation models is the hydrostatic/Boussinesq approximation. This ignores density changes in the fluid except when gravitational forces are concerned.

For numerical models which are aimed at creating realistic simulations of the past (referred to as hindcasts), the use of realistic atmospheric forcing data is necessary to drive the simulation. These include surface radiative, heat and buoyancy (precipitation and evaporation) fluxes, as well as wind stress forcing. What the model can and cannot resolve (both temporally and spatially) is also influenced by the temporal and spatial resolution of these atmospheric forcing variables, which depend on the availability of high quality measurements. In recent years the quantity, distribution and quality of such observations has increased considerably but the further back in time we go, the scarcer the number of measurements. This is especially true for the open ocean, where data on wind, humidity and precipitation fluxes is very limited. Because these fluxes depend on small air-sea temperature and humidity differences, direct measurements of the heat fluxes and freshwater sources with coverage and accuracy required for an ocean model are extremely difficult to obtain over the vast world ocean. While weather prediction models can compute such fluxes, they do not yet produce the data with the sufficient accuracy and mesoscale resolution needed for ocean models. Moreover, forcing the models with climatological estimates of surface fluxes generally results in unrealistic model Sea Surface Temperature (SST), or Sea Surface Salinity (SSS), which then become inconsistent with the imposed surface flux themselves (Barnier, 1998). Many ocean models now use re-analyses of atmospheric data, which are gridded, quality controlled compilations of observational data such as ECMWF ERA40 (Uppala et al., 2005). In these re-analyses, observations from multiple sources are run through an integrated forecasting system using a three dimensional variational technique to provide analyses every six hours. Newer revisions of ERA40 such as ERA-Interim (Dee et al., 2011) and ARPEGE (Beuvier et al., 2010) are dynamical downscales that aim at improving and increasing the resolution of atmospheric data. Because numerical model atmospheric forcing still needs much improvement, imbalances in the freshwater and heat fluxes can cause simulations to drift from stable conditions. What is commonly done to overcome this is to force the model with a simple relaxation of SST or SSS or both to a climatological mean. This approach presents many known drawbacks to represent ocean variability, since mesoscale features such as eddies and fronts are damped unrealistically rapidly by this restoring.

The physical characteristics of the ocean in terms of shape (coastline), topography, channels and straits are also vital for the performance of the model, as they can have important effects on many scales of the circulation. The resolution with which these are resolved can in some cases determine whether the model can simulate realistic circulation patterns at certain locations. Straits and channels are of especial importance since it is here where water and heat flux exchange between seas and basins occur. Another challenge in modelling the topographical characteristics of the ocean are the continental shelves and slopes, which play an important part in ocean circulation, particularly with regards to coastal currents, jets as well as cold water cascading into the deep ocean. Because of the shallow depths involved, circulation on the shelf is forced strongly by winds and astronomical tides, while in the deep ocean it is the density gradients and the winds. Additionally, the transition between shelf and abyssal ocean is quite abrupt with the slope regions having spatial scales of tens of kilometres (compared to thousands in the open ocean). Therefore low or medium resolution models tend to greatly smooth these abrupt topographical features, therefore affecting many of coastal circulation patterns that tend to flow along these features (Kantha and Clayson, 2000).

In general, higher resolution is always preferable although it is limited by computational and storage capabilities and therefore compromises have to be made. High resolution global models (example figure 1.3) are computationally extremely expensive (often requiring the use of"super-computer clusters" for extended periods of time). This is why regional models (example figure 1.4) are capable of operating at higher resolution than global models and thus more practical for regional studies.

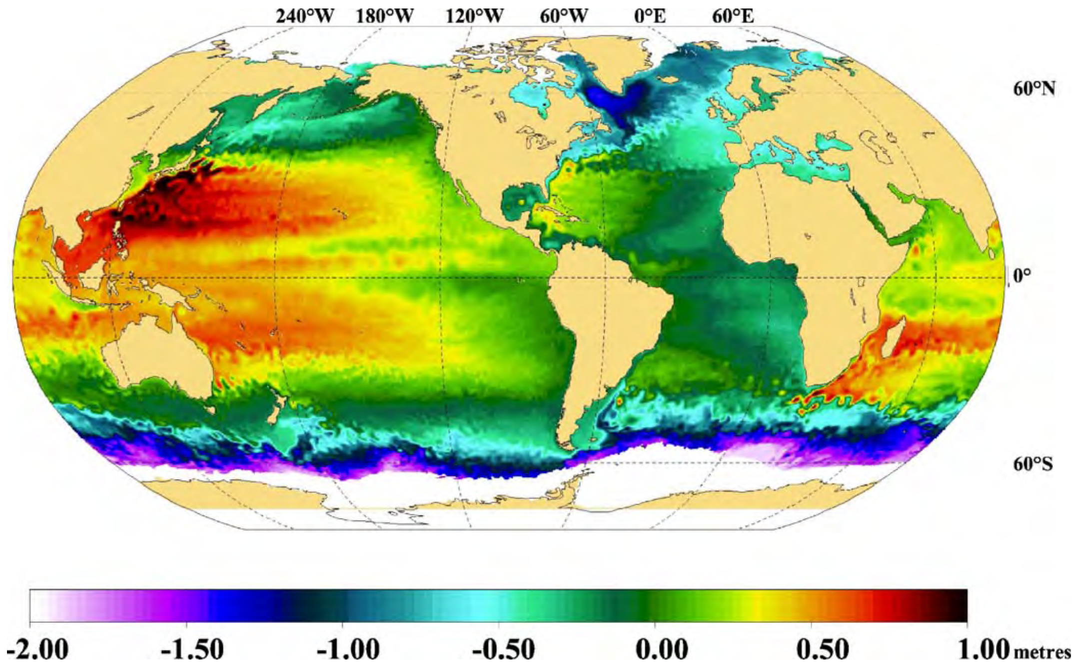

Figure 1.3: Coverage of a global model (ORCA G22) showing a snapshot of sea surface height and ice cover during winter (from Barnier et al. (2006)).

However, regional models are not without their own problems; these models require that their boundary conditions be provided by either nesting into a coarser resolution model or through relaxation to climatology. Nesting within a coarser resolution model can introduce errors due to differences in the parametrization of the physical processes in both models as well as errors due to the numerical techniques used for the nesting, which can propagate these errors into the regional domain having a significant impact on the simulation's evolution.

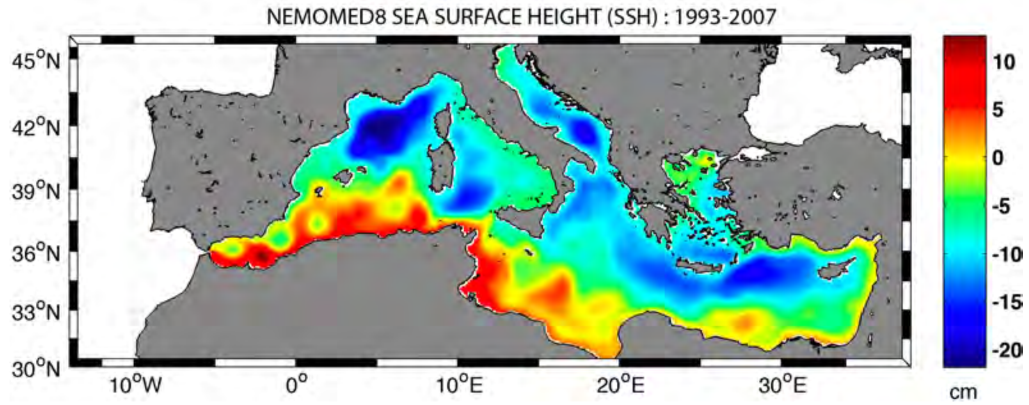

Figure 1.4: Coverage of a regional model (MEMOMED8) showing the sea surface height (SSH) for 1993-2007.

1.3 The Mediterranean Sea

In the context of ocean variability and climate change studies, the Mediterranean Sea (figure 1.5) is considered a "miniature ocean" (Bethoux and Gentili, 1999; CIESM Initiative Group, 2002), a kind of ideal, accessible, reduced scale ocean laboratory where many phenomena present in many different regions of the global ocean can be studied at a smaller scale: deep convection (MEDOC Group, 1970; Leaman and Schott, 1991), shelf-slope exchanges (Bethoux and Gentili, 1999), thermohaline circulation and water mass interaction (Wüst, 1961), mesoscale and submesoscale dynamics (Robinson et al., 2001), etc. Despite its small size, the thermohaline circulation within the basin is particularly active (Wu and Haines, 1996). Robinson et al. (2001) gives a value of 10-14 km for the internal Rossby Radius of Deformation, four times smaller than the typical value in the open ocean. Physical mechanisms are thus better monitored and understood in this ocean basin, contributing then to the advancement of knowledge of physical interactions and biogeochemical coupling at near-shore, local, sub-basin and global scales (Tintore, 2009).

The Mediterranean is a mid-latitude semi-enclosed sea, connected to the Atlantic Ocean through the ~300 m deep Strait of Gibraltar. It is comprised of two main basins, the western (WMED) and eastern (EMED) Mediterranean basins, connected by the Sicily Strait. Each of these basins are composed of several sub-basins, each one characterized by different oceanographic features (different topography, water masses and atmospheric forcing) and separated by straits and channels (Astraldi et al., 1999).

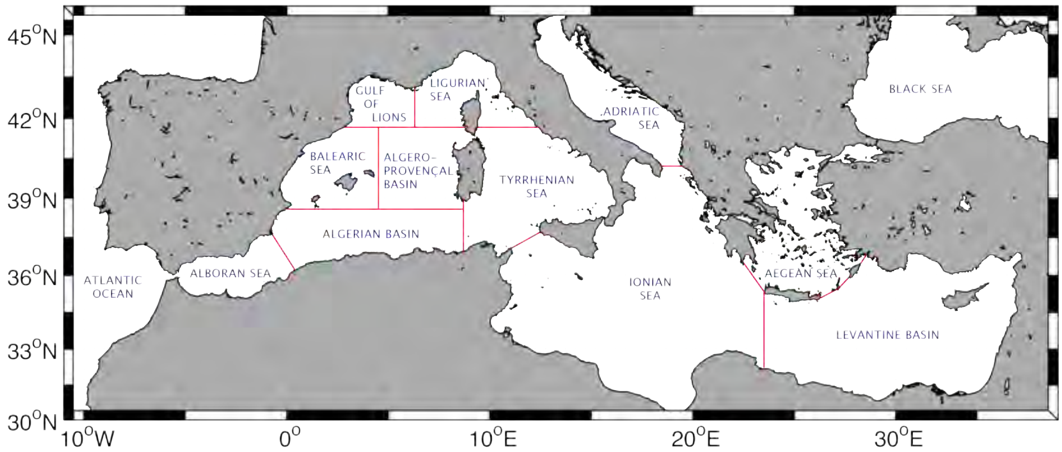

Figure 1.5: The regions and basins of the Mediterranean Sea.

The general picture of the Mediterranean circulation is rather complex due to the presence of multiple interacting scales, including basin, sub-basin scale and mesoscale structures (Robinson and Golnaraghi, 1994). In the Mediterranean one can find strong coastal boundary currents, unstable jets that shed vortices, permanent and recurrent sub-basin gyres, and energetic mesoscale eddies. All these structures interact and give rise to a significant variability in a wide range of temporal scales (mesoscale, seasonal and interannual). This complexity and variability of the ocean circulation arises from multiple driving forces: topographic effects, variable atmospheric forcing and internal dynamical processes.

Another element which is also important in the Mediterranean because of its huge socio-economic impacts is sea level variability. In the Mediterranean, it depends on local as well as remote forcing (sea level changes are linked to the NAO by the combined effect of atmospheric pressure anomalies and changes in evaporation and precipitation (Tsimplis and Josey, 2001)). Global steric expansion occurring outside of the Mediterranean basin can transmit a signal through the Strait of Gibraltar. Within the Mediterranean, inter-annual and higher frequency variability is dominated by wind and atmospheric pressure changes (Gomis et al., 2006) while steric variations, associated changes in the water budget by rivers, evaporation and precipitation driven by the regional atmospheric forcing, all contribute to sea level changes (Tsimplis et al., 2008). The rates of sea level change over the Mediterranean Sea have shown considerable variability over the last century. Before the 1960‘s, relative sea level was increasing at a rate of about 1.2 mm/yr, between 1960 and 1994 sea level was decreasing (Tsimplis and Baker, 2000), and after the mid 1990‘s altimetric measurements suggest rapid sea level rise, especially in the eastern Mediterranean. The spatial variability of sea level is also extremely non-uniform, which was clearly highlighted with the advent of satellite altimetry, capable of mapping the open ocean and its geographical variations of sea level change (Cazenave et al., 2001).

In the following sections we present some of the main circulation features of the Mediterranean Sea and modelling efforts carried out in this region.

1.3.1 Surface Circulation

The general circulation scheme of the Mediterranean Sea is complex and composed of three predominant and interacting spatial scales: basin scale (including thermohaline circulation), sub-basin scale, and mesoscale (Robinson et al., 2001). Mesoscale variability is known as the dominant signal in ocean circulation (Pujol and Larnicol, 2005), and is present throughout most aspects of Mediterranean circulation, from the gyres found in the Alboran Sea and Levantine basin to the eddy vorticity associated with the major currents such as Algerian, Northern and Ionian currents (figures 1.6 and 1.7). It also plays an important role in the formation of deep waters in the Gulf of Lions through mesoscale baroclinic instability (Herrmann et al., 2008a).

The Mediterranean surface circulation circuit starts as Atlantic Water (AW) enters the Mediterranean Sea through the Strait of Gibraltar at surface layers (100-200 m approx.) and into the Alboran Sea. Circulation in this sea is dominated by one or two sub-basin scale anticyclonic gyres (Viúdez et al., 1998), a quasi permanent western anticyclonic gyre (the Western Alboran Gyre, WAG) (figure 1.6) and the intermittent Eastern Alboran Gyre (EAG). While the EAG can also have cyclonic phases (Viúdez and Tintoré, 1995) it is mostly anticyclonic (Tintoré et al., 1988). The eastern boundary of the EAG is known as the Almería-Orán front and marks the beginning of the Algerian current which flows along the African coast. This narrow coastal current is very unstable and produces many anticyclonic eddies of 50-100 km in diameter which can be clearly seen with infrared satellite images (Millot, 1999). For this reason, the Algerian Basin is characterized by intense mesoscale activity. Some of these eddies grow in size and detach from the coast reaching in some cases the southern Balearic Sea (Ruiz et al., 2002). The Algerian Current reaches the Strait of Sicily where it bifurcates in two branches. One branch enters the EMED, while the other branch remains in the WMED.

Circulation at the Strait of Sicily presents a two-layer exchange, at the surface, AW enters the eastern basin, and in the deeper layers, the Levantine Intermediate Water (LIW), which are formed in the Levantine basin, enters the western basin. The AW branch that remains in the WMED follows the Italian, French and Spanish coasts, as the so-called northern current (Millot, 1999), and the LIW follows a similar cyclonic path along the periphery of the WMED at a depth of between 200 and 800 m. The northern current is also fed by AW flowing northward along east of Corsica and eventually flows into the

Balearic Sea, where a part of it crosses the Ibiza and Mallorca Channels and continues its path towards the Alboran Sea. The rest of the Northern Current recirculates to the North-East into the Balearic Current (Alvarez et al., 1994; Pinot et al., 1995; Astraldi et al., 1999; Ruiz et al., 2009). During its path from Gibraltar to the east, AW gradually changes becoming warmer (by 14-15^{o}C below the mixed layer) and saltier from 36.5 at the Strait of Gibraltar to 38.0-38.3 as it reaches the NW Mediterranean Sea (Millot, 1999). When the Northern Current reaches the Balearic Basin, the old AW properties are very different to the recent AW in the south, thus appearing a density front separating those waters (Balearic front).

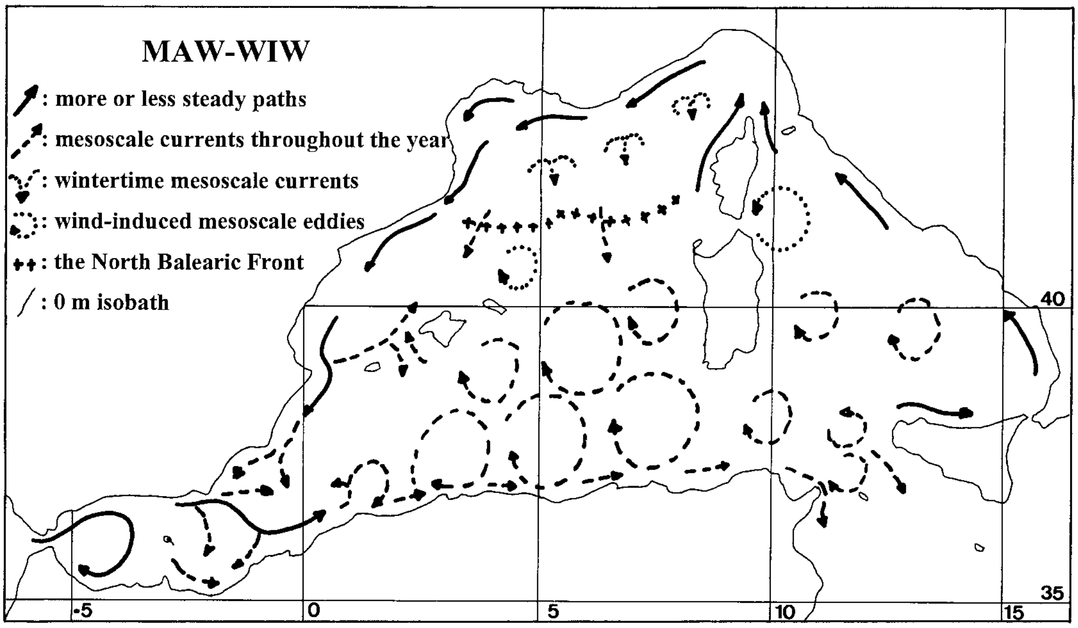

Figure 1.6: Schematic surface circulation in the Western Mediterranean Sea (Millot, 1999)

In the Eastern Mediterranean, the surface waters entering from the Strait of Sicily form the so called Atlantic Ionian Stream, this current is formed by modified AW having a salinity of 38.5 psu. In the Ionian Basin there are two permanent gyres, the anticyclonic Pelops Gyre and the cyclonic Cretan Gyre (figure 1.7). The Ionian stream enters the Levantine Basin, the easternmost basin in the Mediterranean, where the water gets warmer and saltier in the summer due to an excess of surface evaporation. There have been observed two permanent features in this basin, the Mersa-Matruh anti-cyclonic gyre

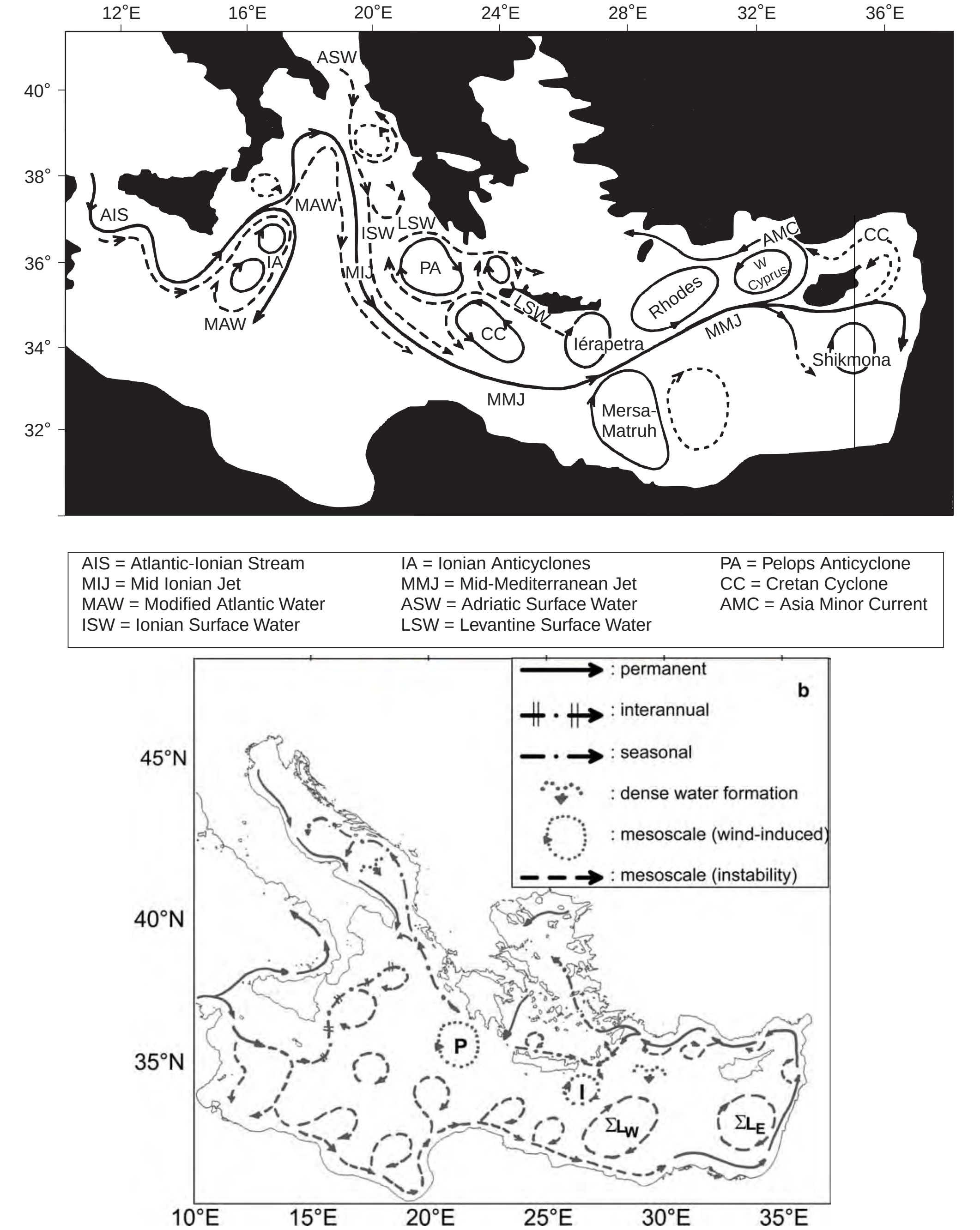

Figure 1.7: Two variations on the schematic surface circulation in the Eastern Mediterranean Sea. Robinson and Golnaraghi (1994) (top), Hamad et al. (2005) (bottom)

and the cyclonic Rhodes Gyre. In winter, the cooling increases the density of surface waters so that it sinks and mixes forming the LIW, which spreads at a depth of 300-500 m, exits from the strait of Sicily to the western Mediterranean and lastly emerges to the Atlantic ocean through the Strait of Gibraltar. The preferred site of LIW formation is the Rhodes gyre region, although there are observations of intermediate water formation in other areas of the Levantine Sea (see review by Lascaratos et al. (1999)).

As mentioned above, an important part of the Mediterranean circulation comes from mesoscale eddies and features. Mesoscale circulation is turbulent and displays significant temporal and spatial variability. Not all areas of the Mediterranean display equal amounts of mesoscale activity. Whereas certain regions display high activity such as the Alboran Sea, along the path of the Algerian Current and also the Levantine Basin below the Cretan Arc, other regions such as the Liguro-Provençal Basin, the Tyrrhenian and Adriatic Seas have low mesoscale activity (Pujol and Larnicol, 2005).

Mesoscale eddies form through instabilities along coastal currents like the Algerian Current, which can eventually detach from the current becoming offshore eddies and interact with the current itself. Eddies can form with both cyclonic and anticyclonic motion, with the former being smaller and short lived (days to weeks), and the latter being larger and capable of lasting from months to as much as a year. Large anticyclonic eddies can have significant effects on circulation over wide areas and long periods of time. They can achieve a considerable size (several tens to a few hundreds of kilometres) and depth, and can interact with coastal currents or even block circulation completely, especially in the proximity of straits and channels (Millot, 1999). This underlines the importance of mesoscale variability studies in comprehending the sea surface circulation in the Mediterranean.

Since the horizontal scale of mesoscale eddies is related to the Rossby radius of deformation, which in the Mediterranean Sea is $\sim$10-14 km, adequate study of mesoscale eddies requires very fine sampling or high resolution modelling.

1.3.2 Deep Water Formation

The Mediterranean Sea has an intense thermohaline circulation, being one of the few regions in the world where open ocean deep convection occurs (Herrmann et al., 2008b) and thus one of the few sites able to redistribute water over great depths (Schroeder et al., 2010). The formation of deep waters is important both for the Mediterranean and the world ocean. It is the main mechanism that allows the exchange of oxygen and nutrients between the surface and deep layers. Deep waters can also act as climatic markers since once they sink to the deep layers, they retain their characteristics that were determined by the prevailing atmospheric conditions at its formation site, allowing the study of past climate as far as the renewal time scales allow (which can be decades to centuries in the Mediterranean) (Lascaratos et al., 1999). Figure 1.8 shows a schematic representation of the thermohaline circulation in the Mediterranean Sea.

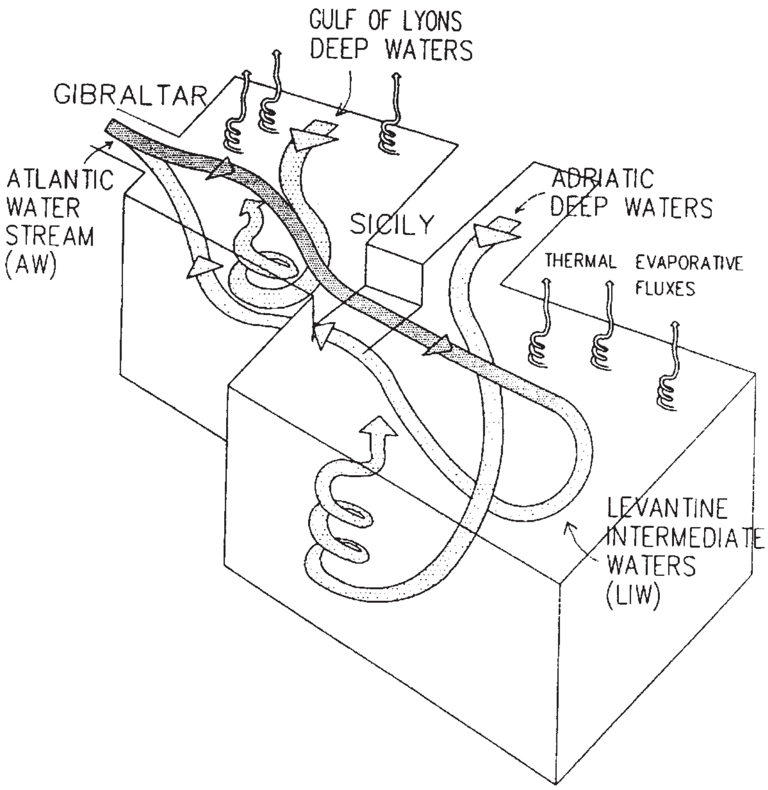

Figure 1.8: Schematic representation of the thermohaline circulation in the Mediterranean Sea from Lascaratos et al. (1999).

The process of deep convection consists of three phases, starting with the pre-conditioning, where the area of deep convection is prepared for vertical mixing. In the Gulf of Lions, the pre-conditioning agent is the cyclonic circulation at its centre, which lifts the isopycnals and exposes the denser, less stratified waters to the atmosphere, facilitating the mixing process. Additionally, a region can retain the signal of convection events from one year, pre-conditioning a deep convection event on the following year. Once the stratification of the water column has been sufficiently degraded by the pre-conditioning, the second phase is the actual deep convection mixing, which can be onset by a single or multiple strong atmospheric events. The third and final stage is the re-stratification of the water column once the turbulence has been dissipated and the density gradients re-established (Juza, 2011).

The North Western Mediterranean (WMED) is one of the main deep water formation sites of the Mediterranean Sea. The principal drivers of deep convection in the NW-MED are atmospheric, namely strong northerly winds and significant heat loss during winter periods combined with a cyclonic gyre in the Gulf of Lions region. These atmospheric conditions (Tramontane, Mistral, cyclogenesis of the Gulf of Genoa, etc) are caused by the local orography of the NW Mediterranean coast (Alps, Pyrenees, Rhone Valley) which channel strong cold winds into the area (Herrmann and Somot, 2008). In this region, dry and cold winds initially mix the surface Atlantic Water (AW) with the underlying warmer and saltier Levantine Intermediate Water (LIW) through violent mixing, which upon further cooling leads to the formation of Western Mediterranean Deep Water (WMDW) (MEDOC Group, 1970; Schroeder et al., 2010) which sinks down to the full depth of the region ∼2000 m. During mild winters, convection still occurs, but the buoyancy loss is not sufficient to produce deep water and thus forms intermediate waters, so-called Western Intermediate Waters (WIW) (Font et al., 1988). Given that these events are a direct consequence of atmospheric forcing, they display a significant interannual variability.

The Eastern Mediterranean basin (EMED) also contains certain areas where deep convection takes place. In this basin, deep waters are mostly formed in the south Adriatic Sea with smaller contributions from the northern part (Lascaratos et al., 1999). The onset of this deep water formation follows a similar process to that of the NW-MED, consisting of strong winds and surface heat loss combined with a permanent cyclonic gyre in the southern Adriatic Sea. These Adriatic Deep Waters (ADW) fill the deepest parts of the Ionian and Levantine Seas. This was the traditional picture of the Eastern Mediterranean Deep Water (EMDW) formation up until the discovery of the Eastern Mediterranean Transient (EMT) during the 1990's (Roether et al., 1996). At the beginning of the 1990's, a change in the location of deep water formation was observed, shifting from the typical southern Adriatic Sea to the Aegean Sea. This was caused by several preconditioning processes and finally triggered by the 1992-1993 winter, which was an exceptional winter in terms of heat loss and wind stress. The deep waters formed in the Aegean then overflowed into the Levantine and Ionian basins through the Cretan Arc Straits, uplifting the old EMDW creating a warm, salty and dense anomaly in the hydrographic characteristics of the deep layers of the EMED and a cold and fresh anomaly in the intermediate layers (Roether et al., 2007; Beuvier et al., 2010). Some Levantine Deep Water (LDW) was also observed at the permanent Rhodes Gyre (Sur et al., 1992).

1.3.3 Numerical Modelling

The Mediterranean presents a very interesting region for ocean modelling. As mentioned above, many of the ocean's dynamical processes take place in the Mediterranean making it a very suitable but challenging region for modelling studies. It is however not without its challenges. The Mediterranean topography is extremely complex (figure 1.9), its water balance is maintained at the Strait of Gibraltar, which is narrow (14.3 km) and shallow (300 m). This requires all but the highest resolution models to make special adjustments at this location to allow for an adequate flow. In addition to Gibraltar, there are many other straits and channels that play vital roles in the water mass circulation around the Mediterranean. The Sicily Strait (145 km, 316 m depth) separates the eastern and western Mediterranean basins, with all the surface and intermediate water mass exchanges happening through it. The Otranto Strait in the Adriatic, the Cretan Arc separating the Aegean from the Levantine basin and the Ibiza and Mallorca Channels are also vital in the regional circulation. Whether a model is capable of adequately representing these topographic features will determine its success at modelling circulation and water mass exchanges.

Figure 1.9: Satellite image of the Mediterranean Sea with the bottom topography overlaid (source: Google Earth), and detail of the various channels and straits.

Mediterranean dynamics are dominated by mesoscale variability therefore models striving to study processes other than large scale mean circulation must have sufficient resolution to resolve the mesoscale. There are also dynamical processes such as deep convection that are vital for Mediterranean and global oceanography and are generally difficult to model because of their dependence on short and intense atmospheric events as well as on small mesoscale baroclinic instabilities (Herrmann et al., 2008a).

Several regional modelling studies have focused on the Mediterranean Sea using high resolution $1/8^o$ and $1/16^o$ regional models such as DieCAST (Fernández et al., 2005), OPAMED8 (Somot et al., 2006), EU-MFSTEP (Tonani et al., 2008), NEMOMED8 (Sevault et al., 2009) and MED16 (Béranger et al., 2010) to name a few. The DieCAST $1/8^o$ simulation used in Fernández et al. (2005) is not a hindcast, it is a simulation run to assess circulation and transport variability in the Mediterranean Sea. It is forced by climatological monthly mean winds and uses relaxation towards monthly climatological surface temperature and salinity. The OPAMED8 $1/8^o$ simulation by Somot et al. (2006) is a scenario of the Mediterranean Sea under climate change IPCC-A2 conditions and run with an atmosphere regional climate model (ARPEGE) over the 1960-2099 period using a hierarchy of three different models. Their objective is to obtain a high resolution atmospheric forcing to run the OPAMED8 simulation (based on the OPA model (Madec et al., 1998) of the Mediterranean Sea under a transient climate change scenario. The EU-MFSTEP $1/16^o$ simulation by Tonani et al. (2008) is a very high resolution model based of the OPA code (Madec et al., 1998) and used for operational daily forecasts of the Mediterranean Sea. It is available since 1997. The NEMOMED8 $1/8^o$ simulation by Sevault et al. (2009) is a simulation focused on the study of the dynamics behind certain features and variability of the Mediterranean Sea, which has also been used in the recent studies by Beuvier et al. (2010) and Herrmann et al. (2010) that focused on the EMT and the 2005-2006 NW Mediterranean convection events respectively. The MED16 (Béranger et al., 2010) is a modelling experiment to assess the performance of atmospheric forcing resolution on winter ocean convection in the Mediterranean Sea by running two 4-year simulations 1998-2002 (with 11 years spin-up), one using ERA40 and one using ECMWF analysed surface fields which have twice the resolution of ERA40. Additionally, some recent studies such as Hu et al. (2009) and Schaeffer et al. (2011) have used short, very high resolution models ($\sim$1 km resolution) to study very specific areas and processes in the Mediterranean (specifically, mesoscale eddies in the

Gulf of Lions).

Throughout this thesis we study the performance of a variety of ocean models in the Mediterranean Sea; from medium resolution $1/4^o$ global models to regional $1/8^o$ and finally a first iteration of a global $1/12^o$ model.

Chapter 2

Motivation and Objectives

The general motivations and objectives of the present thesis are to study the Mediterranean (with a focus on the Western Mediterranean) variability through the analysis and validation of five ocean numerical hindcast simulations by comparing them to different sources of observations (including *in situ* data and remote sensing).

We attempt to perform a comprehensive analysis of the main features and variables that represent the Mediterranean Sea circulation, water masses and dynamics, compare them to real data, and suggest where the simulations have room for improvement. In Chapters 5 and 6 we use low resolution $1/4^o$ hindcasts with the aim of improving our understanding of long term interannual variability at basin scales. In Chapter 7, we use high resolution $1/8^o$ and $1/12^o$ hindcasts to assess the improvements gained by the higher resolution as well as more detailed studies at sub-basin and meso-scales.

Modelling studies demand a large amount of work in their programming, running, diagnostics, etc. Part of the objectives of these studies arise from a collaboration agreement with LEGI (Laboratoire des Ecoulements Gophysiques et Industriels) and MERCATOR-OCEAN to validate their ocean simulations for the Mediterranean Sea region.

Chapter 5 is a first approach at the analysis and validation in the Mediterranean Sea of a global ocean simulation; the ORCA025-G70 simulation. This simulation was chosen because it was, at the time, one of the highest resolution global simulations available, it was modern and had been validated in several regions of the world‘s oceans. However, no particular attention had been paid to its performance in the Mediterranean. Higher resolution regional models were available for the Mediterranean, but no-one had analysed a global model there. The resolution of $1/4^o$ is insufficient to reproduce the mesoscale dynamics, but adequate for the large scale circulation which is the main focus of this chapter (mainly basin scale). Specifically, the scope of this chapter is to assess whether ORCA-G70 is capable of correctly reproducing the state of the ocean with regards to certain key variables; mean temperature and salinity basin scale variability and trends at different depth layers by comparing the simulation to the MEDAR temperature and salinity database, Sea Surface Height and Steric Height time series analysis of seasonal cycle amplitude and phase, interannual variability, trends, as well as the spatial distribution of trends, variance and the annual amplitude. This is done by comparing the simulation to satellite altimetry data. Finally we check whether transport through the two main water inputs into the Mediterranean Sea (Atlantic waters through the Strait of Gibraltar, and freshwater input from the Black Sea) are correct and water balance is maintained through them by comparing with the available literature.

Chapter 6. Following the positive and interesting results obtained when analysing ORCA-G70, the goal of this chapter is to expand on the work carried out in Chapter 5 by adding more simulations with different configurations to the analysis and asses how their different characteristics (same $1/4^o$ resolution) affect their capability to reproduce circulation features in the Western Mediterranean. In addition to ORCA-G70, we analyse ORCA-G85 (a simulation with improved atmospheric forcing, greater vertical resolution and weaker sea surface salinity restoring), and GLORYS1V1 (a shorter simulation with data assimilation). The inclusion of GLORYS1V1 aims at verifying whether reanalysis products that include data assimilation help to improve the description and our understanding of ocean variability in the Western Mediterranean Sea. It will highlight which degree of improvement can be expected from an ocean reanalysis in that region with respect to a free run. In addition to the basin scale analysis performed in Chapter 5, we focus on specific aspects of the circulation in the WMED such as the deep water formation in the Gulf of Lions and transport through the Balearic Channels, assessing how the differences in the model configurations affect their performance. Finally, we analyse the large-scale mean geostrophic circulation in the WMED by breaking it down into its principal components using Empirical Orthogonal Functions (EOFs).

Chapter 7. In this final study, we go a step further and analyse two high resolution models, one global (ORCA12, $1/12^o$ resolution) and one regional (NEMOMED8, $1/8^o$ resolution). With these higher resolution simulations, the objective is to study the mesoscale variability of the WMED circulation. For consistency we also perform the basic temperature and salinity basin scale analysis, as well as looking at the deep-water formation capabilities of these high resolution simulations, since, as concluded by the previous chapters, resolution (both of the simulation and the atmospheric forcing) is one of the limiting factors when reproducing deep convection events in the Gulf of Lions. However the bulk of this chapter is dedicated to investigate the dynamical characteristics of the WMED, and to do so we focus on the geostrophic circulation of the simulations given by their sea surface height and compare it to the geostrophic circulation calculated from altimetry measurements. To assess the mesoscale variability, we analyse the Eddy Kinetic Energy (EKE). Finally, we attempt to analyse and identify the principal components of the WMED mesoscale circulation by performing EOF calculations in three main regions; the Alboran Sea, the Algerian Basin and the North-Western Mediterranean.

Chapter 3

Data and Numerical Simulations

All of the models analysed throughout this Ph.D. Thesis (from global to regional scale) are based on the NEMO2 (Nucleus for European Models of the Ocean) (Madec, 2008) modelling system, which presently includes the latest version of the primitive equation, free surface ocean circulation code OPA9 coupled to the multi layered sea-ice model LIM2. The fundamental equations of ocean dynamics and diagnostic sea surface height used in these models can be consulted in appendix A.

3.1 The ORCA Hindcasts

The ORCA hierarchy of ocean models are coupled ocean/sea-ice global configurations of the NEMO numerical framework implemented by the DRAKKAR group (Barnier et al., 2006) aiming at the study of ocean variability under realistic atmospheric forcing conditions over the last half century. The models simulate the evolution of temperature, salinity, velocity, sea surface height (SSH), sea-ice characteristics, and oceanic concentrations of tracers (CFC_{11} and C_{14}) (Barnier et al., 2007).

The *DRAKKAR collaboration* is a European modelling project which provides the framework for joint and coordinated modelling studies between research groups in France, Germany, Russia and Finland.

Common characteristics of the ORCA models

The model configurations use the ORCA global tri-polar grid at varying resolutions (2^o, 1^o, $1/2^o$, $1/4^o$, $1/12^o$). Effective resolution gets finer with increasing latitudes (the grid size is scaled by the cosine of the latitude, except for the Arctic, figure 3.1), and in the vertical, grid spacing is finer near the surface and increases with depth (max. depth is 5844 m). Bathymetry is derived from the 2-min resolution ETOPO2 bathymetry data of the NOAA National Geophysical Data Centre. Initial conditions for temperature and salinity are derived from the NODC Word Ocean Atlas data set for middle and low latitudes, and for the Mediterranean they are derived from the MEDAR climatology (more details can be found in Barnier et al. (2006) and Molines et al. (2007).

The ORCA hindcasts studied here are driven at the sea surface by realistic atmospheric forcing. One of the great difficulties of "forced" oceanic modelling is the balance of atmospheric fluxes. The uncertainties in air temperature, humidity, winds, rainfall and air-sea fluxes are so large than when one integrates the global heat and freshwater fluxes, there is usually a huge imbalance which drives an unacceptable drift in the ocean model.

3.1.1 $1/4^o$ Global Hindcasts: ORCA G70 and G85

In chapters 5 and 6 we analyse the ORCA-R025 G70 and ORCA-R025 L75.G85 numerical simulations (G70 and G85 hereafter), which are implemented on a $1/4^o$ resolution grid. Effective resolution is ∼27.75 km at the equator, ∼20-22 km in the Mediterranean and ∼13.8 at 60^o N/S). At this resolution, the simulations are eddy permitting but not eddy-resolving in large oceans such as the Atlantic, but not even eddy-permitting in the Mediterranean where the first Rossby radius of deformation is around 10-14 km. Grid, masking, and initial conditions are inherited from the global configuration of the MERCATOR-Ocean operational oceanography center, with 1442x1021 grid points, 46 vertical levels for G70 and 75 vertical levels for G85. Some smoothing is applied when adding the bathymetry (some of the straits are widened to two grid points (∼40 km at Mediterranean latitudes) to allow adequate flow given the coarse resolution of the models). A restoring has been applied towards the Levitus climatology (T,S) at the Gibraltar Strait exit, in the Gulf of Cadiz. This restoring increases from 200 m to 400 m, then remains constant to the bottom. Since this restoring only affects the Mediterranean outflow, its effects are not felt directly within the Mediterranean Sea.

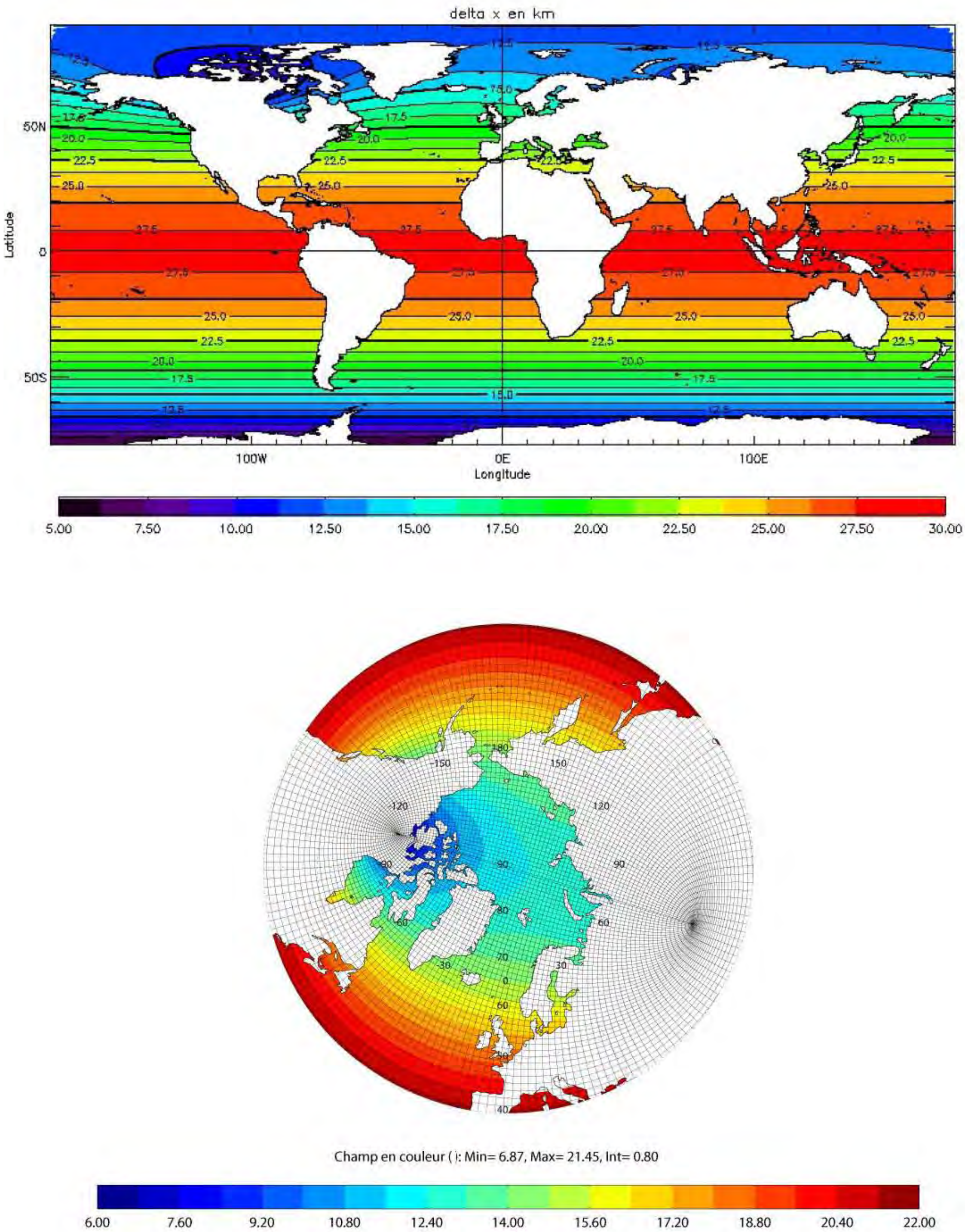

Figure 3.1: Horizontal resolution (in km) of the ORCA 025 1/4^o grid (MERCATOR Projection) (Juza, 2011)

Forcing

Atmospheric forcing for both models is a hybrid forcing based on the ECMWF ERA40 reanalysis (∼125 km resolution) and CORE (Large and Yeager, 2004). Surface momentum flux is directly provided to the ocean/sea-ice model as a wind stress vector. Surface heat fluxes (solar, infra-red, latent, and sensible heat) and freshwater flux for ocean and sea-ice are calculated using the empirical bulk parametrization described by Goosse (1997). Evaporation is derived from the latent heat flux.

In the case of G70 the forcing used is the DFS3 (DRAKKAR Forcing Set 3), which is based on un-corrected surface atmospheric state variables of ERA40 extended in time until 2007 with fields of the ECMWF operational analysis and the radiation and precipitation products of CORE. From the CORE forcing data set, precipitation (rain and snow), downward shortwave and longwave radiations are extracted; and ERA40 (from 1958-2001) and ECMWF operational analysis (2002-2007) provide 10 meter wind, 2 meter air humidity and 2 meter air temperature to compute turbulent air/sea and air/sea-ice fluxes during model integration using the bulk formula proposed by (Large and Yeager, 2004). The frequency of DFS3 is monthly for precipitation, daily for radiation and 6-hourly for turbulent variables. This forcing is globally imbalanced for heat (+12.8 W/m^2) and freshwater (+56 mm/year).

G85 is forced with DFS4 which is an improved version of DFS3 with corrections applied to ECMWF variables (air temperature, air humidity, wind speed) to remove unrealistic time discontinuities (induced by changes in the nature of assimilated observations, especially in 1979 when satellite data began to be assimilated) and obvious global and regional biases in ERA40 fields (by comparison to high quality observations). Corrections also aimed to improve continuity between ERA40 and ECMWF operational analyses in 2002. Wind speed corrections consist in rescaling ERA40 and ECMWF winds with 6 years of QSCAT scatterometer winds. The result for the Mediterranean Sea is that wind speeds are increased by about 10% in DFS4. Finally, the CORE radiation and precipitation fields have been submitted to a small adjustment (in zonal mean) that yields a near-zero global imbalance of heat (+0.3 W/m^2) and freshwater (-0.2 mm/year). Detailed information on ERA40, DFS3 and DFS4 can be found in Brodeau et al. (2010).

Since these simulations do not achieve freshwater balance, and to avoid and prevent an unacceptable drift in the model, a sea surface salinity (SSS) restoring term has been applied. This term attempts to balance the freshwater budget by restoring SSS to climatology (adding evaporation or precipitation where necessary). This restoring term tends to adversely affect the simulation's interannual variability. In G85 the SSS relaxation is $1/6^{th}$ that of G70.

3.1.2 $1/12^o$ Global Hindcast: ORCA-12

The ORCA12.L46-MAL95 (O12 hereafter) is the first global $1/12^o$ simulation performed at MEOM (LEGI, CNRS). It uses the standard ORCA tri-polar grid (4322 x 3059 grid points) with resolution of 10 km at the equator, 5 km at 60^o and 3.5 km at 75^o. It has 46 vertical layers (similar to G70) with a resolution of 6 m near the surface and 250 m in the deep ocean, and is forced by the higher-resolution ERA-Interim ($\sim$80 km resolution) atmospheric forcing. It covers the period from 1989 to 2007. This simulation follows an initial test run (ORCA12.L46-K001) at Kiel (IFM Geomar), which was started in 1979 from Levitus and used the CORE2 forcing fields. The purpose of the O12 run is to learn how to run such a big model and perform a sensitivity experiment between CORE2 and ERA-Interim forcing.

In this run, standard SSS restoring towards Levitus (global) / Medatlas (Mediterranean) is used (with a time scale of 60 days/10 meters, which is considered quite strong). This is similar to the restoring used in G70.

3.2 Global Simulation with Data Assimilation: $1/4^o$ GLORYS1V1

GLORYS1V1 (GLORYS hereafter) is the first of a number of simulations created by the French GLobal Ocean ReanalYsis and Simulations framework and is based on the operational system PSY3V2 used at MERCATOR-OCEAN. It is also a global implementation of the NEMO framework and shares many features with the ORCA-025 simulations described above (particularly G70 with the same forcing and sea-ice model). The simulation spans the Argo era from 2002-2008 and uses data assimilation from a variety of sources including Sea Surface Temperature (SST) maps, along track sea level anomaly (SLA, AVISO delayed mode) and in situ temperature and salinity profiles from the CORA-2 and CORIOLIS databases. The model does not perform any relaxation in SST or SSS. The atmospheric forcing consists in daily averages of atmospheric variables provided by ECMWF operational analyses, and the CLIO bulk formulation (Goosse, 1997) is used. ECMWF precipitation field has been corrected using GPCP monthly data in a similar way to the method proposed by Troccoli and Kallberg (2004)

3.3 Mediterranean Sea Regional Hindcast: $1/8^o$ NEMOMED8

In Chapter 7 we analyse the NEMOMED8 (NM8) model (Beuvier et al., 2008; Sevault et al., 2009), which is a $1/8^o$ Mediterranean configuration of the NEMO numerical framework. It is an updated version of the OPAMED8 model by Somot et al. (2006), which is a regional configuration of the OPA ocean model (Madec et al., 1998).

Most of the description of this numerical simulation is obtained from Beuvier et al. (2010) and Herrmann et al. (2010).

NM8's resolution of $1/8^o$ provides a mesh size in the 9 to 12 km range from the north to the south of the domain, which covers the entire Mediterranean Sea and an Atlantic buffer zone near the Strait of Gibraltar. To better represent the water and heat exchange at the Strait of Gibraltar, the grid is tilted and stretched to better follow the SW-NE axis of the real strait and to increase its resolution up to 6 km (Beranger et al., 2005). NM8 has 43 vertical Z-levels with an inhomogeneous distribution (from $\triangle Z = 6$ m at the surface to $\triangle Z =$ 200 m at the bottom with 25 levels in the first 1000 m). Bathymetry is based on the ETOPO 5'x5' database and the deepest level has a variable height in order to adapt to the real bathymetry.

Sea surface height evolution is parametrized by a filtered free-surface (Roullet and Madec, 2000). With this parametrization, the volume of the Mediterranean Sea is not conserved due to the loss of water induced by evaporation. In order to conserve volume, at each time step, the evaporated water over the whole basin is redistributed in the Atlantic buffer zone west of 7.5^oW.

Atmospheric Forcing

NM8 is forced by the 50 km resolution ARPERA (Herrmann and Somot, 2008; Tsimplis et al., 2008) atmospheric forcing, which is a dynamical downscaling of the ERA40 reanalysis (125 km resolution) from ECMWF (Simmons and Gibson, 2000) driven by the ARPEGE-Climate regional climate model developed at CNRM (Déqué and Piedelievre, 1995). The small scales (under 250 km) of ARPEGE-Climate are allowed to develop freely and the larger scales are driven by ERA40 fields. The synoptic chronology then follows the ERA40 ECMWF fields while the high-resolution structures of the atmospheric flow are created by the model. For the period 1958-2001, ARPEGE-Climate is driven by the ERA40 reanalysis and from 2002 to 2006 fields of ECMWF analysis are used ($\sim$55 km), being downgraded to ERA40 resolution ($\sim$125 km) for consistency.

The forcing fields for NM8 are momentum, freshwater and heat fluxes. A relaxation term toward ERA40 sea surface temperature (SST) is applied for the heat flux. This term actually plays the role of first-order coupling between the SST computed by the ocean model and the atmospheric heat flux, ensuring the consistency between those terms. Following the CLIPPER Project Team (1999), the relaxation coefficient is -40 W $m^{-2}K^{-1}$, equivalent to an 8 day restoring time scale.

No salinity restoring is used at the surface (unlike in the ORCA simulations) and river runoff freshwater flux is explicitly added to complete the surface water budget. The Black Sea is not included in NM8 instead, its freshwater input into the Mediterranean is considered as a river for the Aegean. All river inputs are based on monthly climatologies (constant over the years).

The exchanges with the Atlantic Ocean are performed through a buffer zone from 11^{o}W to 7.5^{o}W. Temperature and salinity in this area are relaxed to the 3-D T-S fields of the seasonal Reynaud et al. (1998) climatology, with a weaker relaxation closer to Gibraltar and stronger further away. Initial conditions for the Mediterranean Sea are given by the MEDATLAS-II climatology MEDAR-Group (2002) and the Reynaud et al. (1998) for the Atlantic.

3.4 *In Situ* Observations

Three different hydrographic datasets were considered to perform the comparison and validation of the different simulations. These datasets are the following:

3.4.1 MEDAR

In an effort to provide an integrated picture of temperature and salinity in the Mediterranean, the MEDAR Group (2002) built a new database interpolating 291,209 T and 124,264 S quality checked profiles onto a $0.2^o \times 0.2^o$ horizontal grid and 25 standard vertical levels (Rixen et al., 2005). The MEDAR dataset contains yearly data for the period 1945-2002. The data interpolation was obtained using the Variational Inverse Method (VIM) and the calibration of the correlation length and the signal-to-noise ratio were obtained by Generalised Cross Validation.

It is important to note that although the database is available for a long period, the number of profiles at the beginning, and especially in the WMED prior to the 1970‘s, is scarce. In addition, sampling of the Mediterranean is biased towards the areas of deep and intermediate water formation, while areas near the African coasts have not been sampled adequately (figure 3.2). Moreover the data are also seasonally biased Tsimplis and Rixen (2002) as most measurements have been taken during the spring and summer periods. This can lead to significant interpolation errors.

There is a separate product, the MEDAR climatology, which is comprised of monthly averages without interannual variability. That is to say, one average for every January, every February, and so on. This climatology is also used in this study to look at the seasonal cycle of the steric signal.

3.4.2 ISHII

The Ishii dataset (Ishii and Kimoto, 2009) (ISHII here-on) which consists of monthly $1^o \times 1^o$ gridded global T and S fields spanning the period 1945-2006 and covering from surface to 700 m. The ISHII dataset comes from an objective analysis of different kinds of *in situ* ocean T and S data (bottle, CTD, ARGO, XBT and MBT). XBT and MBT data are corrected for depth bias.

3.4.3 EN3-V2a

The ENACT/ENSEMBLES version 3 (EN3-v2a) dataset (EN3 here-on) (Ingleby and Huddleston, 2007) was produced by objective analysis of the T and S profiles of the World Ocean Database 05, the Global Temperature and

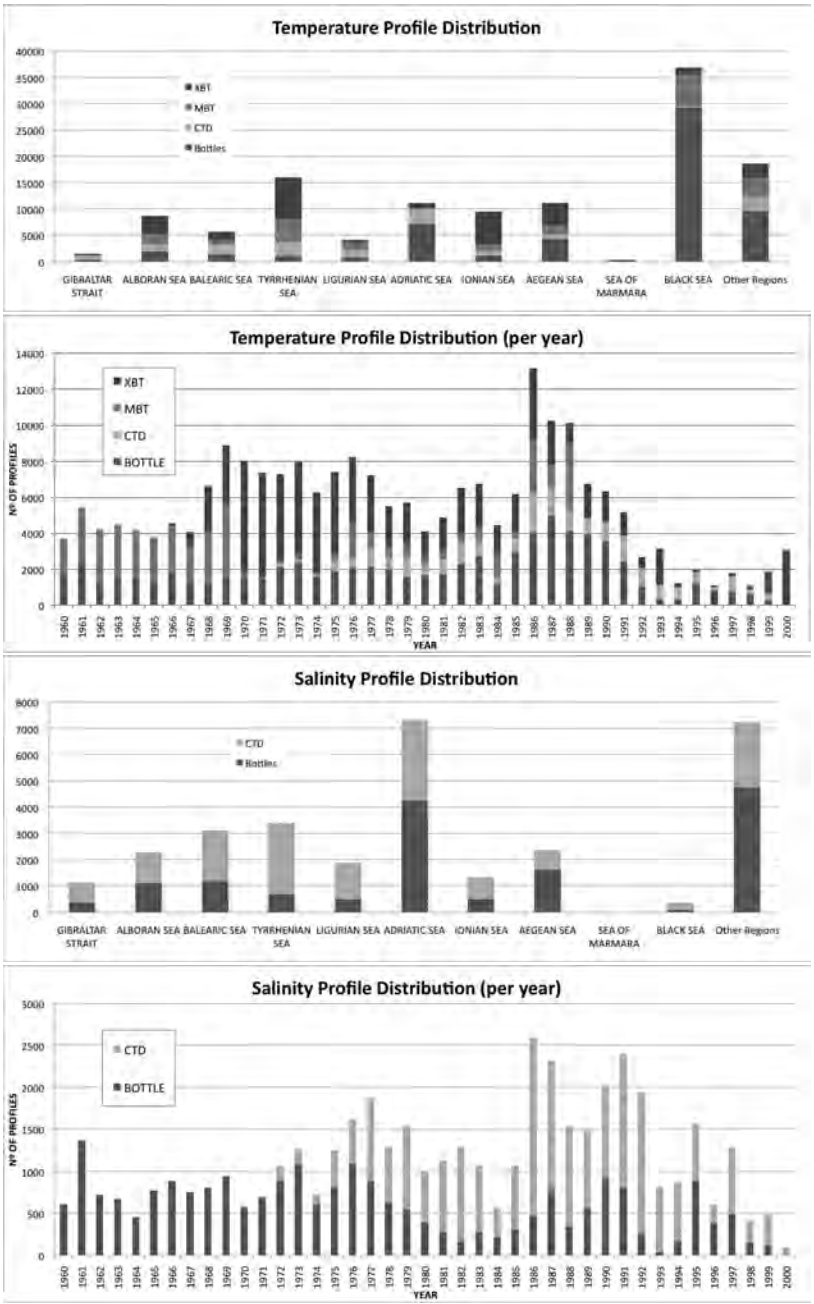

Figure 3.2: Distribution of Temperature and Salinity profiles in the MEDAR database (Vidal-Vijande et al., 2011).

Salinity Profile Project, Argo and the Arctic Synoptic Basin-Wide Oceanography Project. EN3 contains observations from bathythermographs (XBTs and MBTs), hydrographic profiles (CTDs and predecessors), moored buoys and ARGO drifters. The dataset consists of quality controlled, global, monthly T and S fields on a $1^o \times 1^o$ grid covering the period 1950 to the present. The vertical domain extends down to 5000 m, with data on 42 levels.

Data coverage is highly non-uniform, especially at the beginning, with huge gaps in in parts of the tropics and southern hemisphere contrasted with a few highly sampled ship tracks (mostly MBTs). This distribution improves over time, but large areas of the world ocean still remain with inadequate temporal and spatial sampling (Ingleby and Huddleston, 2007).

3.5 Satellite Altimetry

Satellite altimetry provides realistic high-resolution sea surface height (SSH) observations making it a useful tool in the validation of sea level and surface circulation numerical models (further details on the altimetry principle are provided in appendix B). However, altimeter measurements also include Earth‘s geoid which varies tens of meters across the ocean and needs to be subtracted from altimetry data to obtain a usable product (Dobricic, 2005). Since the exact shape of the geoid is largely unknown (the best data available comes from the GRACE satellite measurements and they have a resolution of approximately 300 km, which is only sufficient for large scale studies) the typical solution to circumvent this limitation is to subtract a temporal mean of sea surface height at each location leading to only the variable part of sea surface height, known as sea level anomaly (SLA).

Satellite altimetry data are available as a global product at $1/4^o$ resolution but in this thesis we use the higher-resolution product specific for the Mediterranean. It is the REF MERGED SLA product which is freely available through the AVISO FTP (http://www.aviso.oceanobs.com). These data consist of gridded, delayed time sea level anomaly fields specific for the Mediterranean Sea merging several altimeter missions (Topex/Poseidon, Jason-1/2, ERS 1/2, ENVISAT) provided weekly with a resolution of $1/8^o$. The reference product has been selected in order to have a homogeneous time series with the same configuration of satellite altimeters included in the objective analysis scheme.

The methodology used in AVISO (Ssalto/Duacs system) to process altimetric data is to build up a homogeneous and inter-calibrated dataset based on a global crossover adjustment using Topex/Poseidon as the reference (Le Traon et al., 1998). Sea surface height measurements are then geophysically corrected (tides, wet/dry atmosphere, ionosphere) with the atmospheric correction applied in order to minimize aliasing effects and to recover total sea level. The classical Inverted Barometer correction has been replaced by the MOG2D barotropic correction (Carrère and Lyard, 2003) which improves the representation of high frequency atmospheric forcing as it takes into account wind and pressure effects. Then, along-track data are resampled every 7 km using cubic splines and SLA is computed by removing a 7-year mean corresponding to the 1993-1999 period. Measurement noise is reduced by applying Lanczos (cut-off and median) filters. The mapping method to produce gridded SLA fields from along-track data is described in Le Traon et al. (2003). The long-wavelength error parameters are presently adjusted according to the most recent geophysical corrections. For more details on the altimeter data processing the reader is referred to Pujol and Larnicol (2005). This change, as shown in (Pascual et al., 2009), constitutes an important step forward with respect to previous altimeter products (e.g. those used in Brachet et al. (2004) and (Pascual et al., 2007)). This is particularly relevant close to the coast (defining here the coastal ocean as the region over the continental shelf and slope, ranging from 0-100 km from the coast), where altimetric observations often are of lower accuracy or not interpretable due to a number of factors including inaccurate tidal corrections, incorrect removal of atmospheric (wind and pressure) effects at the sea surface (Volkov et al., 2007), as well as the radar signal being contaminated by land up to a distance of around 40 kilometres from the coast. In a small sea with many narrow straits and basins such as the Mediterranean, major features which are normally found further out at sea are usually not affected, however coastal currents can show significant error due to land proximity (Vignudelli et al., 2005). To overcome this problem, several groups from Europe are working on these issues in the frame of projects funded by Space Agencies (such as PISTACH funded by CNES and COASTALT funded by ESA). Essentially, improved altimeter corrections and increasing the data recovery near the coast, are the main tasks within those projects (Bouffard et al., 2009; Volkov et al., 2007). Despite its limitations, altimetry has become an invaluable tool for the study of sea level variability across the worlds oceans.

For this study, monthly means have been computed from weekly gridded maps (averaging 4-5 maps for every month).

3.6 Mean Dynamic Topographies

An important issue to be analysed in the models described in this work is to evaluate the capability to reproduce the main features of mean circulation. However, as mentioned above, the Sea Level Anomaly altimetry fields only include the variable part of the total sea level signal. Thus, the mean circulation has to be analysed from alternative sources. One of the methods is to use approximations derived from numerical models as a first guess and then make local corrections using *in situ* observations. Here we use two different MDTs, one by Rio et al. (2007) and one by Dobricic (2005). Rio et al. (2007) use an average over 1993-1999 of dynamic topography outputs from MFS (Tonani et al., 2008) as a first guess. This is then improved in a second step by combining drift buoy velocities and altimetry using a synthetic method to obtain local estimates of the mean geostrophic circulation which are then used to improve the first guess through an inverse technique to map the Synthetic MDT onto a $1/8^o$ grid. Dobricic (2005) uses a different method; they use the statistics from the MFS operational assimilation system, monitoring the long-term bias in the SLA assimilation (using the period Sept 1999 to Sept 2002) and try to eliminate it.

Chapter 4

Methods

In this thesis we have used a variety of statistical methods to analyse the different datasets. In this chapter we describe these methodologies and add references to the chapters in which they have been used.

4.1 General Statistics

Throughout the works presented in this Ph.D. thesis we use a series of standard statistical analysis methods to analyse the various datasets and variables. These are the main ones used:

Means - In some cases we use temporal means, creating two-dimensional maps, and in other cases we use spatial means, creating time-series plots of seas, basins or smaller regions.

Variance is a measure of the amount of variation of the values of a particular variable. We use variance to assess the spatial variability of certain variables (e.g. sea surface height) by calculating the variance over a certain period for each grid point of the dataset and creating a two-dimensional variance map. This is used in Chapter 5.

Trends are useful to describe the long term behaviour of a dataset or timeseries. Since the data used throughout this PhD thesis is of a fairly low frequency, made up of monthly or yearly averages of gridded data, we calculate trends using simple linear regression (by least squares) and then get the confidence levels at the 95% for the slope of the fit:

$$\hat{a} = \frac{\sum_{i=1}^{n} y_i(t_i - \bar{t})}{\sum_{i=1}^{n}(t_i - \bar{t})^2} \tag{4.1}$$

$$d = \pm \frac{\hat{s}}{\sqrt{\sum_{i=1}^{n}(t_i - \bar{t})^2}} T_{n-2}(1 - \alpha/2) \tag{4.2}$$

where $\hat{a}$ is the estimation of the slope, d is the confidence interval at the α level of significance, $\hat{s}$ is the estimation of the standard deviation, and T_{n-2} is the inverse of the t-student cumulative probability function with n-2 degrees of freedom (Vargas-Yáñez et al., 2005). The trend can be calculated either with the full signal or with the signal minus the seasonal cycle. The final step is to fit a straight line to the dataset using the function $f = \hat{a}x + \hat{b}$.

The **Correlation Coefficient** is a measure of the statistical relationship between two dependant datasets. Correlations have been calculated using the following formula:

$$r = \frac{\sum_m \sum_n (A_{mn} - \overline{A})(B_{mn} - \overline{B})}{\sqrt{(\sum_m \sum_n (A_{mn} - \overline{A})^2)(\sum_m \sum_n (B_{mn} - \overline{B})^2}} \tag{4.3}$$

where $\overline{A}$ is the matrix mean of A, and $\overline{B}$ is the matrix mean of B.

Annual cycles. Throughout this thesis we use two different methods to calculate the annual (seasonal) cycle; in Chapter 5 we obtain the annual cycle by fitting two harmonic functions using a least squares method to assess whether the amplitude of the spatial patterns along the annual cycles of model and observations coincide.

$$y(t) = A_a \cos\left(\frac{2\pi}{365.25}t - \phi_a\right) + A_{sa} \cos\left(\frac{2\pi}{182.63}t - \phi_{sa}\right) \tag{4.4}$$

where A_a and ϕ_a are the amplitude and phase of the annual cycle, and A_{sa} and ϕ_{sa} are the amplitude and phase of the semi-annual cycle (Pascual et al., 2008).

In most cases when we wish to study the interannual variability of a certain signal, the seasonal cycle, which is usually the dominant signal, has a much higher amplitude than all other signals, therefore making interpretation of interannual variability harder. We therefore remove the seasonal cycle by subtracting it from the total signal. The removal of the seasonal cycle for timeseries analysis is done by removing a monthly climatology from the timeseries data. The climatology is created by calculating the mean of every month of the year (i.e. mean of all Januarys, Februarys, etc).

4.2 Empirical Orthogonal Functions (EOFs)

EOFs are used to identify and quantify the spatial and temporal variability consistently reducing the dimensions of large datasets to few significant orthogonal (uncorrelated) modes of variability, and to estimate the amount of variance associated to each mode of variability in percentage terms.

Despite the dimension reduction of the datasets performed by the EOF method, the spatial patterns and their expansion coefficients (principal components (PC), i.e., the evolution in time of the spatial modes) are not always easy to interpret, especially referring to PC of secondary modes of variability, often complicated by non-periodic signals. It is important to take into account that the modes of variability contain information about the dataset that is not necessarily related to physical features (Olita et al., 2011).

In Chapters 6 and 7 we use EOFs to decompose the complex ocean circulation signal into its Principal Components (PC) of spatial variability $F_k(x, y)$ and their associated temporal components $a_k(t)$ making it easier to analyse and describe them separately.

The signal $O(x, y, t)$ is decomposed in the using the following formulation:

$$O(x, y, t) = \sqrt{n-1} \sum_{k=1}^{n} F_k(x, y) a_k(t) \tag{4.5}$$

where $\mid a_k \mid = 1$ and $\mid F_k \mid \neq 1$

4.3 Water Mass Transports

Transport through straits and channels is calculated by integrating the zonal velocities provided by the simulations at either North-South, East-West, or diagonal transects. Positive values are considered transport due East (e.g.. Atlantic inflow into the Mediterranean Sea) or North, and negative values were considered transports due West (e.g.. Mediterranean outflow into the Atlantic Ocean) or South. In the case of diagonal transects, which in this study only refers to the Mallorca Channel, positive values are considered for flows with a dominant Northward component and negative values are considered for flows with dominant Southward component.

4.4 Hovmöller Diagrams

In this thesis we use Hovmöller diagrams to plot the time evolution of vertical profiles of temperature and salinity. The X and Y axes are time and depth respectively with the value of temperature or salinity represented by the color gradients. These are used in Chapters 6 and 7 to study the time-evolution of deep convection events in the Gulf of Lion.

4.5 Eddy Kinetic Energy (EKE)

The Eddy Kinetic Energy is a measure of the degree of variability and may identify regions with highly variable phenomena such as eddies, current meanders, fronts or filaments. It is calculated from the sea level anomaly (altimetry) or sea surface height anomaly (models) (η') by making the assumption of geostrophy :

$$EKE = \frac{1}{2}[U_g'^2 + V_g'^2] \tag{4.6}$$

$$U_g' = -\frac{g}{f}\frac{\partial \eta'}{\partial y} \tag{4.7}$$

$$V_g^{'} = \frac{g}{f}\frac{\partial \eta^{'}}{\partial x} \tag{4.8}$$

where $U_g^{'}$ and $V_g^{'}$ denote the zonal and meridional geostrophic velocity anomalies. f is the Coriolis parameter, g is the acceleration of gravity and the derivatives $\frac{\partial \eta^{'}}{\partial y}$ and $\frac{\partial \eta^{'}}{\partial x}$ are computed by finite differences where x and y are the distances in longitude and latitude, respectively (Pascual et al., 2007).

Chapter 5

Basin Scale analysis in the Mediterranean Sea using a $1/4^o$ simulation

5.1 Introduction

This chapter is based on the article :

Vidal-Vijande, E., A. Pascual, B. Barnier, J.-M. Molines, and J. Tintoré, 2011: Analysis of a 44-year hindcast for the Mediterranean sea: comparison with altimetry and in situ observations. *Scientia Marina*, **75** (1),

In this chapter we study the interannual and seasonal variability in the Mediterranean Sea by performing a model assessment of the global ORCA-R025 G70 (G70 here-on) simulation, and comparing it with altimetry and the MEDAR (temperature and salinity) observational database. We also analyse the prognostic sea surface height (SSH) from the simulation, and try to identify the drift problems common in the SSH of most models. Also, using a global model (with suitably resolved straits) reduces certain issues related to boundary conditions. We analyse the model's output using a series of techniques, attempting to identify its strengths, and especially its weaknesses in order to improve future simulations.

5.2 Temperature

In order to better understand the time evolution and vertical distribution of temperature in the Mediterranean, it was separated into basins and vertical layers (Fig. 5.1) identical to those used by Rixen et al. (2005). This allows a better comparison between the model and observations. Figure 5.2 provides a list of the numerical values seen in Figure 5.1 for easy comparison.

For these comparisons, the model data were filtered out with a 1-year running average in order to remove the intra-annual variability not resolved by MEDAR.

The surface layer (top 150 m) shows good agreement between the model and observations, with correlations of 0.8 in the WMED and 0.5-0.6 in the EMED, and is capable of reproducing signals such as the temperature anomaly round 1990-1995. Tsimplis and Rixen (2002) relate this temperature fluctuation with the EMT. However the model is slightly warmer, between 0.08^{o}C and 0.16^{o}C than the observational data, which may be related to the underestimation of total winter period heat loss (Herrmann and Somot, 2008) caused by the low resolution of ERA40.

Trend values for both G70 and MEDAR show a positive trend in the WMED (0.51± 0.28^{o}C/100 yr and 0.81± 0.29^{o}C/100 yr respectively), and coincide in sign with other studies by Tsimplis and Rixen (2002), Rixen et al. (2005) and Salat and Pascual (2006). The EMED shows a strong negative trend for the second half of the 20th century in MEDAR (-1.21± 0.33^{o}C/100 yr) but no significant trend in G70, also coinciding with the studies referenced above. However, these trends are usually difficult to detect reliably because surface layers are subjected to seasonal and high frequency variability, where the noise superimposed on mean climatological values or trends is very large (Vargas-Yáñez et al., 2009).

Intermediate layers (150-600 m), which are dominated by the Levantine Intermediate Water (LIW), show a clear trend difference in the WMED with warming in G70 (0.67± 0.12^{o}C/100 yr) and cooling in MEDAR (-0.33± 0.13^{o}C/100 yr). In contrast, the EMED shows essentially no trend in G70 and a stringer cooling in MEDAR (-0.96± 0.14^{o}C/100 yr). Vargas-Yáñez et al. (2009) provide a compilation of studies such as those by Bethoux and Gentili (1999) (1959-1997, for the Ligurian Sea) and Sparnocchia et al. (1994) (1950-1987, for the Ligurian Sea and Sicily Strait), obtaining similar trends to G70, but these

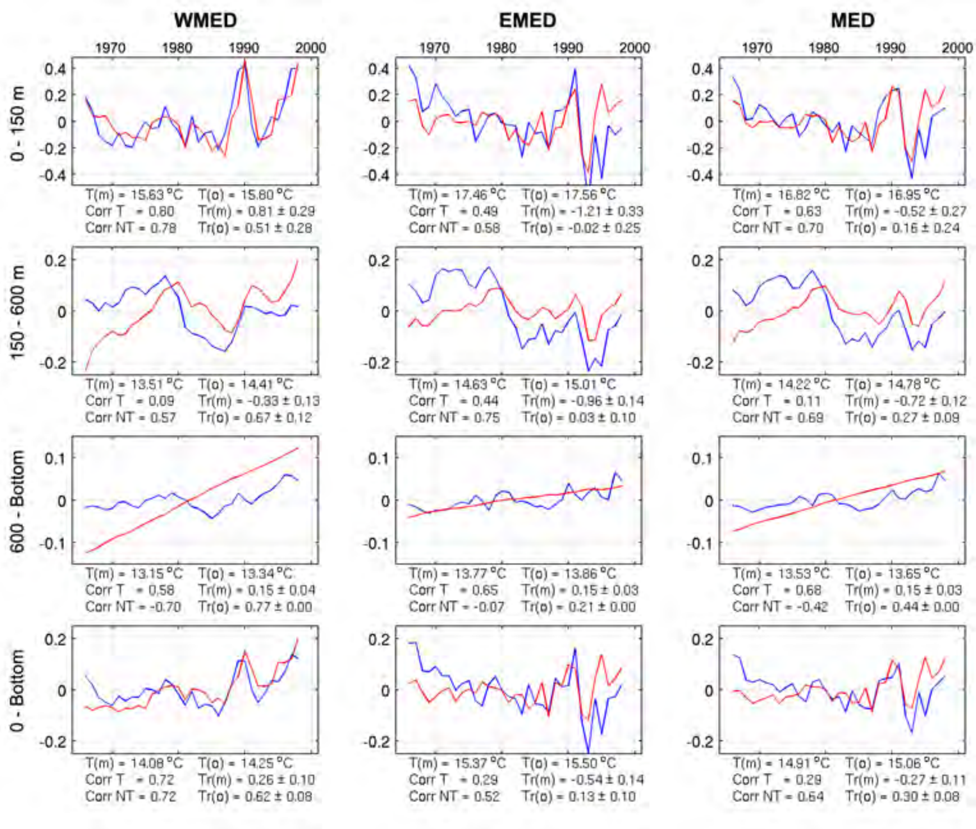

Figure 5.1: ORCA (red) and MEDAR (blue) temperature time-series divided into basins and layers (1965-1998). **T** refers to the mean temperature. **Corr T** refers to the correlation of the time-series with their respective trends. **Corr NT** refers to the de-trended correlation values. **Tr** refers to the trend value

Depth range	Basin	Tmean (medr) ºC	Tmean (orca) ºC	Correlation (with trend)	Correlation (no trend)	Trend (medar) ºC/100yr	Trend (orca) ºC/100yr
0-150 m	WMED	15.63	15.80	**0.80**	**0.78**	0.81±0.29	0.51±0.28
	EMED	17.46	17.56	**0.49**	**0.58**	-1.21±0.33	-0.02±0.25
	MED	16.82	16.95	**0.63**	**0.70**	-0.52±0.27	0.16±0.24
150-600 m	WMED	13.51	14.41	0.09	**0.57**	-0.33±0.13	0.67±0.12
	EMED	14.63	15.01	**0.44**	**0.75**	-0.96±0.14	0.03±0.10
	MED	14.22	14.78	0.11	**0.69**	-0.72±0.12	0.27±0.09
600-Bottom	WMED	13.15	13.34	**0.58**	-0.70	0.15±0.04	0.77±0.00
	EMED	13.77	13.86	**0.65**	-0.07	0.15±0.03	0.21±0.00
	MED	13.53	13.65	**0.68**	-0.42	0.15±0.03	0.44±0.00
0-max	WMED	14.08	14.25	**0.72**	**0.72**	0.26±0.10	0.62±0.08
	EMED	15.37	15.50	**0.29**	**0.52**	-0.54±0.14	0.13±0.10
	MED	14.91	15.06	**0.29**	**0.64**	-0.27±0.11	0.30±0.08

Figure 5.2: ORCA and MEDAR temperature statistics related to Figure 5.1. Correlation values that are significant to 99% are in bold.

studies may not be directly comparable due to the trends' strong dependence on area, depth range and period of study. Other results by Krahmann and Schott (1998) and Rixen et al. (2005) describe the period as having decadal variability but no discernible trend. Trends in intermediate layers still do not agree even between observations.

Removing the trend from the model's data reveals that the variability is actually well resolved in both basins (de-trended correlations of 0.57 in the WMED and 0.75 in the EMED). The MEDAR data show a considerable drop in temperature around the 1979-1983 period in both basins; this drop is well represented by the model in the WMED (de-trended) but not in the EMED, where the model shows a more modest drop.

Deep layers (600 m to bottom) show a large temperature trend difference in the WMED. Here, G70 shows no interannual variability and severely overestimates the trend at 0.77± 0.00^{o}C/100 yr, five times higher than the trend observed in MEDAR (0.15± 0.04^{o}C/100 yr). Other deep layer temperature studies such as Bethoux and Gentili (1996), Bethoux et al. (1998), Bethoux and Gentili (1999), Krahmann and Schott (1998) and Tsimplis and Baker (2000) have generally found lower temperature trends (between 0.16 and 0.36^{o}C/100 yr) than those obtained by G70. Relevant work by Rixen et al. (2005) is not compared here since the MEDAR data used in their study is essentially the same. A possible reason for exaggerated warming trends in the deep layers of the model could be related to the resolution of the atmospheric forcing. Most deep-water formation events in the Mediterranean occur during short, cold and strong events over relatively small areas). With an atmospheric forcing resolution of 125 km, these events are not allowed to properly develop. Therefore deep layers are not replenished with cold, dense waters and eventually heat up by diffusion. In fact, calculating the heat flux from the DFS3 atmospheric forcing reveals that the Mediterranean Sea is gaining heat at a rate of 3.88 W/m^2, whereas the established observational-based heat flux coming in through the Strait of Gibraltar is of -5 W/m^2 (so the same amount should be lost by the atmosphere to maintain a state of equilibrium).

5.3 Salinity

The salinity analysis shows that the correlations between G70 and MEDAR are indeed much lower (figure 5.3) than those of temperature. At all layers, the interannual variability has been almost obliterated by the sea surface salinity restoring term. Data for the WMED display very low or even negative correlations at all depth levels with large differences in the interannual variability of both datasets. The EMED shows statistically significant positive correlations at all depths (except the intermediate layer) however the interannual variability from the model is much lower than the MEDAR database. It is worth noting that the mean surface salinity for the entire Mediterranean basin is significantly lower in G70 than in MEDAR ($\sim$0.3 psu), this is replicated in intermediate and deep layers to a lesser degree. Therefore the salinity restoring term still applies insufficient evaporation to compensate for the weak ERA40 water loss flux (Hermann et al., 2008; Josey, 2003; and Mariotti et al., 2002). However one must also be cautious regarding the MEDAR dataset since its quality depends directly on the amount and distribution of real data (Figure 1), an there are less than half as many salinity profiles as temperature ones as well as a heavy northern bias.

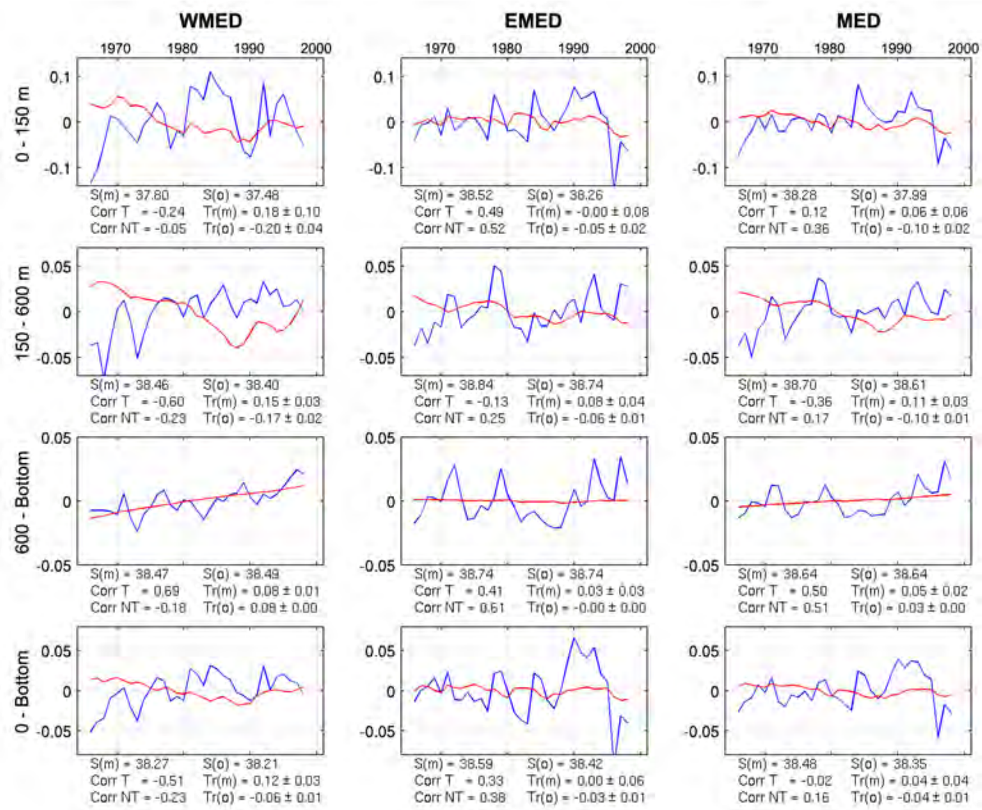

Figure 5.3: ORCA (red) and MEDAR (blue) salinity time-series divided into basins and layers (1965-1998). **S** refers to the mean salinity. **Corr T** refers to the correlation of the time-series with their respective trends. **Corr NT** refers to the de-trended correlation values. **Tr** refers to the trend value

Depth range	Basin	Smean (medr)	Smean (orca)	Correlation (with trend)	Correlation (no trend)	Trend (medar) psu/100yr	Trend (orca) psu/100yr
0-150 m	WMED	37.80	37.48	-0.24	-0.05	0.18±0.10	-0.17±0.02
	EMED	38.52	38.26	**0.49**	**0.52**	-0.00±0.08	-0.05±0.02
	MED	38.28	37.99	0.12	**0.36**	0.06±0.06	-0.10±0.02
150-600 m	WMED	38.46	38.40	-0.60	-0.23	0.15±0.03	-0.17±0.02
	EMED	38.84	38.74	-0.13	**0.25**	0.08±0.04	-0.06±0.01
	MED	38.70	38.61	-0.36	0.17	0.11±0.03	-0.10±0.01
600-Bottom	WMED	38.47	38.49	**0.69**	-0.18	0.08±0.01	0.08±0.00
	EMED	38.74	38.74	**0.41**	**0.61**	0.03±0.03	-0.00±0.00
	MED	38.64	38.64	**0.50**	**0.51**	0.05±0.02	0.03±0.00
0-max	WMED	38.27	38.21	-0.51	-0.23	0.12±0.03	-0.06±0.01
	EMED	38.59	38.42	**0.33**	**0.38**	0.00±0.06	-0.03±0.01
	MED	38.48	38.35	-0.02	0.16	0.04±0.04	-0.04±0.01

Figure 5.4: ORCA and MEDAR salinity statistics related to Figure 5.3. Correlation values that are significant to 99% are in bold.

5.4 Seasonal Steric Signal

As opposed to G70, the MEDAR data is only available in annual time steps for the second half of the 20th century. This does not allow for the representation of the seasonal cycle. There is however a monthly MEDAR climatology (monthly averages without interannual variability) for this period, which can be used to determine the differences and similarities of the steric signal for both G70 and MEDAR. The steric height (SH) is the component of sea level driven by the expansion/contraction due to changes in temperature and salinity. It is computed for each grid point of the model as the vertical integration from surface to the bottom of the specific volume anomaly (α) (respect to the specific volume at 35 psu and 0^{o}C caused by changes in potential temperature (T) and salinity (S):

$$Steric\,Sea\,Level = 1/g\int_{-H}^{0}\alpha\,dx \tag{5.1}$$

Figure 5.5 shows the computed steric height for the Mediterranean basin from the climatological data (from the surface to the full depth). Amplitudes coincide perfectly (~5 - 6 cm), and phases are very similar with only very minor differences. The most notable result is the absolute height difference between both datasets, with G70 being an average of 14.33 centimetres higher than MEDAR. This is because the mean salinity for the entire Mediterranean basin is significantly lower in G70 than in MEDAR, while temperature is slightly higher. A simple test of adding a bias of 0.13 psu to the salinity (which is the mean difference observed for the whole Mediterranean integrated from the surface to the sea floor in Figure 5.3) made the absolute steric height of MEDAR change by ~17 cm. Halosteric and thermosteric sensitivity analysis shows that about 85% of the steric signal is due to temperature (amplitude of ~8-10 cm) and 15% due to salinity (amplitude of ~2 cm) (not shown).

The term *Dynamic Height* is similar to steric height, but the integration is done from the surface to a chosen reference level (usually referred to as the level of zero-motion). The steric signal / dynamic height is very important, not only because of its effect on sea level, but because from it, one can compute an important component of the ocean; the geostrophic currents. These currents exist due to a balance of forces caused by the distribution of horizontal

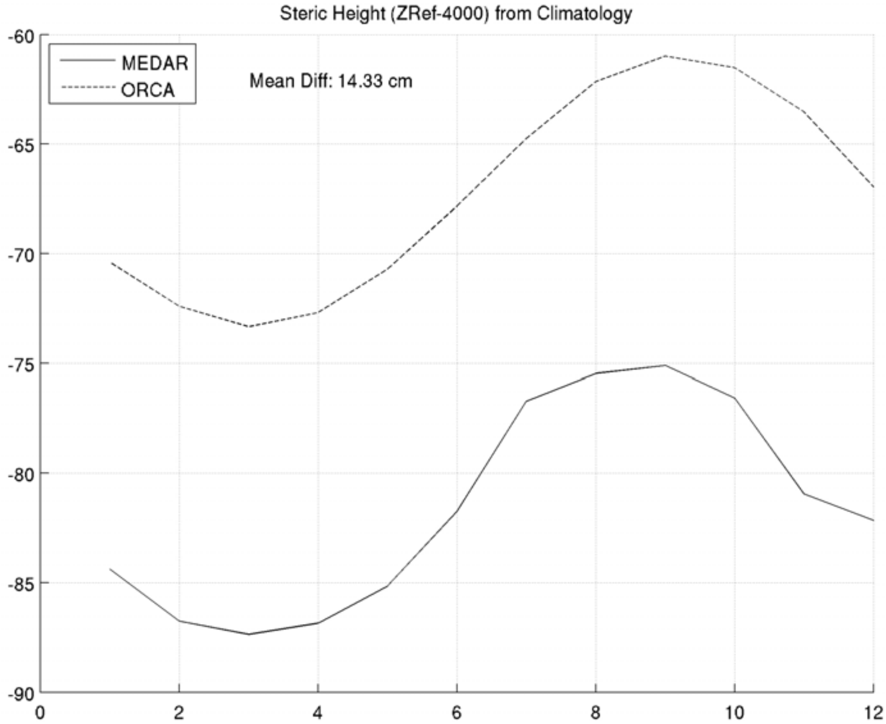

Figure 5.5: ORCA G70 (dashed-line) and MEDAR of steric height calculated from a reference (solid-line) climatology depth level of 4000 m.

density/pressure gradient fields (computed empirically from measurements of temperature and salinity) and the Coriolis force (for a more complete description, please see Pickard and Emery (1990)).

5.5 Sea Level: Comparison with Altimetry

In addition to temperature and salinity, the Sea Surface Height performance of the model was also analysed and compared to Altimetry data. Since the altimetry dataset is only available since 1993, only the period from 1993-2004 was analysed in this section. This analysis was also performed on the computed steric height of the model. Other studies by Tsimplis et al. (2008) have compared numerical models such as ORCA G70 and OPAMED8 (Somot, 2005) to tide gauges for a longer time period, 1960-2000.

5.5.1 Mean Sea Level

We look at the time evolution of the sea surface height variables over the Mediterranean and its two main basins, the EMED and WMED basins. Figure 5.6 shows the Mediterraneans basins mean anomaly time-series for the models SSH, SH and altimetry for the 1993-2004 period, where the main component of this signal is clearly due to the seasonal cycle.

From these results, it is clear that the model is perfectly capable of accurately reproducing the phase and amplitude of the seasonal cycle with very good comparison between the models SSH and the Altimetry (which in theory are observing the same processes), with correlations of $\sim$0.8 (0.89 with the signals de-trended). A clear example of this is the sea level signal linked with the 1996 negative NAO (North Atlantic Oscillation, Woolfe et al. (2003)), which according to Tsimplis et al. (2008) is the strongest signal of the last four decades (particularly in the WMED). When computing the models steric height, the specific volume anomaly was integrated from the surface to the full depth of the model.

Figure 5.6 shows that the steric component accounts for about half of the total sea level signal. The computed steric height of the model shows an annual cycle amplitude of $\sim$5 cm, and the full SSH signal as diagnosed by the model of $\sim$10 cm. These values coincide with the altimetry data and are confirmed by Bouzinac et al. (2003) and Larnicol et al. (1995).

A notable limitation of the model is its ability to reproduce long-term SSH trends. With an average trend of 14.95$\pm$1.52 mm/year for the whole Mediterranean, the model overestimates 4-5 times the trend observed by altimetry (3.6$\pm$1.54 mm/year). The trend is higher in the EMED than in the WMED,

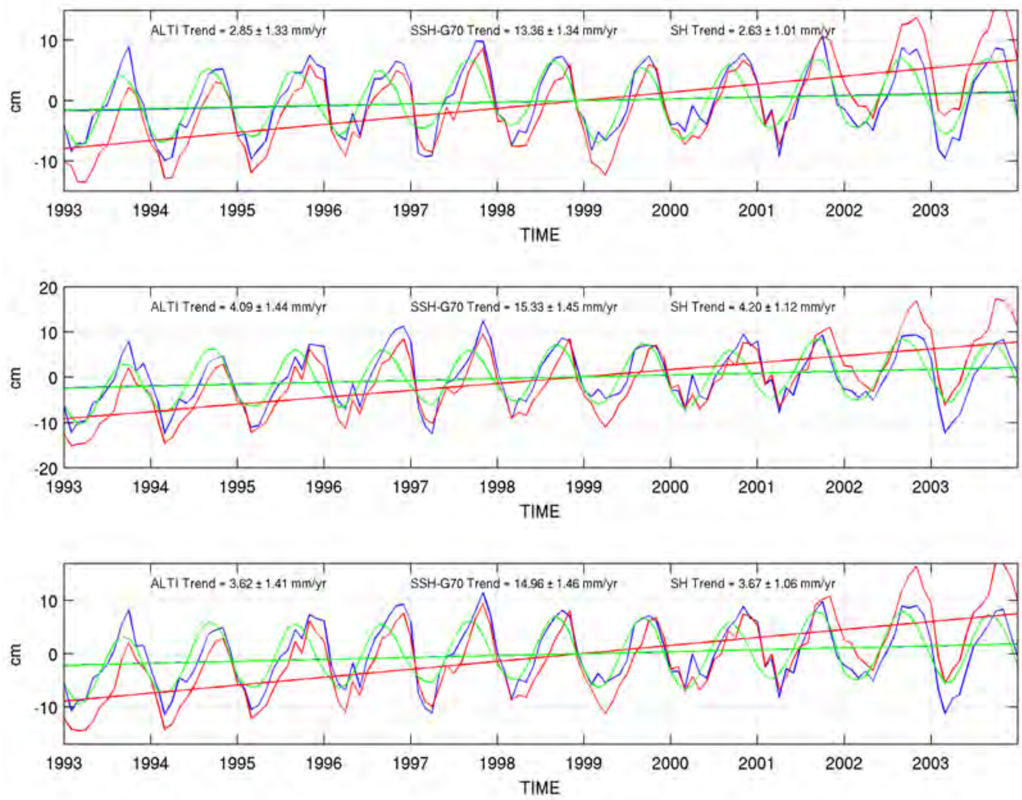

Figure 5.6: Timeseries of G70 sea surface height (SSH, red), steric height (SH, green) and altimetry (ALTI, blue) for the WMED (top), EMED (middle) and whole Mediterranean (bottom)

but this coincides with Altimetry. A surprising result is that the steric height computed from the models temperature and salinity data does not display the same exaggerated trend, moreover, the trend is almost identical to the altimetry trend (3.66±1.16 mm/year). However, the fact that the steric heights trend coincides with altimetry should be interpreted with caution due to the discrepancies observed in the temperature trends between ORCA and MEDAR (especially at intermediate and deep layers, Figure 5.1).

The spatial distribution of trends (not shown) for SSH and altimetry confirms that the models trend overestimation is a global feature of the model (in the Mediterranean 8 - 18 mm/year, average 14.95 mm/year), whereas altimetry displays areas of both positive and negative trends (-16 to +10 mm/year, average 3.6 mm/year).

These trends calculated using basin averages are useful to provide a general idea of the basins behaviour but may not be truly representative of many areas within the basins themselves. These must therefore be analysed with caution. Tsimplis and Rixen (2002) found that given the strong spatial variability of the trends, a basin average could not be used to realistically assess its behaviour (as a consequence, further studies will include smaller, sub-basin scales). As an example, altimetry in the EMED shows a strong sea level drop in the northern Ionian basin (∼10 mm/yr) and the opposite in the Levantine basin (∼14-18 mm/yr). Up to now, no numerical study has been able to reproduce this sea level drop in the northern Ionian basin, instead showing an intense sea level rise over the EMED with similar values to the altimetry trend in the Levantine basin (Tsimplis et al., 2008).

In order to study the interannual variability of the signals, the seasonal cycle and trend are removed. Examining figure 5.7 shows that most of the peaks in the model coincide with those in the altimetry data despite some differences in the intensities. Altimetry generally appears to show a more intense interannual variability than SSH however standard deviation calculations revealed that the model and altimetry show similar values over the period studied. Interestingly, the model shows a lower frequency $\sim$ 4 year signal, with a positive trend from 1993 to 1996, negative from 1996 to 2000, and positive again from 2000 to 2004.

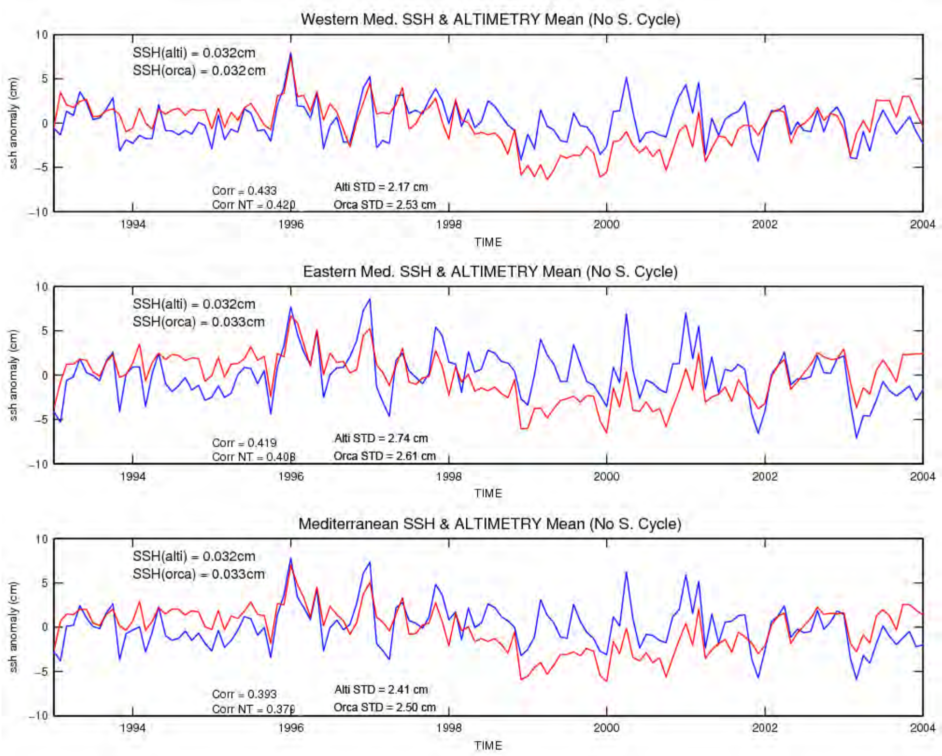

Figure 5.7: Timeseries (with the seasonal cycle and trends removed) of ORCA sea surface height (red) and altimetry (blue) for the WMED, EMED and whole Mediterranean. STD refers to the standard deviation values for each time-series. Corr and Corr NT refer to correlation and de-trended correlation respectively.

5.5.2 Trend

As observed in section 5.5.1, the model displays a significant positive trend which is much higher than observed values. In Figure 5.8 we look at the spatial distribution of the trends for SSH and altimetry. While altimetry shows areas of both positive and negative trends with values from -16 to +10 mm/year (average 3.6 mm/year), the model shows a completely positive trend scenarios with values ranging from 8 - 18 mm/year (average 14.95 mm/year).

An interesting signal in the Altimetry trend is a negative patch in the Ionian basin. This is most likely due to the circulation changes occurred during the EMT (East Mediterranean Transient), where the areas of deep water formation shifted from the Adriatic Sea to the Aegean (Roether et al., 1996). This signal has not been reproduced by the model. Then again, it is not expected for a global model, especially since this signal has been very difficult to reproduce in dedicated studies.

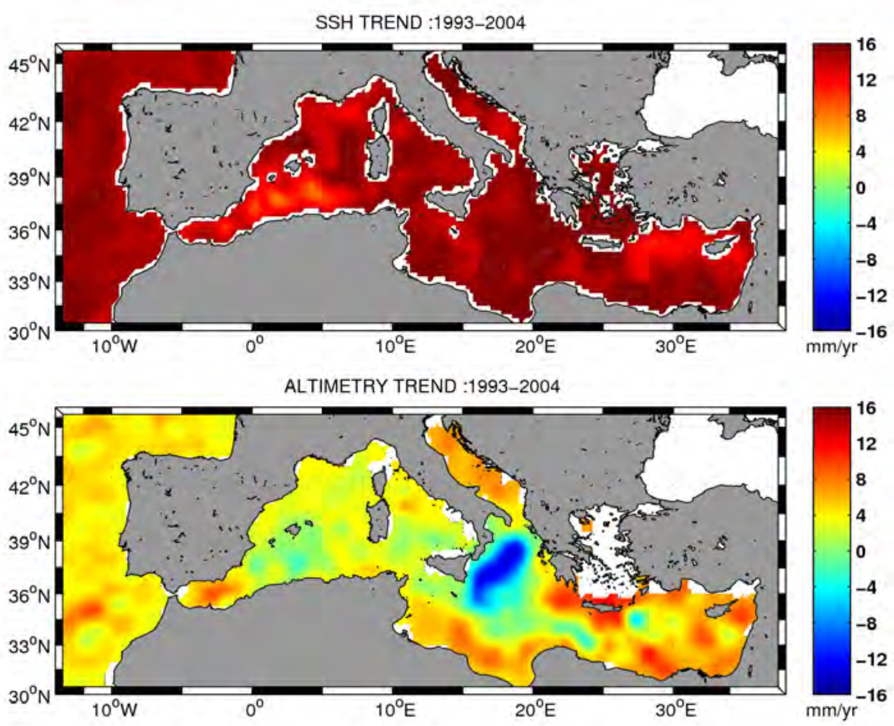

Figure 5.8: G70 SSH and Altimetry Trend maps for the 1993-2004 period

5.5.3 Variance

Figure 5.9 shows the maps of variance for the 1993-2004 period of the model's SSH, the steric height and satellite altimetry. Comparing the model's SSH and computed steric height (SH) shows a large difference between them, with SH's variability having a much lower overall intensity than the SSH.

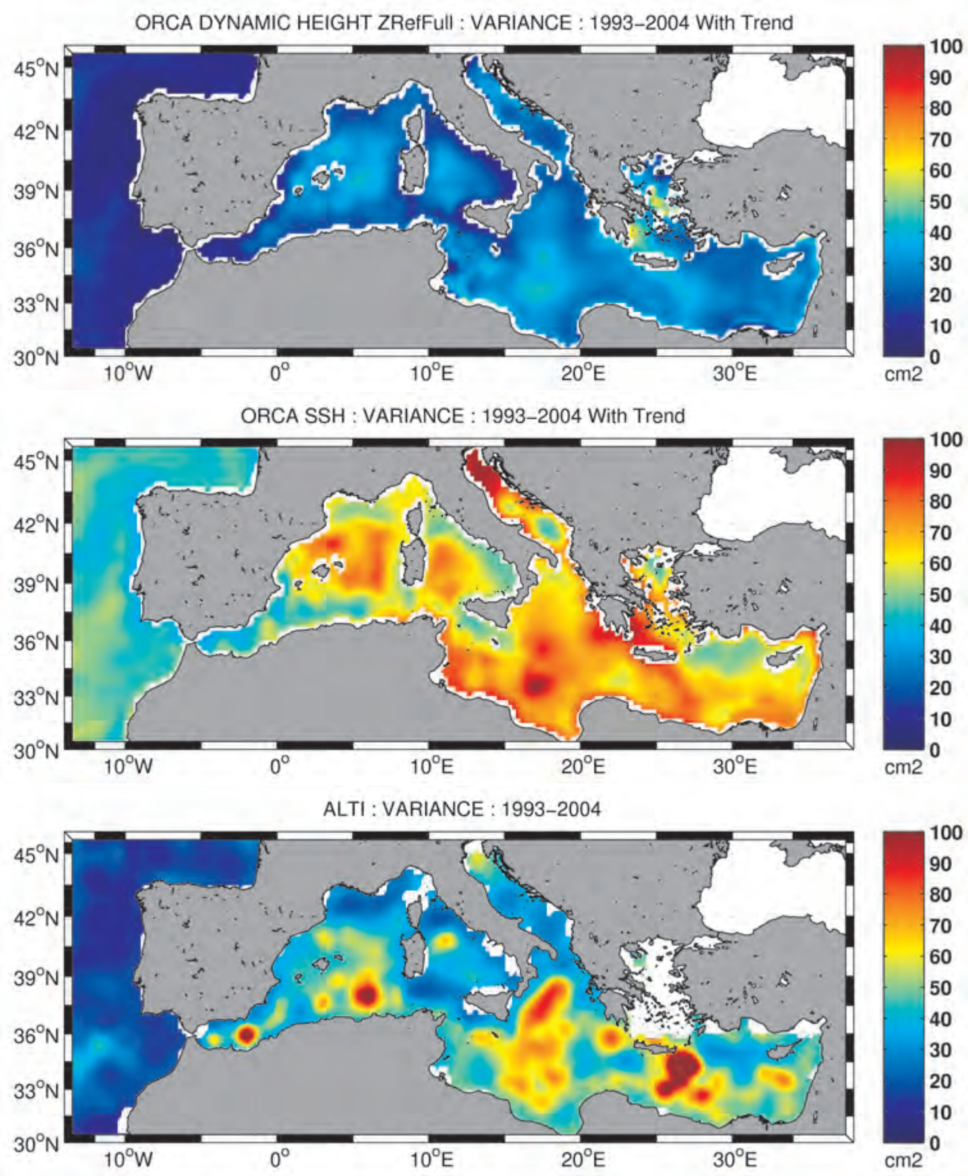

Figure 5.9: G70 Steric Height(top), G70 Sea Surface Height (middle), and Altimetry (bottom) variance maps for the 1993-2004 period.

The steric effect is an important part of the sea level seasonal cycle, accounting for roughly half of the total sea level signal. This means that the overall variance of the steric height should behave similarly with respect to the variance from the SSH. However, figure 5.9 shows that the SSH variance is significantly more than double the steric height variance. For example, east of the Balearic Islands, the SSH variance is ∼70-80 cm^2 whereas the steric height variance is ∼25-30 cm^2. As identified in sections 5.5.1 and 5.5.2, the SSH signal displays an exaggerated positive trend in SSH. Removing this trend from the variance (figure 5.10) for both steric height and SSH shows little change in the steric height but a significant reduction in the SSH variance, bringing the ratios much closer to the expected values (e.g. east of the Balearic Islands, SSH = ∼50-60 cm^2 while SH variance remains similar ∼25-30 cm^2). By comparing the de-trended SSH map with altimetry it is clear that the model is not capable of resolving the intense mesoscale features which are detected by the altimetry, however, ignoring this fact (that was expected given the models spatial resolution), the average variance values of both SSH and altimetry are quite similar.

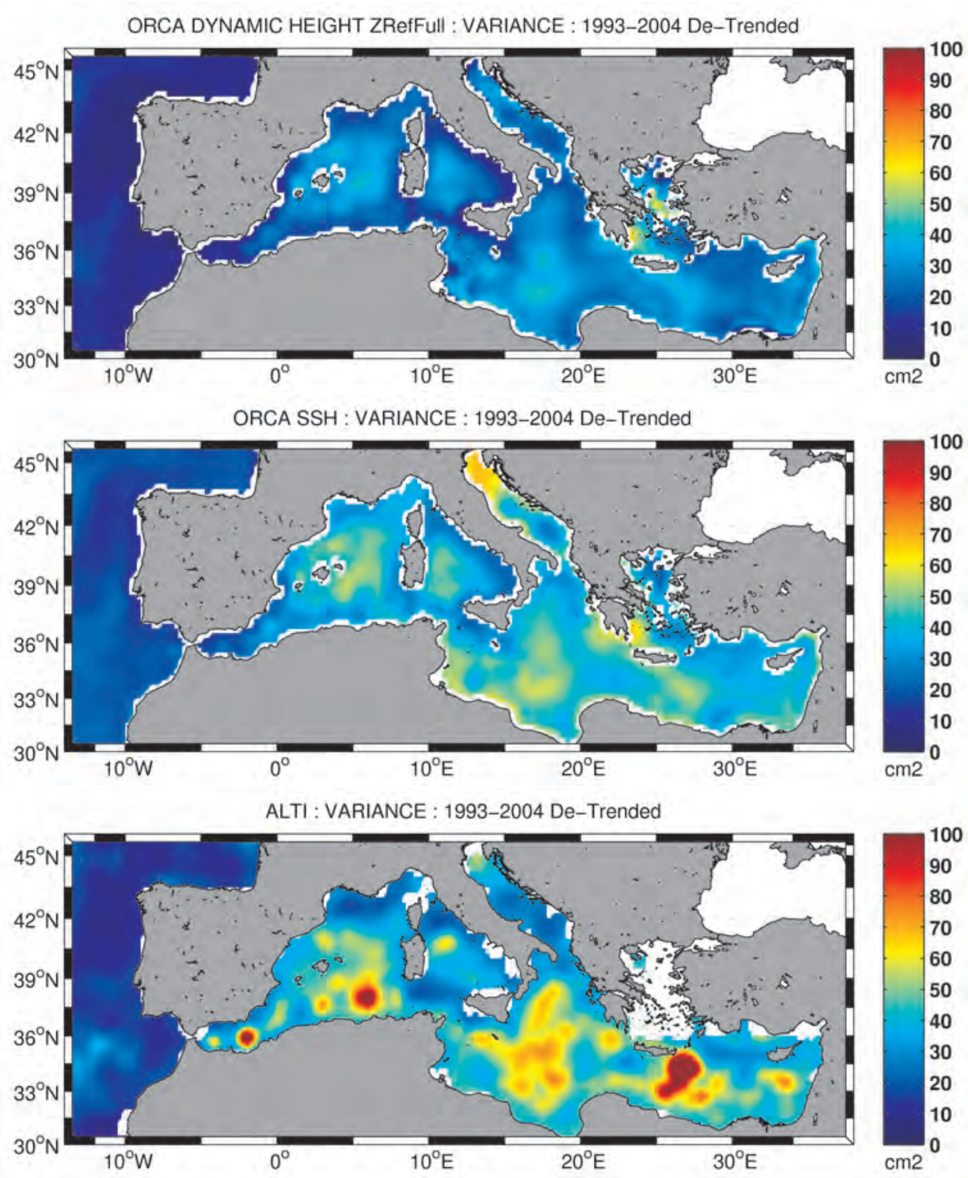

Figure 5.10: G70 Steric Height(top) and G70 Sea Surface Height (middle) and altimetry (bottom) de-trended variance maps for the 1993-2004 period

5.5.4 Annual Amplitude

As seen in figure 5.6, the amplitude of the seasonal cycle is very well reproduced. Both datasets display an amplitude of around 10 cm. Looking at the spatial distribution of the amplitude (figure 5.11) shows that both ORCA and Altimetry show similar distribution of high and low amplitude features. Altimetry exhibits more intense structure but this is most likely due to its higher resolution. From the spatial distribution maps, it can be confirmed that the model does not have sufficient resolution to accurately reproduce the mesoscale activity in the Alboran Sea and the Algerian Current.

One can argue whether the seasonal cycle of sea level has an impact on the geostrophic currents. However since the heating and cooling is relatively uniform, the small spatial variations of the amplitude of the seasonal cycle cause small gradients (around 3 cm in 100 km). Using the equation for geostrophic current velocities to make a quick approximation:

$$V \propto \frac{g}{f}\frac{\partial \eta}{\partial x} \tag{5.2}$$

Where f is the Coriolis parameter and $\partial \eta$ is the sea level difference.

$$V \propto \frac{10ms^{-1}}{10^{-4}s^{-1}}\frac{3 \times 10^{-2}m}{100 \times 10^{3}m} \tag{5.3}$$

$$V \propto \frac{3}{100}ms^{-1} = 3cms^{-1} \tag{5.4}$$

From the above approximation, we see that the spatial variations in the amplitude of the seasonal cycle cause a very small effect on the geostrophic current velocities (~3 cm/s).

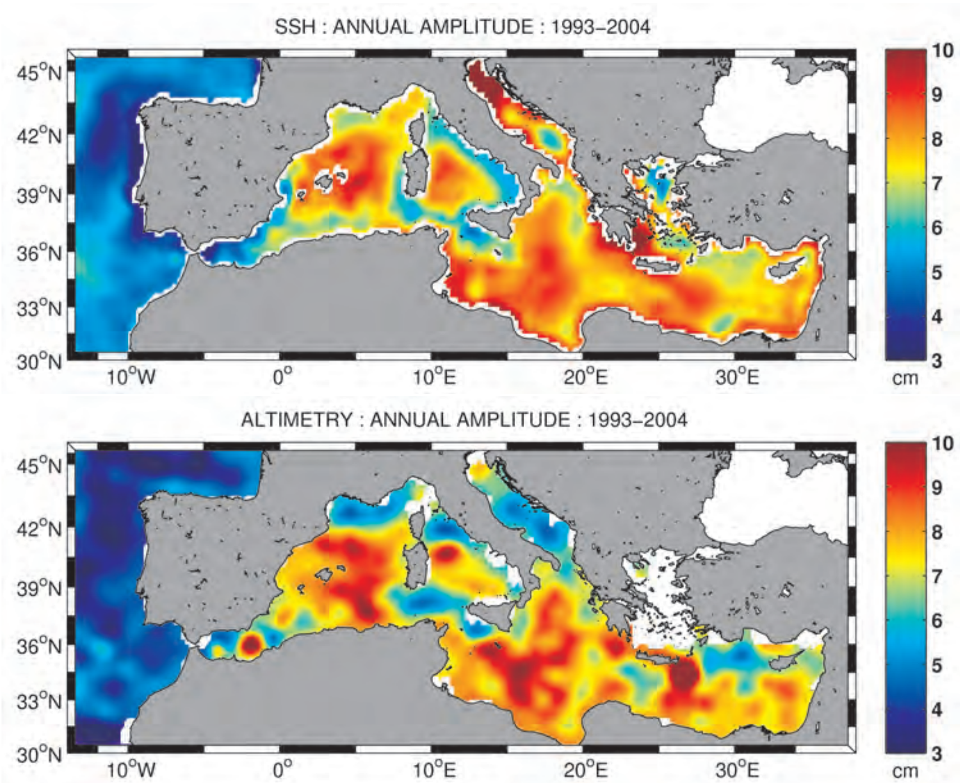

Figure 5.11: G70 SSH and Altimetry Annual Amplitude maps for 1993-2004

5.6 Surface Currents

A snapshot for June 2000 of surface currents is provided to visualize the circulation for the Western Mediterranean basin. Current velocities are overlaid on the Sea Surface Height for the same time step. Figure 5.12 (top) clearly shows how the model reproduces the main features of the WMED (Western Alboran Gyre, Algerian Current and its associated eddies, Northern and Balearic currents) in agreement with figure 1.6. In the EMED figure 5.12 (bottom), the Atlantic Ionian Stream is visible in agreement with figure 1.7 (top). It is also visible how the currents follow the main SSH features, this demonstrates that the circulation in the Mediterranean Sea is mainly geostrophic in nature.

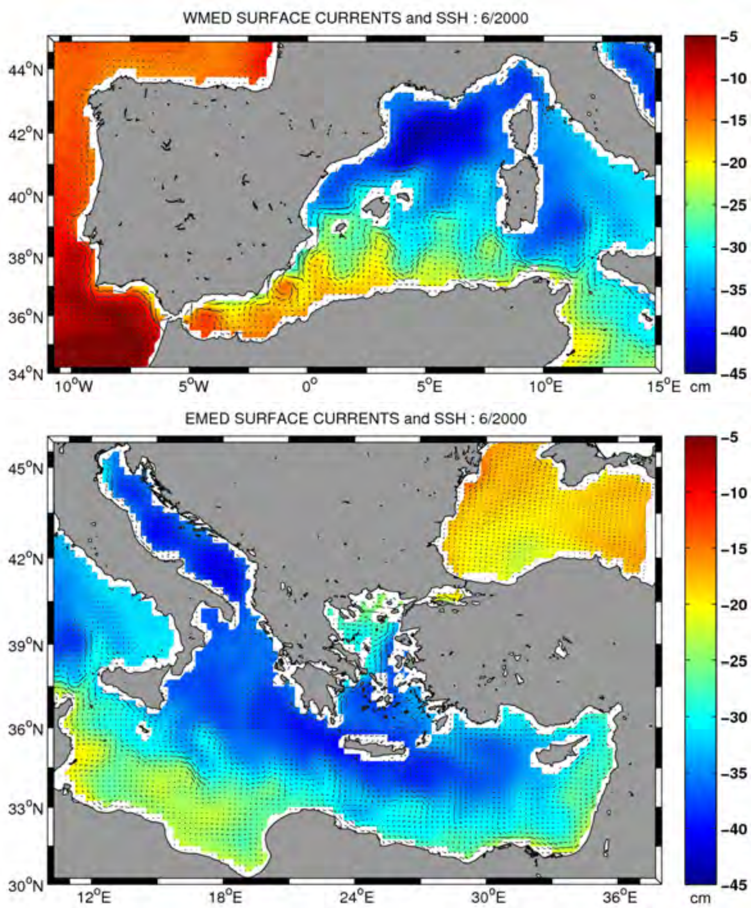

Figure 5.12: G70 SSH and Surface Current snapshot map for June 2000

5.7 Transports

5.7.1 Strait of Gibraltar

Many studies have focused on the Strait of Gibraltar as it is the only point of contact between the Mediterranean and the open ocean, and is through where the water balance in the Mediterranean is maintained. The correct representation of this transport is crucial for a model to work properly within the Mediterranean. Figure 5.13 shows transport through the Strait of Gibraltar calculated from the G70 horizontal velocity fields. The transport values obtained by G70 are 1.076±0.078 Sv of inflow and 1.008±0.089 Sv of outflow, with a net inflow of 0.067±0.064 Sv (for the period 1993-2004). Flow variability displayed by the model is quite low compared to the observational studies since the model data used is comprised of monthly averages and the observations contain higher frequency variability.

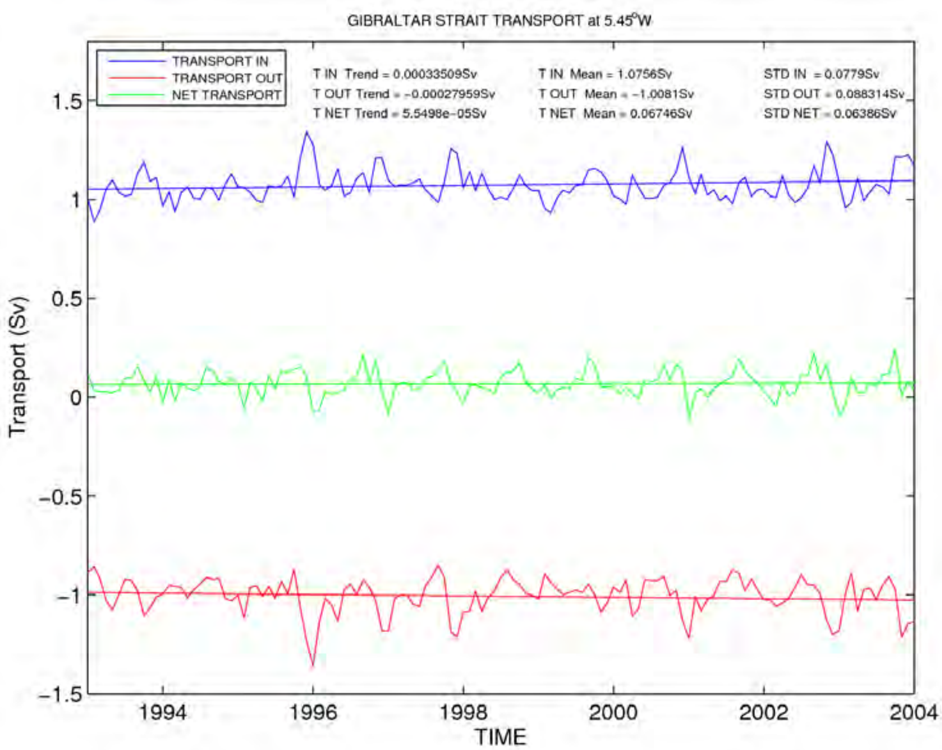

Figure 5.13: Transport through the Strait of Gibraltar

Astraldi et al. (1999) provides a summary table of different transport estimates by a variety of authors up to 1999. In many cases the estimated transports are derived from heat, salt and water budgets for the Mediterranean Sea. The large uncertainty regarding this transport is mainly due to the lack of long-term direct measurements, the complexity of the horizontal and vertical profile of the strait, and the presence of strong tidal currents (Tsimplis and Bryden (2000), Gomis et al. (2006)).

To date, no observational studies have been carried out for long enough to calculate a long-term mean. Most estimates are based on short (less than one year) mooring deployments and short cruises, and most studies assume a certain vertical and horizontal uniformity of the inflow/outflow. The longest study is by Candela (2001), 2 years from October 1994 to October 1996 of continuous current profile measurements at a mid-sill location on Gibraltar's main sill, as well as two hydrographic cruises. The results from this study give a mean inflow of 1.01 Sv, outflow of 0.97 Sv and a mean inflow of 0.04 Sv. Other studies include Tsimplis and Bryden (2000) who estimated a mean inflow of 0.789 Sv, outflow of 0.634 Sv and a net inflow of 0.156$\pm$0.696 Sv from the 23rd of January to the 23rd of April 1997. Also García-Lafuente et al. (2002) estimated a mean inflow of 0.724 Sv, outflow of 0.741 Sv and a net outflow of 0.018$\pm$0.502 Sv from the 16th of October 1997 to the 27th of March 1998. Transport values obtained by G70 are close to those estimated by Candela (2001), but show a more intense inflow/outflow than Tsimplis and Bryden (2000) and García-Lafuente et al. (2002), however given the general uncertainty, these values do enter well within the generally accepted transport values for the Strait of Gibraltar.

5.7.2 Black Sea

The water volume contribution from the Black Sea is also important to complete the freshwater budget of the Mediterranean. The calculated transport values for the model (Figure 5.14) are of 0.019$\pm$0.021 Sv into the Mediterranean Sea. As opposed to the Strait of Gibraltar, very few studies have looked at the water transport from the Black Sea into the Mediterranean Sea. Mass balance estimates by Unluata et al. (1990) and Özsoy and Unluata (1998) yielded a net vertically averaged transport of 0.0095 Sv, and Peneva et al. (2001) used Sea Level Anomaly from Topex/Poseidon to calculate a net transport of 0.016$\pm$0.0057 Sv. These values are within the same order of magnitude as those obtained from ORCA given the margin of error. This is a remarkable result for a 1/4^o global model, especially given the complexity of the Turkish Straits system. Nevertheless, the error associated with this transport is likely an important source of error for the freshwater balance calculation (section 5.8).

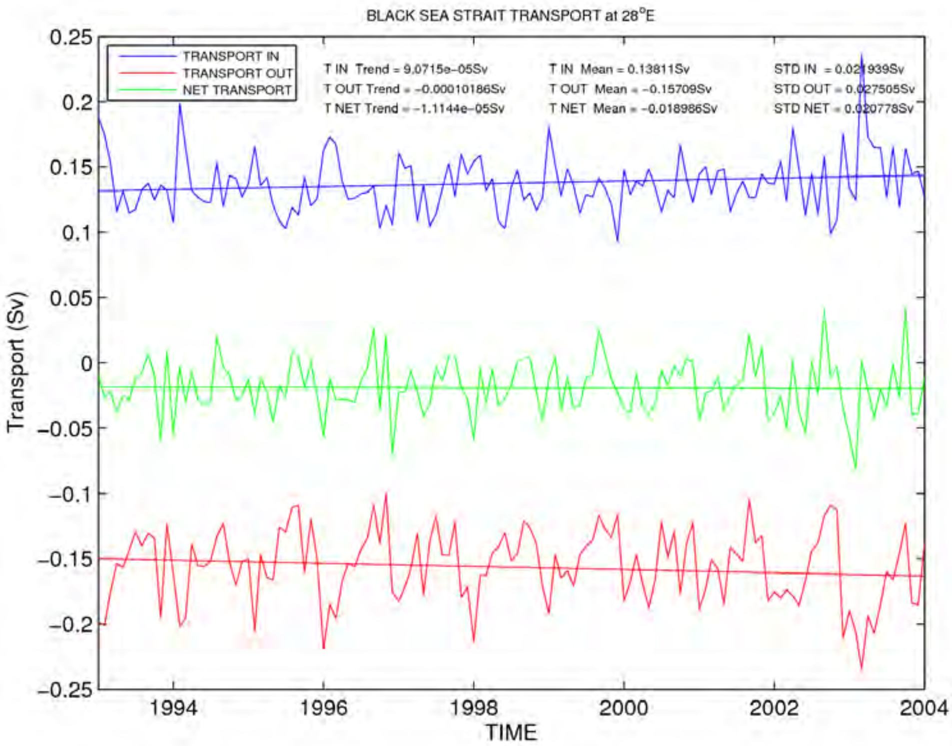

Figure 5.14: Transport from the Black Sea into Mediterranean

5.8 Freshwater Balance of the Mediterranean

As seen in section 5.5.1, the SSH calculated by the model shows a significant positive trend. In an attempt to identify the possible source of this trend, a water budget calculation was made for the Mediterranean Sea. The water budget is the balance between the water coming into the Mediterranean through its main straits; the Strait of Gibraltar and the Turkish Straits (connecting the Mediterranean Sea to the Black Sea), and the net downward/upward water flux (precipitation minus the evaporation plus the river run-off; P - E + R).

The transports were calculated in section 5.7, with mean transport values into the Mediterranean Sea for the Strait of Gibraltar and the Turkish Straits of 0.0674 Sv and 0.0189 Sv respectively. The net sea level change due to horizontal water transports was obtained by dividing the total volume of water entering into the Mediterranean Sea by its area (giving a net trend of water inflow of 1.083 x 103±51.7 mm/yr). From this term, the Net Downward Water Flux (NDWF, which includes the salinity restoring term) was subtracted (1.0291 x 103±32.5 mm/yr), giving a total net positive sea level change trend for the Mediterranean Sea of 54 mm/yr with an associated error of 44 mm/yr (calculated by a bootstrap method). These trend values, when taking into account the associated error, fall within the trends observed for the models SSH in section 5.5.1 (around 15 mm/yr). The salinity restoring term applied to the model increases evaporation in the NDWF an equivalent to 8.06±4.1 mm/yr, however this is insufficient to compensate for the low evaporation rate of the atmospheric forcing, resulting in an imbalance between the horizontal and vertical water fluxes.

Given that the water transport into the Mediterranean Sea is within the range of values obtained in the literature (although transport through the Turkish Straits can show significant error and make a contribution to the sea level trend), the positive trend observed in the models SSH is likely related to an imbalance of the water and heat fluxes of the model.

5.9 Summary

This chapter has focused on studying the interannual and seasonal variability in the Mediterranean Sea by performing a model assessment of the ORCA-R025 G70 Simulation, and comparing it with Altimetry and the MEDAR (temperature and salinity) observational database.

When comparing the ORCA outputs with the MEDAR database we have found that the mean surface temperature values and the surface layer (0-150 m) over the 1962-2001 period were quite accurately represented with regard to temperature (de-trended correlations of 0.7) However, the sea surface salinity restoring term applied to the model eliminates most of the interannual variability (de-trended correlations of 0.36).

Mean temperatures for this layer are slightly higher in the model (0.08 - 0.16^{o}C), very likely related to the atmospheric forcings (ERA40) known underestimation of the total heat loss ($\sim$3.88 W/m^2 for ORCA in the Mediterranean as opposed to the well established observation based value of $\sim$5 W/m^2 inferred from heat transport at Gibraltar, meaning that the Mediterranean is gaining heat. However, this result is actually within the range of other observational and modelling studies. Ruiz et al. (2008) puts together a table of the different heat flux studies and the values range between -11 W/m^2 and 29 W/m^2).

Intermediate (150-600 m) and deep (600 m- bottom) layers show a clear positive trend that was not seen in MEDAR. This is possibly due to the atmospheric forcings resolution which prevents the formation of deep water resulting in cold, dense waters not reaching the deep ocean which eventually heated up through diffusion. Our results have shown that the mean surface salinity for the entire Mediterranean basin is significantly lower in G70 than in MEDAR ($\sim$0.3 psu), which is replicated in intermediate and deep layers to a lesser degree and could be a consequence of a weak sea surface salinity restoring, without sufficient evaporation to compensate for a weak ERA40 water loss flux.

The evaluation of G70 with regard to sea level (both in terms of absolute sea surface height (SSH) and its steric component) has revealed that the model reproduces the large scale interannual variability reasonably well, as well as the seasonal cycle when compared to the altimetric data. However the model presents an unrealistic SSH positive trend ($\sim$15 mm/year). Given that the water transport into the Mediterranean is within the range of values obtained in the literature (although transport through the Turkish Straits can show significant error and make a contribution to the sea level trend), the positive trend observed in the models SSH is likely related to an imbalance of the water budget of the model (E-P-R).

As expected with this models 1/4^o resolution, which is eddy-permitting but not eddy-resolving, the model is incapable of correctly reproducing most mesoscale features. This is especially notable in the Alboran Sea and Algerian Current where the model is unable to reproduce the gyres and eddies that are formed in these regions. Besides the mesoscale and sea level trends, this global ocean model behaves well in the Mediterranean Sea, taking into account its relatively low resolution for the dynamic features of this semi-enclosed sea. With a few key issues (such as surface salinity restoring and atmospheric forcing) that, once identified, can be improved, the G70 ocean model can provide a very promising tool for the study of the Mediterranean seasonal cycle and inter-annual variability characteristics.

Chapter 6 will expand on the knowledge acquired during the model assessment and incorporate analysis of new model runs (from the ORCA series). These new and improved simulations cover a longer time period (up to 2007), have improved the atmospheric forcing (requiring a weaker salinity restoring) and increased the number of vertical levels.

Chapter 6

Western Mediterranean Analysis using three $1/4^o$ simulations

This Chapter is based on the article (in press) :

Vidal-Vijande, E., A. Pascual, B. Barnier, J.-M. Molines, N. Ferry, and J. Tintoré, 2012: Multiparametric Analysis and Validation in the Western Mediterranean of three global OGCM Hindcasts. *Scientia Marina*, **EOF-2011 Special Edition**.

6.1 Introduction

In this Chapter expand on Chapter 5 which is based on the article by Vidal-Vijande et al. (2011) and perform the validation in the Western Mediterranean Sea of a series of $1/4^o$ global ocean simulations based on the NEMO code (Madec, 2008): two climatic scale hindcasts (ORCA025 G70 and ORCA025 L75.G85) and one shorter simulation with data assimilation (GLORYS1V1). The inclusion of GLORYS1V1 reanalysis in this study aims at verifying that reanalysis products that include data assimilation help to improve the description and our understanding of ocean variability. It will highlight which degree of improvement can be expected from an ocean reanalysis in that region with respect to a free run. This study will focus primarily in the Western Mediterranean, which is a region of significant interest for our research centre (IMEDEA). After carrying out a general assessment of temperature and salinity, particular attention will be paid to the models capability to reproduce the deep water formation in the Gulf of Lions and its transport through the Balearic Sea. The basin average sea level trends will be compared against satellite altimetry and the mean circulation evaluated with two different mean dynamic topographies. The transport in Gibraltar will be also analysed as well as the exchanges at the Balearic Channels, (Mallorca and Ibiza) where most of the WMED North-South exchanges of heat and water takes place (Pinot et al., 2002).

6.2 Temperature

In order to assess the performance of the models with regards to temperature and salinity, the WMED was divided into vertical layers (figures 6.1 and 6.2) following a similar pattern to Chapter 5 which was based on the system used by Rixen et al. (2005). The numerical models have been compared to the EN3 hydrographic database. For these comparisons, both the simulation data for G70 and G85 and the EN3 hydrographic data have been filtered using a 1-year running average in order to remove the intra annual variability and focus on the longer 44-47 year period variability. For GLORYS, since the simulation is much shorter (2002-2009) the data have not been annually filtered.

Figure 6.1 shows the temperature timeseries averaged over the WMED at different depth layers. Figure 6.1(a) is the initial comparison of the three observational datasets (MEDAR, ISHII and EN3). All three datasets behave similarly except for ISHII at deep layers (since it only reaches 700 m) and for salinity in intermediate and deep layers where the variability is much higher than the other two. Of all three datasets, EN3 was deemed the most appropriate due to its compromise between temporal resolution (monthly), depth range (0-5000 m) and period (1950 to present).

Figure 6.1(b) shows the comparison between EN3, G70 and G85. Both G70 and G85 have near identical variability at the surface layers, and are in good agreement with EN3. G85 correlates especially well with EN3 (de-trended correlation of 0.87). The major difference found between the three datasets at surface layers is a bias in mean temperature. Taking EN3 as the reference, G85 is 0.44^{o}C cooler and G70 is 0.55^{o}C warmer.

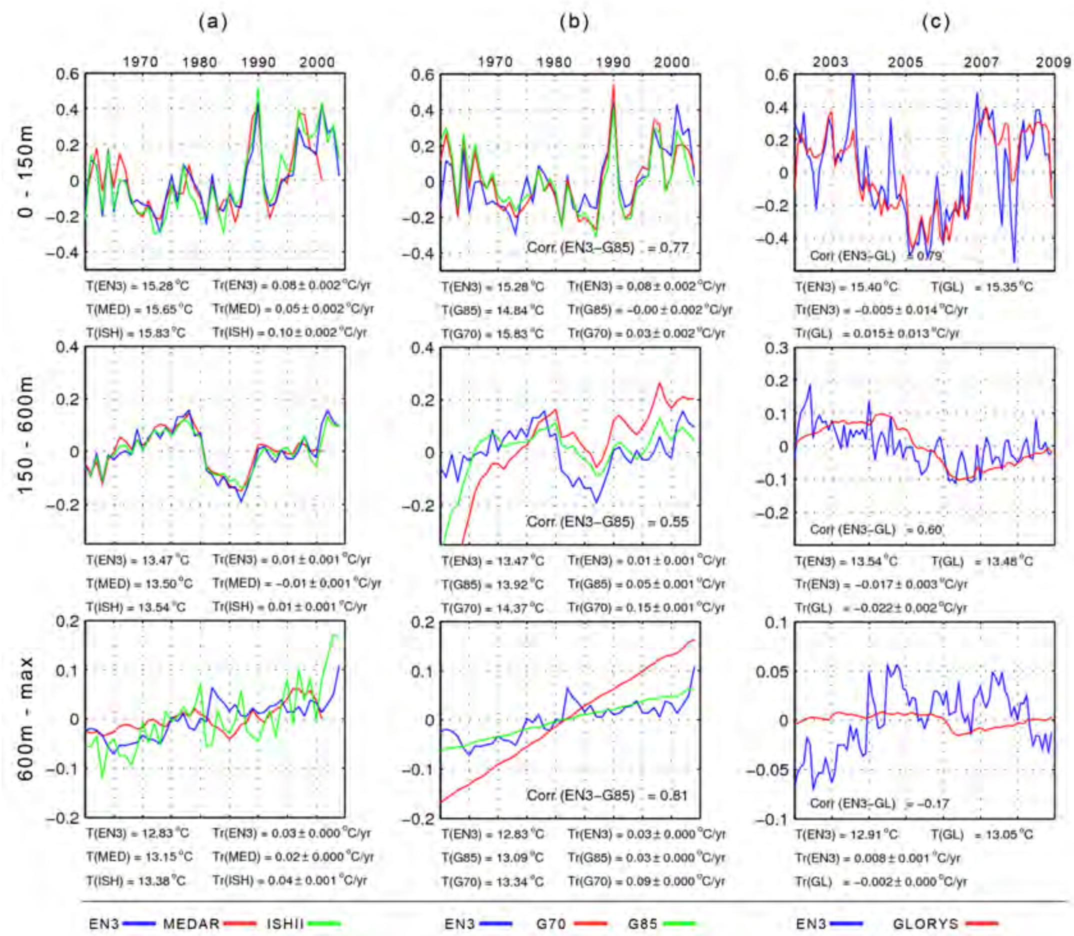

Figure 6.1: WMED mean temperature anomaly of the interannual variability at different layers. (a) is the comparison between EN3 (blue), MEDAR (red) and ISHII (green) from 1960 to 2004. (b) is the comparison between EN3 (blue), G70 (red) and G85 (green) from 1960 to 2004. (c) is the comparison between EN3 (blue) and GLORYS (red) from 2002-2009. Mean temperatures (T) and trends (Tr) with their error are given below each image for the different data streams

At intermediate layers (150-600 m), G70 presents an exaggerated positive trend that is reduced in G85 when compared to EN3 (G70 = 0.15^{o}C/yr, G85 = 0.05^{o}C/yr and EN3 = 0.01^{o}C/yr) and mean temperature values (G85 = 13.92^{o}C, EN3 = 13.47^{o}C). Deep layers also show significant improvement, with G85 and EN3 showing similar trends and closer mean values (although interannual variability is non existent in both simulations).

The improvement in temperature trends in G85 can be attributed to two factors; the better time continuity of the DFS4 forcing which has an impact on long term trends, and the increased vertical resolution which has a strong effect on the vertical mixing coefficient of the turbulent closure scheme.

The differences in mean temperatures are also result of the atmospheric forcing parameters; DFS3 (G70) is globally imbalanced for heat resulting in a warming ocean, hence higher mean temperatures. On the other hand, DFS4 (G85) maintains a near-zero global heat balance. DFS4 also has stronger wind speeds causing a global cooling of surface waters, which together with the better vertical mixing coefficients due to increased vertical resolution helps propagate the effects of the atmospheric forcing throughout the water column and maintain a better correspondence with the observations. However, as will be discussed in the following section, the inability of the model to reproduce normal winter convection causes temperatures at intermediate and deep layers to warm up, showing a positive temperature bias.

As is to be expected from a model with data assimilation, GLORYS performs well when compared with the EN3 observational data (Figure 6.1(c)). At surface layers, GLORYS has slightly weaker peaks in its interannual variability but the overall pattern of variability is very similar with high correlations of 0.77 over the WMED. Intermediate layers also show relatively good performance with slightly lower correlations of 0.66, although the model shows very low interannual variability, similar to the behaviour of the ORCA models. This might probably be due to a reduced number of sub-surface observations included in the data assimilation. At deep layers, the basin mean temperature does not show the spike in 2004 caused by the production of anomalously warm and salty deep water during the winters of 2004-2005 and 2005-2006 (Schroeder et al. (2008a), Schroeder et al. (2010)), however, as seen in Figure 6.6 the simulation does indeed create a strong convection event in the 2005-2006 winter. The behaviour of the models with respect to observations at different frequency bands has also been analysed using spectral analysis (not shown). WMED spatially averaged power spectra were computed showing that for the simulations a predominant peak is registered in surface temperature at 10-12 months corresponding to the annual cycle, and the same occurring for EN3. A weaker semiannual peak at 6 months also appears in the simulations which is not clearly found in the observations.

6.3 Salinity

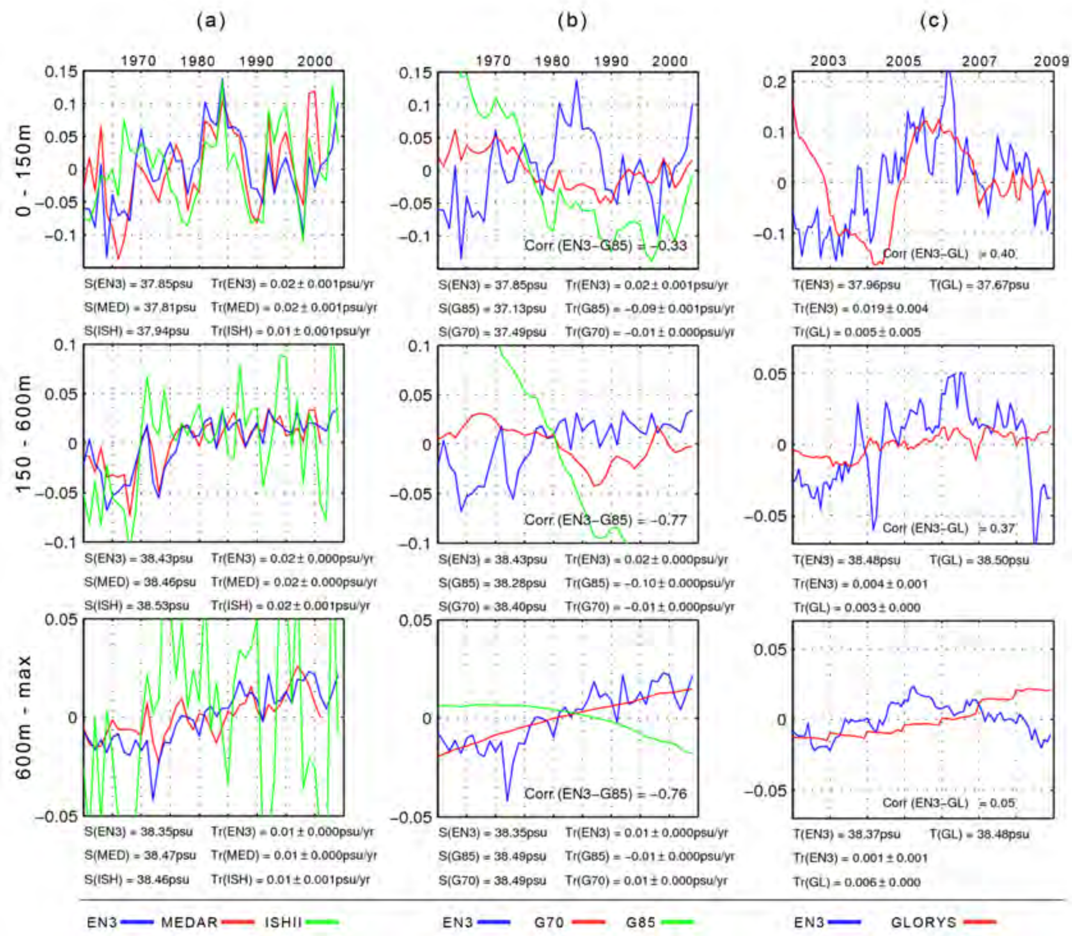

Figure 6.2: WMED mean salinity anomaly of the interannual variability at different layers. (a) is the comparison between EN3 (blue), MEDAR (red) and ISHII (green) from 1960 to 2004. (b) is the comparison between EN3 (blue), G70 (red) and G85 (green) from 1960 to 2004. (c) is the comparison between EN3 (blue) and GLORYS (red) from 2002-2009. Mean salinity (S) and trends (Tr) with their error are given below each image for the different data streams

While EN3 salinity trends are always either slightly positive or close to zero, both G85 and G70 simulations show negative trends at surface and intermediate layers, with G85 displaying trends 5 to 8 times stronger than G70. This is due to the salinity relaxation in the G85 simulation that is 1/6th of that imposed in G70. This lower relaxation applies less evaporation to the simulation causing a very strong and unrealistic negative trend in salinity, also rendering the mean values over the period studied much lower (at surface layers, EN3=37.93, G85=37.13) than those obtained from the EN3 observational data. Consequently, the power spectra of G85 and EN3 are very different (not shown). At deep layers, G70 and EN3 coincide with slight positive trends ($\sim$0.03 - 0.05 psu/yr) but G85 remains negative at $\sim$0.08 psu/yr). Caution must be taken when analysing observational salinity data in deep layers as it is very scarce and unevenly spread out therefore prone to significant averaging error. Salinity in GLORYS appears slightly better than in the ORCA models but still does not produce good results. At surface layers, the model shows a strong deviation with regards to EN3 ($\sim$0.25 psu in salinity anomaly in the WMED) towards the beginning of the simulation but manages to stabilize and approximate EN3 by 2005. This deviation during the initial years may be due to GLORYS using the ARIVO climatology (Gaillard et al. (2008), Gaillard and Charraudeau (2008)), which is different from the climatology used in the background field in the EN3 optimal interpolation. Additionally, salinity data in 2002 and 2003 is very scarce, reducing the confidence in the EN3 dataset. Also GLORYS assimilation of observations other than in situ profiles, namely altimetry and SST and could be part of the difference (through the use of multivariate covariances). At intermediate and deep layers, GLORYS seems to show a positive drift in salinity with very marked and unrealistic steps at the end of every year (especially in deep layers). EN3 displays a significant increase in salinity in deep layers of approximately 0.05 psu peaking in 2005 and a reduction after that. This behaviour is difficult to explain. It could be related to the 2005-2006 deep convection events that caused an increase in salinity at those depths and were studied by Schroeder et al. (2006), Schroeder et al. (2008b), Schroeder et al. (2010), Herrmann et al. (2010), Font et al. (2007) and Smith et al. (2008). Another possible explanation is that the peak in EN3 may be due to lack of observations at that depth. This is not observed in the model.

6.4 Deep Water Formation in the Gulf of Lion

One important issue to be explored is the capability of these models to reproduce deep-water formation events. Given the nature of these events, which are caused by localized extreme weather (wind and cold) events, the spatial and temporal resolution of the simulations are a heavily limiting factor, as well as the low resolution of the atmospheric forcing.. Despite these limitations, in this section we evaluate the interannual variability of deep water using Hovmöller Diagrams of mean vertical temperature and salinity profiles from the Gulf of Lion deep-water formation sites.

Figure 6.3 shows the temporal evolution of the vertical temperature and salinity profiles (the mean of a 1^o x 1^o centred at 42.6^{o}N, 4.4^{o}E) for G85. Every winter, cold water sinks down the water column to about 200-300 m. For the entire G85 simulation period (1960 to 2007, not shown), the propagation of these colder waters does not seem to go beyond that level, instead stopping as it encounters the Levantine Intermediate Waters (LIW). However, the winters of 2004-2005 and 2005-2006 show the propagation of these colder waters penetrate into the intermediate layers and significantly modify its signature, with the latter producing a thin tongue of colder water reaching beyond 750 m and into the deep layers. As can be seen in Figure 6.4 which shows the Net Downward Heat Flux (NDHF) and Net Upward Water Flux (NUWF), the winters of 2005 and 2006 also show very intense evaporation and heat loss ($\sim$240 W/m^2), setting the appropriate conditions for deep water formation. One notable difference between EN3 (figure 6.5) and G85 is the warmer intermediate waters by approximately 0.5^{o}C in the simulation prior to the onset of these two exceptional winters. As is evidenced by the two strong convection events, these have an important role in conditioning the temperature of intermediate layers by mixing down colder waters. Given the low resolution of the model, but especially of the atmospheric forcing, weaker deep convection events are not reproduced by the simulation and cause intermediate layers to heat up by diffusion (the initial years of the simulation have similar temperatures to observations but from 1960 to 1965 there is a rapid warming of this layer).

The 2005 and 2006 events are clearly visible in the EN3 dataset (figure 6.5), with both years producing strong convection. These results correspond to the deep-water formation events described in Schroeder et al. (2006), Schroeder et al. (2008b), Schroeder et al. (2010), Herrmann et al. (2010), Font et al. (2007) and Smith et al. (2008) that were produced by extremely strong forcing

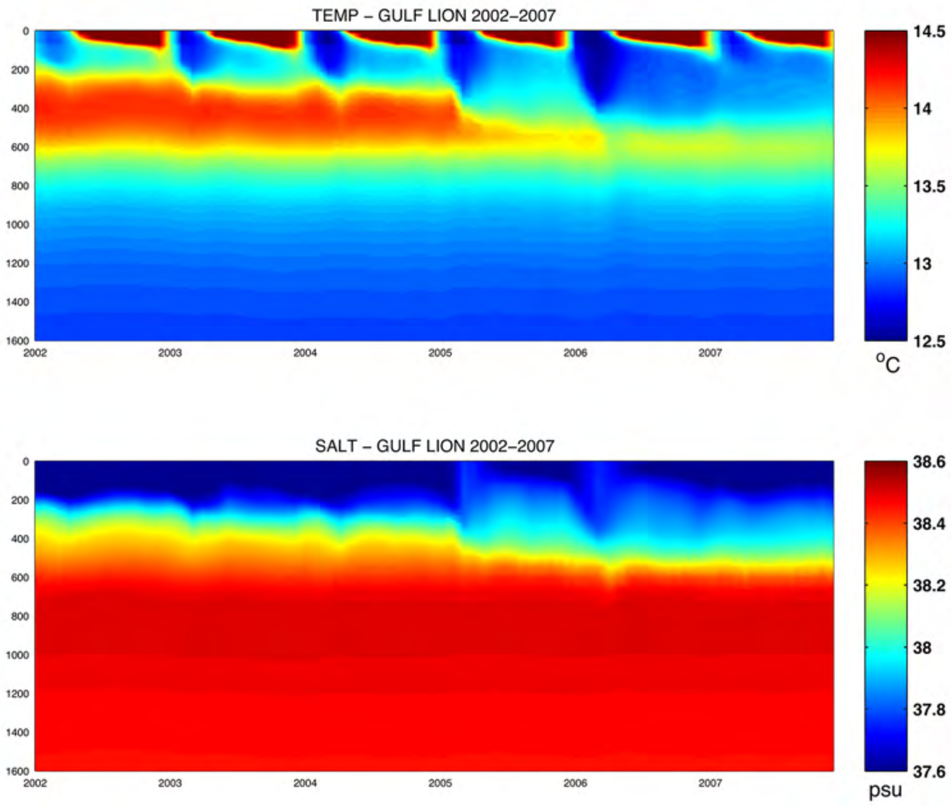

Figure 6.3: Hovmöller diagrams showing the temporal evolution of temperature (top) and salinity (bottom) of a 1^o x 1^o area at the center of the Gulf of Lion for the G85 simulation.

during these two winters (heat loss 70% above average according to López-Jurado et al. (2005) and low precipitation according to Font et al. (2007)). In fact, the ARPERA dataset (Herrmann et al., 2008b), which is a dynamical downscaling of the ERA40 dataset (from 150 to 50 km) gives a net winter heat loss for that area of 308 W/m^2 for the 2004-2005 winter, whereas other winters show net losses of $\sim$200 W/m^2 (table 1 in Schroeder et al. (2010)). A similar difference is seen in G85 although the total heat loss is less due to the lower resolution of the ERA40 atmospheric forcing (240 W/m^2 in 2004-2005 vs $\sim$150 W/m^2 during most other winters). The effects of the atmospheric forcing resolution (temporal and spatial) on deep convection were studied by Béranger et al. (2010) using high resolution (1/16^o) numerical simulations and running both ERA40 ($\sim$125 km) and ECMWF ($\sim$55 km) forcing. They concluded that the higher resolution forcing generated the more realistic (and stronger) winds and winter heat loss necessary for the formation of deep convection events.

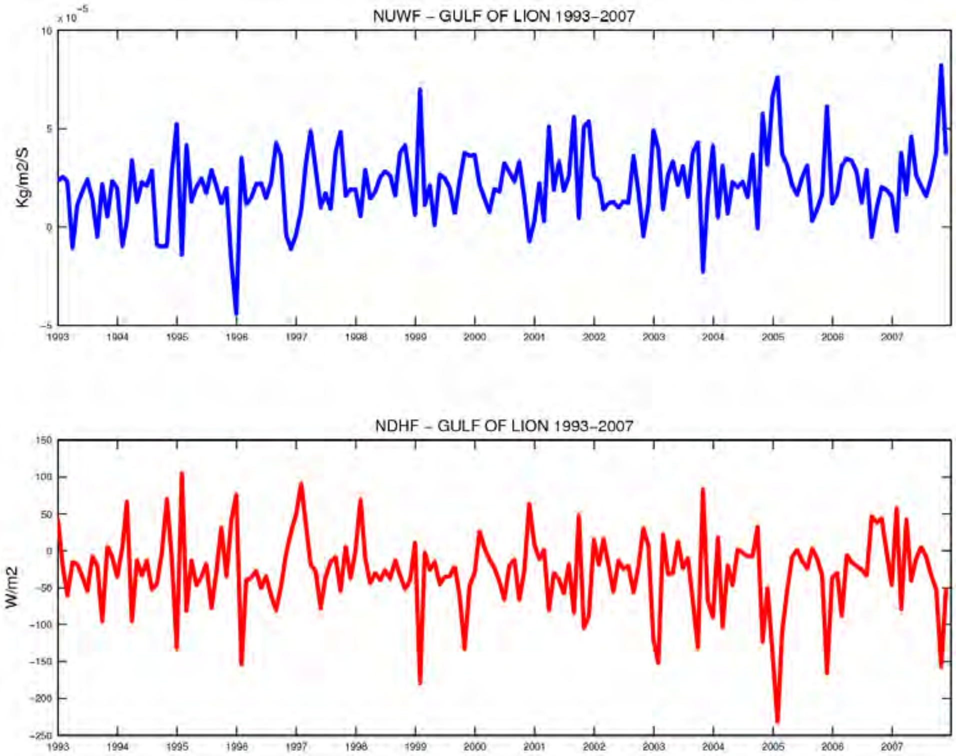

Figure 6.4: Timeseries plots of Net Upward Water Flux (NUWF) (top, blue) and Net Downward Heat Flux (NDHF) (bottom, red) over a 1^o x 1^o area of the Gulf of Lion for the G85 simulation.

Similar analysis was performed with GLORYS over the period 2002-2009 (figure 6.6). Daily outputs were available for this simulation, greatly increasing temporal resolution, a factor which is very important in these localized deep water formation events. In GLORYS the year of most intense cooling was 2006 with a very distinct cooling signal throughout the water column reaching the deep layers and changing the properties of intermediate and deep waters for the following years. However, the 2005 event is weaker than the observations and does not reach beyond the intermediate layers. This disparity between GLORYS, which assimilates data and EN3 could be due to several factors; the ECMWF operational system which provides the ocean-atmosphere fluxes for the simulation increased its resolution from 0.5^o to 0.25^o in February 2006, just prior to the onset of the deep convection event. This resolution increase would clearly benefit the formation of deep convection events and could partly explain the difference with the previous year. EN3 and the assimilated CORA database may contain different profiles (due to differences in quality control

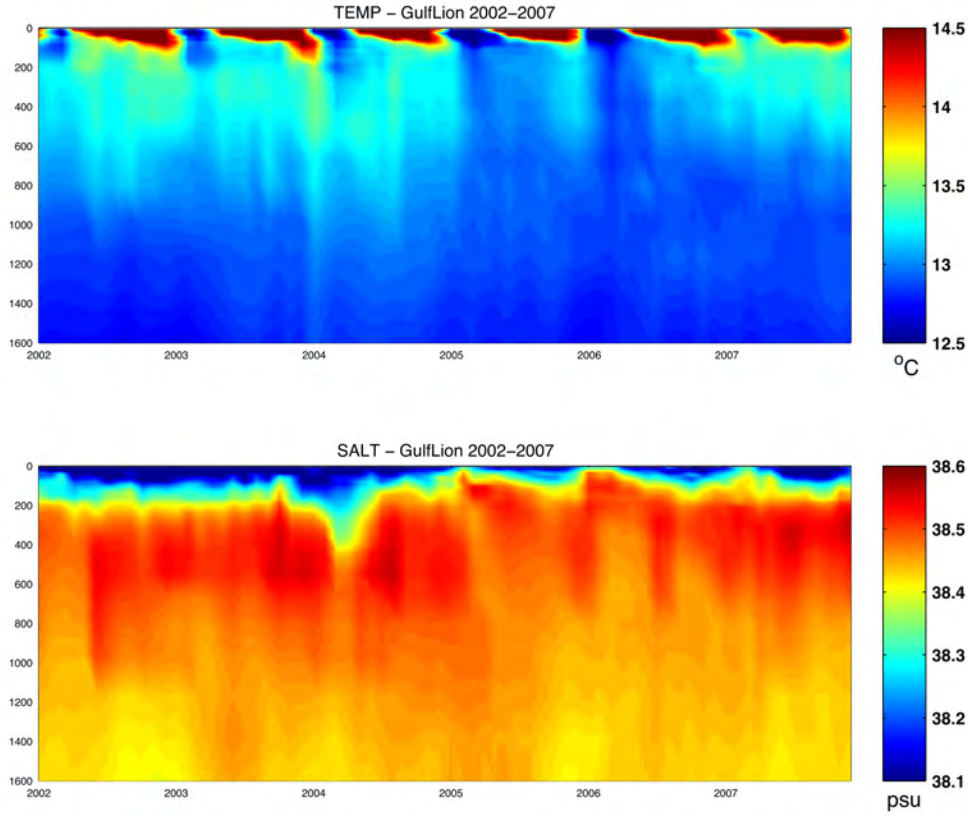

Figure 6.5: Hovmöller diagrams showing the temporal evolution of temperature (top) and salinity (bottom) of a 1^o x 1^o area at the centre of the Gulf of Lion for the EN3 database.

parameters or source data).

Additional tests were performed in different areas of the WMED, similar 1^o x 1^o squares were taken in the Ibiza Channel and the Alboran Sea just before the Strait of Gibraltar. At the Ibiza Channel (figure 6.7), similar (but less intense) cooling of the upper and intermediate layers occurs in G85 but is not so clear in EN3 (figure 6.8).

Figure 10 is a composite of TS Diagrams for the years 1996, 1997, 2003 and 2006 at the Ibiza Channel. Presence of LIW and WMDW is clear in all four years but 1996 and 2006 also show a clear presence of Western Mediterranean Intermediate Water (WIW) with a temperature minima between 13^{o}C and 12.5^{o}C. The years 1996 and 1997 were chosen because Pinot et al. (2002) performed extensive measurements during the CANALES experiment in the Ibiza and Mallorca channels, and thus can be readily compared to the simula-

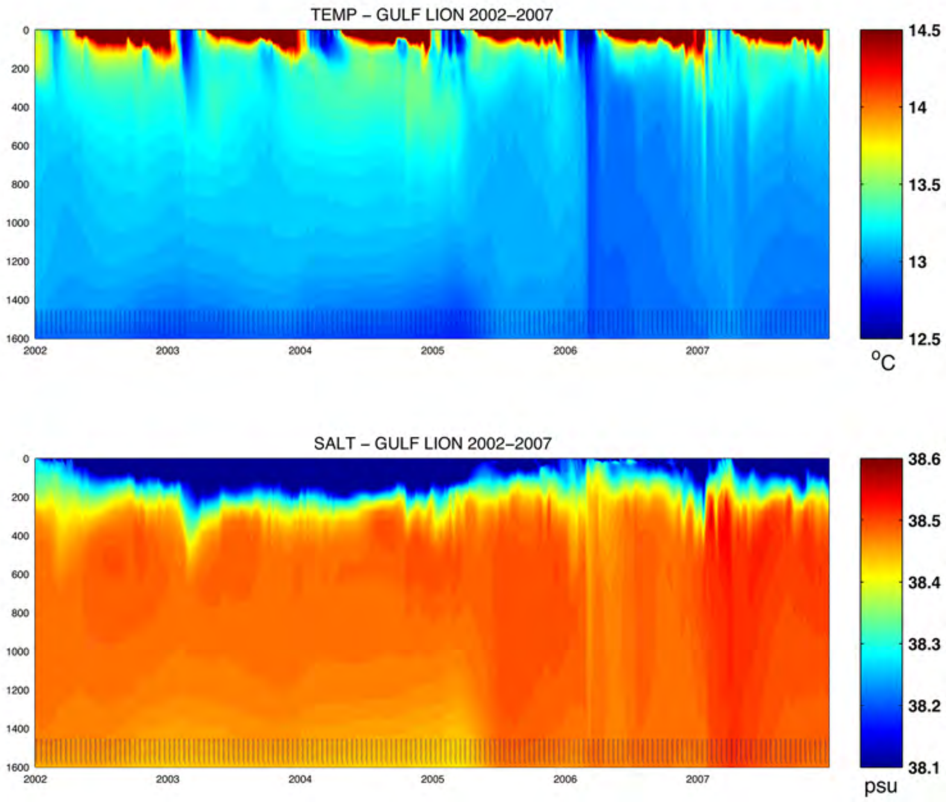

Figure 6.6: Hovmöller diagrams showing the temporal evolution of temperature (top) and salinity (bottom) of a 1^o x 1^o area at the center of the Gulf of Lion for the GLORYS simulation.

tion data. The 1996 WIW peak in the G85 TS Diagram and the temperature minima coincide with Pinot et al. (2002), as well as the lack of WIW in 1997. At the Alboran site, the effects of these two winters are felt far weaker however the modification of intermediate waters seems to reach this location by middle of 2006.

These deep-water formation events were reproduced to some extent due to the extremity of the atmospheric forcing. Li et al. (2006) and Herrmann et al. (2008b) concluded that the necessary resolution for atmospheric forcing in order to simulate Mediterranean convection and deep water formation is about 50 km. Therefore normal deep-water formation events are likely not reproduced by the ORCA025 simulations.

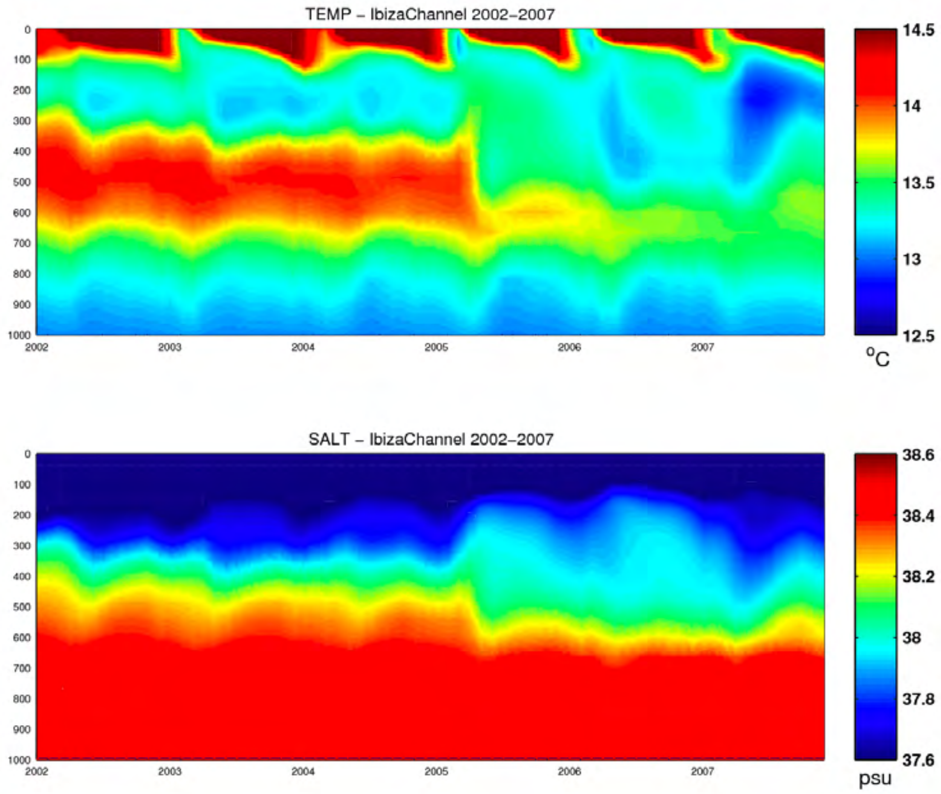

Figure 6.7: Hovmöller diagrams showing the temporal evolution of temperature (top) and salinity (bottom) of a 1^o x 1^o area at the center of the Ibiza Channel for the G85 simulation.

6.5 Mean Sea Level

Performance regarding sea level in the simulations is analysed by comparing them to altimetry over the available common period (1993-2004/2007/2009)(Figure 6.10). Detailed comparison of mean sea level from altimetry and sea surface height from G70 can be found on Chapter 5 and will not be repeated here. However, the main result in this regard was that the model was capable of correctly reproducing the seasonal cycle in both phase and amplitude as well as the interannual variability but SSH from the model showed a exaggerated positive trend of 14.96±1.46 mm/yr when the trend for altimetry was 3.62±1.32 mm/yr. G85 also displays a correct seasonal cycle but the trend has increased even further to 20.27±1.37 mm/yr due to the effect of a reduced salinity relaxation term, which implies lower evaporation and in consequence an increase in sea level. These positive trends of the ORCA models are not an isolated feature of the Mediterranean, but global due to an imbalanced freshwater bud-

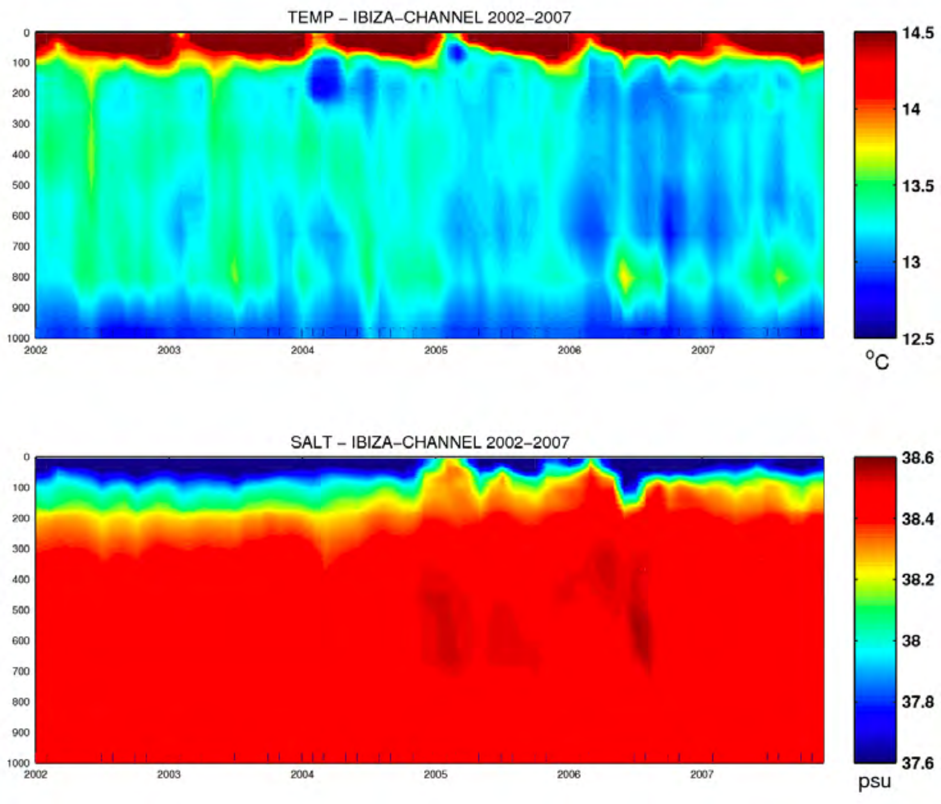

Figure 6.8: Hovmöller diagrams showing the temporal evolution of temperature (top) and salinity (bottom) of a 1^o x 1^o area at the center of the Ibiza Channel for the EN3 database.

get. The freshwater budget is of vital importance since it contributes to the mean sea level budget closure, impacting sea level rise and density driven circulation (Ferry et al., 2010), however its different contributors (precipitation, evaporation, river run-off and glacier melt) have large uncertainties making the achievement of a balance very difficult. If the trends are removed, the power spectra (Figure 6.11) of G85 and altimetry are very similar in terms of peaks and energy. Essentially both spectra present a marked annual cycle at 10-12 months and a less well defined semiannual peak, but it trends are not removed, higher energy is seen in G85 at lower frequencies.

In GLORYS, the net water budget is artificially set to zero in each time step becoming perfectly balanced and therefore it does not affect the mean sea level (MSL) of the model. The consequence is that any changes in MSL are due to the assimilated data provided by altimetry (Ferry et al., 2010). As a result, the comparison between GLORYS and altimetry data yields almost

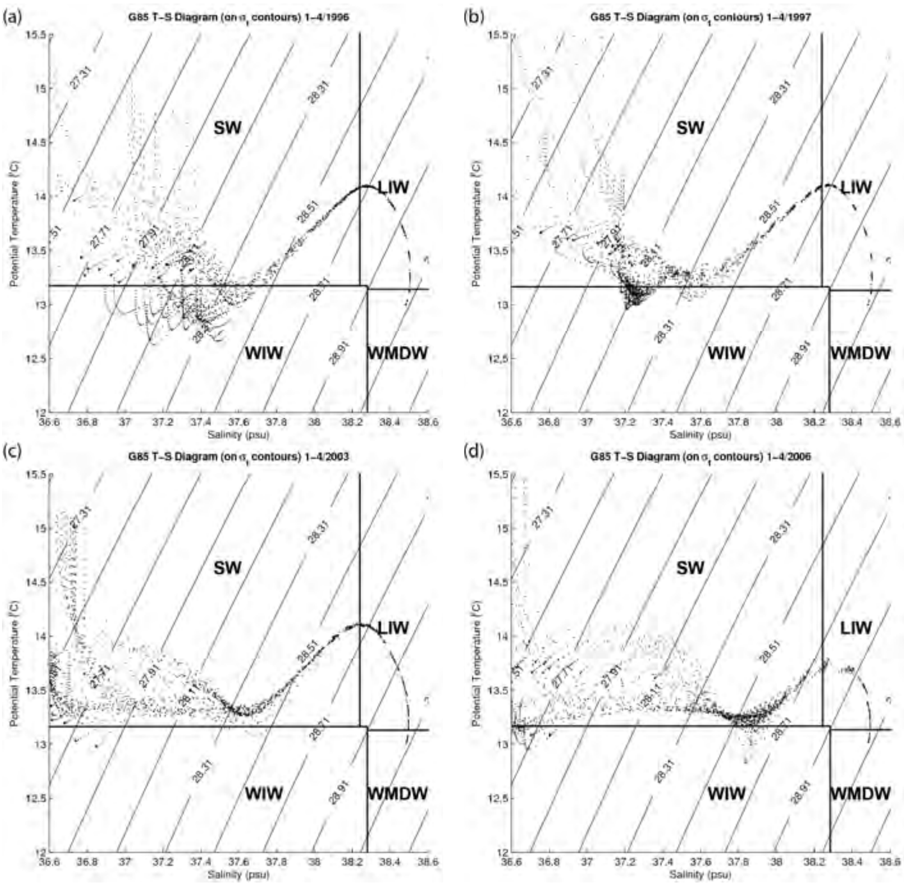

Figure 6.9: TS Diagrams of a 1^o x 1^o area at the center of the Ibiza Channel for the G85 simulation for the period of January to April of 1996 (a), 1997 (b), 2003 (c) and 2006 (d). SW stands for Surface Waters, the rest of the acronyms are detailed in the text.

identical results, with no drift in the models SSH and a trend very similar to altimetry.

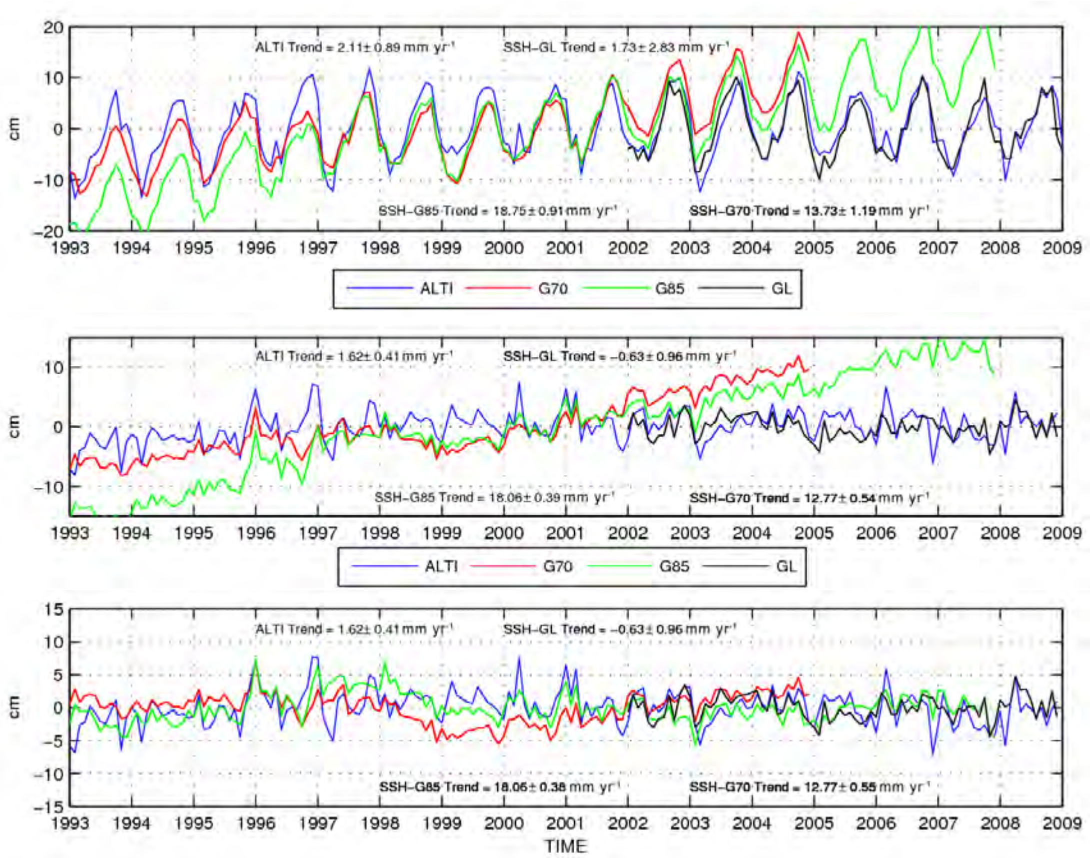

Figure 6.10: ORCA G70 (red), G85 (green) and GLORYS (GL, black) SSH plotted against altimetry mean sea level anomaly (blue) for the WMED. (top) full signal (middle) with the seasonal cycle removed (bottom) with seasonal cycle and trends removed (the numerical values indicate the trend that has been removed).

6.6 Mean Surface Circulation

We contrast the mean circulation of G70 and G85 derived from mean SSH and surface velocity currents over the 1993-2004 period with the available literature. The mean circulation in the Western Mediterranean is well known. Atlantic waters enter the Strait of Gibraltar into Alboran Sea (Astraldi et al. (1999), Beranger et al. (2005), Tsimplis and Bryden (2000), Sánchez-Román et al. (2009), García-Lafuente et al. (2002), Gomis et al. (2006)) and form the Western Alboran Gyre (WAG) and Eastern Alboran Gyre (EAG) (Viúdez et al., 1998). The circulation continues out of the Alboran Sea as the Algerian Current (AC) (Millot, 1999). The AC shows significant mesoscale activity as it continues towards the Sicily Channel. Part of it crosses the channel and

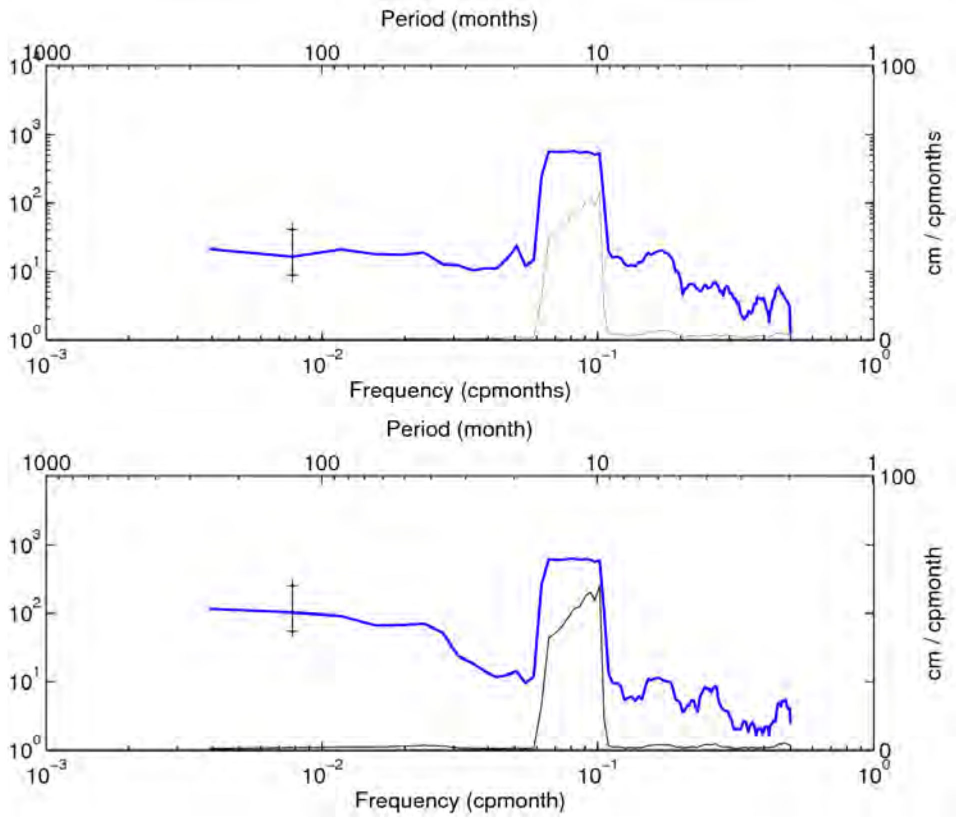

Figure 6.11: Altimetry (top) and G85 (bottom) power spectra for mean SSH for the period 1993-2007.

the rest recirculates into the Tyrrhenian Sea, moving along the Italian Coast and becoming the Northern Current as it passes into the Ligurian, through the Gulf of Lion and into the Balearic Sea. The Northern Current recirculates before it reaches the Ibiza Channel and becomes the Balearic current (Pinot et al. (1995), Alvarez et al. (1994), Astraldi et al. (1999), Ruiz et al. (2009)). The ORCA models show the same general circulation pattern (figure 6.12). In more detail, both G70 and G85 show the presence of WAG and EAG, with G70 showing a more prominent WAG. Given the coarse resolution, both models aggregate the Algerian current and the area of intense mesoscale activity above the Algerian current into one meandering, high-intensity band, with G85 reaching further north than G70. Both models show a low minima to the SE of the Gulf of Lions and between Sardinia and Sicily, with G70 being more intense in the former and G85 in the latter. In the Balearic Sea, G70 reproduces the recirculation of the Northern Current further south than G85, closer to Ibiza channel.

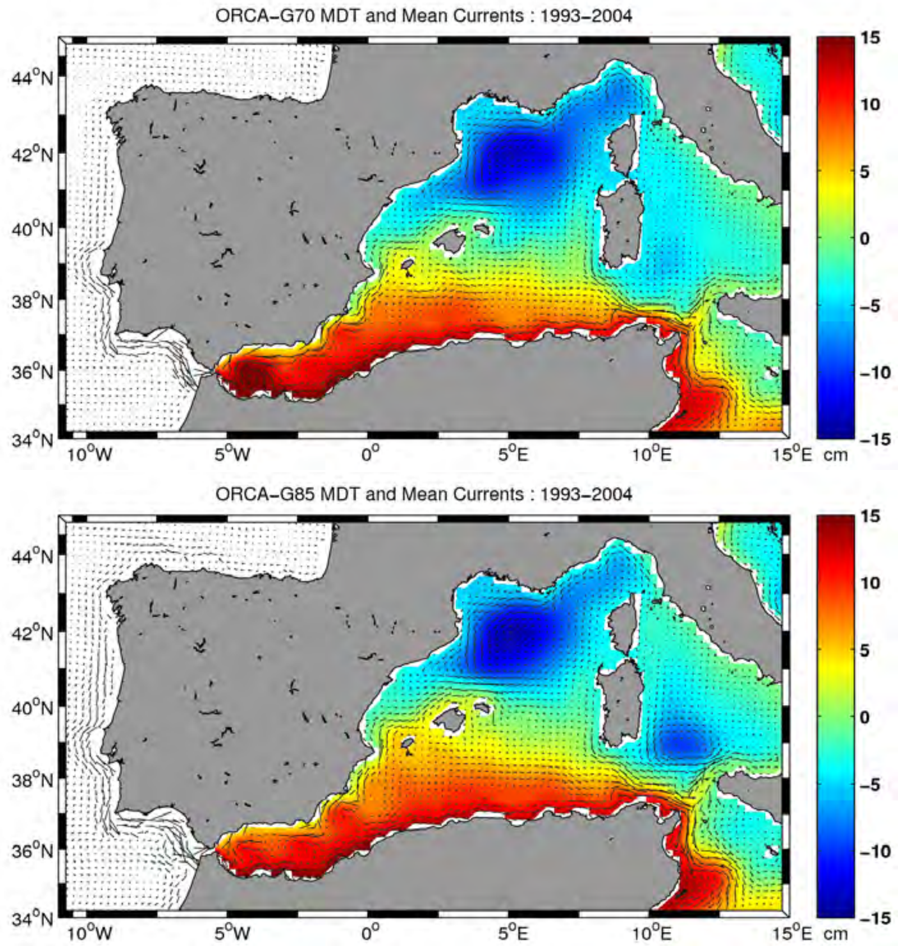

Figure 6.12: Mean Sea Surface Height maps from G70 (top) and G85 (bottom) with surface velocity vectors added.

6.7 EOF Analysis of SSH

We further evaluate the main patterns of variability of G85 by using Empirical Orthogonal Functions (EOFs) and comparing with altimetry. Figures 6.13 and 6.14 present the first EOF mode of altimetry and G85 SSH respectively. The first EOF mode of altimetry, which explains 72.6% of the covariance, shows the strong seasonal variability of the Alboran Gyres with maximum amplitude in autumn (Larnicol et al., 2002). Also seen is the autumn/winter intensification of the cyclonic circulation in the Gulf of Lions. In the first EOF mode of G85 (86.2% cov.) the seasonality of the cyclonic gyre in the Gulf of Lions is also observed to a certain degree, weaker and more towards the north. The signature of the Alboran anticyclonic gyres is almost negligible in G85. Along the path of the Algerian Current, G85 does not show the mesoscale variability seen in altimetry as expected, although it does exhibit a North-South gradient.

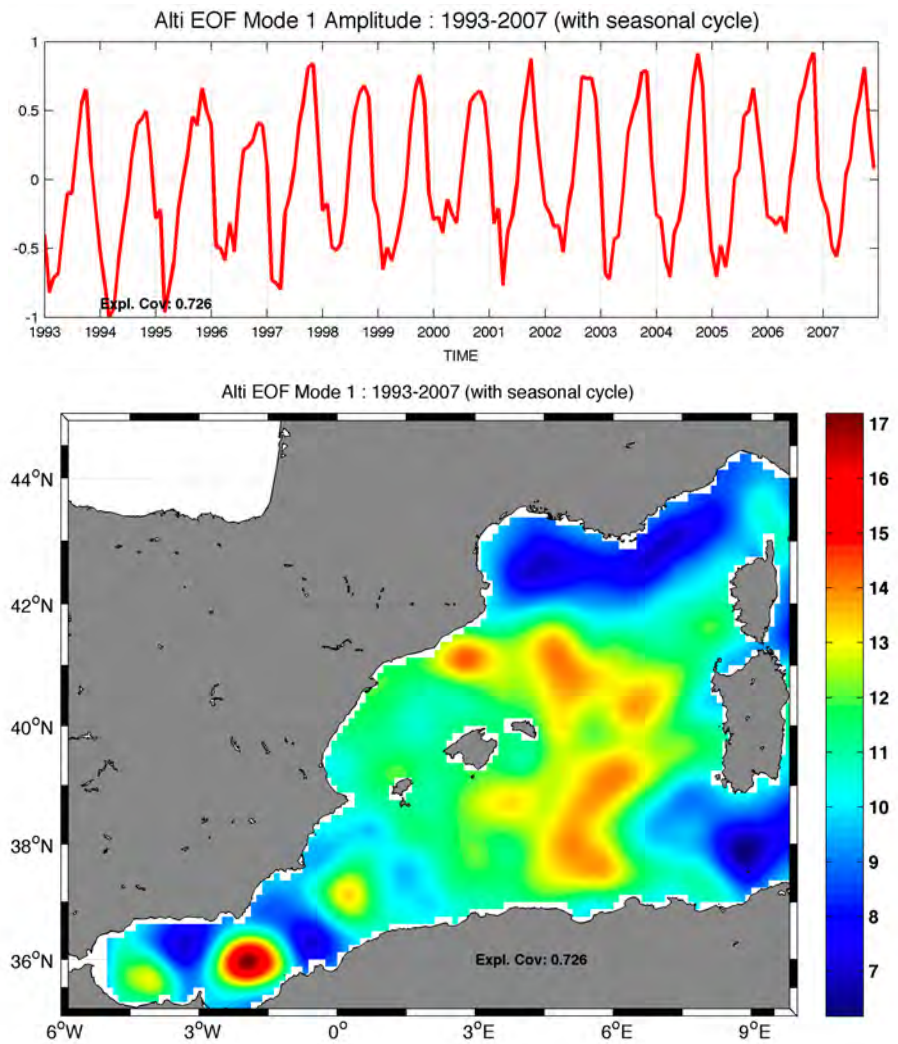

Figure 6.13: The first EOF mode for altimetry SLA (sea level anomaly) with the amplitude (top) and pattern (bottom).

Figures 6.15 and 6.16 show the first EOF mode of both datasets with the seasonal cycle removed. As is to be expected, altimetry displays more intricate mesoscale patterns and better defined eddy structures such as the WAG and EAG. Despite the weaker Alboran gyres seen in G85 and the stronger pattern in the area of the Gulf of Lion, the simulation does show similar (but more diffuse) mesoscale patterns along the path of the Algerian current; particularly the eddy east of the Almería-Orán front and the two eddies southeast of the Balearic Islands. The normalized amplitude timeseries of the first EOF mode

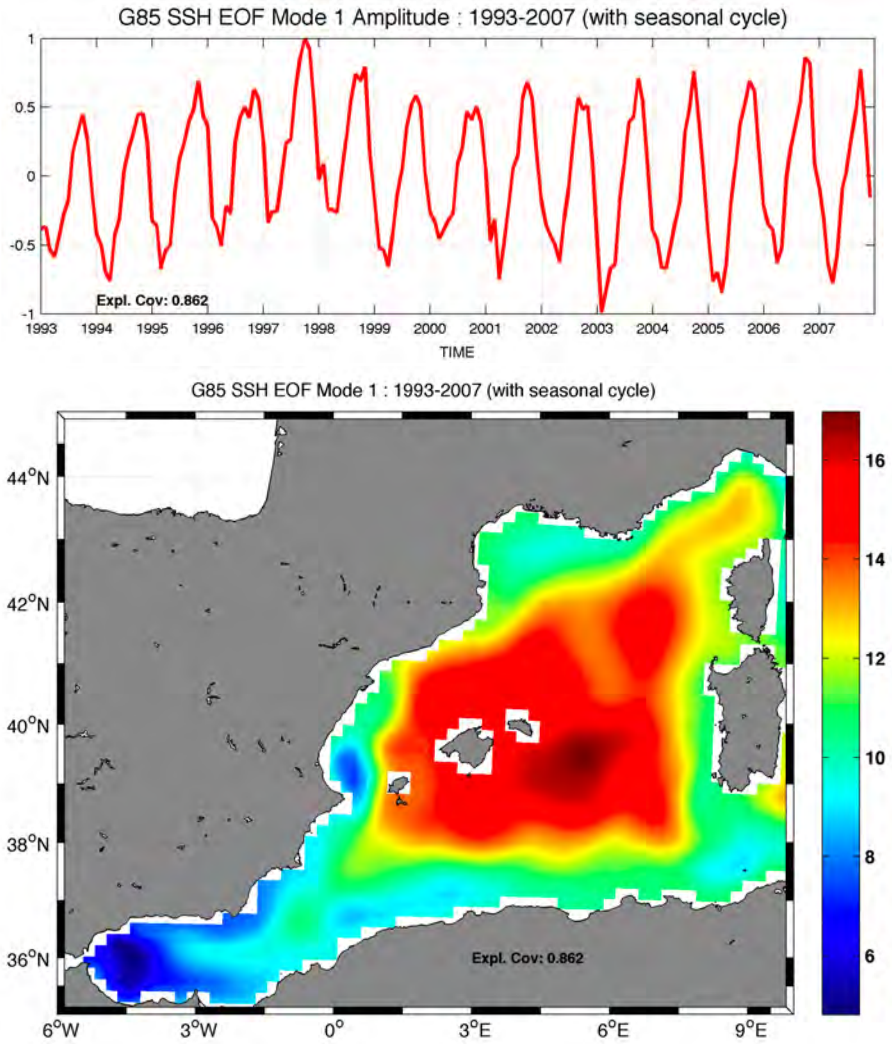

Figure 6.14: The first EOF mode for G85 SSH with the amplitude (top) and pattern (bottom).

show important disparities, although there are coincidences in the position of some peaks such as 1996. The difference in the explained covariance of both datasets can be attributed to resolution. In altimetry, subsequent modes (not shown) correspond mainly to marked mesoscale eddy features which the model cannot resolve.

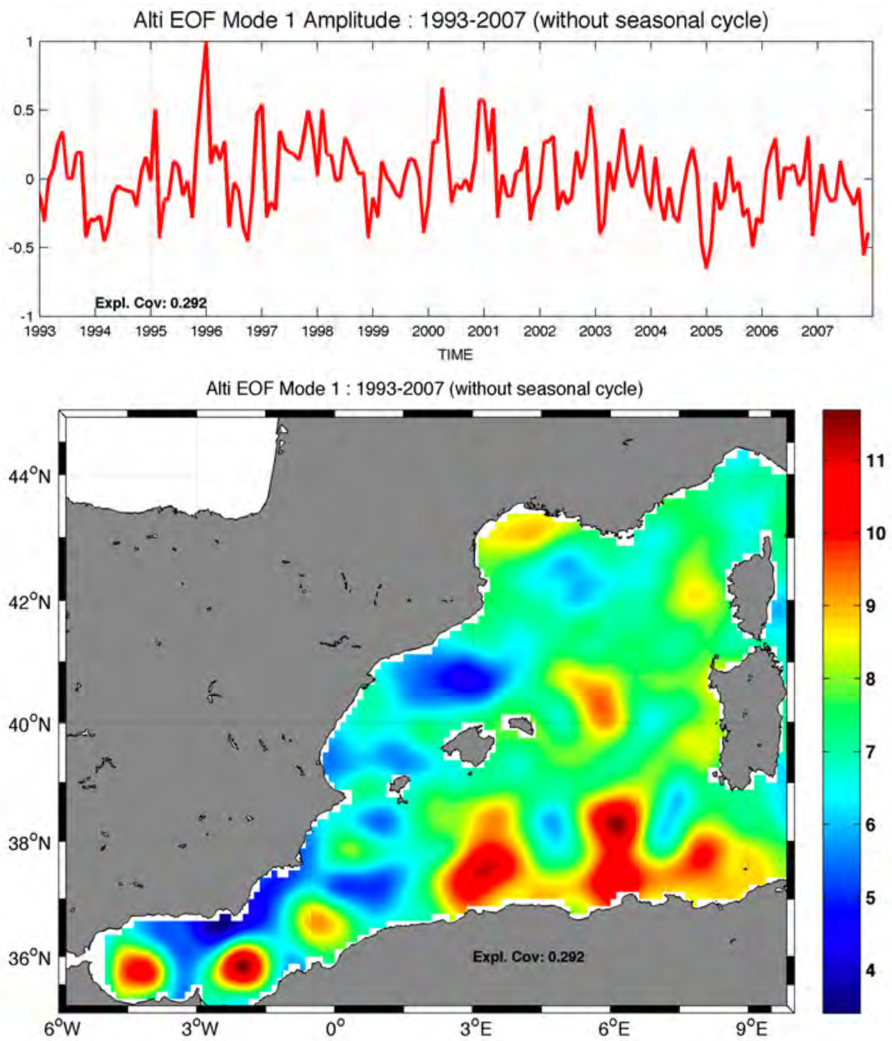

Figure 6.15: The first EOF mode for altimetry (without seasonal cycle) with the amplitude (top) and pattern (bottom).

6.8 Transports

6.8.1 Strait of Gibraltar

Table 6.1 shows the transport values for the different simulations analysed in this study. G70 has an inflow of 1.076±0.08 Sv, an outflow of 1.008±0.09 Sv and a net inflow of 0.067±0.06 Sv. G85 has a slightly less intense exchange with 1.006±0.09 Sv inflow, 0.948±0.1 Sv outflow and a weaker 0.05±0.06 Sv net inflow. GLORYS shows a more intense exchange (1.296±0.12 Sv inflow, -1.243±0.10 Sv outflow) but similar net flow to G85 (0.052±0.1 Sv). In this

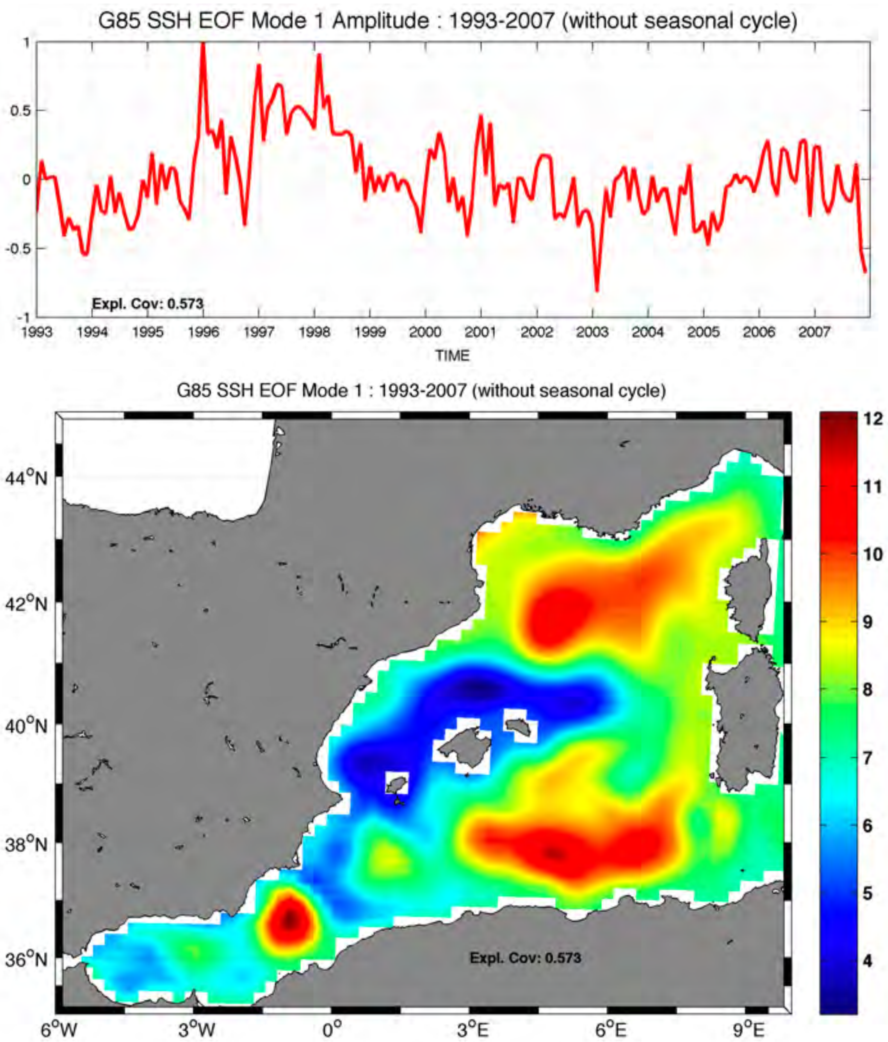

Figure 6.16: The first EOF mode for G85 SSH (without seasonal cycle) with the amplitude (top) and pattern (bottom).

regard, all three models fall within the established observational values which in themselves show a large uncertainty due to the lack of long-term direct measurements, the complexity of horizontal and vertical profile of the flow, and the presence of strong tidal currents (Tsimplis and Bryden (2000), Gomis et al. (2006)). To date, no observational efforts have been maintained long enough to calculate a long-term mean. The longest study to date is by Soto-Navarro et al. (2010) who combined atmospheric data from reanalysis, satellite and experimental observations to calculate a 4 year time series of the Atlantic inflow using the net flow estimated from the Mediterranean water budget and the Mediterranean outflow derived from current meter observations. They ob-

SIMULATIONS	ORCA G70	ORCA G85	GLORYS
IN	1.076±0.08 Sv	1.006±0.09 Sv	1.296±0.12 Sv
OUT	1.008±0.09 Sv	0.955±0.10 Sv	1.243±0.10 Sv
NET	0.67±0.06 Sv	0.50±0.06 Sv	0.52±0.08 Sv

Table 6.1: Transports at the Strait of Gibraltar for G70 (1993-2004), G85 (1993-2007) and GLORYS (2002-2009).

tained a mean Atlantic inflow of 0.81±0.06 Sv, a mean Mediterranean outflow of 0.78±0.05 Sv and a net flow of 0.038±0.007 Sv. Another study by Candela (2001), 2 years from October 1994 to October 1996 using current profile measurements obtained inflows of 1.01 Sv, outflows of 0.97 Sv and a net inflow of 0.04 Sv. Other studies by Tsimplis and Bryden (2000) and (García-Lafuente et al., 2002) show weaker exchange and net flows but their studies were performed over periods of 4 and 6 months respectively, thus not capturing a full years cycle.

6.8.2 Ibiza and Mallorca Channels

The Ibiza Channel together with the Mallorca Channel, are two passages where significant north-south water exchange in the WMED takes place (Fernández et al., 2005), with Ibiza being the most important of the two with over twice the amount of flux. Across the Ibiza Channel, transport shows a marked seasonal cycle with maximum southward flow during winter months (January-March), and the opposite happening with northward flow in summer. In the Mallorca Channel, a seasonal cycle is also present but there is flow in both directions throughout the year. In this study we focus primarily on the Ibiza Channel. At the Ibiza Channel, both G70 and G85 (figure 6.17) display the appropriate north-south seasonal variability with similar flow values. G70 shows mean northward transport of 0.628±0.3 Sv, southward transport of 0.225±0.14 Sv and a net northward transport of 0.403±0.37 Sv. G85 has slightly stronger northward transport 0.717±0.34 , a slightly more intense southward transport at 0.228±0.23 Sv and a net northward transport of 0.489±0.51 Sv. The associated error is slightly higher in G85. By computing transport at different layers, it was determined that northward transport occurs in surface layers and southward transport occurs mainly in intermediate and deep layers

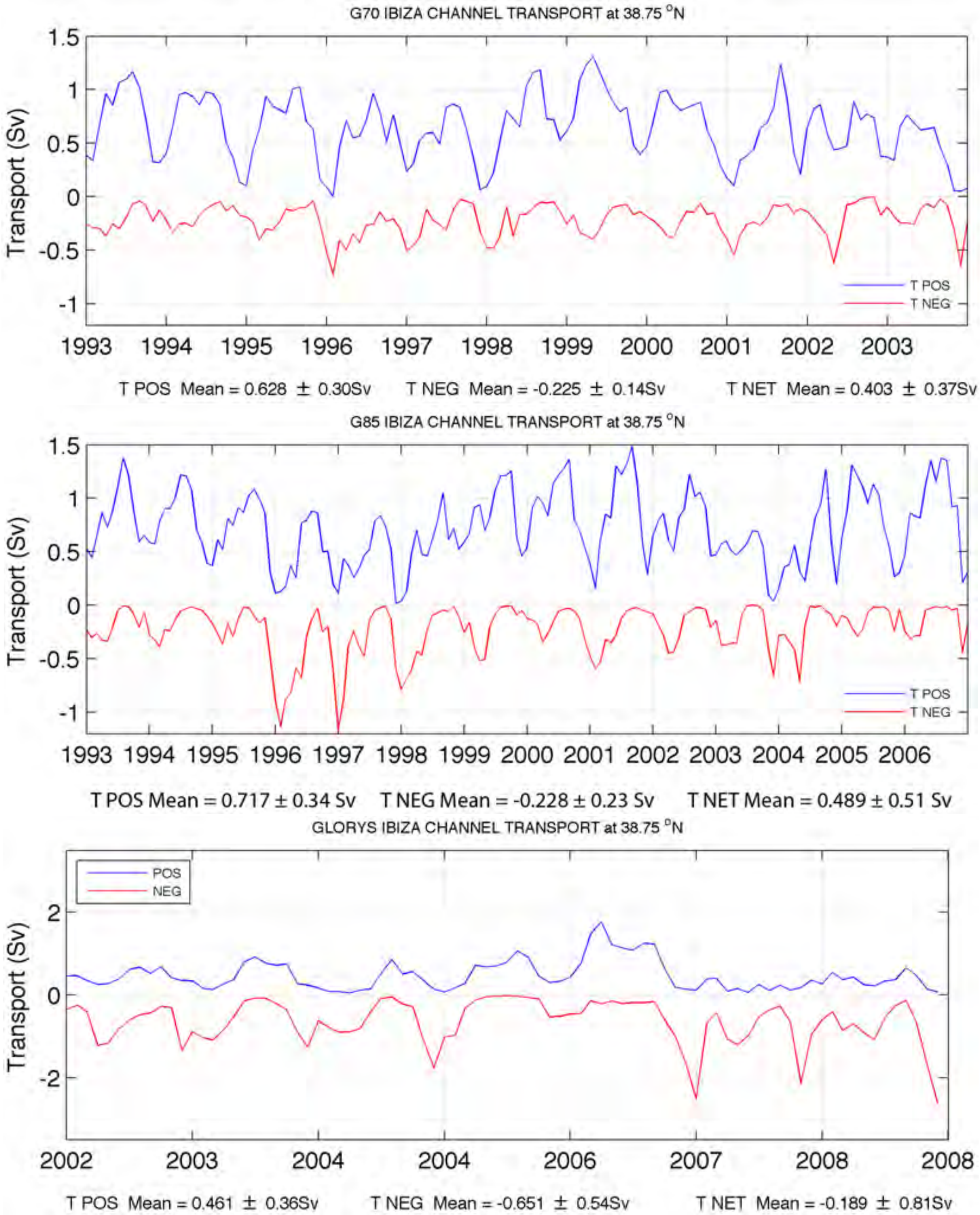

Figure 6.17: Transport timeseries for G70 (top), G85 (middle) and GLORYS (bottom) at the Ibiza Channel. Mean transport values are given below the figure. POS means flow in positive directions (north and east). NEG means flow in the negative directions (south and west).

GLORYS (figure 6.17) has a northward transport similar in magnitude to the other two models but its southward transport is far more intense with an average of 0.668±0.56 Sv, normal annual peaks of over 1 Sv and intense peaks of 2-2.5 Sv (winters of 2007 to 2009). These intense peaks are far greater than those found in the literature. It must be noted that these peaks occur in the final years of the simulation, where no direct observational data has been published yet, and could very well be exceptional years.

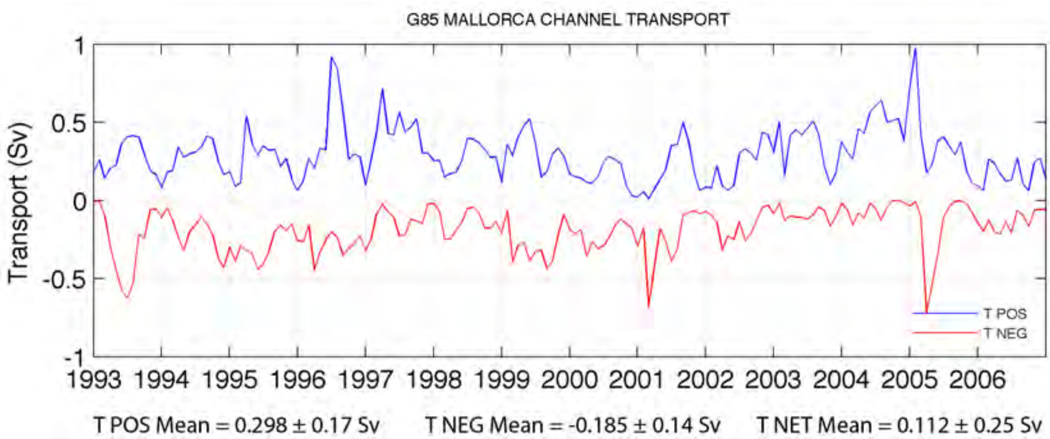

Figure 6.18: Transport timeseries for the G85 simulation at the Mallorca Channel for the period 1993-2007. Mean transport values are given below the figure. POS means flow in positive directions (north and east). NEG means flow in the negative directions (south and west).

Fernández et al. (2005) calculated transports through several transects, straits and channels using data from the DieCAST 1/8^o numerical model. They obtained maximum southward transports of 0.9 Sv in winter and northward transports in summer of 1 - 1.4 Sv (with very little northward transport in the winter). His data agrees with both ORCA simulations although G70 does not reach the maximum 0.9 Sv of southward transport. GLORYS agrees in the northward flow but generally overshoots the measured 0.9 Sv. One of the most exhaustive observational studies in the Balearic Sea was undertaken by Pinot et al. (2002) and consisted of two years of hydrography experiments (The CANALES Experiment) from 1996 to 1998. These included several sampling techniques to measure the flow through the Mallorca and Ibiza Channels. They provide very detailed transport measurements over the two-year period, which coincide reasonably well with G85 in both the magnitude of transports and some of the smaller-scale variability. In the simulations, the Ibiza Channel (figure 6.17, middle) coincides better with the observational data than the

Mallorca Channel (figure 6.18). Pinot et al. (2002) measured peaks of 1.05 Sv moving southward through the Ibiza Channel (IC) during winter of 1996, falling to 0.5 Sv by spring and fully reversing by summer with a northward flow of recent Atlantic Water (AW). By the beginning of winter, the flow has reversed again with dominating southward flow from the Northern Current (NC). 1997 begins with a similar pattern to that of the previous year (0.9 Sv) and shows a very sharp decline with the beginning of spring due to an eddy blocking the channel. G85 displays this sharp decline as well however it is probably not due to an eddy since the model is not capable of reproducing eddies of this small size. G70 does show similar variability but its maximum southward transport values seem to be underestimated. This could be due to the reduced vertical resolution of G70, especially in the intermediate and deeper layers where most of the southward transport through the IC takes place. This appears to indicate that vertical resolution of the simulations is an important element in correctly reproducing transports.

6.9 Summary

We have analysed the performance of three global numerical simulations, G70, G85 and GLORYS (with data assimilation) building on Chapter 5 (which is based on Vidal-Vijande et al. (2011)) but focusing on the WMED. All three simulations are based on a similar 1/4^o NEMO (Madec, 2008) code configuration on an ORCA grid. G70 and G85 are hindcasts of the past half century developed by the DRAKKAR Group (Barnier et al., 2007), they differ in vertical resolution (G70 has 46 vertical levels and G85 has 75), slightly different forcing based on ERA40 (G70 has DFS3 and G85 the improved DFS4) and intensity of the surface salinity restoring term with G85 being six times weaker than G70. The salinity restoring term is applied it order to correct for drift in the freshwater balance of the simulations, it adds freshwater or increases evaporation where needed based on a climatology. GLORYS has a similar configuration to G70 but includes data assimilation and runs over the period of 2002 to 2008.

Mean temperature variability is well reproduced at surface and intermediate layers although G70 shows trends at deep and intermediate layers that are larger to those obtained from observational databases. The improved continuity of the DFS4 atmospheric forcing together with a higher vertical resolution greatly improves these trends in G85. The combined effect of a more consistent atmospheric forcing (interfacing between the ERA40 and ECMWF in 2002), corrected fluxes and more realistic wind stress ($\sim$10% stronger, (Brodeau et al., 2010) together with the increased vertical resolution which improves the vertical mixing coefficient cause a marked improvement in the intermediate and deep layer trends.

Salinity is the most problematic variable. Neither the interannual variability nor the trends coincide well with observations. SSS relaxation obliterates interannual variability and the degree of restoring directly affects the salinity trend. This is evident by G85 that shows very strong negative trends in surface and especially intermediate layers. Salinity is directly affected by the atmospheric forcing and freshwater balance of the simulations. Further work improving the quality and resolution of atmospheric forcing is likely to improve salinity results.

The exceptional deep convection events of 2004-2005 and 2005-2006 (Schroeder et al. (2006), Schroeder et al. (2008a), Schroeder et al. (2010) Herrmann et al.

(2010), Font et al. (2007), Smith et al. (2008)) in the NW Mediterranean were analysed in more detail using the G85 and GLORYS simulations (G70 finishes in 2004), as well as their propagation towards the Balearic Channels. These channels are of vital importance as it is where a large part of the North-South water and heat exchanges in the WMED takes part. These two exceptional winters were characterized by extreme evaporation and heat loss in the Gulf of Lion area, leading to very strong deep convection events which also modified the properties of the Levantine Intermediate Waters. In G85, the strong convection and modification of LIW is clearly visible, with the 2005-2006 winter convection actually penetrating below the LIW into deep layers. However the low resolution of the model and especially of the atmospheric forcing cause that weaker convection events do not penetrate the LIW. This causes the intermediate layers to heat up since evidenced by the 2004-2006 years, the winter entrainment of colder waters plays a vital role in maintaining the temperature of the LIW close to the observations. GLORYS shows the strong convection event in the 2005-2006 winter, and due to the availability of daily resolution the convection is very clearly marked and isolated. This is backed by the EN3 results that also show the deep convection on both winters, with 2005-2006 being the strongest. These results show that as long as the forcing conditions are strong enough, these simulations are capable of producing deep waters despite the low atmospheric forcing resolution. However, during normal convection conditions these models are not capable of propagating the convection into deep waters due to the low spatial resolution of both the model and the atmospheric forcing, which needs to be at least 50 km in order to allow the simulation of Mediterranean convection ((Li et al., 2006), (Herrmann and Somot, 2008), (Béranger et al., 2010)).

Regarding sea level, all models correctly reproduce the seasonal cycle and interannual variability but since the simulations without assimilation (G70 and G85) do not maintain the freshwater balance and underestimate evaporation (Herrmann et al., 2008b) they display exaggerated positive trends. G70 displays a trend of 14.96$\pm$1.46 mm/yr and G85 with a weaker SSS restoring shows a greater positive trend (20.27$\pm$1.37 mm/yr), indicating that at present these simulations require the restoring term in order to keep trends within acceptable levels. GLORYS has its water balance artificially adjusted at every time step therefore does not suffer this problem.

We have found that all simulations recreate the mean surface circulation correctly within their resolution limits, which prevents them from resolving the mesoscale although through EOF pattern analysis, some larger mesoscale features are indeed reproduced. Transport through the Strait of Gibraltar is within the established observational estimates (Candela (2001), Tsimplis and Bryden (2000), García Lafuente et al. (2002)), showing correct inflow (G70: 1.078 Sv, G85: 1.006 Sv), outflow (G70: 1.008 Sv, G85: 0.955 Sv) and net values (G70: 0.067, G85: 0.050 Sv). Only GLORYS appears to have a more intense exchange (1.296 Sv in, 1.243 Sv out) but correct net flow (0.052 Sv). The Ibiza and Mallorca Channels play a vital role in the WMED as it is through these channels that a large part of the North-South exchange of heat and water occurs. All simulations display the correct seasonal variability at the Ibiza Channel, with predominant southward transport in winter and northward in the summer. G70 has correct mean values but does not reproduce the 1996-1998 high southward transport events. These events are reproduced by G85 and coincide with the observations by Pinot et al. (2002) during the CANALES Experiment. It is important to note that according to G85, these years are exceptional. GLORYS produces very intense southward flow (1.5 to 2.5 Sv), far exceeding the other simulations. Observations are not available for the GLORYS years so they cannot be directly compared, however available observational data of previous years show weaker transports (0.6 to 1.3 Sv). This study contributes to the improvement of the ORCA hierarchy of simulations and points out the strengths and weaknesses of these simulations in the Mediterranean Sea.

Chapter 7

Western Mediterranean Analysis using two higher resolution simulations: NEMOMED8 ($1/8^o$) and ORCA12 ($1/12^o$)

This Chapter is based on the an article which is currenly in preparation with the following authors: Vidal-Vijande, E., A. Pascual, S. Somot, B. Barnier, J.-M. Molines, and J. Tintoré,

7.1 Introduction

In previous chapters, we have analysed simulations that due to their limited resolution, could not resolve or even produce Mediterranean mesoscale features. Given a Rossby Radius of Deformation of 10-15 km, numerical modelling studies attempting to study dynamical features and processes in the Mediterranean must be of high enough resolution to resolve them. G70, G85 and GLORYS having a $1/4^o$ coarse resolution were simulations mainly focused on large scale or basin scale processes, not the mesoscale features that dominate the Mediterranean dynamics.

This chapter builds upon the previous work by incorporating two higher resolution simulations, NEMOMED8 (1/8^o) and ORCA12 (1/12^o). To assess their behaviour in relation to the 1/4^o simulations, we start with similar basin scale analysis as seen in the previous chapters, and then we expand on the dynamic features such as the mesoscale circulation and eddy kinetic energy.

Before proceeding to the results, we should recall that unlike NEMOMED8, which is a mature simulation specifically fine-tuned to the Mediterranean Sea, ORCA12 is the first hindcast produced by the DRAKKAR group at this resolution and is aimed at assessing the capabilities of the global ORCA models at this resolution. And thus, much improvement is to be expected after this first attempt.

7.2 Temperature

We assess the basin scale mean temperature and salinity for the WMED comparing EN3 to NEMOMED8 and ORCA12. Since ORCA12 is a shorter simulation than previous models, we focus on the altimetry period 1993-2007. Due to the shorter period studied, in this case we have used the available monthly data instead of annual means seen in figures 5.1, 5.3, 6.1 and 6.2. The seasonal cycle has been removed.

As is to be expected, monthly data yield higher variability in both the simulations and the hydrography. As mentioned in previous chapters, caution must be taken when considering the hydrography variability since sustained monthly observations are scarce and not uniform in space.

Figure 7.1 (a) shows the temperature variability at surface, intermediate and deep layers in the WMED. At surface layers, the three datasets show good agreement as has been the case in previous chapters, with high correlations of 0.76 for NM8 and 0.69 for O12. Both the NM8 and O12 simulations behave very similarly and follow EN3 closely. EN3 displays higher variability at certain peaks. There is a significant difference in mean surface layer temperature between EN3 and the simulations, with EN3 at 16.84^{o}C, O12 15.84^{o}C and NM8 at 15.65^{o}C.

At intermediate layers (150-600 m) EN3 shows a higher degree of variability than the simulations. NM8 follows the overall pattern set by EN3 without defined peaks (correlation of 0.47), and O12 displays a positive trend up to 2005 with upwards step pattern every winter. The mean temperatures of the

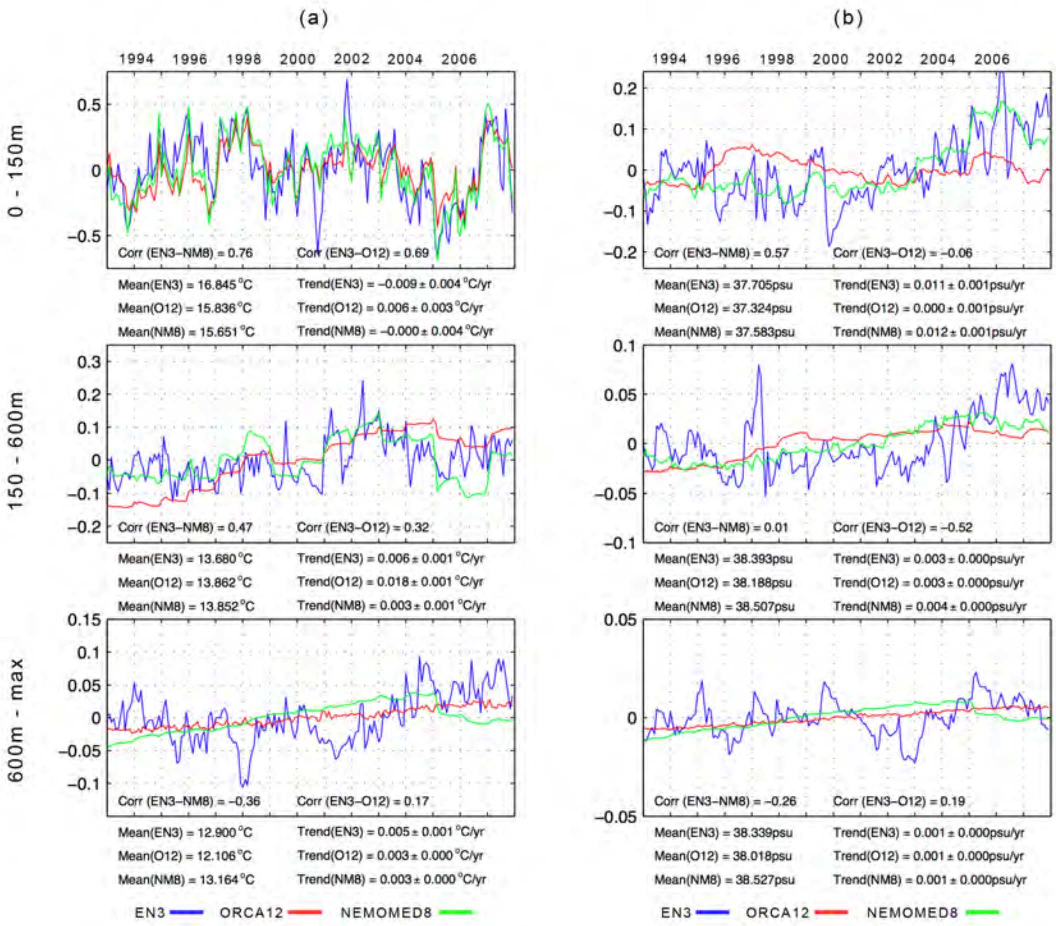

Figure 7.1: WMED mean temperature (a) and salinity (b) anomaly at different layers. Comparison between EN3 (blue), ORCA12 (red) and NEMOMED8(green) 1994 to 2007.

three datasets are much closer in this case, with the simulations essentially the same and EN3 just $\sim$0.2^{o}C lower.

At deep layers (600 m to bottom), the simulations have very low variability and negligible trend (although slightly positive). EN3 on the other hand shows considerable variability, which is harder to positively rely on due to the low number of actual measurements that reach into this layer. The few CTD measurements that reach beyond 600 m would certainly be scarce and not uniform throughout the WMED. Regarding mean temperatures, ORCA12 is significantly colder than both EN3 and NEMOMED8.

7.3 Salinity

Figure 7.1 (b) represents the salinity at different layers. As with the previous ORCA simulations, salinity is a parameter that is hard for simulations to reproduce because it depends on several atmospheric forcing factors which have considerable error over the open ocean (such as precipitation, wind stress and evaporation). In this regard, O12 does not give very good results at surface layers, with its variability not coinciding at all with EN3 and having statistically insignificant or even negative correlations, it is however a better result than seen in the $1/4^o$ G70 and G85 simulations since the trend remains stable. On the other hand NM8 is a considerable improvement; although the variability is lower than EN3, NM8 does follow the same lower frequency pattern as the hydrography and actually has a significant positive correlation of 0.57.

This becomes less so at intermediate and deep layers, where NM8 and O12 do follow the overall trend but do not show a particularly good agreement with EN3 variability. We must again be cautious to consider the EN3 variability due to the frequency and spatial distribution of the actual measurements, which in the case of salinity are even lower than those of temperature.

One of the problems of numerical models and salinity is that some of them require surface salinity restoring in order to avoid significant drift. Salinity relaxation can be useful in many of the world's large oceans where the variability is dominated by the seasonal cycle, thus restoring salinity to a climatology helps keep realistic salinity values. However, the Mediterranean variability is extremely complex, and while there is a dominant seasonal cycle, many other important factors play into the total variability signal. For this reason, a standard salinity restoring to a climatology does not work well in the Mediterranean. In fact, the salinity forcing and its interannual variability is essential for the reproduction and understanding of certain key Mediterranean processes such as the EMT. Therefore SSS relaxation as well as any other modelling trick limiting the spatial and temporal variability of the 3D thermohaline structure of the Mediterranean should be avoided (Beuvier et al., 2010). In this case, O12 is using a fairly strong surface salinity restoring (more details in Chapter 3) whereas NM8 actually does not apply any salinity restoring to its simulation.

7.4 Deep Water Formation in the Gulf of Lion

We analyse the deep water formation capabilities of NM8 and O12 in the Gulf of Lions and compare it with EN3. It must be noted that NM8 has already been extensively tested in this area by Herrmann et al. (2010), however we include our analysis for completeness using hovmöller diagrams for comparing with the ORCA simulations (which is not done by the aforementioned authors). As in section 6.4, we analyse the temporal evolution of the vertical temperature and salinity profiles (mean of a 1^{o}x1^o square centred at 42.6^{o}N, 4.4^{o}E). Figure 7.2 shows the EN3 reference dataset. The seasonal summer warming and winter cooling at the surface is clearly visible, with warming reaching down to a maximum depth of about 100 - 150 meters and winter cooling which causes vertical mixing and convection normally reaching the intermediate layer at $\sim$300 - 400 meters. The deep convection events display a marked interannual variability, with years of intense and deep convection and years of very reduced vertical mixing.

The NEMOMED8 simulation (Figure 7.4) clearly displays the interannual variability in the strength of vertical mixing, with intermittent events of deep convection where the mixing reaches below 1000 meters. As opposed to the simulations studied in previous chapters (G70, G85, GLORYS), deep convection is not limited to the very intense atmospheric forcing years of 2005-2006, but also occur with less intensity in previous years, more in agreement with the observational datasets. In salinity this is also visible, with freshening of the water column during these deep convection events, being more intense in during the 2004-2005 and 2005-2006 winters. A notable difference between NM8 and EN3 is the intermediate layer temperature, with NM8 being slightly warmer $\sim$13.8^{o}C with regards to EN3 $\sim$13.4^{o}C. Likewise in salinity, the intermediate layer salinity for NM8 is saltier ($\sim$38.65 psu) than EN3 ($\sim$36.50 psu).

The ORCA-12 simulation (Figure 7.4 has a very different vertical temperature profile than EN3 and NM8. Whereas in both NM8 an EN3, the bottom limit if the intermediate waters is not well defined, cooling progressively from the maxima at around 400 meters down to about 800 meters, the intermediate waters in O12 have their lower limit at a very marked thermocline between 400 and 500 meters depth. They are also significantly warmer than NM8 and EN3 at between 14.2 and 14.7^{o}C. Deep layer temperatures are similar to the observations, creating a very strong thermocline.

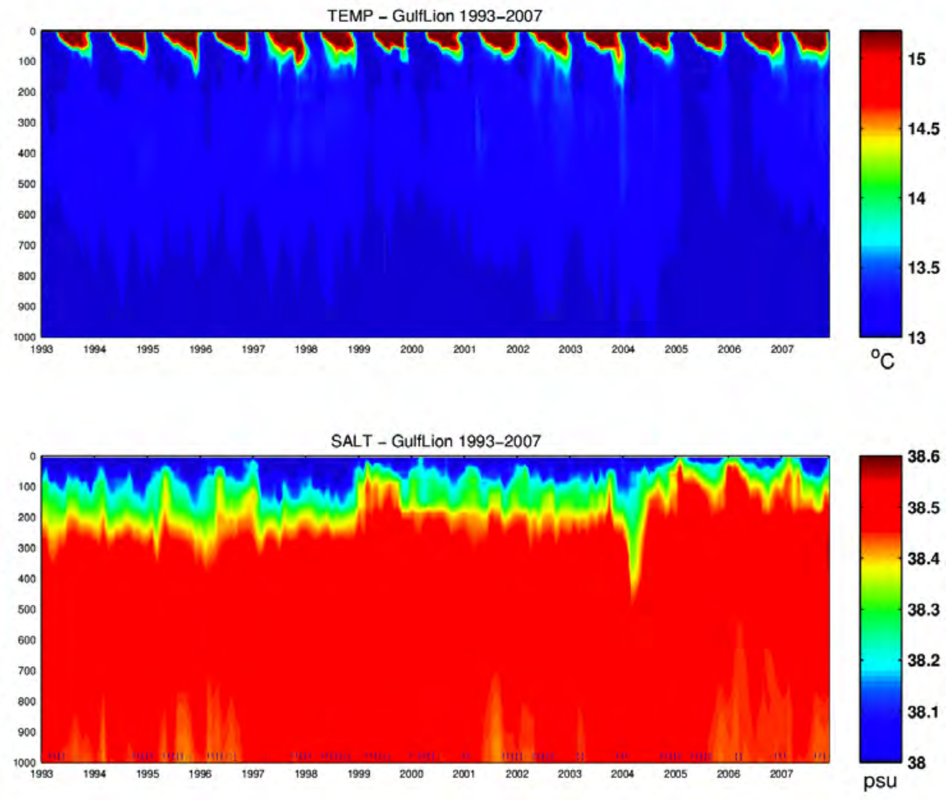

Figure 7.2: Hovmöller diagrams showing the temporal evolution of temperature (top) and salinity (bottom) of a 1^o x 1^o area at the center of the Gulf of Lion for the EN3 hydrographic dataset.

Interannual variability in the winter convection events is also clearly observed in O12 although the water in these events is warmer than EN3 and NM8 and does not appear to significantly cross the thermocline at the deep limit of the intermediate waters. It therefore appears that deep convection does not occur, probably related to the strength of the thermocline at ∼500 meters. The warmer (less dense) waters mixing down from the surface are not dense enough to cross the thermocline which is too stable for winter vertical mixing to break it up. This appears to be the case even in the severe 2004-2005 and 2005-2006 winters.

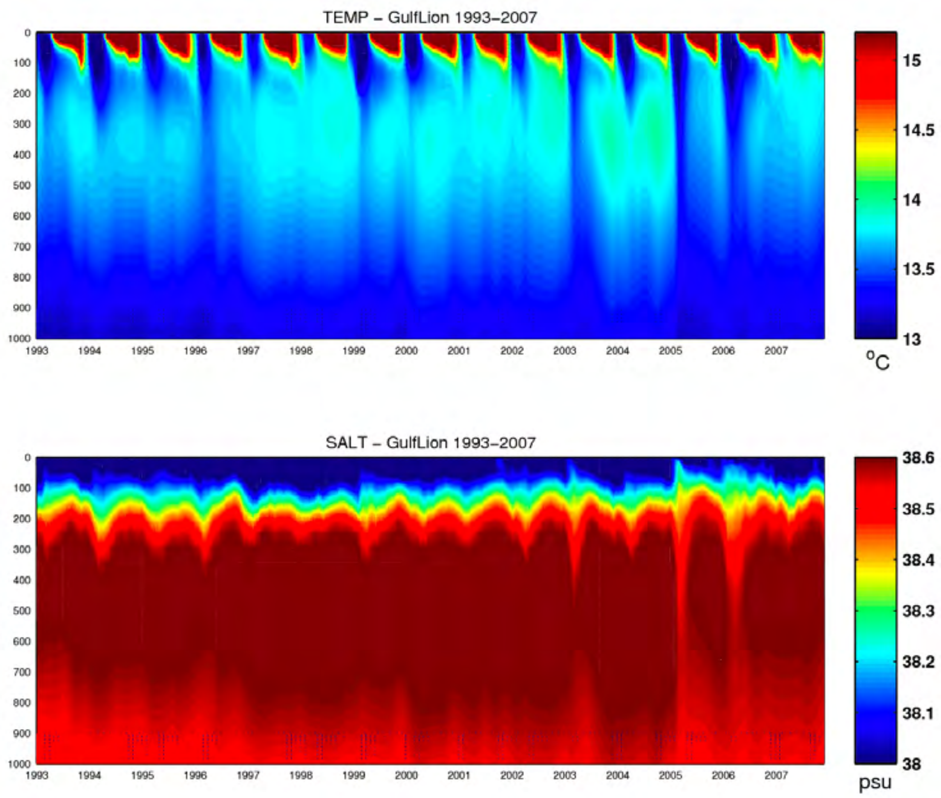

Figure 7.3: Hovmöller diagrams showing the temporal evolution of temperature (top) and salinity (bottom) of a 1^o x 1^o area at the center of the Gulf of Lion for the NEMOMED8 simulation.

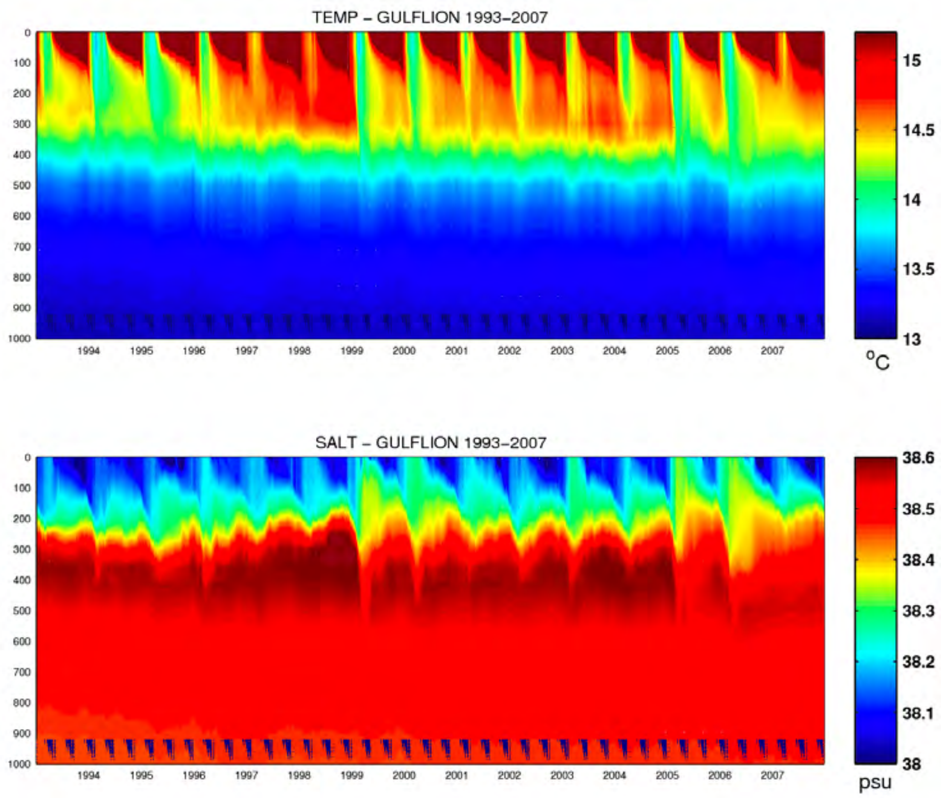

Figure 7.4: Hovmöller diagrams showing the temporal evolution of temperature (top) and salinity (bottom) of a 1^o x 1^o area at the center of the Gulf of Lion for the ORCA-12 simulation.

7.5 Mean Surface Circulation

In the following sections we will focus on the dynamical characteristics of the WMED and how the NM8 and O12 simulations reproduce them by comparing to altimetry. These simulations with their higher resolution are now theoretically capable of producing Mediterranean mesoscale, something the ones used in previous chapters could not do.

We start by looking at the mean circulation of the three datasets in the WMED. This will provide a baseline on whether the simulations are getting the "basics" right and where they could be failing. Although we take altimetry as the reference when assessing the simulations' performance, one must not forget that altimetry is not perfect, especially regarding the mean circulation. Most of the mean circulation pattern derived from altimetry actually comes from the Mean Dynamic Topography (MDT) (Rio et al., 2007) which is added to altimetry to get the Absolute Dynamic Topography (ADT). As described in section 3.6 the MDT itself is actually mathematically derived from a variety of sources including numerical simulations, drifter tracks and other observations. All of these data sources have their own associated errors.

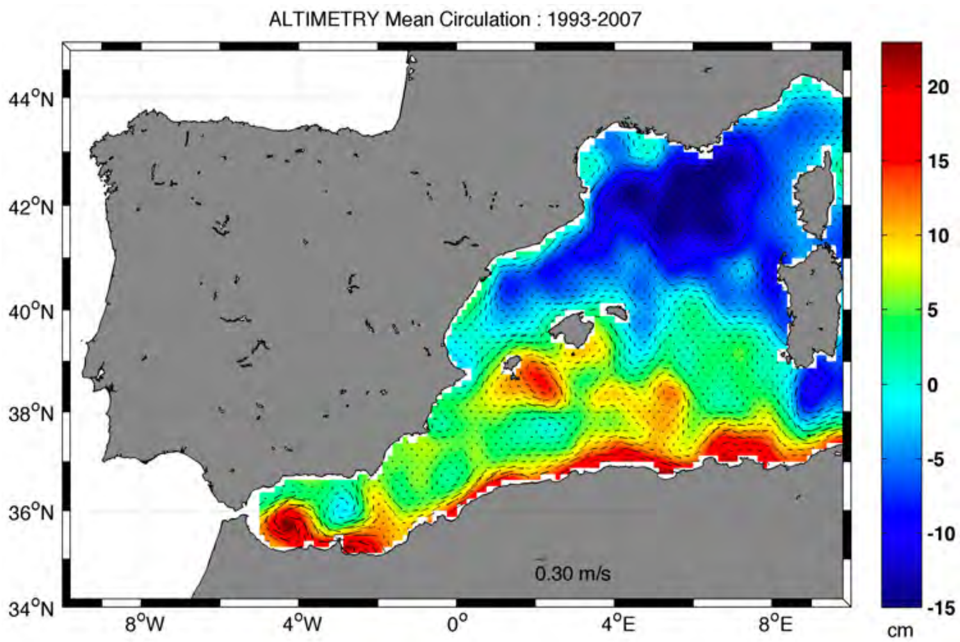

Figure 7.5: Altimetry mean geostrophic circulation in the WMED derived from the ADT (MDT+SLA) for the 1993-2007 period.

Figure 7.5 presents the WMED mean circulation derived from altimetry. We start at the Alboran Sea, which is the location where exchange of water between the Atlantic and the Mediterranean takes place through the Strait of Gibraltar. As such, it is characterized by an intense inflow/outflow regime and complex circulation patterns. Atlantic waters enter through the Gibraltar Strait at surface and form a powerful inflow current called the Atlantic Jet. This jet meanders and forms a quasi-permanent gyre at the western part of the Alboran Sea called the West Alboran Gyre (WAG) (Viúdez et al. (1998), Baldacci et al. (2001), Flexas et al. (2006)), and an intermittent Eastern Alboran Gyre (EAG). The eastern boundary of the EAG usually forms the well known Almería-Orán front (Tintoré et al., 1988) and marks the start of the Algerian Current (AC) (Astraldi et al. (1999), Millot (1999)). At its start close to 0^o, the AC is relatively narrow (30-50 km), flowing very close to the coast. As it progresses eastward, its width and separation from the coast vary, and due to baroclinic instabilities in its flow, regularly forms meanders that can eventually detach from the current and become both cyclonic and anticyclonic coastal eddies (Olita et al., 2011). Some of the stronger eddies, which are mostly anticyclonic, may become "open sea eddies" reaching the Balearic Islands and the Liguro-Provençal Basin (Millot, 1999). The AC and its associated eddy-generating capacity dominate the circulation of the Algerian Basin.

The northern part of the WMED is in turn dominated by the Northern Current, which flows along the coasts of Italy, France and Spain following the bathymetry. Flux is maximum during a long winter period (Dec-May) with significant mesoscale variability, and weakens during the summer (Millot, 1999). The Gulf of Lions is a site of intense mesoscale activity and winter deep water formation (MEDOC Group, 1970). Due to the action of the Northern Current, the circulation here is generally cyclonic in nature. The Northern Current flows southward along the Iberian coast and splits in two branches, one recirculating into the Balearic Current (Ruiz et al., 2009) and the other continuing south through the Ibiza Channel (Pinot et al., 2002).

As mentioned at the beginning of this section, the mean circulation patterns derived from altimetry, while assumed to be mostly correct, can have errors associated to the MDT. A clear example of this is the anticyclonic eddy found just south-east of Ibiza. This is probably an artefact of the MDT (A. Pascual, personal communication from several observational studies not yet published) and may not be a predominant circulation feature.

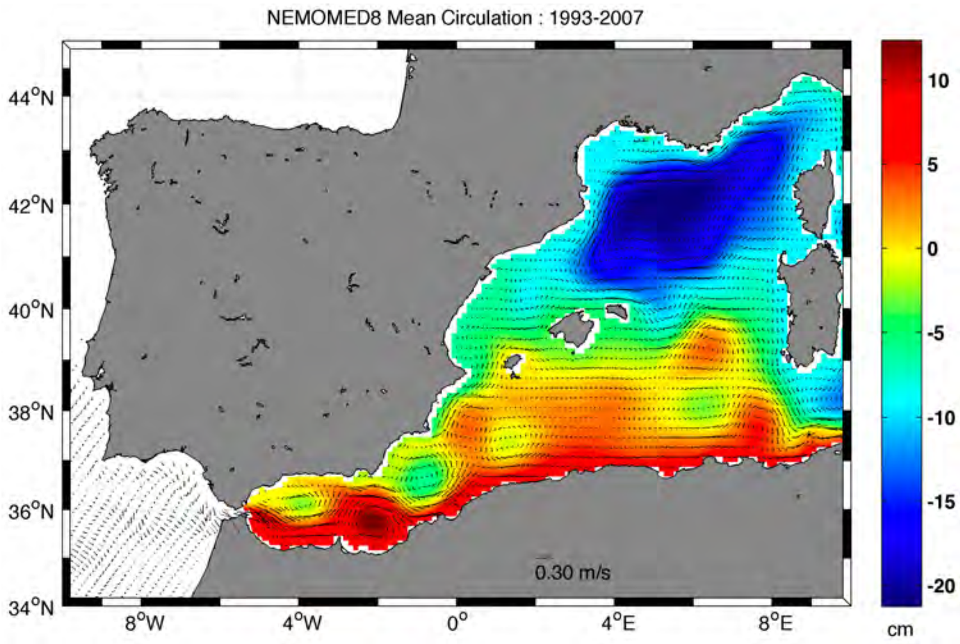

Figure 7.6: NM8 mean geostrophic circulation in the WMED derived from the full SSH signal for the 1993-2007 period.

Figure 7.6 presents the WMED mean circulation derived from NM8 sea surface height. At first glance, the overall circulation displays a smoother field with less intricate mesoscale structure. In the Alboran Sea the WAG is not present, only the EAG, which in this case is more intense than in altimetry. The Almería-Orán Front that sits between the EAG and an intense cyclonic gyre to the north-east is very strong. The AC which flows east is not so clearly defined, with its outer edge extending further out into sea and becoming confused with the anticyclonic mesoscale activity in the center of the Algerian Basin. In the northern part of the WMED, the Northern Current and the intense cyclonic circulation of the Gulf of Lions are clearly visible. The Northern Current has most of its recirculation occurring further north, with a weaker signal reaching west of Mallorca and recirculating into the Balearic Current. Also visible is the flow through the Ibiza Channel, completing the circulation loop of the Mediterranean.

Figure 7.7 presents the WMED mean circulation derived from O12 sea surface height. Despite having higher resolution than the other two datasets (at 1/12^o), the mean circulation field of O12 is the smoothest of the three with very few discernible mesoscale features. In the Alboran Sea, the WAG appears in a displaced mode (Viúdez et al., 1998; Vargas-Yáñez et al., 2002; Flexas

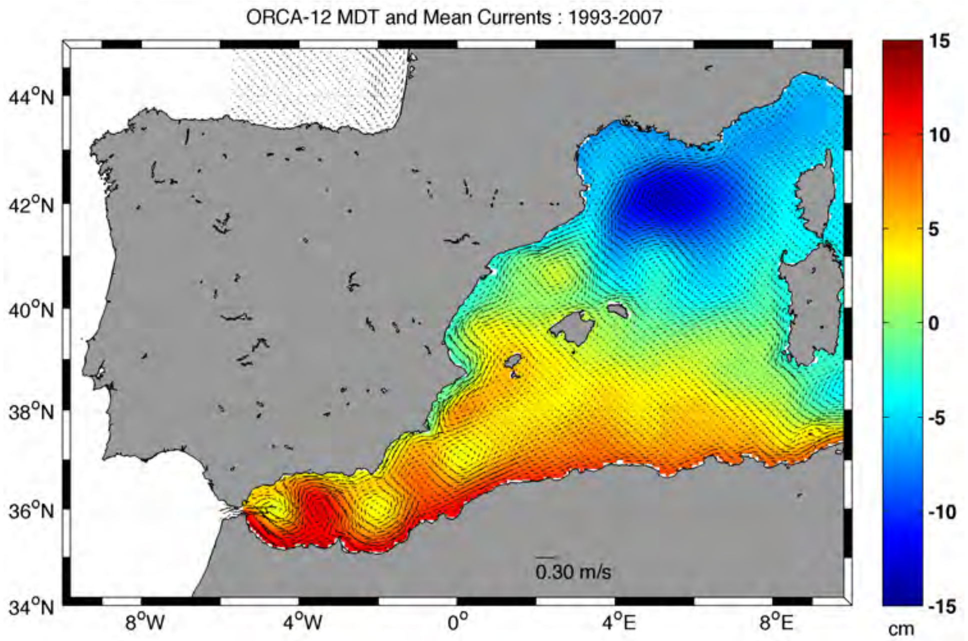

Figure 7.7: O12 mean geostrophic circulation in the WMED derived from the full SSH signal for the 1993-2007 period.

et al., 2006) and the EAG is not present. Instead, two cyclonic eddies are formed in their place by the meandering Atlantic Jet. The Algerian Current is visible although its outer border is not well defined, becoming more of a smooth gradient which mixes with the Algerian Basin mesoscale activity. The Northern Current appears as a large cyclonic circulation feature in the outer Gulf of Lions, with an anticyclonic eddy centred at 41^{o}N, 3^{o}E blocking its way further south into the Balearic Sea. Therefore the Northern Current's recirculation happens very far north. In fact, one of the strongest currents is the northward flow through the Ibiza Channel, which follows the bathymetry close to the Iberian Peninsula. When this northward current meets the Northern Current flowing south-west, the aforementioned blocking anticyclonic eddy forms.

As can be seen, the circulation scheme of O12, while overall correct (at basin scale) in the direction and intensity of the flow, the finer detail of mesoscale circulation is not adequately resolved.

7.6 Eddy Kinetic Energy

Eddy Kinetic Energy (EKE) is an excellent way to characterize the mesoscale activity of the ocean, which in turn is one of the dominant signals of ocean circulation, however few studies have focused on the study of EKE in the Mediterranean Sea. Some of the current available studies that include Kinetic Energy (KE) are from Demirov and Pinardi (2002) and Molcard et al. (2002) based on numerical simulations (total KE), Poulain and Zambianchi (2007) using drifters and Iudicone et al. (1998), Ayoub et al. (1998) and Pujol and Larnicol (2005) using altimetry (EKE), showing that KE/EKE display significant temporal variability. Numerical models and altimetry are currently the two best methods to study basin scale EKE due to their complete temporal and spatial coverage. Current measurements from drifters or stationary moorings can be more accurate but their spatial distribution is not sufficient for adequate coverage.

In this section, we study the sea surface variability by analysing the geostrophic eddy kinetic energy (EKEg) from O12, NM8 and altimetry. This is the eddy kinetic energy calculated from the sea level anomaly (SLA) signal. For altimetry, we use the direct SLA fields without adding the mean dynamic topography (MDT). For the simulations, we first subtract the mean sea level signal for the 1993-2007 period and then calculate the geostrophic currents from the SLA slope.

Figure 7.8 shows the mean EKEg calculated from altimetry for the 1993-2007 period. There is a clear north-south difference in EKEg levels, with maximum values corresponding to the Alboran Sea and the path of the Algerian Current. In contrast, the northern WMED has very low values. The highest values of EKEg are associated with the eastern boundary of the West Alboran Gyre (WAG), the full structure of the WAG is not visible since it is a quasi-permanent feature which is not present in the SLA. The intermittent Eastern Alboran Gyre (EAG) is clearly visible, as well as several mesoscale features along the Algerian coastline. Another area of high EKEg is the region south-west of Sardinia, which is characterized by the regular formation of anticyclonic eddies that propagate both towards the east and north. A weaker signal corresponding to the 1998 anticyclonic eddy north of Mallorca (Pascual et al., 2002) is also visible. This is important since the 1998 eddy was a unique feature that was only present for a few months, however it leaves an impression over the mean of the 14 year period studied. Therefore singular instances of

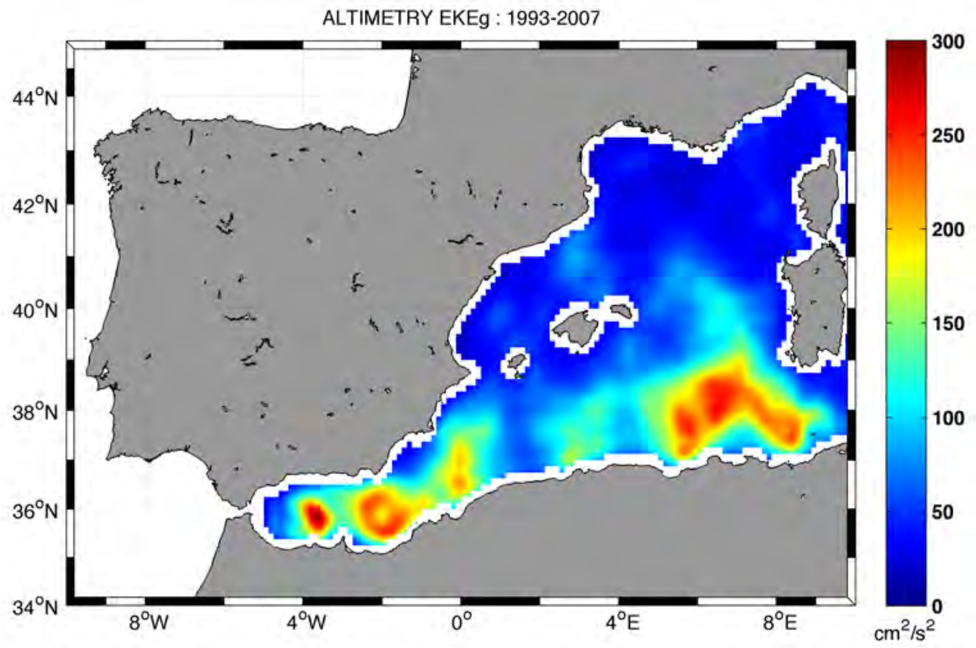

Figure 7.8: WMED mean Geostrophic Eddy Kinetic Energy (EKEg) map calculated from altimetry SLA for the period 1993-2007.

high EKEg signals can skew the overall mean, complicating the interpretation of the mean EKEg state of the ocean (Pujol and Larnicol, 2005). It is therefore also useful to study the mean temporal EKEg evolution. Figure 7.9 shows the temporal evolution EKEg for the three regions of the WMED with most of the variability; the Alboran Sea, the Algerian Basin and the North Balearic Sea.

The Alboran Sea is the region where higher EKEg is found (with typical maxima of ∼450 to 500 cm^2/s^2), with intense interannual variability but few distinct peaks. This denotes an area where EKEg is regularly high, and the mean spatial EKEg signal is probably representative of the mean state. In the Algerian Basin a ∼2.5 year signal is seen below the interannual variability between 1997 and 1999. According to Pujol and Larnicol (2005) this is due to the presence of two anticyclonic eddies detected in 1997, these were also studied by (Puillat et al., 2002) and had a lifetime of about two to three years, therefore considerably influencing the EKE variability. In the North-Balearic Sea, the clear spike related to the 1998 anticyclonic eddy is also affecting the overall mean state of the region.

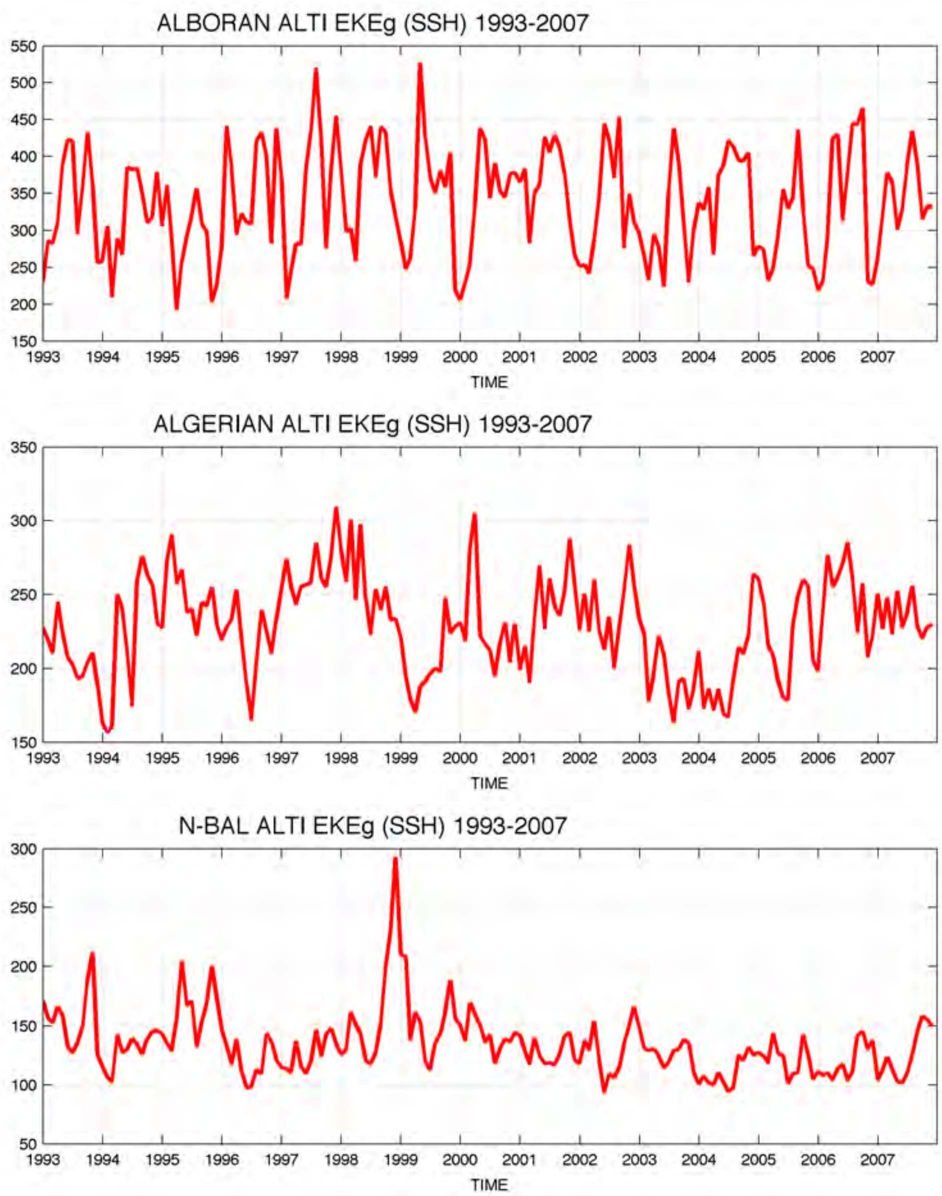

Figure 7.9: Mean altimetry EKEg timeseries for the Alboran Sea (top), Algerian Basin (middle) and North Balearic Sea (bottom).

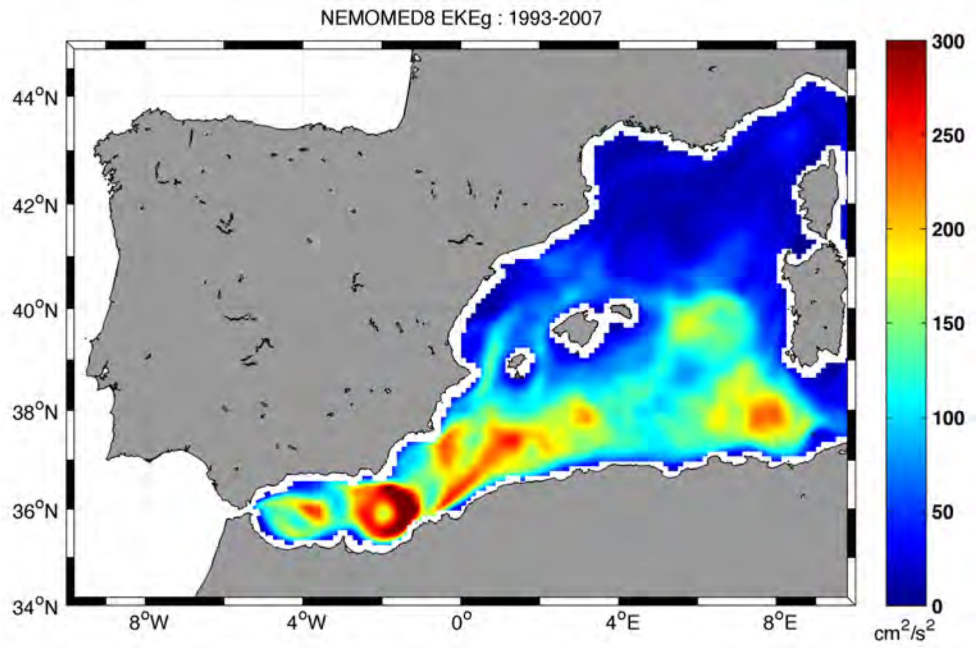

Figure 7.10: WMED mean Geostrophic Eddy Kinetic Energy (EKEg) map calculated from NM8 for the period 1993-2007.

Figure 7.10 shows the mean EKEg calculated from NM8 for the 1993-2007 period. NM8 has a similar overall distribution of high EKEg regions, with maxima in the Alboran Sea and Algerian Basin. In this case, the strongest signal is seen in the EAG, which is very clearly defined. The WAG is also visible, with a maxima at the eastern edge, but with the presence of the entire gyre unlike in altimetry. This denotes a more variable WAG with respect to altimetry SLA observations. Higher EKEg is also found at the start of the Algerian Current but not so much to the south-west of Sardinia. Overall the EKEg levels are similar to altimetry in the 0 to 300 cm^2/s^2 range. What is present in NM8 but not clearly visible in altimetry is the flow through the Ibiza Channel and to a lower extent the Mallorca Channel, as well as their continuation as the Balearic Current.

The temporal evolution of NM8 EKEg (Figure 7.11) also presents the occurrence of singular events with the potential to influence the mean spatial EKEg patterns. In the Alboran Sea a very intense peak at the end of 1993 with a value of $\sim$700 cm^2/s^2 which likely represents a very intense EAG is

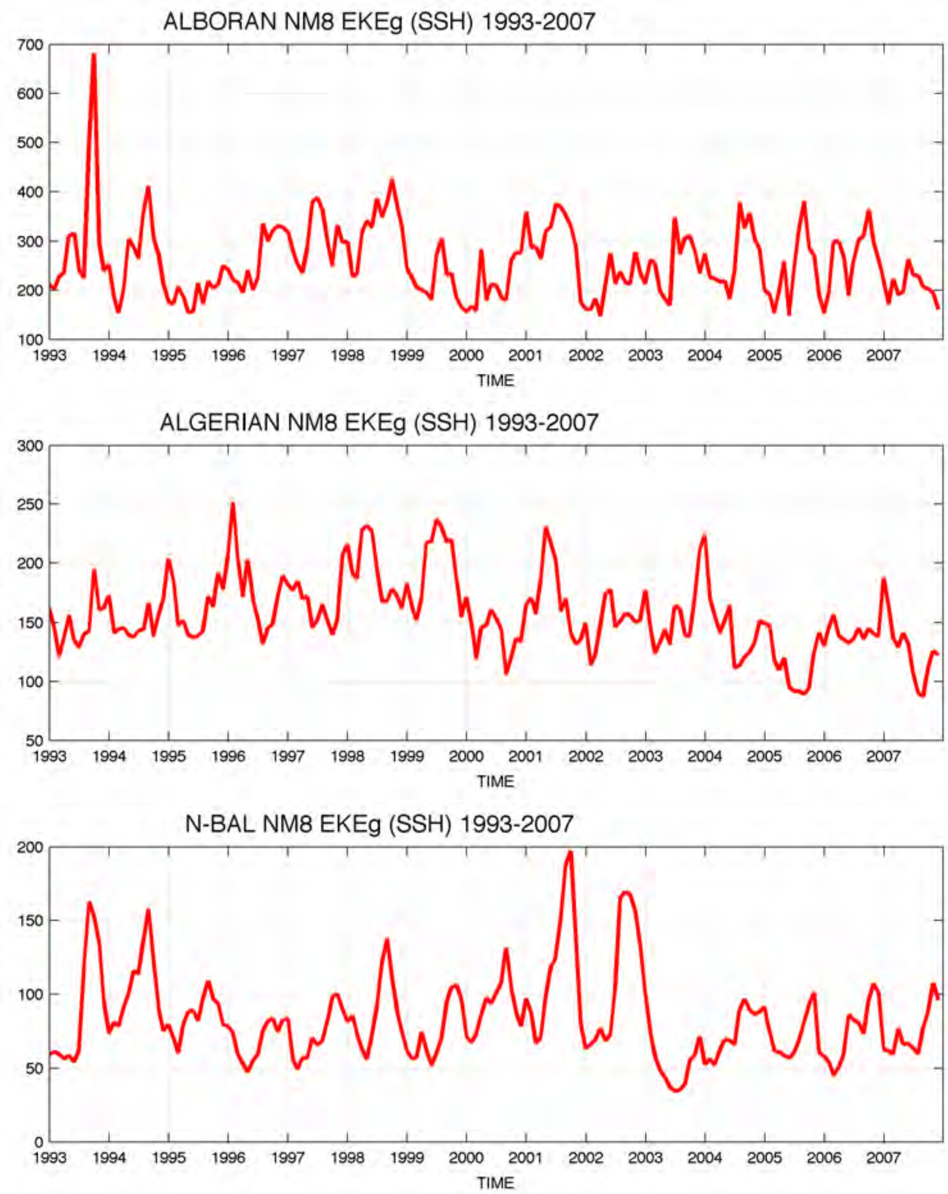

Figure 7.11: Mean NM8 EKEg timeseries for the Alboran Sea (top), Algerian Basin (middle) and North Balearic Sea (bottom).

certainly affecting the distribution of EKEg values in the spatial means. In the Alboran Sea, there are seasonal maxima but no discernible outlying peaks. In the N-Bal region, a few higher EKEg peaks, likely related to increased flow through the Ibiza Strait are leaving an impression on the spatial means.

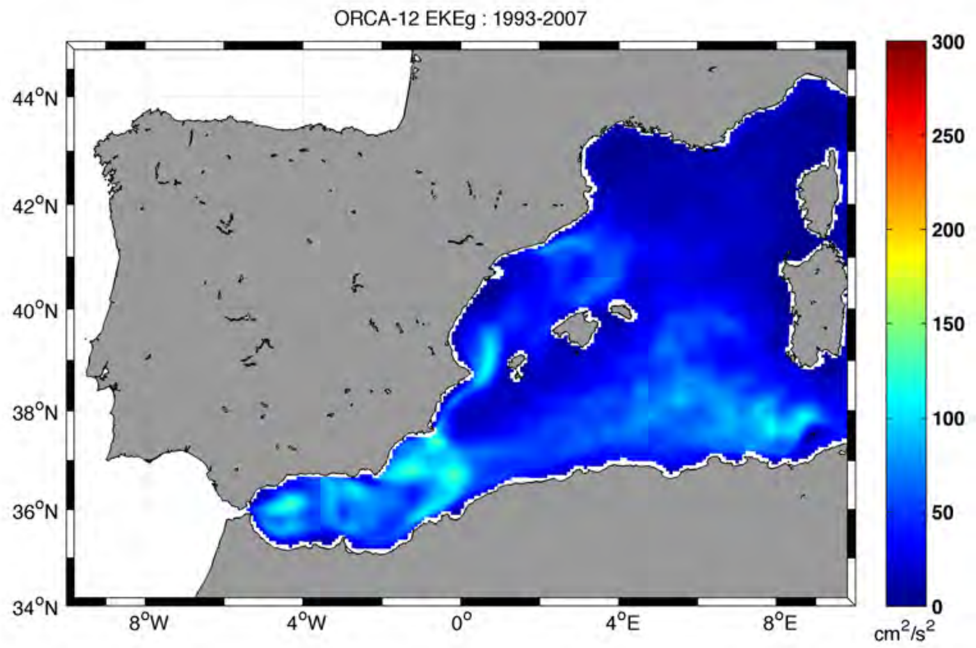

Figure 7.12: WMED mean Geostrophic Eddy Kinetic Energy (EKEg) map calculated from O12 for the period 1993-2007.

Figure 7.12 shows the mean EKEg calculated from O12 for the 1993-2007 period. Immediately visible are the reduced levels of EKEg, which are less than half those of altimetry and NM8. This is due to a relatively stable mean circulation with little variability outside of the mean, therefore when subtracting the MDT to leave the SLA, a larger part of the variability is gone with it. Despite the reduced EKEg values, the locations of maximum EKEg remain similar to NM8 albeit with some differences. In the Alboran Sea, the WAG and EAG are partially visible, but not as clearly as in NM8 or altimetry. The high EKEg region at the start of the AC is the most intense region in the entire domain. The flow through the Ibiza Channel is also very intense, showing that this location has high variability (not removed with the MDT). In the Algerian Basin, there is also a high EKEg region to the south-west of

Sardinia as with NM8 and altimetry.

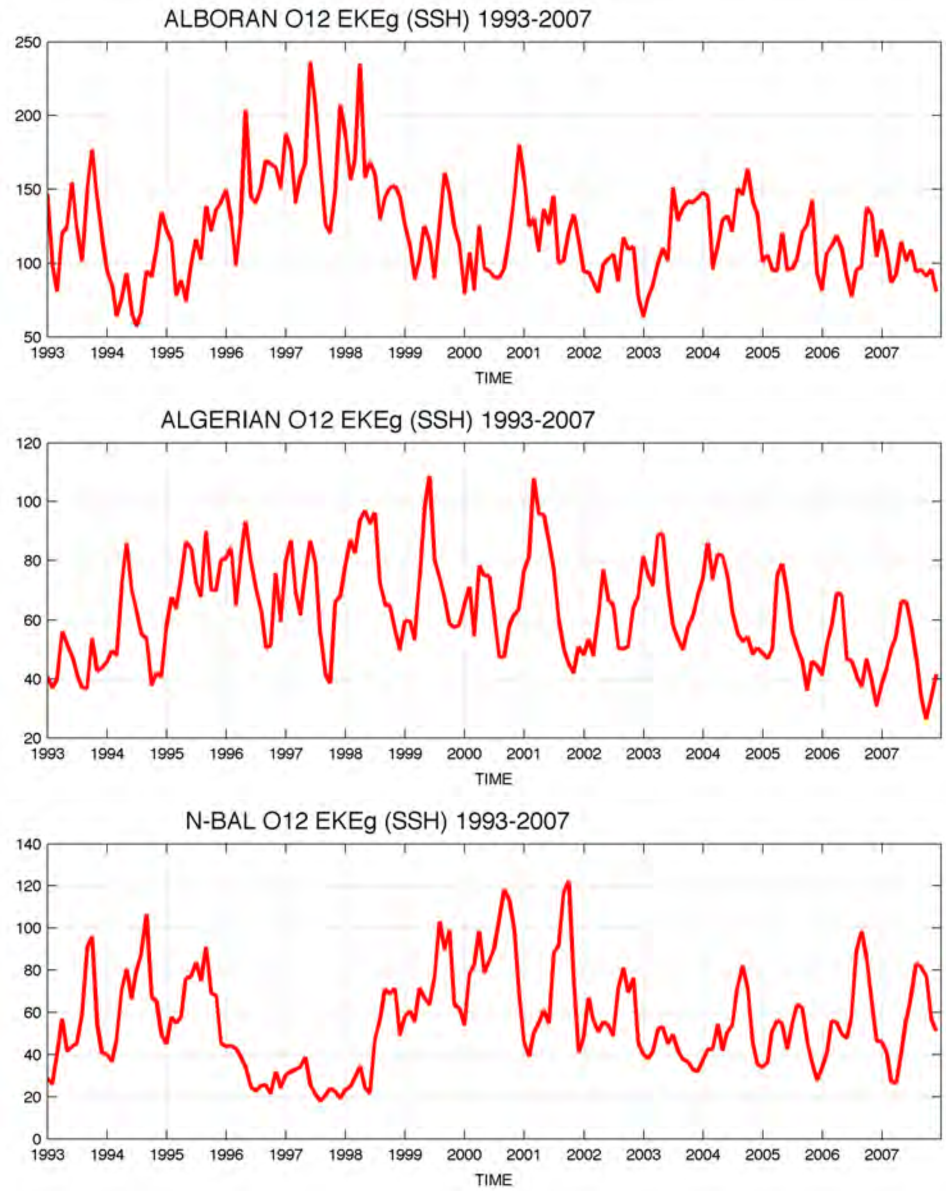

Figure 7.13: Mean O12 EKEg timeseries for the Alboran Sea (top), Algerian Basin (middle) and North Balearic Sea (bottom).

The temporal evolution of O12 EKEg (Figure 7.13) shows interannual variability in all three regions being studied, without any particular outliers which could obviously skew the mean spatial patterns. The peaks display a seasonality in the Algerian Basin (with maxima in winter) and the North Balearic Sea (with maxima in summer). In the Alboran Sea, the seasonal maxima are hard to pinpoint since they do not appear to happen regularly in any particular season.

7.7 Mean Circulation Component Analysis using EOFs

We analyse the mean circulation in three different regions of the WMED (Alboran Sea, Algerian Basin and North WMED) using Empirical Orthogonal Functions (EOFs) on the Absolute Dynamic Topography (ADT = MDT + SLA) of altimetry, and the sea surface height (SSH) parameter of NEMOMED8 and ORCA-12. We calculate EOFs on the full SSH /ADT signal (hereafter EOF-F) and also on the SSH/ADT anomaly by removing a temporal mean (1993-2007) at each grid point (hereafter EOF-A). The analysis of both EOF-F and EOF-A is useful because in the case of EOF-Fs, the different components of the mean circulation can be analysed and quantified separately. EOF-As allow the study of different variability signals which are obscured by the dominating mean circulation.

For the following analysis, we divide the WMED into subregions to better account for the variability in each subregion. For ease of understanding the analysis, we recall the season definitions : Winter (January - March), Spring (April - June), Summer (July - September), Autumn (October - December).

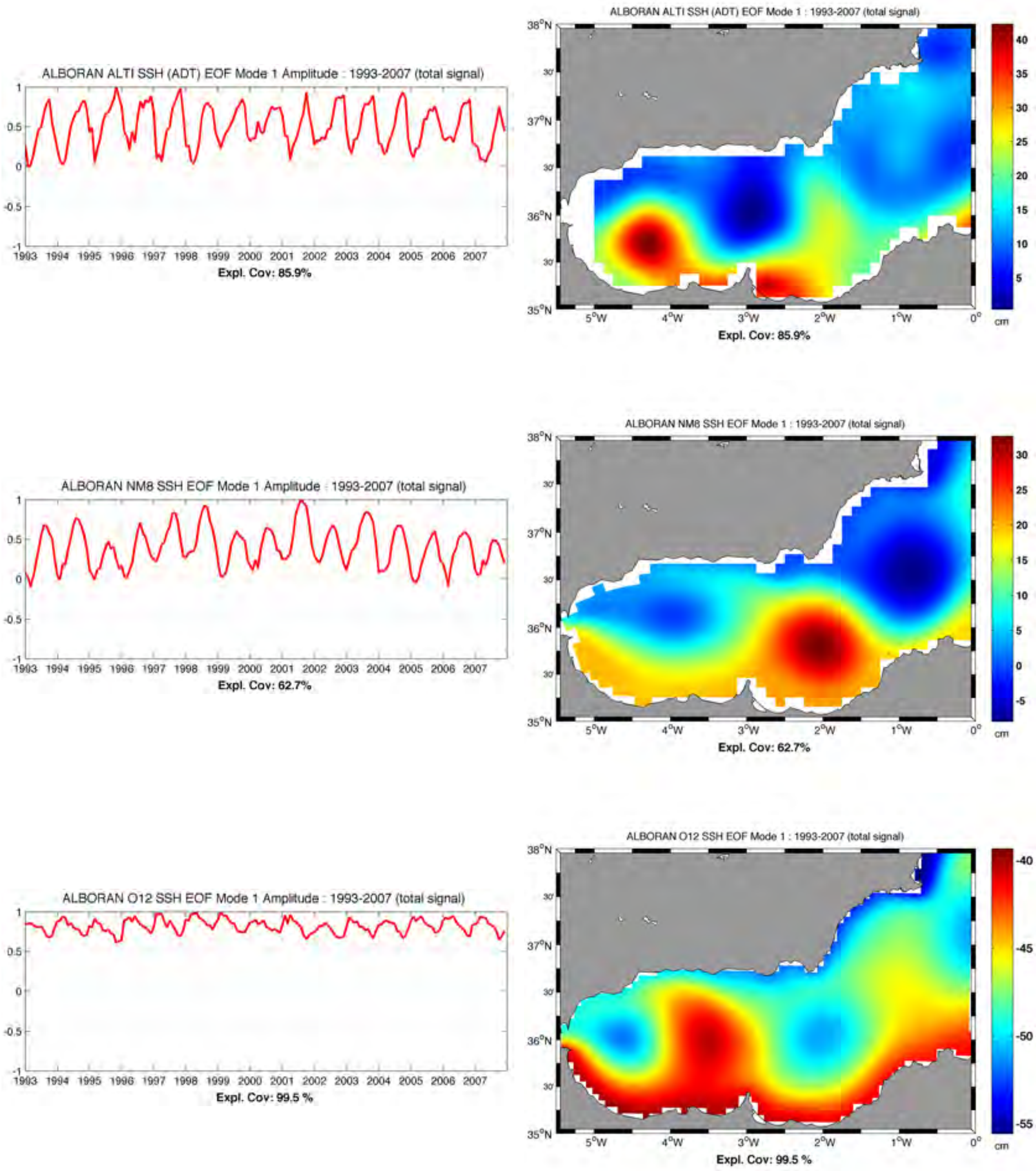

Figure 7.14: 1st EOF-F mode of total SSH for the Alboran Sea with amplitude (left) and pattern (right). Altimetry (top), NEMOMED8 (middle) and ORCA12 (bottom)

Alboran Sea

1st EOF-F Mode (Figure 7.14)

For altimetry, the first EOF-F mode accounts for most of the variance (85.9%) and explains the seasonality of the region. Both the WAG and EAG gyres are present but with clear predominance of the WAG (reflected by the gradient and covariance explained by this mode), which is present all year round with a minima in winter and maximum towards the end of summer. There is never an inversion of the anticyclonic circulation (amplitude is always positive, never negative). Note that this first EOF-F mode is very similar to the MDT (Rio et al., 2007).

For NM8 the seasonal variability coincides with altimetry in phase and amplitude, with more interannual variability. The EOF-F pattern does not reproduce the WAG, only the Atlantic Jet with some curvature. Conversely, the variability of the EAG is the predominant signal as well as an intense cyclonic gyre located north-east of the EAG marking a sharp front between both gyres, clearly defining the Almería-Orán front. The south-east boundary of the cyclonic eddy may correspond to the beginning of the AC. The explained covariance is lower than for altimetry but is still high explaining 62.7% of the covariance.

O12 displays a different spatial pattern, in this case the WAG appears displaced eastward, a situation that has been observed by authors such as Viúdez et al. (1998), (Vargas-Yáñez et al., 2002) and Flexas et al. (2006) where the WAG can migrate northwards and be ”pushed” eastwards by the Atlantic Jet, although this is not the known predominant state of the Alboran Sea. East and West of the WAG are two cyclonic gyres caused by the meandering flow of the strong Atlantic Jet. There is no presence of the EAG or the Almería-Orán front. This first EOF-F mode explains 99.5% of the covariance and has little seasonal and interannual variability suggesting this spatial pattern is very stable.

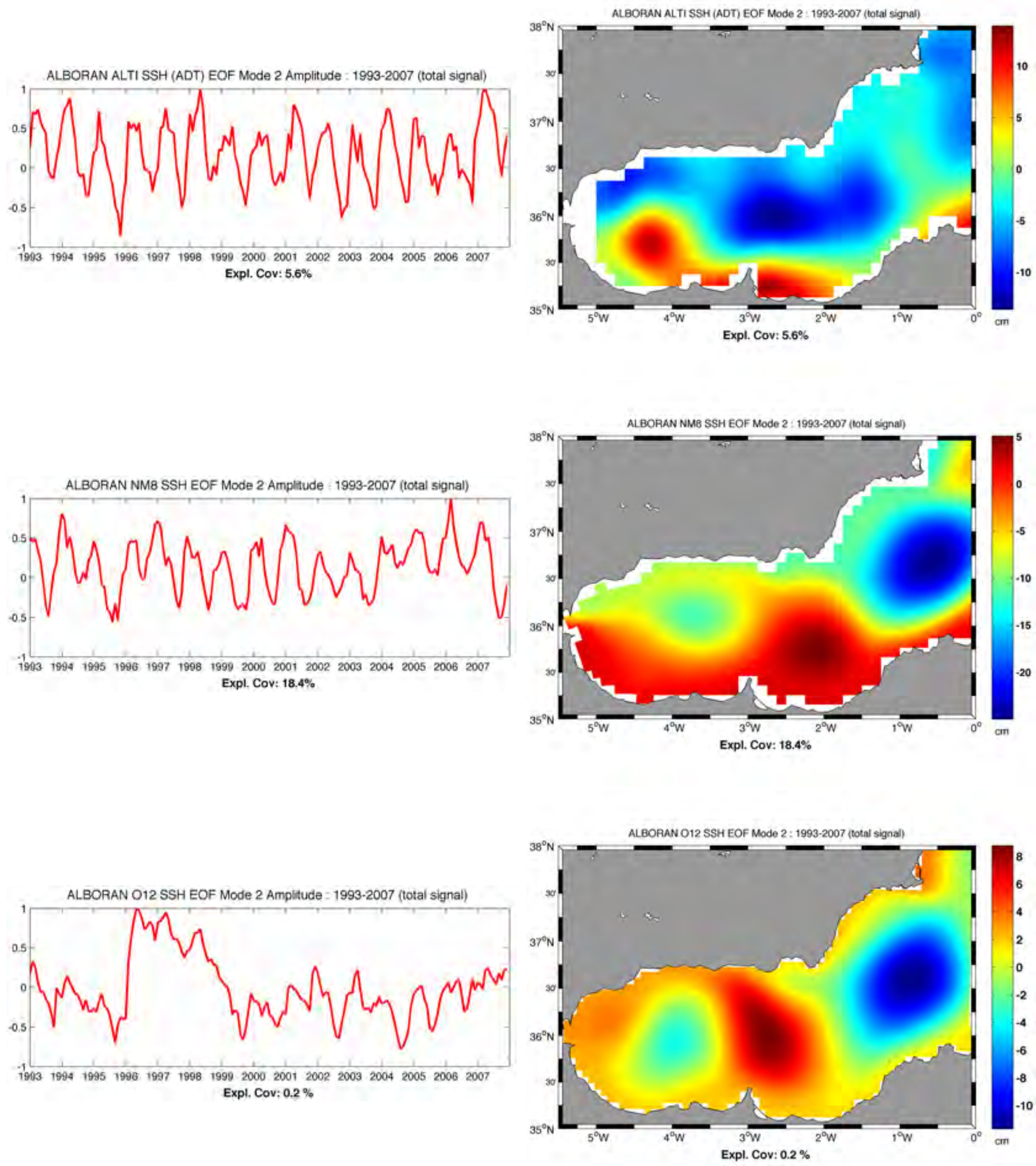

Figure 7.15: 2nd EOF-F mode of total SSH for the Alboran Sea with amplitude (left) and pattern (right). Altimetry (top), NEMOMED8 (middle) and ORCA12 (bottom)

2nd EOF-F Mode (Figure 7.15)

The second altimetry EOF-F mode has a similar pattern in the WAG area with respect to the first EOF-F mode but with an inverted phase in the temporal amplitude, essentially balancing out the variability of the WAG in the first EOF-F mode. While the 1st EOF-F has only positive amplitude values, the 2nd EOF-F has both positive and negative values, with almost 180 degrees lag between them; the addition of both results in a quasi permanent positive signal. On the other hand, in the EAG area, both the temporal amplitude and the mode are inverted with respect to the first EOF-F mode, amplifying the EAG variability. However it should be noted that this mode explains less than 6% of the covariance.

As with altimetry, NM8 shows a similar pattern to the first mode with an inverted phase, but this time for the intense dipole formed by the EAG and a cyclonic eddy to the north-east, enhancing the well known Almería-Orán front and the beginning of the AC. In this mode, the amplitude of the EAG is much lower than the first mode ($\sim$5 cm vs $\sim$25 cm), therefore the stabilizing effect of the inverted phase will not affect the inherent variability of the EAG.

For O12, the second EOF-F mode only explains a 0.2% of the covariance and is not statistically significant.

1st EOF-A Mode (Figure 7.16)

By looking at the EOF anomalies (EOF-A), we remove the mean circulation signals. The first EOF-A mode is characterized by the variability of the EAG, and in smaller measure the WAG variability. As in figure 7.14 the temporal amplitude is maximum in September-November and minimum in winter (February-March). In this case since we are working with anomalies the minimum values are negative representing the weakest phase of anticyclonic circulation. The first EOF-A has a lower explained covariance than the full signal but is still very high (70.6%).

NM8 shows a similar pattern and amplitude to altimetry, without the presence of the WAG, and a positive anomaly on the eastern boundary of the domain. As with altimetry, the explained covariance, is lower with the first EOF-A but the difference is not as large.

O12 also presents mesoscale variability with temporal and spatial patterns of similar size but not occurring in the right locations, with a clear dominance of a anticyclonic signal centred at 0.5^{o}W. Regarding the explained covariance, same comments as above.

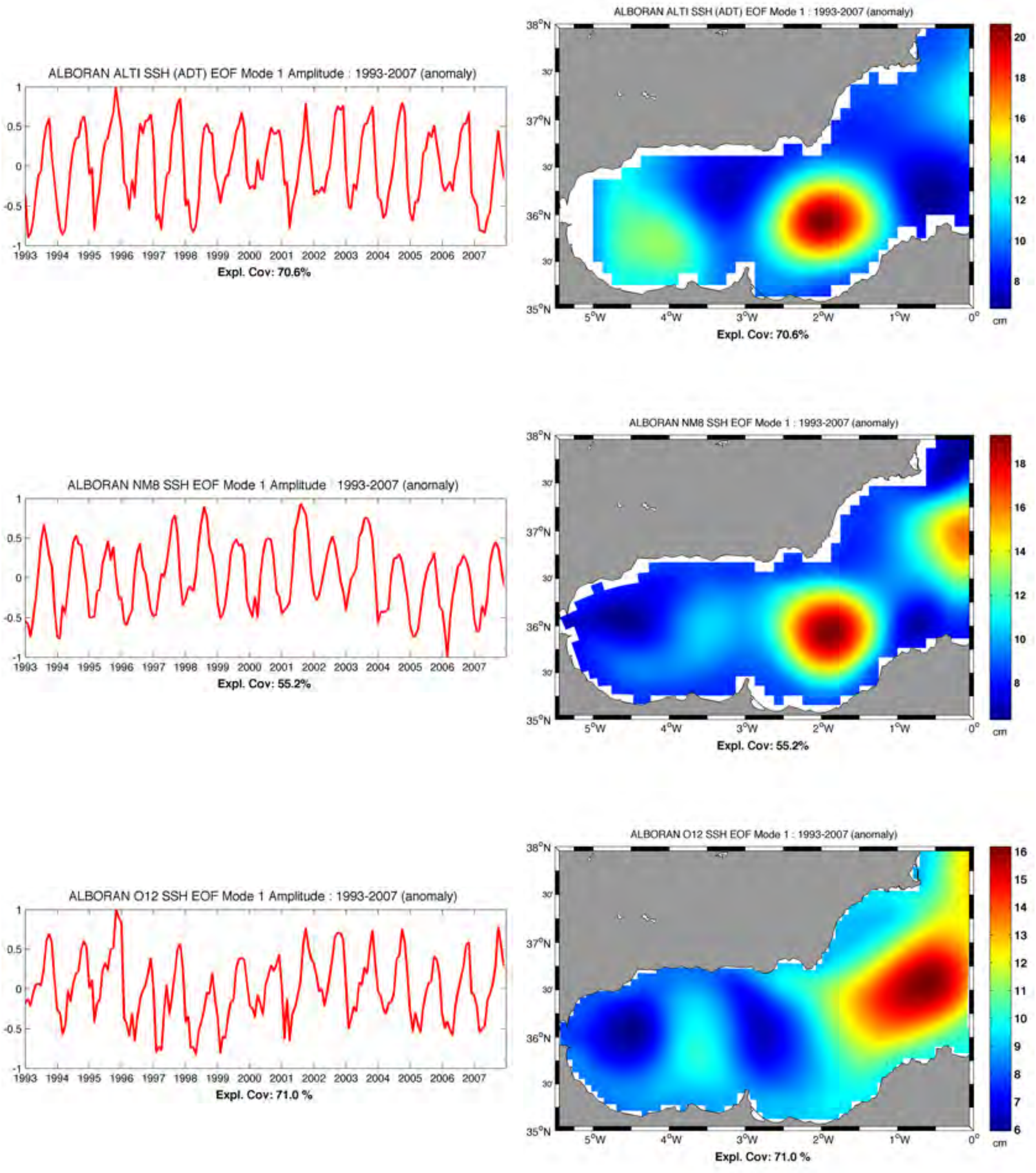

Figure 7.16: 1st EOF-A mode of total SSH for the Alboran Sea with amplitude (left) and pattern (right). Altimetry (top), NEMOMED8 (middle) and ORCA12 (bottom)

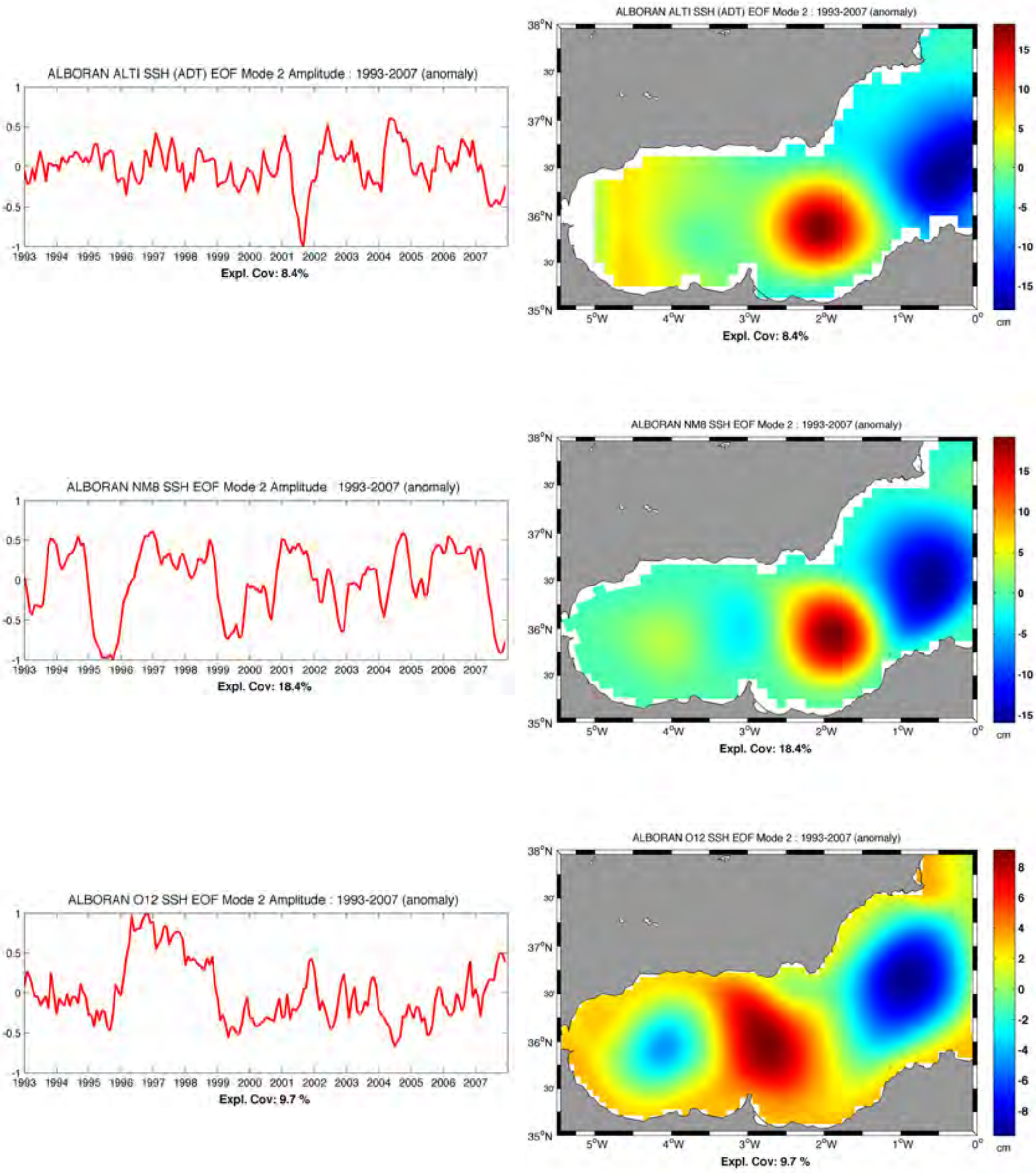

Figure 7.17: 2nd EOF-A mode of total SSH for the Alboran Sea with amplitude (left) and pattern (right). Altimetry (top), NEMOMED8 (middle) and ORCA12 (bottom)

2nd EOF-A Mode (Figure 7.17)

For altimetry the second EOF-A mode does not present seasonal variability, but only interannual variability with a marked peak around August 2001 and the spatial patten reveals a marked dipole between the EAG and the cyclonic eddy east of the EAG, with a very intense Almería-Orán front. The explained covariance is low since this mode explains mostly a specific event in time.

The spatial pattern of NM8 is extremely similar to altimetry, with almost identical gradients, but with different temporal variability. This is expected since NM8 does not have data assimilation with limited capabilities for reproducing real interannual mesoscale signals.

O12 tends to create an anticyclonic mesoscale features centred at 3^o which could correspond to a migrated WAG as seen and described in the first EOF-F mode.

Algerian Basin

1st EOF-F Mode (Figure 7.18)

The first EOF-F mode of altimetry in the Algerian basin represents mainly the Algerian Current flowing very close to the North African coastline. This current is maximum in late summer and minimum towards the end of winter. This mode explains 76.6% of the covariance. Essentially, this mode is dominated by the MDT (with a degree of modulation) which defines the mean circulation. Another feature that can be observed in this mode is a smaller mesoscale feature to the southeast of Ibiza. This is actually believed to be an artefact caused by the MDT added to the altimetry products.

In NM8, the Algerian Current is also the dominant feature of the first EOF-F mode, although it is not as confined to the coast as altimetry. There are also two intense features east (5^{o}E) and south-east (6^{o}E) of the Balearic Islands that contribute to the first EOF, as well as a well developed meander in the Algerian Current (8^{o}E) that could evolve into a separated eddy through baroclinic instability and detach from the AC. In this case the amplitude appears to be inverted with maximum intensity in winter with some inversion of the flow towards the end of summer. This phase difference may be due to the contribution of intense mesoscale activity characteristic of the Algerian basin. The covariance explained by this mode is lower at 41.7%, giving some

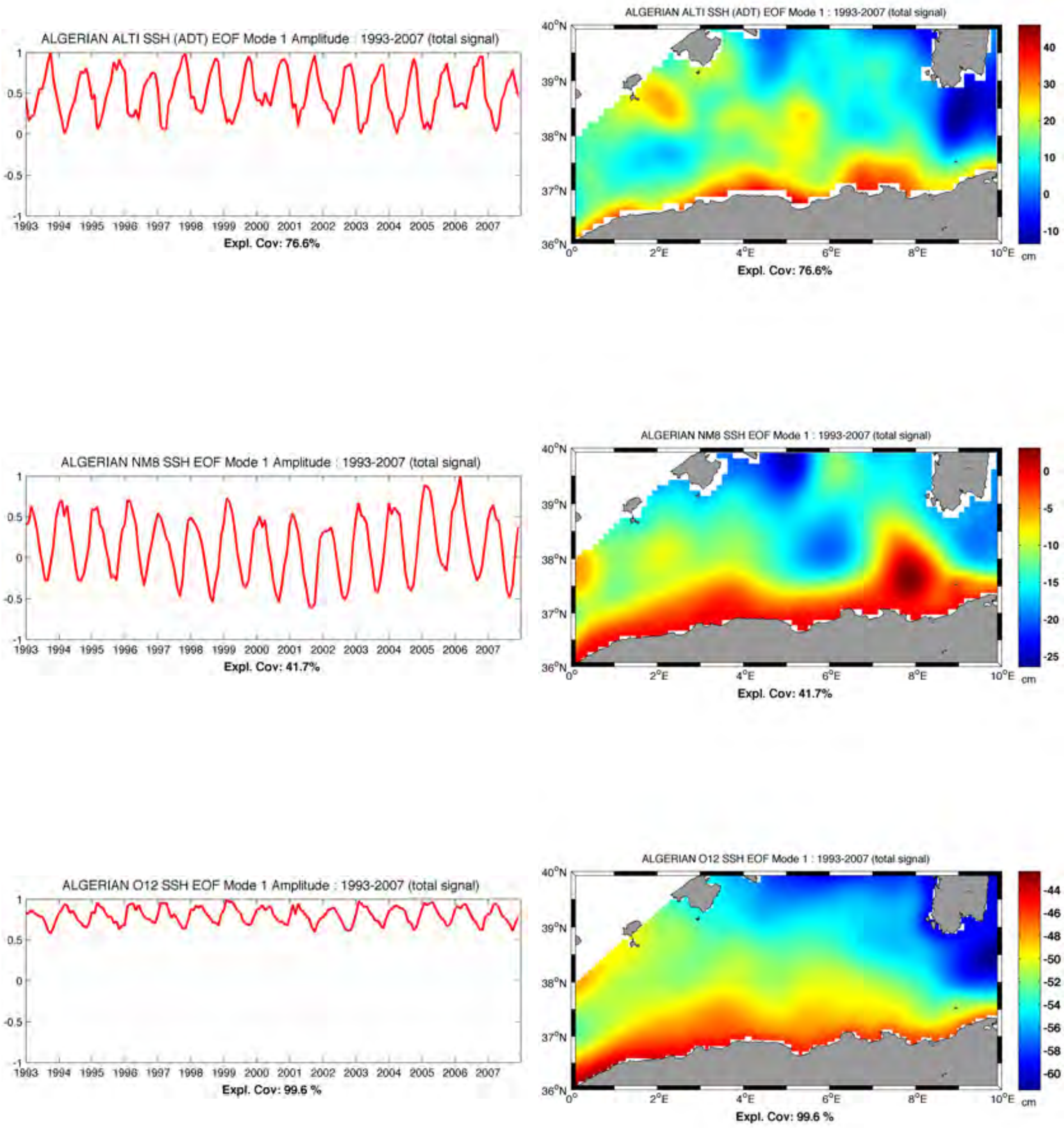

Figure 7.18: 1st EOF-F mode of total SSH for the Algerian Basin with amplitude (left) and pattern (right). Altimetry (top), NEMOMED8 (middle) and ORCA12 (bottom)

indication that the variability is not dominated by a single feature.

The first EOF-F mode of O12 also shows the AC as its main feature, though in this case the outer edge of the current is less well defined, becoming more of a smooth gradient covering most of the Algerian basin. The covariance explained by this mode is extremely high at 99.6% and the temporal amplitude shows very little variation indicating that this current is extremely stable in the simulation. As in NM8, maximum is in winter with minimum at the beginning of autumn.

2nd EOF-F Mode (Figure 7.19)

For altimetry, the second EOF-F mode is also mainly associated with the variability of the Algerian Current, with a very similar pattern to the first mode but this time the temporal amplitude has both positive and negative values and showing a maximum in winter (as with the first modes of NM8 and O12). The explained covariance is lower (11.5%) but the horizontal gradients are similar ($\sim$20 cm across the current boundary). Thus to fully understand the EOF-Fs in the AC it is necessary to consider both the first and second EOF-Fs and compare with the simulations. The first mode defines the permanent direction of the flow with relatively low variability, but the second mode modulates its intensity and phase, which when adding both modes is actually inverted causing a maximum in winter and minimum in summer, coinciding with the simulations.

The second EOF-F mode in NM8 is dominated by the anticyclonic mesoscale variability associated with the Algerian Current (shedding off eddies into the center of the Algerian basin as the current moves eastward). This mode has a marked seasonal cycle but always positive meaning that the mesoscale activity weakens in winter but is always anticyclonic in nature. The explained covariance is 31%, contributing almost as much as the first mode to the region's variability.

The second EOF-F mode of O12 also shows the AC but the explained covariance is so low (0.1%) that it is statistically insignificant.

1st EOF-A Mode (Figure 7.20)

The first EOF-A of altimetry is dominated (67.9%) by a well defined dipole between an anticyclonic eddy to the south of Sardinia and a cyclonic mesoscale

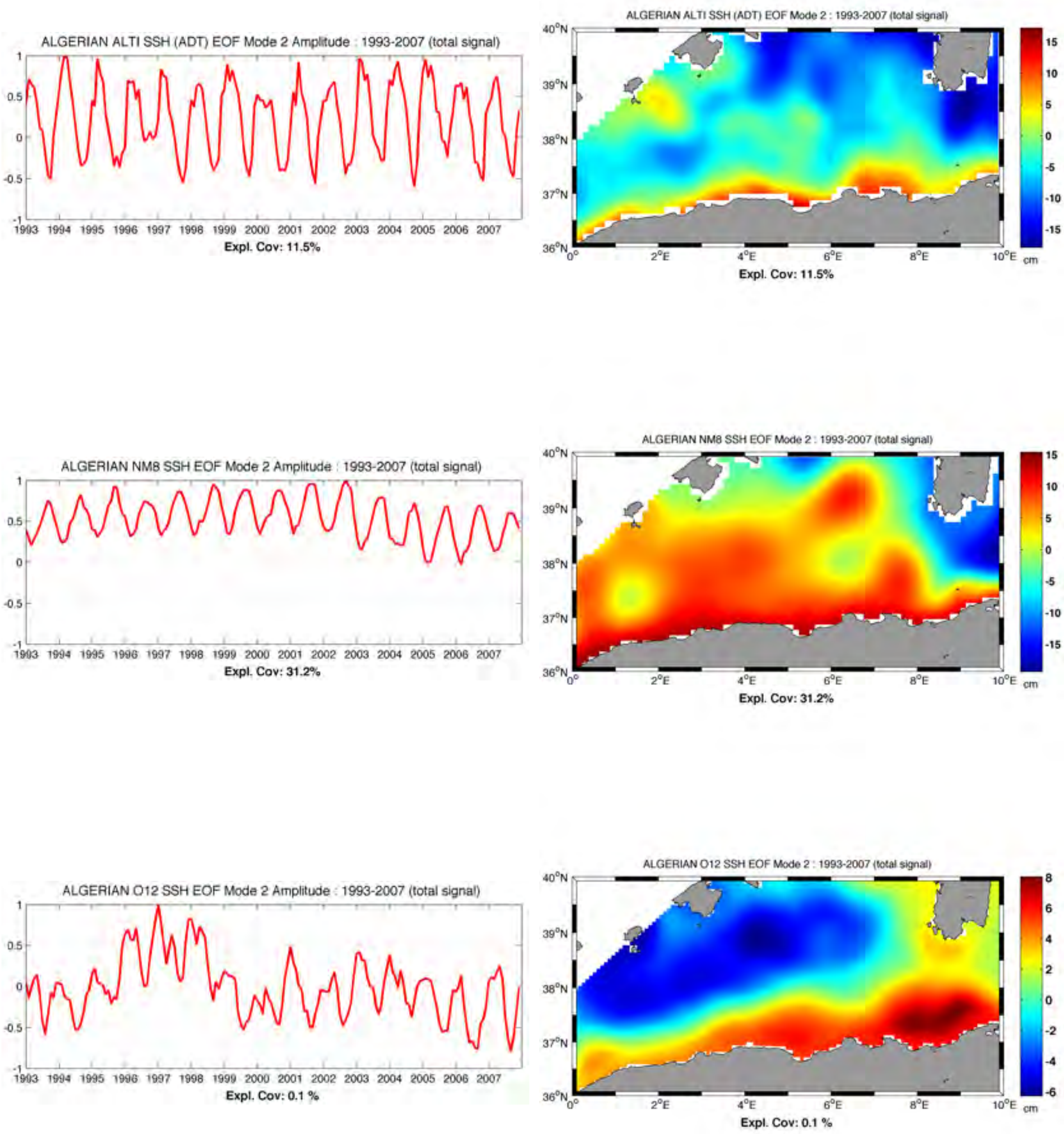

Figure 7.19: 2nd EOF-F mode of total SSH for the Algerian Basin with amplitude (left) and pattern (right). Altimetry (top), NEMOMED8 (middle) and ORCA12 (bottom)

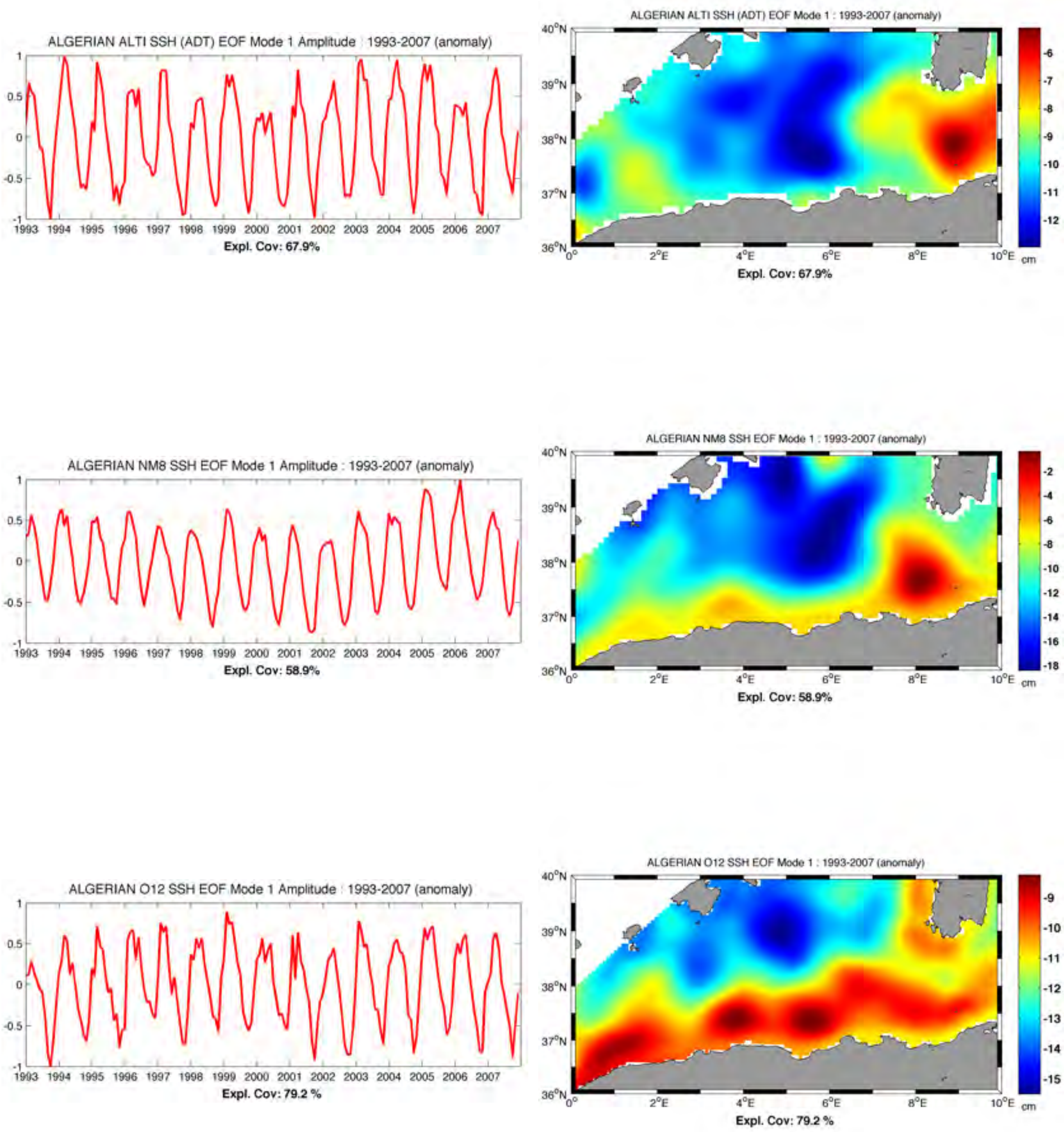

Figure 7.20: 1st EOF-A mode of total SSH for the Algerian Basin with amplitude (left) and pattern (right). Altimetry (top), NEMOMED8 (middle) and ORCA12 (bottom)

feature to the south-east of the Balearic islands. This pattern is maximum in winter and inverts in the summer. The Algerian Current is hardly present in this first EOF-A mode.

NM8 shows a very similar spatial pattern and amplitude to altimetry with the dipole mentioned above. In this case, the gradient between both cyclonic and anticyclonic features is stronger as their nuclei are closer together and slightly more intense. The explained covariance (58.9%) is also of a similar magnitude to altimetry. In this case, there is a fainter appearance of the AC.

The first EOF-A mode of O12 is clearly dominated by the mesoscale features found within the path of the Algerian Current but well detached from the coast, again with maximum in winter. These mesoscale features could correspond to the typical "coastal eddies" associated with the AC (Millot, 1999). This mode explains a high 79.2% of the covariance but does not match what is seen by altimetry and NM8 in their respective first EOF-A modes.

2nd EOF-A Mode (Figure 7.21)

The second EOF-A mode of both altimetry and NM8 show another strong dipole to the south-west of Sardinia formed by a cyclonic eddy to the west and an anticyclonic eddy to the east (the anticyclonic eddy is sometimes referred to as the Southeast Sardinia Gyre (Astraldi et al., 2002)). In this case it is far more defined, with a stronger horizontal gradient. They both explain a similar covariance (altimetry = 5% and NM8 = 4.4%). In the case of altimetry the signal is mainly due to isolated events in 1997, 2003 and 2006, whereas in NM8 they are more regular. In NM8 there are also a number of weaker mesoscale signals along the North-African coastline associated to the AC variability.

For O12, this mode is related to some variability of the AC, in this case closer to the African coastline, revealing some seasonal and interannual variability.

North-Western Mediterranean Basin (N-WMED)

The N-WMED domain used for this analysis covers part of the Ligurian Basin, the Gulf of Lions, the Balearic Sea and part of the Liguro-Provençal Basin.

1st EOF-F Mode (Figure 7.22)

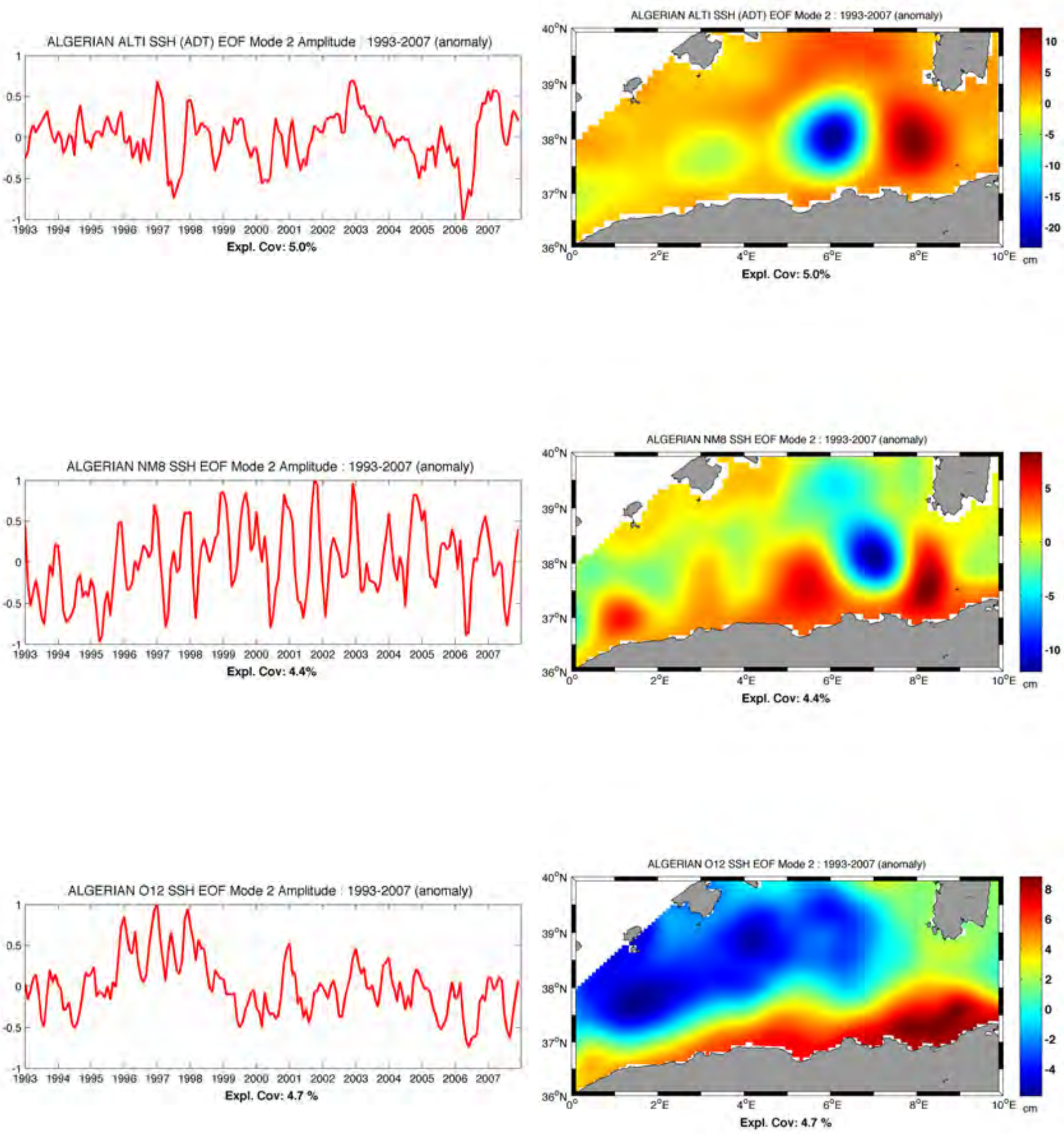

Figure 7.21: 2nd EOF-A mode of total SSH for the Algerian Basin with amplitude (left) and pattern (right). Altimetry (top), NEMOMED8 (middle) and ORCA12 (bottom)

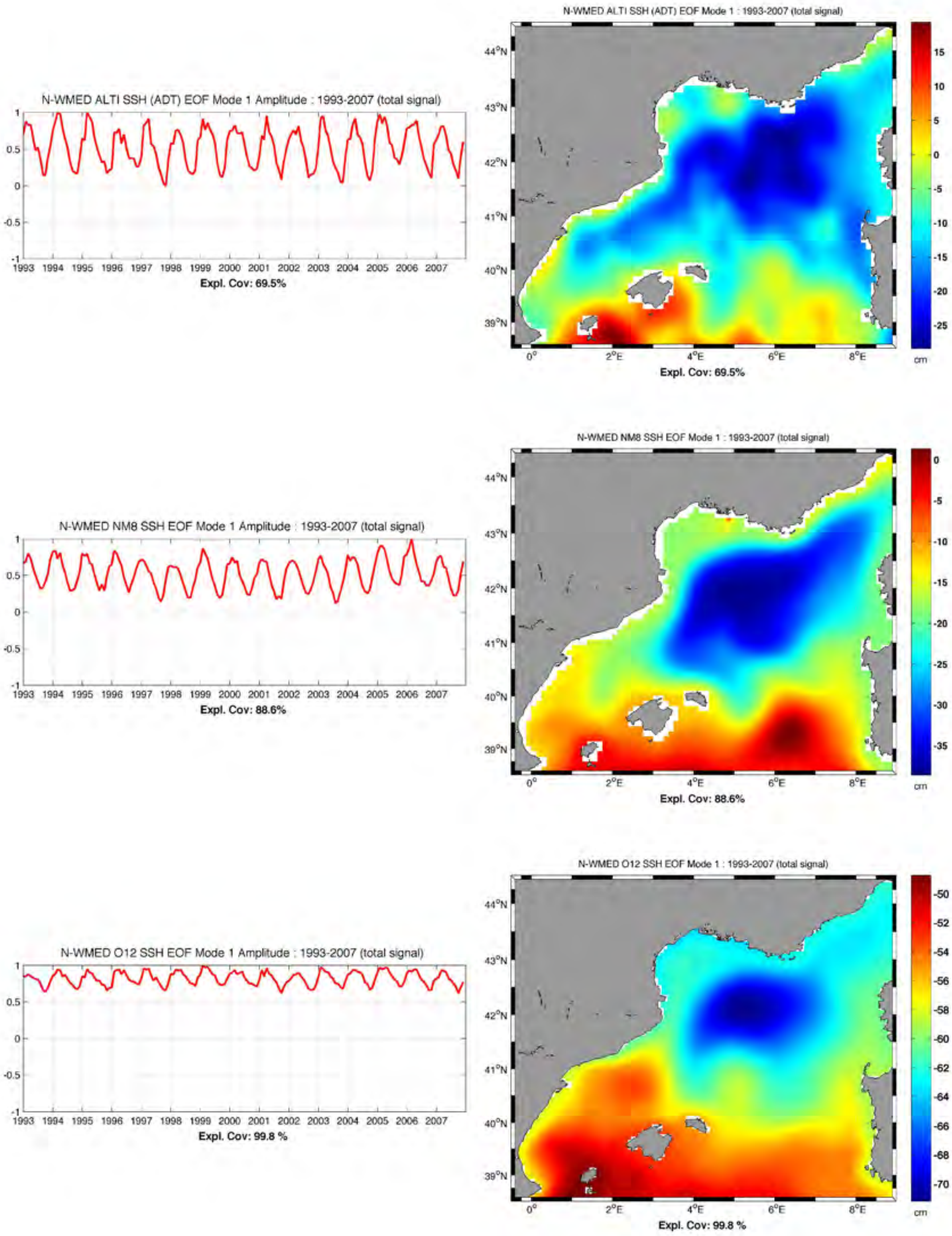

Figure 7.22: 1st EOF-F mode of total SSH for the N-WMED with amplitude (left) and pattern (right). Altimetry (top), NEMOMED8 (middle) and ORCA12 (bottom)

The first EOF-F mode of altimetry in the North-WMED (69.5% explained covariance) is dominated by the cyclonic circulation in the Gulf of Lions and the Northern Current which reaches the Balearic Sea (NW of Mallorca) and recirculates into the Balearic Current (Lopez García et al. (1994), Ruiz et al. (2009)). This mode shows a clear seasonal cycle with maximum intensity in winter and minimum in autumn. Since the sign of the temporal amplitude never becomes negative, the pattern weakens but never reverses.

In the case of NM8, there is a very strong cyclonic signal in the Gulf of Lions, with an intense Northern Current. However the recirculation happens mainly further North than in altimetry (to the north-west of Menorca) with a weaker signal actually reaching north-west of Mallorca. Some recirculation at that location still occurs but is less predominant. The phase of the seasonal cycle coincides with altimetry. The explained covariance is higher than altimetry at 88.6%.

For O12, the main feature is the cyclonic circulation in the Gulf of Lions, with no protrusion of the Northern Current into the Balearic Sea. The recirculation happens even further north than NM8 and an anticyclonic mesoscale signal appears to block the Northern Current from reaching further south. The phase of the temporal amplitude is similar to both altimetry and NM8 but has lower variability as well as a very high explained covariance (99.8%), again suggesting a stable pattern of the first EOF mode.

2nd EOF-F Mode (Figure 7.23)

The second altimetry EOF-F mode is also associated with the variability of the cyclonic circulation in the Gulf of Lions as well as the weaker signal of the Northern Current's recirculation in the Balearic Sea. The phase is inverted with respect to the first EOF-F amplitude, therefore this mode is related to the weaker circulation of the Northern Current in the summer. As with the AC discussed above, the second modulates the first, reducing part of its maximum intensity in winter and increasing its minimum in summer. Also visible is the surface transport through the Ibiza Strait, which is northward in the summer and southward in the winter in agreement with previous *in situ* observations (Pinot et al., 2002).

For NM8, the second EOF-F mode shows a similar pattern and temporal amplitude to altimetry with the cyclonic circulation in the Gulf of Lions. In this case, the transport through the Ibiza Strait is more intense, clearly con-

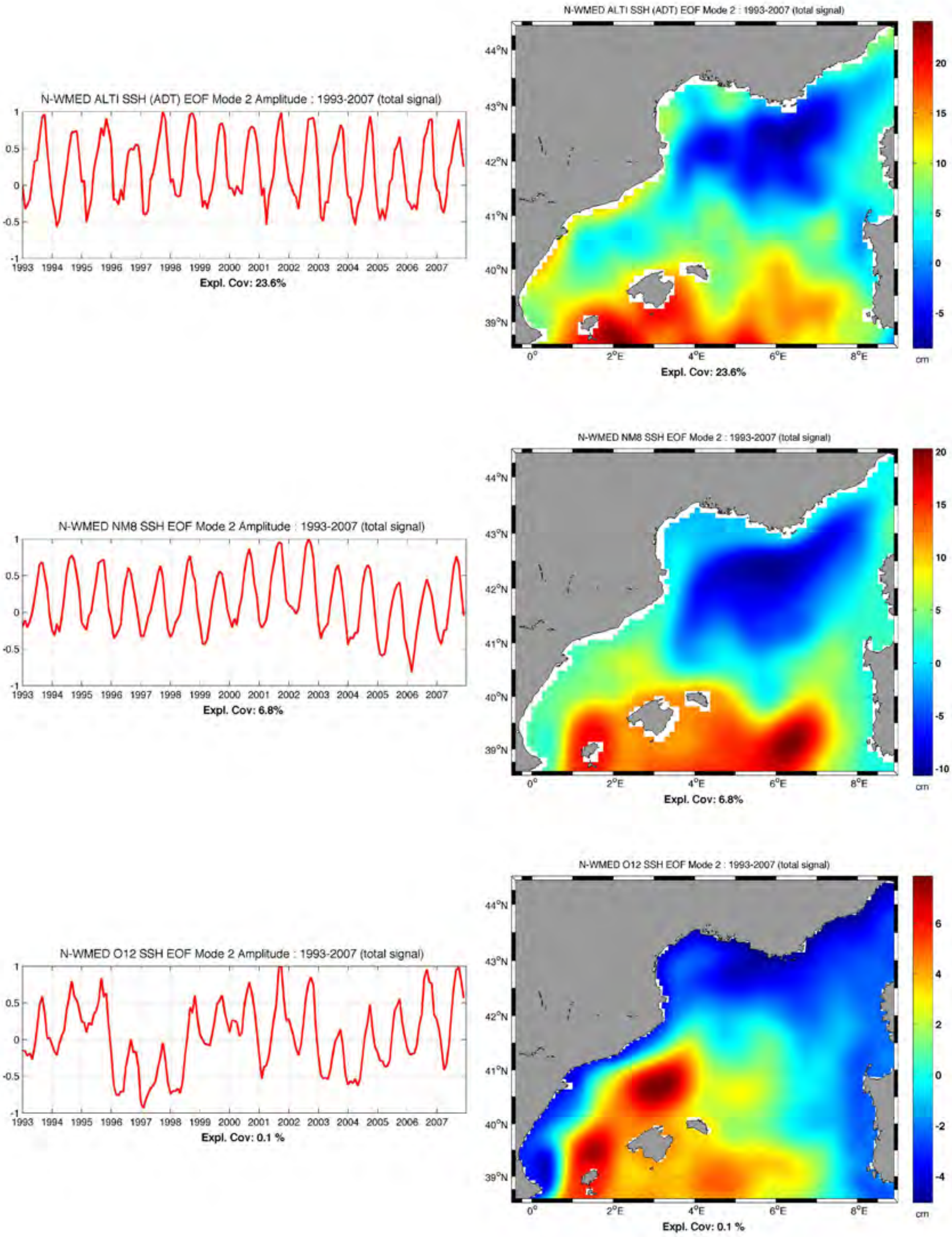

Figure 7.23: 2nd EOF-F mode of total SSH for the N-WMED with amplitude (left) and pattern (right). Altimetry (top), NEMOMED8 (middle) and ORCA12 (bottom)

tinuing north-east as the Balearic Current and eventually becoming part of a mesoscale feature west of Sardinia.

Again, for O12 this mode explains a very low percentage of the covariance (0.1%) therefore is not statistically significant. Its main features are the transport through the Ibiza Strait and two anticyclonic mesoscale eddies to the west and north of Mallorca.

1st EOF-A Mode (Figure 7.24)

The first EOF-A mode of altimetry is associated with an intense north-south front centred at 42^{o}N usually referred to as the North Balearic Front (Lopez García et al. (1994), Millot (1999), Olita et al. (2011)). This front is caused by the wind channelling effect of the Pyrenees, especially in the summer where the more stable weather conditions in the N-WMED are disturbed by this effect.

NM8 also displays the occurrence of the North Balearic Front, albeit with lower intensity. This mode also corresponds to the transport through the Ibiza Channel seen in the second EOF-F mode and mesoscale activity in the Liguro-Provençal Basin.

The first EOF-A mode of O12 is similar to the second EOF-F mode suggesting that the pattern was so stable in the first EOF-F mode that removing a temporal mean at each grid point essentially removed this first mode. O12 displays a different pattern to both altimetry and NM8, with a very intense northward flow through the Ibiza Strait (maximum at the end of summer), which continues north closer to the Iberian Peninsula than the Balearic Islands. This is not the location where northward flow is known to occur (Millot (1999), (Pinot et al., 1995), (Ruiz et al., 2009)). Northward flow is usually associated with the Balearic Current which flows very close to the Balearic Islands. In this case, two anticyclonic mesoscale features appear to be constraining the flow further northward.

2nd EOF-A Mode (Figure 7.25)

The second EOF-A mode for all three datasets is dominated by discrete mesoscale features in the northern Balearic Sea. In altimetry, a the main signal is an anticyclonic eddy that occurred north of Mallorca in 1998 and studied in depth by Pascual et al. (2002). O12 shows a similar eddy although it happens

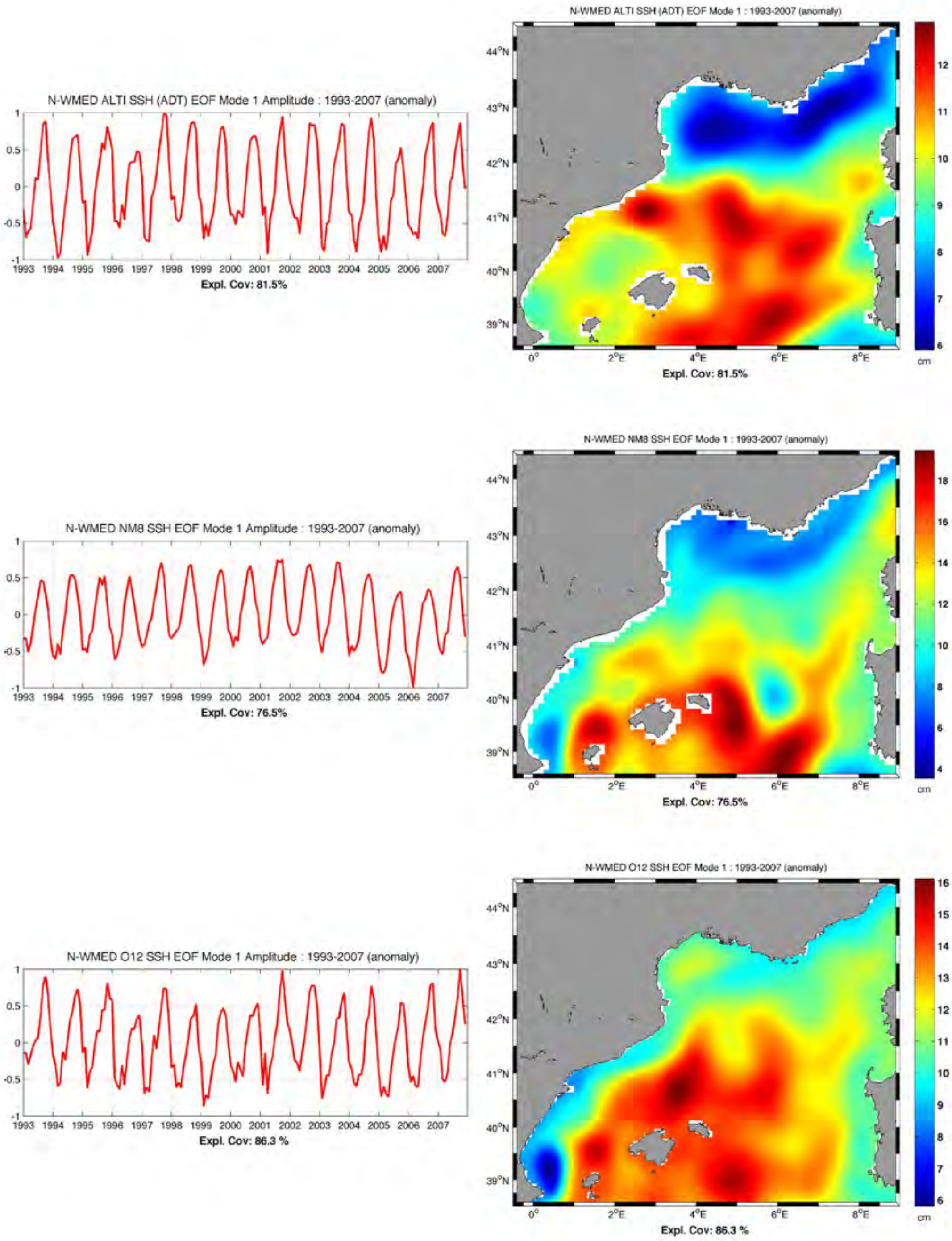

Figure 7.24: 1st EOF-A mode of total SSH for the N-WMED with amplitude (left) and pattern (right). Altimetry (top), NEMOMED8 (middle) and ORCA12 (bottom)

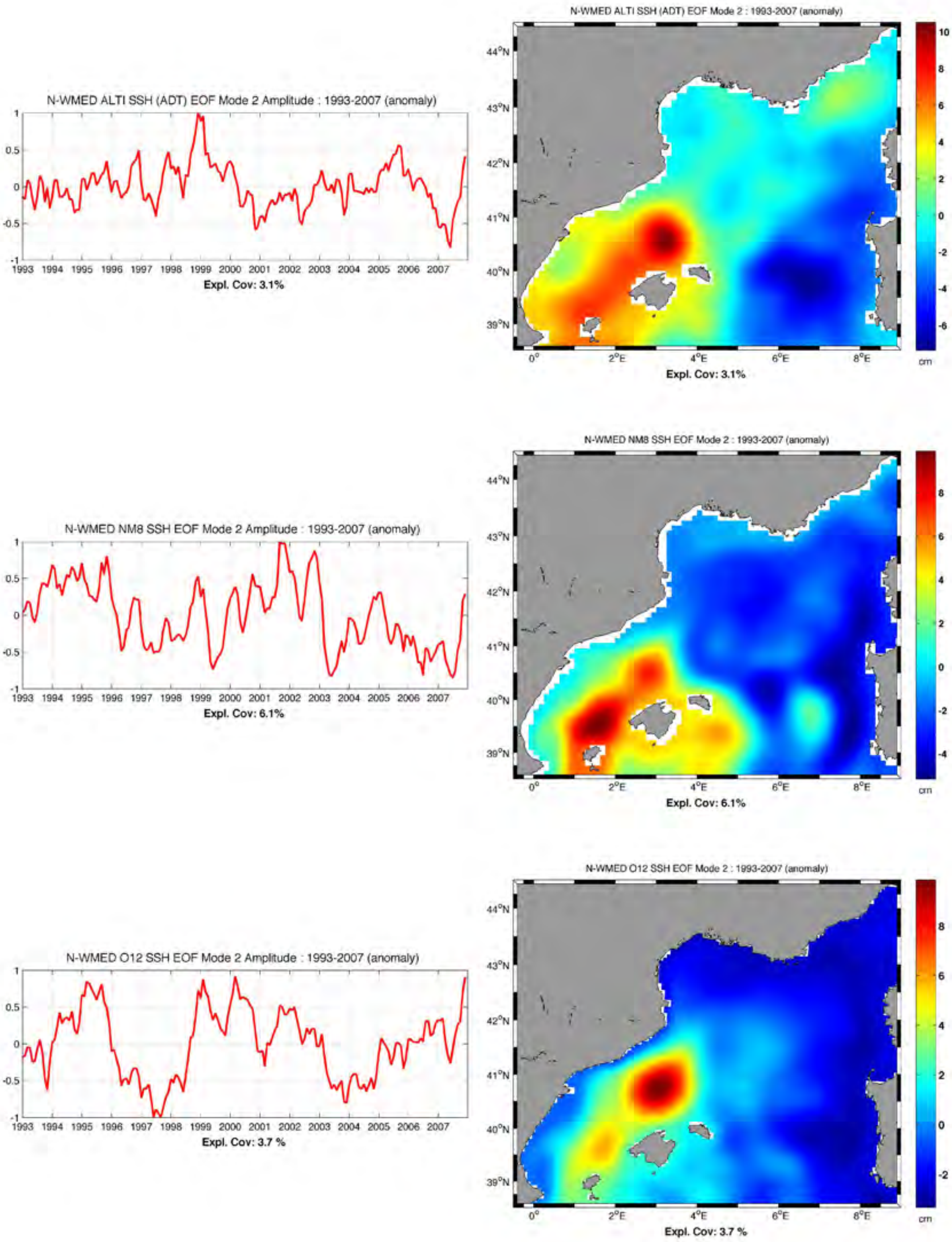

Figure 7.25: 2nd EOF-A mode of total SSH for the N-WMED with amplitude (left) and pattern (right). Altimetry (top), NEMOMED8 (middle) and ORCA12 (bottom)

more often. NM8 shows a weaker signal at that location, instead a stronger eddy is found north of Ibiza.

7.8 Discussion and Summary

Two high resolution numerical simulations, NEMOMED8 ($1/8^o$) and ORCA-12 ($1/12^o$), have been analysed and compared to several observational datasets (EN3 for temperature and salinity and altimetry for mean circulation and dynamical analysis). Through these comparisons, several aspects of the dynamical features of WMED circulation have been studied.

As opposed to previous chapters where the numerical simulations used had a resolution too low to produce Mediterranean mesoscale variability, NM8 and O12 both have theoretically sufficient resolution to produce, although perhaps not fully resolve, it. Apart from the resolution difference, NM8 and O12 are very different simulations. NM8 is a matured simulation, evolved from OPAMED8 (Somot et al., 2006), and tailored to the Mediterranean Sea. The atmospheric forcing used, ARPERA is a dynamical downscale of the ECMWF/ERA-40 fields, also tested and optimized for the Mediterranean, and finally there is no salinity restoring. In contrast, O12 is the first iteration (of many to come) of the ORCA global simulations at $1/12^o$. It uses the ERA-Interim atmospheric forcing which is also a downscale of ECMWF/ERA-40 fields although it is not specifically tuned for the Mediterranean. Overall this simulation is perhaps premature, but nonetheless is an interesting simulation to analyse for the first time.

Since NM8 is a more mature and fine-tuned simulation, it tends to perform better than O12 in practically all the analyses. Given the complexity of numerical models, resolution alone is not enough to improve the results.

In the temperature and salinity analysis (section 7.2), surface temperature performance is good for both simulations, as it has been in all previous chapters, primarily because the surface layer is heavily influenced by the atmospheric forcing which is based on similar real observations. Salinity remains a difficult parameter for these simulations, although NM8 showed a significantly better performance at surface and intermediate layers than O12 and previous ORCA simulations (G70 and G85) despite not having any salinity restoring. This is a good result and a marked improvement.

Another interesting aspect that was studied in Chapter 6 is the formation of deep waters in the Gulf of Lions. Conclusions from the analysis performed in Chapter 6 indicated that in order for numerical simulations to reliably reproduce deep convection events, improvements in the resolution of both the simulation and the atmospheric forcing were needed (as well as correcting known underestimations in the atmospheric forcing). The results obtained in this chapter are interesting because while those conclusions hold true for NM8, they do not for O12. In both cases, both the simulations and atmospheric forcing are of higher resolution, but it is the fine-tuning of the latter that makes the difference. NM8 performed very well in reproducing the deep convection events and vertical structure of the water column in the Gulf of Lions, which again was one of the main purposes of this simulation (extensive studies in Herrmann et al. (2010)). On the other hand, O12 produced an excessively warm intermediate layer preventing deep convection to reach beyond this layer.

The mean geostrophic circulation scheme of the WMED was also analysed and compared with altimetry. The simulations displayed a correct overall circulation pattern but they both had discrepancies with respect to altimetry in specific areas of the WMED. Both simulations produced an overall smoother field than altimetry, with O12 being even smoother than NM8, a result which is surprising given the higher resolution of the former. NM8 did not reproduce the Western Alboran Gyre (WAG) and had a less defined Algerian Current (AC). It reproduced the Northern Current quite well, but the recirculation that happens to the west of Mallorca is weaker, with most of it happening further north. O12 did not produce neither the WAG nor the EAG in their normal locations, instead it produced a displaced WAG (Flexas et al., 2006). In this simulation, the AC is not well defined and constrained to the coast, instead it is represented as a wide gradient merging the AC with the anticyclonic mesoscale activity characteristic of the Algerian Basin. The Northern Current is represented as a cyclonic circulation in the Gulf of Lions, with no southward protrusion into the Balearic Sea due to the blockage of a permanent anticyclonic eddy.

Another way to assess ocean circulation is to analyse the geostrophic eddy kinetic energy (EKEg), which is calculated from sea level anomalies and gives a measure of the mesoscale activity. In this regard, all three datasets (altimetry, NM8 and O12) coincide in the regions of maximum EKEg as being mainly the Alboran Sea and Algerian Basin. Altimetry and NM8 have similar levels of EKEg and reproduce both the WAG and EAG variability as well as the high EKEg regions along the path of the AC. O12 shows EKEg levels which are less than half those of altimetry and NM8. This is due to the low variability of the circulation scheme, which is consequently removed when calculating the anomalies leaving lower EKEg values.

Analysis of mean circulation is adequate as a broad view of whether the simulations are producing correct circulation, however it is too broad to delve into the different processes that drive this circulation as all the signals are mixed together. For this reason, the main components of the circulation were separated and analysed using empirical orthogonal functions (EOFs) of both the full mean circulation signal and also the spatial anomaly. Separating the circulation into its main components makes it possible to analyse them separately and with better success.

The first and second EOF-F modes in all cases mainly referred to the mean circulation modulated by a relatively weak temporal variability (seasonal and interannual), and produced similar patterns to those seen in section 7.5, however in the case of the simulations in the Algerian Basin, this technique was particularly helpful in separating the AC from the mesoscale variability of the basin (this was very clear in NM8).

The anomaly EOF-A modes proved to be especially interesting, displaying variability which is hard to see in the mean circulation. In both the first and second EOF-A modes, NM8 proved an exceptional performance when compared to altimetry in all regions, with very similar spatial patterns and appropriate temporal phase (although the interannual variability did not match, which is expected since the simulation does not assimilate data and would be very difficult for it to reproduce actual mesoscale interannual variability). An interesting feature which did appear and was not visible in the mean circulation was the North Balearic Front. This front was visible in the first EOF-A mode of all three datasets (although a bit weaker in O12).

In conclusion, the analysis of these two high resolution numerical simulations provided an interesting opportunity to study the dynamics of WMED variability and also the characteristics and behaviours of two very different simulations. NEMOMED8 appears as a mature and solid simulation, consistently producing good results when validated against observational datasets. Despite its good results, NM8 still leaves room for improvement. Some key circulation features such as the WAG are not reproduced properly and its resolution is still not sufficient to accurately resolve the mesoscale and submesoscale. A 1/16^o or 1/32^o simulation with similar performance would be a very interesting tool for Mediterranean variability studies.

ORCA12.L46-MAL95, as the first iteration of a 1/12^o global simulations is an interesting push forward with the capabilities of resolving in greater detail the physical characteristics of the ocean. It is also of sufficient resolution to become a useful tool for variability studies in the Mediterranean Sea. However, this first iteration is still in its early stages of development and needs to be fine-tuned to produce better and realistic results. In the WMED, although the basin scale circulation schemes are correct, the finer mesoscale circulation and location of certain gyres (WAG, EAG) and currents (Balearic Current, Northern Current) still requires improvement.

Chapter 8

Conclusions and Perspectives

This thesis has focused on exploring the different aspects of the Mediterranean Sea variability through the validation of a series of ocean numerical models. We have performed a comprehensive analysis of the main features and variables that define its circulation, its water mass characteristics and its dynamics. In order to do so, we have combined the study of numerical simulations with a number of different sources of observational data. By using several ocean models with different configurations and characteristics, we have been able to explore which model configurations offered the best results in different areas and where they need to improve. Through the various statistical methods used in the validation against observations, we have learnt the strengths and weaknesses of both models and observations. Whereas extensive observational databases are great for the study of the state of the ocean, the truth is that many gaps in both time and space still exist in many regions of the World‘s Oceans (including the Mediterranean Sea). Numerical simulations on the other hand provide a complete picture of the state of the ocean, and with the recent simulations spanning the last half century, climatic scale studies start to be possible. This, in theory, makes models a perfect tool to study all kinds of oceanic processes as long as the model resolution is sufficient to resolve them.

However, due to computational limitations (and also, of our understanding of the physics behind some of the processes that govern ocean dynamics), numerical models still rely on simplifications and parametrizations for processes that they cannot resolve. For simulations like the ones studied here, which aim at producing realistic results, and that rely on external forcing based on observations, it is also the quality and resolution of these observations which becomes a limiting factor. We are simply not able to feed the models with good enough data to perfectly simulate the state of the ocean and its medium-to-long term trends.

Whereas our results show that in many cases, the simulations are adequate for studies involving circulation patterns, interannual variability and seasonal cycles, the same results evidence that climatic trends are still an area where models need improve their robustness before using these results to make statements about the future evolution of the ocean and climate. For example, sea level trends are generally not maintained within observational values when allowed to develop freely (how can we make statements about future trends if the models cannot reproduce known past trends?). The same goes for temperature in some of the simulations. Salinity, which is a key variable in the thermohaline circulation of the world‘s oceans, is generally problematic for ocean models, in many cases requiring strong restoring to climatology in order to avoid significant drift.

These limitations makes the validation of simulations against real data a vital process in order to consider them reliable enough for the study of certain processes, especially when it comes to climatic trends.

In this chapter we summarize the most important conclusions outlined along this thesis and suggest some ideas for future work.

Temperature We have analysed the basin scale mean temperature evolution of all the simulations (G70, G85, GLORYS, O12 and NM8) at different depth layers. At surface layers, all simulations produce good results. This is not surprising since as they are all driven by realistic (and similar) atmospheric forcing, the surface temperatures compare well with observations. This confirms that the models have good air-sea interaction physics. At intermediate and deep layers, the performance is not as good and the differences are marked by the quality of the atmospheric forcing. With the G70 and G85 simulations, which are differentiated by the atmospheric forcing (G70 uses DFS3 and G85 uses DFS4) and vertical resolution, G85 shows much improved trends at intermediate and deep layers due to the better time continuity of DFS4 (interface between ERA40 and ECMWF, corrected fluxes, more realistic wind stress). One issue displayed by the $1/4^o$ simulations is a deviation in mean temperatures, especially at intermediate layers where they tend to be considerably warmer than the observations. The higher resolution O12 and NM8, which are based on improved, higher resolution atmospheric forcing show good trend and variability results at all depths.

Salinity As mentioned above, salinity is generally a problematic variable for numerical simulations. This is mainly due to imbalances in the freshwater fluxes of the atmospheric forcing, derived from lack of quality information on precipitation/evaporation in the open ocean, but also on the fewer salinity observations available for validation (although new technologies such as the recent SMOS satellite will improve surface salinity observations). These imbalances require that many of the models apply a strong restoring to climatology that negatively affects variability. Consequently, models which apply restoring have very bad correlations with observations. Unless the freshwater fluxes are balanced, this restoring is necessary as evidenced by the G85 results, where applying a weak restoring results in a very strong negative salinity drift (which also affects sea level in the opposite direction). On the other hand, NM8, which is a mature regional simulation tailored to the Mediterranean Sea with a balanced water budget does not need to apply surface salinity restoring to reproduces salinity interannual variability reasonably well.

Deep Convection in the Gulf of Lions We focused a part of this study on the capabilities of the simulations to reproduce deep water formation events in the Gulf of Lions. These events are vital for the renewal of waters at the abyssal plains and are part of the thermohaline circulation of the Mediterranean. Deep convection usually occurs during short events of strong, cold wind forcing over relatively small areas of the Gulf of Lions. These conditions in principle require that any model aiming at reproducing such events have enough spatial resolution to do so (both in the model as well as the atmospheric forcing). This is evidenced by the results from NM8, very similar to observations when reproducing the strong 2004-2006 events as well as the weaker events. O12 is also capable of reproducing the weaker events but due to an overly warm intermediate layer, these don not reach full depth. In the $1/4^o$ simulations, G85 is only capable of reproducing the exceptionally strong 2004-2006 events. Its resolution in terms of both grid and atmospheric forcing (ERA40 $\sim$150 km) is insufficient for the weaker events.

Sea Level This is one of the key climatic variables. All simulations correctly reproduce the seasonal cycle and the interannual variability, however in the case of the global simulations, the trend is not realistic. This is due to the freshwater imbalance mentioned above, which causes a significant positive drift (getting worse if less salinity relaxation is applied).

Surface Circulation & Transports What simulations can and cannot reproduce in terms of circulation depends in great measure on their spatial resolution. As is to be expected the $1/4^o$ simulations can only reproduce the large scale circulation of the WMED, which they actually do reasonably well. This includes transports through the Strait of Gibraltar and Balearic Channels. The higher resolution models, NM8 and O12 do have the resolving power to reproduce most of the mesoscale variability of the WMED. We used EOFs to analyse the circulation features of the WMED in depth, and this methodology provided very interesting insights into the signals the models could reproduce. In this regard, and when comparing to the geostrophic circulation inferred from altimetry, NM8 performs exceptionally well, with mesoscale variability very similar to the observations despite some discrepancies in specific locations (e.g. absence of the WAG in the Alboran Sea). O12 on the other hand, and despite its higher resolving power, shows that it is a first-generation simulation at this resolution. Its general circulation is correct, but the fields are very smooth with little variability. The comparison between NM8 and O12 shows that given the complexity of ocean models, resolution alone is not enough to get the best performance.

Overall this study has allowed us to investigate very interesting aspects of how models work in simulating the real ocean, where they perform strongly and where they show room for improvement. One of the clear conclusions of this thesis is that regardless of the resolution of the model, an important factor when trying to create a realistic hindcast is the quality of the atmospheric forcing. Other factors are also important, such as a better representation of the Strait of Gibraltar (like in NEMOMED8), improved bathymetry and also lack of need for relaxation. Further work needs to be conducted in estimating and correcting the underestimations and biases that exist in current atmospheric forcing data. Dynamical downscales such as the ARPERA (tweaked and adjusted for the Mediterranean) used in NM8 seem to be producing very positive results.

It is also evident, that the amount of observations is still limited, especially for variables such as salinity, and also for many areas of the deep ocean. This makes model validation for certain variables and regions much harder since the reliability of the data reanalysis available is reduced.

When working with numerical models, the amount of variables available for study is staggering. One must therefore choose well the focus of their study in order to perform an in depth analysis. Because of this, there is always room for improvement and further study.

Future work should include better quantification and analysis of the parameters in the atmospheric forcing that are the source of simulation imbalances (including water and heat fluxes). In terms of ocean circulation and dynamical features, this thesis has provided an overview of the mean circulation features, but with the availability of better and higher resolution simulations, one can go into much more detail quantifying and analysing specific processes. Whilst it has been briefly touched upon, data assimilation into numerical models can provide an excellent tool to better understand dynamical processes. In order to do so, it is also necessary to include new observations provided by the various platforms which have become very active in recent years: ARGO, gliders, SMOS satellite data for sea surface salinity, SWOT (new generation altimeter), etc. All these sources of new data help to improve the current knowledge of the oceans and the processes affecting it, and can only lead to new and improved advances in ocean modelling and understanding.

Appendix A

Fundamental Equations of Ocean Dynamics

The following general description of the equations governing the model dynamics is taken from Juza (2011).

These models use the discretised form of the **fundamental equations of ocean dynamics** to describe the state of the ocean and its evolution. It is based on the following oceanic variables: the horizontal velocity components $\vec{u_h}$, density ρ, potential temperature T, salinity S and pressure P.

- *Navier-Stokes Equations* of momentum conservation:

$$\frac{D\vec{u}}{Dt} = -\frac{\vec{\nabla}}{\rho} + \vec{g} - 2\vec{\Omega} \times \vec{u} + \vec{D} + \vec{F} \tag{A.1}$$

where $\vec{u} = \vec{u_h} + \omega\vec{k}$ is the three-dimensional velocity vector, P is the pressure, ρ is the volumetric mass, $\vec{g}$ is the gravity acceleration, $\vec{\Omega}$ is Earth‘s rotation vector, $\vec{D}$ and $\vec{F}$ are the terms of dissipation and momentum. The operator $\frac{D\vec{u}}{Dt}$ represents the Lagrangian derivative, which is linked to the Eularian derivative by the following relation:

$$\frac{D}{Dt} = \frac{\partial}{\partial t} + \vec{u}.\vec{\nabla} \tag{A.2}$$

• *Equations of the evolution of temperature and salinity* for conservation of heat and salt content:

$$\frac{\partial T}{\partial t} = -\nabla.(\vec{u}T) + D^T + F^T \tag{A.3}$$

$$\frac{\partial S}{\partial t} = -\nabla.(\vec{u}S) + D^S \tag{A.4}$$

where T is the potential temperature, S is the salinity, D^T and D^S are the diffusion terms, and F^T is the source term.

• *The non-linear equation of state of seawater*:

$$\rho = \rho(T, S, P) \tag{A.5}$$

• *The continuity equation* for conservation of mass :

$$\frac{\partial \rho}{\partial t} + \vec{\nabla}(\rho\vec{u}) = 0 \tag{A.6}$$

Approximations

In order to simplify and resolve the equations of ocean dynamics, the following approximations are applied:

• Spherical Earth approximation: geopotential surfaces are assumed to be spherical and the acceleration due to gravity is parallel to the Earth‘s surface.

• Thin layer approximation: the depth of the oceans is small compared to the horizontal dimensions. The effects of curvature are neglected in the equations.

• Hypothesis of ocean incompressibility: the divergence of the velocity field is zero.

• Boussinesq approximation: the density variations ρ' are negligible with respect to the reference value ρ_0, except in their contribution to buoyancy forces.

$$\rho = \rho_0 + \rho' \text{ and } \rho' << \rho$$

• Hydrostatic approximation: assuming that the scales of horizontal dynamics are much larger than those of vertical dynamics, a balance between the pressure gradient and buoyancy is obtained.

$$\frac{\partial P}{\partial z} = -\rho g \tag{A.7}$$

Primitive Equations

The ocean model resolves the equations of fluid dynamics using the above approximations in a stratified and rotating medium. The system of equations is as follows:

$$\frac{\partial \vec{u}_h}{\partial t} = [(\nabla \times \vec{u}) \times \vec{u} + \frac{1}{2}\nabla(\vec{u}^2)]_h - f\vec{k} \times \vec{u}_h - \frac{1}{\rho_0}\nabla_h P + \vec{D}^u \tag{A.8}$$

$$\frac{\partial P}{\partial z} = -\rho g \tag{A.9}$$

$$\nabla.\vec{u} = 0 \tag{A.10}$$

$$\frac{\partial T}{\partial t} = -\nabla.(\vec{u}T) + D^T + F_{sol}(z) \tag{A.11}$$

$$\frac{\partial S}{\partial t} = -\nabla.(\vec{u}S) + D^S \tag{A.12}$$

$$\rho = \rho(T, S, P) \tag{A.13}$$

where f is the Coriolis parameter as a function of latitude. $F_{sol}(z)$ is the incoming solar heat flux. $\vec{D}^u$, D^T and D^S are the subgrid viscosity and diffusivity parametrizations. The atmospheric forcing is also included in these parametrizations as boundary conditions at surface.

Diagnostic of Sea Surface Height

The NEMO code uses the Boussinesq approximation (the model conserves volume rather than mass) and the **Free Surface Formulation** calculates Sea Surface Height as a diagnostic variable given by the equation :

$$\frac{\partial \eta}{\partial t} = -D + P - E \tag{A.14}$$

where

$$D = \nabla \cdot [(H + \eta)\bar{U}_h] \tag{A.15}$$

where the $P - E$ component is the net downward water flux, also includes the river run-off and the sea surface salinity restoring term. H is the depth of the sea floor, η is the height of the sea surface and $\bar{U}_h$ is the vertically integrated flow.

Appendix B

Radar Altimetry

In the following we present a more detailed description of the altimetric principle shown in figure B.1. For further information please see Ikeda and Dobson (1995) and the AVISO Website : http://www.aviso.oceanobs.com/.

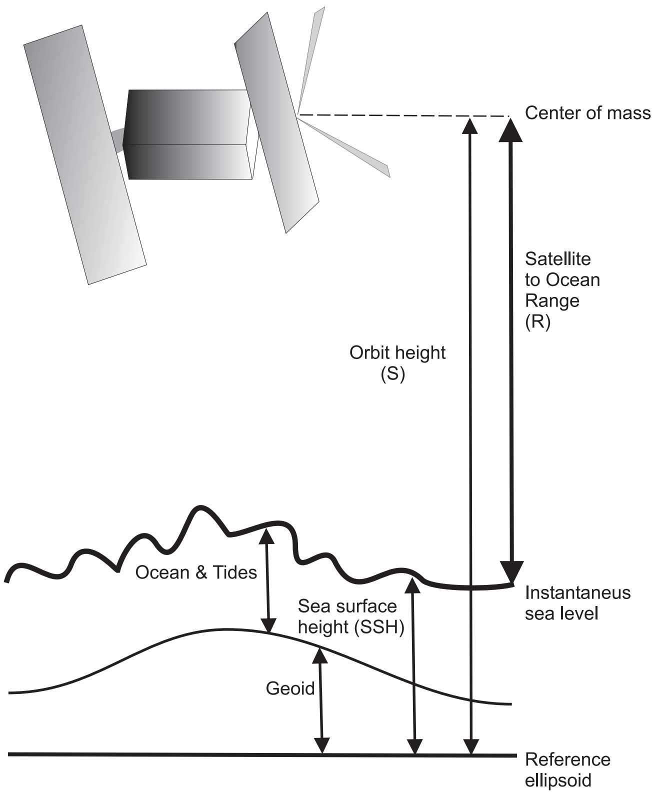

Figure B.1: Altimetric principle

Satellite-to-ocean range (R) Radar altimeters on board satellites permanently transmit signals at high frequency (over 1700 pulses per second) to Earth, and receive the echo from the sea surface. This is analysed to derive a precise measurement of the round-trip time between the satellite and the sea surface. The time measurement, scaled by the speed of light (at which electromagnetic waves travel), yields a range measurement. By averaging the estimates over a second, this produces a very accurate measurement of the satellite-to-ocean range. However, as electromagnetic waves travel through the atmosphere, they can be decelerated by water vapour or by ionization. Once these phenomena are corrected for, the final height is estimated within 2 cm. The ultimate aim is to measure sea level relative to a terrestrial reference frame. This requires independent measurements of the satellite orbital trajectory, i.e. exact latitude, longitude and altitude coordinates.

Satellite orbit height and tracking (S) The critical orbital parameters for satellite altimeter missions are altitude, inclination and period. For example, the TOPEX/POSEIDON satellite flies at an altitude of 1330 km, on an orbit inclined at 66^o to Earth's polar axis. The satellite on its so-called "repeat orbit" passes over the same ground position every 9.9156 days, uniformly sampling the Earth's surface. The satellite can be accurately tracked in a number of ways. The DORIS system on board TOPEX/POSEIDON uses a network of 50 ground beacons, worldwide, transmitting to the satellite. DORIS uses the Doppler shift on the beacon signals to accurately determine the velocity of the satellite on its orbit, and dynamic orbitography models to deduce the satellite trajectory relative to Earth.

This position is determined relative to an arbitrary reference surface, an ellipsoid. This reference ellipsoid is a raw approximation of Earth's surface, a sphere flattened at the poles. The satellite altitude above the reference ellipsoid, distance S, is available to within 3 cm.

Sea surface height (SSH) The sea surface height (SSH), is the range at a given instant from the sea surface to a reference ellipsoid. Since the sea depth is not known accurately everywhere, this reference provides accurate, homogeneous measurements. In practice, SSH is simply computed as the difference between the satellite orbit height (S) and the altimeter range (R):

$$SSH = S - R \tag{B.1}$$

The SSH value takes into account several different signals that can be described as:

$$SSH = G + \eta + \eta' + \epsilon_{orb} + \epsilon + n \tag{B.2}$$

G is the geoid, that is, the equipotential surface of the earth gravity field to which a motionless ocean surface would conform. It is due to major mass and density differences on the sea floor. For example, a denser rock zone on the sea floor would deform sea level and be visible as a hill on the geoid. The geoid variation ranges from a few meters to more than 100 m and it corresponds to the main contribution in SSH. η is the permanent dynamic topography, and η' is its variable part, which are both of the order of one meter, i.e. two orders of magnitude less than the geoid. ϵ_{orb} is the orbit error while ϵ are other altimeter errors (propagation effects in the troposphere and the ionosphere, tides, electromagnetic bias, inverse barometer effect) and n is the altimeter measurement noise (white noise).

Thus, to derive the dynamic topography the easiest way would be to subtract the geoid height, G, from SSH. In practice, the geoid is not yet known accurately enough, and mean sea level is subtracted instead. This yields the variable part of the ocean signal, referred to as Sea Level Anomaly (SLA).

Appendix C

Resumen en Español

La oceanografía es la rama de la ciencia que estudia los océanos. Es un término global que incluye todos los aspectos y procesos que ocurren y gobiernan el océano; organismos marinos y su dinámica de ecosistemas, geología marina, química y bioquímica, procesos físicos y dinámica de los océanos. La oceanografía es un campo de la ciencia relativamente joven, con poco más de un siglo de historia. La mayoría de los avances de la oceanografía se han producido en los últimos 50-60 años, con unarápida aceleracin hacia el final del siglo XX. En este momento, la oceanografía física ha pasado de ser un campo que se refiere principalmente a la exploración del Océano Mundial, a enfocarse a preguntas mucho más detalladas que implican mecanismos que subyacen a la circulación oceánica y su papel en el clima.

Debido al papel central que desempeñan los océanos en muchas de las cuestiones que afectan a la humanidad (clima, recursos, demografía, política, etc), el interés por el estudio de los océanos ha aumentado considerablemente en los últimos 50 años. Hasta hace poco tiempo, nuestra comprensión de la variabilidad del océano se ha visto limitada por la falta de observaciones históricas. En las últimas décadas, la calidad de las observaciones oceánicas, ha aumentado considerablemente, especialmente durante el Experimento Mundial sobre la Circulación Oceánica (WOCE) y más recientemente con la ayuda de la tecnología moderna de telemetría. El auge de las observaciones por satélite (altimetría, microondas, infrarrojos, y el color del océano), así como el uso generalizado de redes de fondeos de larga duración, boyas de deriva Lagrangianas, y los más recientes vehículos autónomos inteligentes (AUV, planeadores, etc.) están transformando la manera en que observamos y comprendemos los océanos. A pesar de este incremento en los datos disponibles, todavía hay muchas regiones de los océanos que tienen muy pocas o ningunas observaciones *in situ*, principalmente en el hemisferio sur. Incluso con una cobertura global por satélite, estos sensores se basan en la energía electromagnética que no pueden penetrar en el interior del océano. Por lo tanto la mayoría de las mediciones se limitan a la superficie. Con el aumento exponencial de la potencia de procesamiento en los ordenadores modernos, los modelos numéricos, que han experimentado un crecimiento equivalente, tanto en el rendimiento como en la complejidad, ayudan a completar la imagen mediante la vinculación de todas las observaciones y conocimientos sobre los océanos para realizar predicciones y análisis retrospectivos en tres dimensiones, potencialmente permitiendo el estudio de los procesos oceánicos con un nivel de detalle imposible hasta la fecha con observaciones por sí solas.

La oceanografía ha cobrado especial relevancia en los últimos años, al convertirse el cambio climático en una enorme fuente de interés para la comunidad científica y el público en general. El clima de la Tierra está en constante cambio, y aunque su variabilidad principal proviene de los procesos naturales, el término *cambio climático* se utiliza generalmente para referirse a los cambios en nuestro clima que se han identificado desde la primera parte del siglo 20. Los cambios observados en los últimos años y los que están previstos durante el próximo siglo se cree que son, principalmente de origen antropogénico, más que debido a los cambios naturales en el océano y la atmósfera, sin embargo esto sigue siendo un tema de debate y estudio.

Con su capacidad calórica, que es mil veces mayor que la de la atmósfera, el océano juega un papel fundamental en la lenta evolución del clima en nuestro planeta, moderando las temperaturas promedio y el clima a largo plazo posibilitando la existencia de la vida. Los océanos son también enormes reservas de gases atmosféricos como el CO_2, absorbiéndolo y encerrándolo durante largos períodos de tiempo (hasta 1000 años), amortiguando en cierta medida, el efecto del aumento de CO_2 sobre el clima. Debido a este papel vital, y con el fin de comprender y predecir el cambio climático, debemos primero comprender los procesos oceánicos que lo afectan y lo controlan.

Variabilidad del Océano

El uso generalizado de la telemetría moderna y los sistemas de observación que proporcionen una visión global de los océanos (con diversos grados de resolución temporal, espacial y vertical) han puesto de relieve la complejidad de la variabilidad del océano a lo largo de una amplia gama de escalas espaciales y temporales. Las escalas de longitud de las estructuras oceánicas (figura C.1) puede variar desde unos pocos kilómetros (e.j., filamentos costeros) a las estructuras a escala de cuenca (e.j. la corriente del Golfo), incluidas las estructuras intermedias del orden de 10-100 km (e.j. remolinos de mesoescala). Las escalas temporales de la variabilidad de estas estructuras puede ir desde días hasta años, o incluso décadas. La presencia en el océano de todas estas estructuras, con diferentes escalas de variabilidad y la interacción entre ellas, hace que el océano real sea un sistema muy complejo. Esta complejidad es inducida por varios mecanismos físicos, de los cuales uno de los principales componentes es el forzamiento atmosférico (principalmente, el viento y los flujos de calor y de agua dulce), que influye directamente en la superficie del océano. En una visión simplificada, el ciclo estacional del flujo de calor en el océano provoca una fluctuación estacional de la temperatura superficial del mar, mientras que el cambio estacional en la velocidad y la dirección de los vientos medios cambia la intensidad y la dirección de los giros y corrientes oceánicas medias. Además, el forzamiento atmosférico promedio puede mostrar una variabilidad considerable de año en año (e.j. inviernos suaves o severos), así como eventos atmosféricos sinópticos (e.j. ráfagas de viento fuertes y localizadas, tormentas, etc), y tener un gran impacto a escala local (corrientes, temperatura, salinidad, etc.) Estos procesos combinados alteran el ciclo estacional dando lugar a la variabilidad interanual del océano.

El océano puede ser considerado, para una amplia gama estudios, un fluido cuasi-no viscoso y estratificado bajo la influencia de la rotación de la Tierra, y donde las inestabilidades dinámicas del flujo medio pueden aparecer por separado de la acción directa del forzamiento atmosférico (capítulo 13, Gill (1982)). Estas inestabilidades dinámicas (tanto baroclinas o barotrópicas) pueden crecer y generar remolinos de mesoescala y marcados frentes oceánicos con una variabilidad de mesoescala asociada. La escala natural asociada a la variabilidad de mesoescala en el océano es el radio de deformación de Rossby o el radio interno de deformación, que es básicamente la escala de longitud horizontal en la que los efectos de rotación pasan a ser tan importante como los efectos de flotabilidad (o gradiente de presión. En muchos casos, los remolinos de mesoescala aparecen y evolucionan de forma independiente del forzamiento atmosférico externo, así como potencialmente interactuan con las corrientes y la topografía, produciendo respuestas a largo plazo en la circulación oceánica y dando lugar a una variabilidad interna interanual del océano.

En el contexto de la variabilidad interanual, con este sistema complejo compuesto por tantos procesos interrelacionados, se hace muy difícil distinguir

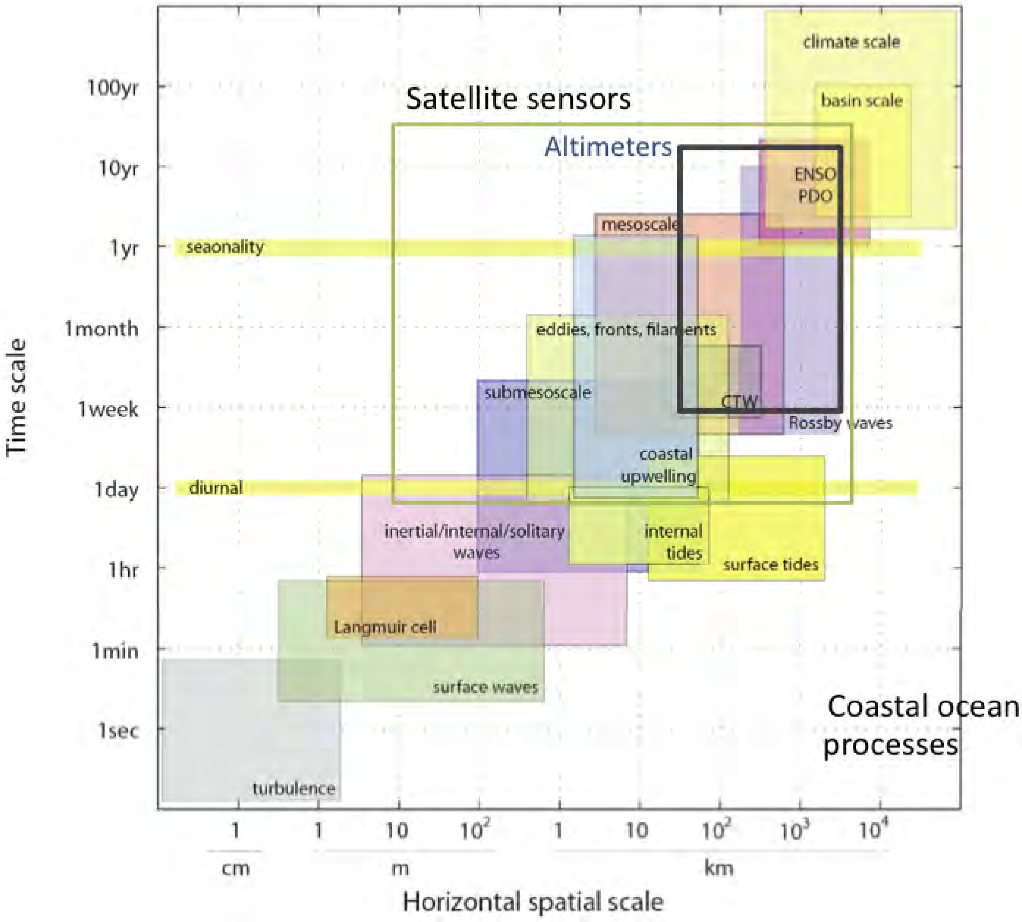

Figure C.1: Escalas espaciales y temporales en el océano (basado en Chelton et al. (2001)

entre la variabilidad natural del sistema y de las alteraciones causadas por la actividad humana. A pesar del progreso significativo, las bases de datos observacionales siguen siendo demasiado cortas, demasiado superficiales (satélites) o demasiado dispersas en el tiempo y el espacio (boyas y fondeos) para permitir estudios detallados de los procesos físicos a lo largo de su amplia gama de escalas (figura C.2 muestra la disponibilidad de observaciones *in situ* desde 1958). Con el fin de estudiar la importancia relativa de cada uno de los mecanismos que desempeñan un papel en la variabilidad del océano (el forzamiento externo o la variabilidad interna de los océanos), es fundamental complementar toda la información de datos *in situ* estudios de modelización numérica.

Modelización Numérica Oceánica

La *modelización numérica de circulación oceánica* consiste en técnicas numéricas para calcular soluciones aproximadas de las ecuaciones diferenciales parciales complejas, no lineales y multidimensionales que rigen la dinámica de los océanos. Los modelos oceánicos han demostrado ser una poderosa herramienta para estudiar la dinámica de los océanos y su variabilidad, especialmente debido al aumento en el poder computacional logrado durante las últimas dos décadas.

Recientes simulaciones numéricas (análisis retrospectivos) ofrecen la evolución continua y completa de los océanos para el período de simulación pero requieren cuidadosas valoraciones cuantitativas y la evaluaciones del desajuste entre modelos y observaciones para guiar los estudios dinámicos y nuevas mejoras del modelo (Penduff et al., 2007).

Debido a que los modelos oceánicos son totalmente flexibles en su configuración, y se pueden diseñar de muchas maneras diferentes para estudiar los distintos procesos oceánicos, es importante entender en primer lugar, cuál va a ser exactamente su función, y en segundo lugar, sus limitaciones en términos de las escalas que pueden ser representadas o resueltas por el modelo, las escalas que deben ser parametrizadas, y finalmente las escalas que están siendo representados de manera imperfecta. La circulación de los océanos es una función complicada de la estructura de la densidad de las masas de agua que componen las cuencas oceánicas, los flujos de radiación en superficie, y el forzamiento atmosférico impuesto en la superficie. Este forzamiento contiene una variedad de escalas temporales (desde horas hasta variaciones de decenios) y espaciales (que van desde el kilómetro a las escalas de la cuenca).

Debido a esta complejidad extraordinaria, y debido a las limitaciones computacionales, los modelos oceánicos deben comprometer su configuración en

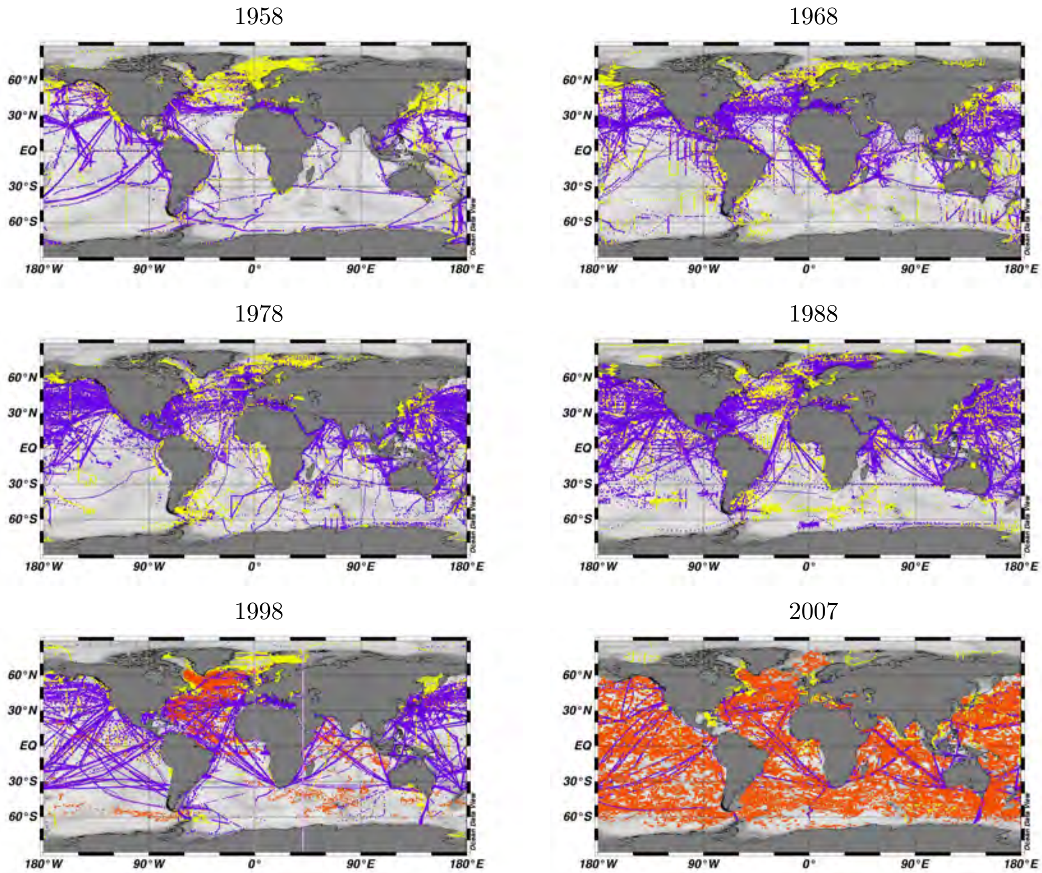

Figure C.2: Cobertura espacial de observaciones *in situ* en los años 1958, 1968, 1978, 1998, y 2007 de diferentes instrumentos: batitermógrafos=MBT, XBT (en violeta), TESAC (en amarillo) y Boyas ARGO (en naranja) (de Juza (2011)).

términos de resolución, cobertura espacial, aproximaciones/simplificaciones en las ecuaciones y otras parametrizaciones. Como tal, hay muchos tipos de modelos oceánicos y Kantha and Clayson (2000) presentan una revisión exhaustiva.

Para esta tesis en la que nos interesa la variabilidad del océano en tres dimensiones, los modelos deben ser baroclinos, globales o regionales, con una resolución suficiente para resolver las características objeto de estudio, mantener una formulación de superficie libre (para el nivel del mar y la adición de masas como características a ser estudiadas) y estar vinculada a la atmósfera ya sea a través de un forzamiento atmosférico externo o mediante modelos atmosféricos acoplados.

Una de las simplificaciones típicas utilizadas en modelos a gran escala de la circulación oceánica es la aproximación hidrostática / Boussinesq. ésta ignora los cambios de densidad en el fluido, excepto cuando se refiere a las fuerzas gravitatorias. Esta simplificación es adecuada cuando se modelan las características horizontales superiores a 10 km (de 10 a 1.000 kilometros desde remolinos de mesoescala a giros oceánicos) ya que por debajo de esta resolución la aproximación hidrostática no se mantiene.

Para los modelos numéricos que tienen por objeto la creación de simulaciones realistas del pasado (análisis retrospectivo), el uso de datos de forzamiento atmosférico realistas es necesario para forzar la simulación. Estos incluyen flujos en superficie de radiación, calor y la flotabilidad (precipitación y evaporación), así como la fuerza del viento. Lo que el modelo puede y no puede resolver (tanto temporal como espacialmente) también se ve influenciado por la resolución temporal y espacial de estas variables de forzamiento atmosférico, que dependen de la disponibilidad de mediciones de alta calidad. En los últimos años la cantidad, distribución y calidad de las observaciones ha aumentado considerablemente, pero cuanto más se retrocede en el tiempo, más escaso es el número de mediciones. Esto es especialmente cierto para el mar abierto, donde los datos sobre flujos de viento, la humedad y la precipitación son muy limitados. Debido a que estos flujos dependen de pequeñas diferencias de temperatura y humedad en la interfaz entre el mar y la atmósfera, las mediciones directas de los flujos de agua y calor con la cobertura y la precisión que se requiere para un modelo oceánico son muy difíciles de obtener sobre la enorme extensión de los océanos globales. Mientras que los modelos de predicción meteorológica pueden calcular los flujos de este tipo, aún no producen los datos con la suficiente precisión y resolución de mesoescala necesaria para los modelos oceánicos. Por otra parte, forzando los modelos con estimaciones climatológicas de flujos superficiales generalmente resulta en valores irrealistas de temperatura y salinidad superficiales, que acaban siendo inconsistentes con los propios flujos impuestos en superficie (Barnier, 1998). Actualmente, muchos de los modelos oceánicos utilizan re-análisis de datos atmosféricos, que son compilaciones de observaciones dispuestas en mallas regulares y que pasan un control de calidad, como puede ser ECMWF ERA40 (Uppala et al., 2005). En estos re-análisis, las observaciones procedentes de múltiples fuentes se insertan en un sistema integrado de predicción que utiliza una técnica variacional en tres dimensiones para proporcionar análisis cada seis horas. Las nuevas revisiones de ERA40 como ERA-Interim (Dee et al., 2011) y ARPEGE (Beuvier et al., 2010) son "downscales" dinámicas que tienen como objetivo mejorar y aumentar la resolución de los datos atmosféricos. Debido a que el forzamiento atmosférico de los modelos numéricos todavía debe mejorar considerablemente, los desequilibrios en el balance de agua y los flujos de calor pueden resultar en una deriva de simulaciones de las condiciones estables. Lo que comúnmente se hace para resolver este problema es forzar el modelo con una simple relajación de la temperatura o salinidad superficial (o ambas) hacia una media climatológica. Este enfoque presenta muchos inconvenientes en la representación de la variabilidad del océano, ya que las características de mesoescala, como remolinos y frentes se suavizan irrealmente rápido debido a esta relajación.

Las características físicas de los océanos en cuanto a forma (costa), topografía, y canales y estrechos también son vitales para el funcionamiento del modelo, ya que pueden tener efectos importantes en muchas escalas de la circulación. La resolución con la que se resuelven puede en algunos casos determinar si el modelo es capaz de simular patrones realistas de circulación en ciertos lugares. Los estrechos y canales son de especial importancia ya que es aquí donde el intercambio de agua y flujos de calor entre mares y cuencas se produce. Otro de los retos en el modelado de las características topográficas del océano son las plataformas y taludes continentales, los cuales juegan un papel importante en la circulación oceánica, especialmente en lo que respecta a las corrientes costeras, "jets", así como el derramamiento de aguas frías y densas hacia el océano profundo. Debido a la poca profundidad , la circulación en la plataforma es forzada fuertemente por los vientos y las mareas astronómicas, mientras que sobre el océano profundo son los gradientes de densidad y los vientos. Además, la transición entre la plataforma y el océano abisal es muy abrupta con las zonas de pendiente teniendo escalas espaciales de decenas de kilómetros (en comparación con miles en el océano abierto). Por lo tanto, los modelos de resolución baja o media tienden a suavizar en gran medida estas características topográficas abruptas, afectando a muchos de los patrones de circulación costera, que tienden a fluir a lo largo de estas características topográficas (Kantha and Clayson, 2000).

En general, una mayor resolución siempre es preferible, aunque está limitada por la capacidad computacional y de almacenamiento, y por lo tanto deben hacerse compromisos. Los modelos globales de alta resolución (e.j. figura C.3) son computacionalmente muy costosos (a menudo requieren el uso de grandes clústeres de ordenadores durante largos períodos de tiempo). Es por ello qué los modelos regionales (e.j. figura C.4) son capaces de funcionar a una resolución más alta que los modelos globales y por lo tanto más prácticos para estudios regionales.

Sin embargo, los modelos regionales tienen sus propios problemas, estos modelos requieren que sus condiciones de contorno sean proporcionadas por anidación en un modelo de menor resolución o mediante la relajación a una climatología. El anidamiento dentro de un modelo de menor resolución puede introducir errores debido a las diferencias en la parametrización de los procesos físicos en ambos modelos, así como los errores debidos a las técnicas numéricas

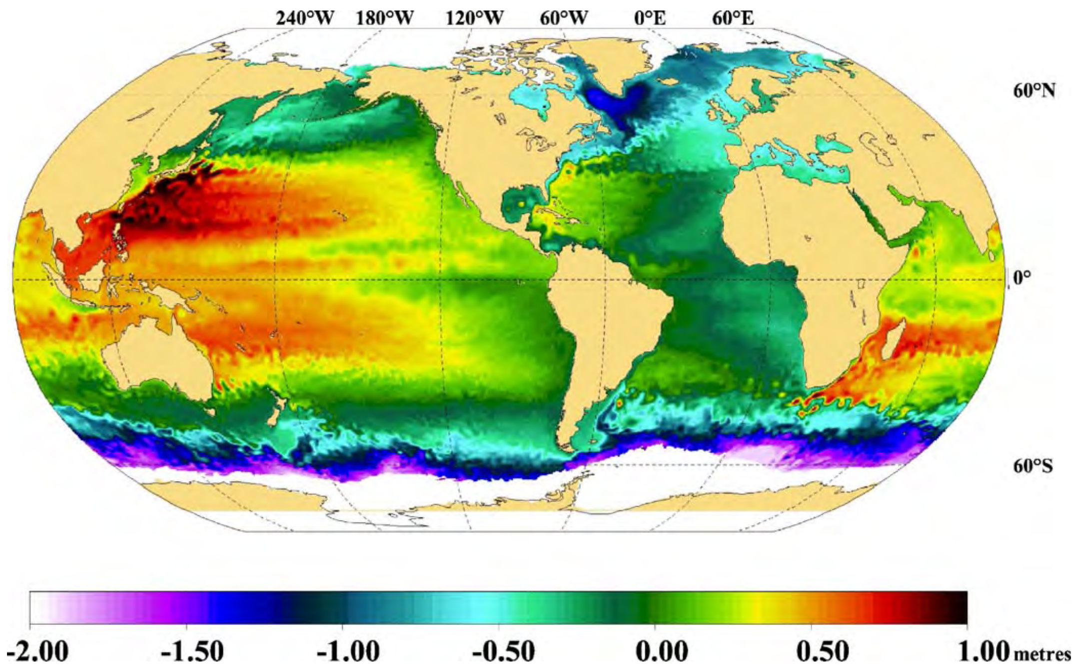

Figure C.3: Cobertura de un modelo global (ORCA G22) mostrando una instantánea de altura de nivel del mar y cobertura de hielo durante el invierno (de Barnier et al. (2006)).

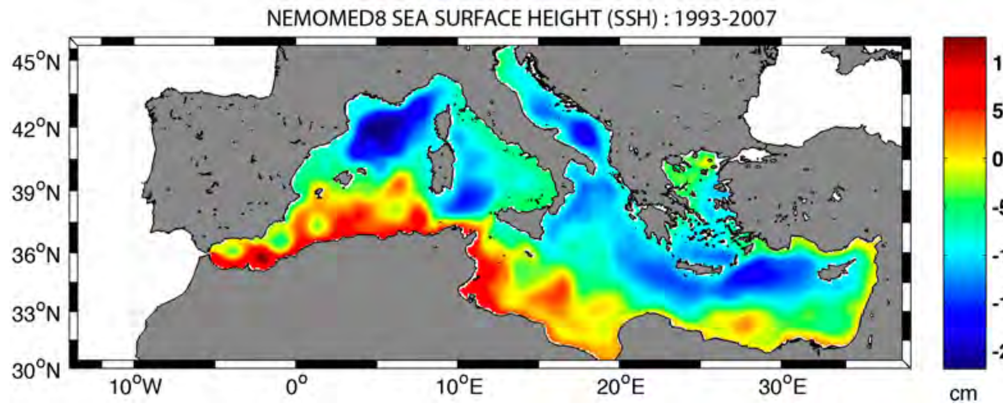

Figure C.4: Cobertura de un modelo regional (MEMOMED8) mostrando un promedio de altura de nivel del mar para el periodo 1993-2007.

utilizadas para la anidación, que se pueden propagar al dominio regional con un impacto significativo en la evolución de la simulación.

El Mar Mediterráneo

En el contexto de la variabilidad oceánica y los estudios sobre el cambio climático, el Mar Mediterráneo (Figura C.5) se considera un "océano en miniatura" (Bethoux and Gentili, 1999; CIESM Initiative Group, 2002), una especie de laboratorio oceánico ideal y accesible a escala reducida, donde muchos de los fenómenos presentes en diferentes regiones del océano global pueden ser estudiados en una escala más pequeña: la convección profunda (MEDOC Group, 1970; Leaman and Schott, 1991), intercambios entre el talud y la plataforma (Bethoux and Gentili, 1999), circulación termohalina e interacción entre masas de agua (Wüst, 1961), dinámica de mesoescala y submesoescala (Robinson et al., 2001), etc. A pesar de su pequeño tamaño, la circulación termohalina en la cuenca es particularmente activa (Wu and Haines, 1996). (Robinson et al., 2001) da un valor de 10 a 14 km para el radio interno de deformación de Rossby, cuatro veces menor que el valor normal en el océano abierto. Por lo tanto los mecanismos físicos pueden ser mejor monitorizados y comprendidos en esta "cuenca oceánica", contribuyendo al avance del conocimiento de las interacciones físicas y acoplamiento biogeoquímico a escalas costeras, locales de sub-cuenca y globales (Tintore, 2009).

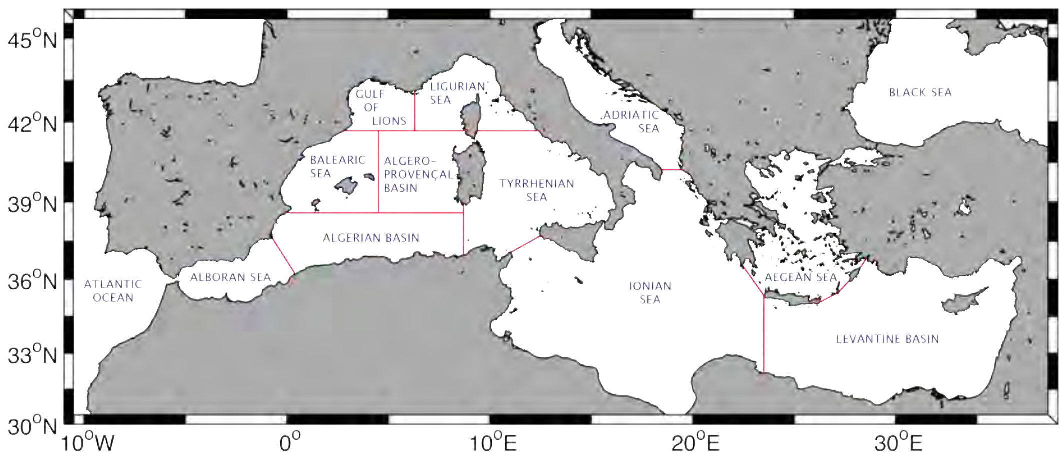

Figure C.5: Regiones y cuencas del Mar Mediterráneo.

El Mediterráneo es mar semicerrado de latitud media conectado con el Océano Atlántico a través del Estrecho de Gibraltar ($\sim$300 m de profundidad). Se compone de dos cuencas principales, las cuencas conectadas occidental (WMED) y oriental (EMED) conectadas por el Estrecho de Sicilia. Cada una de estas cuencas están compuestas de varias sub-cuencas caracterizadas por diferentes características oceanográficas (topografía, masas de agua y forzamiento atmosférico) y separadas por estrechos y canales (Astraldi et al., 1999).

El esquema general de la circulación del Mediterráneo es bastante complejo debido a la interacción de múltiples escalas, incluyendo estructuras de escala de cuenca, sub-cuenca y mesoescala (Robinson and Golnaraghi, 1994). En el Mediterráneo se encuentran fuertes corrientes costeras, "jets" inestables que generan vórtices, giros de sub-cuenca permanentes y recurrentes, y enérgicos remolinos de mesoescala. Todas estas estructuras interactúan y dan lugar a una gran variabilidad en un amplio rango de escalas temporales (mesoescala, estacional e interanual). Esta complejidad y la variabilidad de la circulación de los océanos proviene de múltiples fuerzas impulsoras: efectos topográficos, forzamientos atmosféricos variables, y procesos dinámicos internos.

Otro elemento que también es importante en el Mediterráneo debido a sus enormes impactos socio-económicos es la variabilidad del nivel del mar. En el Mediterráneo, depende tanto de forzamientos locales como remotos (los cambios del nivel del mar están relacionadas con la NAO por el efecto combinado de las anomalías de presión atmosférica y los cambios en la evaporación y la precipitación (Tsimplis and Josey, 2001)). La expansión estérica global que ocurre fuera de la cuenca del Mediterráneo puede transmitir una señal a través del Estrecho de Gibraltar. Dentro del Mediterráneo, la variabilidad interanual y de más alta frecuencia está dominada por el viento y los cambios de presión atmosférica (Gomis et al., 2006) a la vez que variaciones estéricas, cambios asociados en la cantidad de agua proveniente de los ríos, la evaporación y la precipitación impulsada por el forzamiento atmosférico regional, contribuyen a los cambios del nivel del mar (Tsimplis et al., 2008). El ritmo de variación del nivel del mar en el Mediterráneo ha mostrado una variabilidad considerable en el último siglo. Antes de la década de 1960, el nivel del mar relativo aumentaba a un ritmo de alrededor de 1,2 mm / año. Entre 1960 y 1994 el nivel del mar caía (Tsimplis and Baker, 2000), y a partir de mediados de la década de 1990, las mediciones altimétricas sugieren un rápido aumento del nivel del mar, especialmente en el Mediterráneo oriental. La variabilidad espacial del nivel del mar es también extremadamente no uniforme, lo cual se puso claramente de relieve con la llegada de la altimetría por satélite, capaz de cartografiar el océano abierto y las variaciones geográficas de los cambios del nivel del mar (Cazenave et al., 2001).

En las siguientes secciones se presentan algunas de las características principales de circulación del mar Mediterráneo y los esfuerzos de modelización realizados en esta región.

Circulación Superficial

El esquema de circulación general del Mar Mediterráneo es complejo y consta de tres escalas espaciales predominantes que interactúan entre sí: escala de la cuenca (incluyendo la circulación termohalina), la escala de sub-cuenca, y la mesoescala (Robinson et al., 2001). La variabilidad de mesoescala se conoce como la señal dominante en la circulación oceánica (Pujol and Larnicol, 2005), y está presente en la mayoría de los aspectos de la circulación del Mediterráneo, desde los giros que se encuentran en el Mar de Alborán y la cuenca Levantina a la vorticidad de los remolinos de mesoescala relacionados con las corrientes más importantes, como la Corriente Argelina, La Corriente del Norte y la Corriente del Jónico (figuras C.6 y C.7). También juega un papel importante en la formación de aguas profundas en el Golfo de León a través de la inestabilidad baroclína de mesoescala (Herrmann et al., 2008a).

El circuito de la circulación superficial del Mediterráneo comienza con el Agua Atlántica (AW) entrando en el Mar Mediterráneo hacia el Mar de Alborán a través del Estrecho de Gibraltar en las capas superficiales (100-200 m aprox.). La circulación en este mar está dominada por uno o dos grandes giros anticiclónicos (Viúdez et al., 1998), un giro anticiclónico occidental cuasi-permanente (Giro Oeste de Alborán, WAG) (figura C.6) y el intermitente Giro Este de Alborán (EAG). Mientras que el EAG también puede tener fases ciclónicas (Viúdez and Tintoré, 1995) es sobre todo anticiclónico (Tintoré et al., 1988). El límite oriental del EAG se conoce como el frente Almería-Orán y marca el inicio de Corriente Argelina, que fluye a lo largo de la costa africana. Esta estrecha corriente costera es muy inestable y produce muchos remolinos anticiclónicos de 50-100 km de diámetro que pueden verse claramente con imágenes de satélite infrarrojas (Millot, 1999). Por esta razón, la Cuenca Argelina se caracteriza por una intensa actividad de mesoescala. Algunos de estos remolinos pueden crecer y desprenderse de la costa alcanzando en algunos casos el sur del Mar Balear (Ruiz et al., 2002). La Corriente Argelina llega al estrecho de Sicilia, donde se bifurca en dos ramas. Una rama entra en el Mediterráneo Oriental, mientras que la otra rama se queda en el Mediterráneo Occidental.

La circulación en el Estrecho de Sicilia presenta un intercambio en dos capas: en la superficie, las AW entran en la cuenca oriental, y en las capas más profundas, el agua levantina intermedia (LIW), que se forma en la cuenca Levantina, entra en la cuenca occidental. La rama de AW que permanece en el Mediterráneo Occidental fluye a lo largo de las costas italianas, francesas y españolas, como la denominada Corriente del Norte (Millot, 1999) y la LIW sigue un camino ciclónico similar a lo largo de la periferia del Mediterráneo Occidental a una profundidad de entre 200 y 800 m. La Corriente del Norte, que también se alimenta por AW que fluyen hacia el norte a lo largo del este de Córcega, finalmente fluye hacia el Mar Balear, donde una parte atraviesa los canales de Ibiza y Mallorca y sigue su camino hacia el Mar de Alborán. El resto de la Corriente del Norte recircula hacia el Norte-Este convertida en la Corriente Balear (Alvarez et al., 1994; Pinot et al., 1995; Astraldi et al., 1999; Ruiz et al., 2009). Durante su trayectoria desde Gibraltar hacia el este, las AW cambian gradualmente haciéndose cada vez más cálidas (de 14 a 15 ^{o}C por debajo de la capa de mezcla) y más salinas de $\sim$36,5 en el Estrecho de Gibraltar a 38,0-38,3, tras completar su ciclo alcanzando el Mediterráneo Nor-Occidental (Millot, 1999). Cuando la corriente alcanza el norte de la cuenca Balear, las propiedades de las AW antiguas son muy distintas de las AW recientes al sur, formándose así un frente de densidad que las separa (Frente Balear).

En el Mediterráneo Oriental, las aguas superficiales que entran por el Estrecho de Sicilia forman la llamada Corriente Jónica-Atlántica, esta corriente está formada por las AW modificadas con una salinidad de 38,5 psu. En la

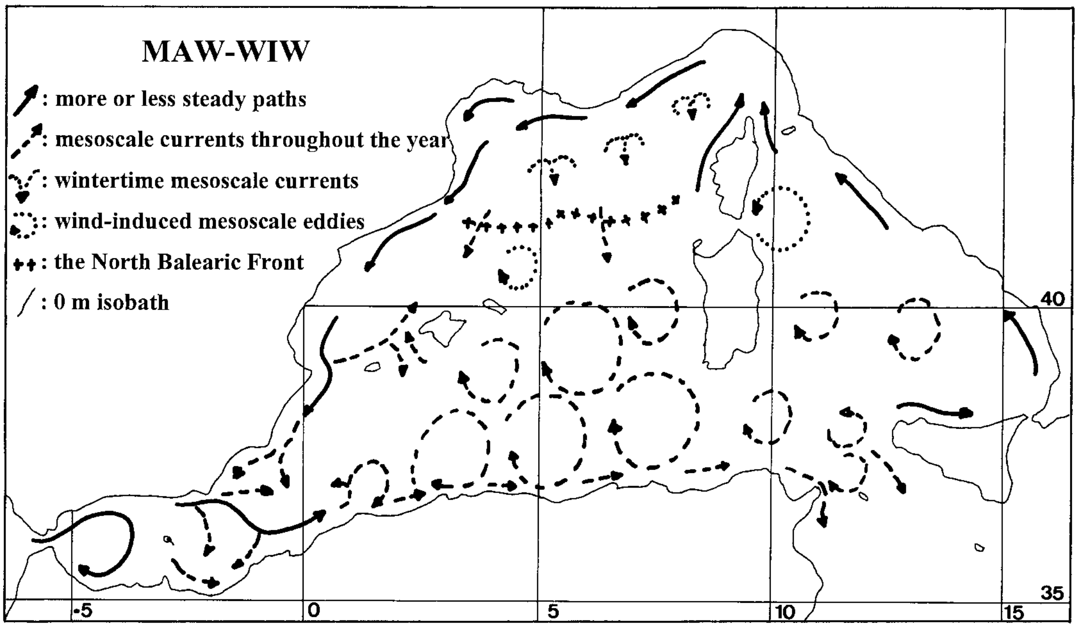

Figure C.6: Esquema de la circulación superficial en el Mediterráneo Occidental (Millot, 1999)

cuenca del Jónico, hay dos giros permanentes, el giro anticiclónico de Pelops y el giro ciclónico de Creta (figura C.7). La Corriente Jónica entra en la cuenca Levantina, la cuenca más oriental del Mediterráneo, donde el agua se calienta y se vuelve más salada durante el verano debido a un exceso de evaporación en superficie. Se han observado dos características permanentes en esta cuenca, el giro anticiclónico de Mersa-Matruh y el giro ciclónico de Rodas. En invierno, el enfriamiento incrementa la densidad de las aguas superficiales haciendo que se hundan y se mezclen formando la LIW, que se extiende a una profundidad de 300-500 m, sale a través del Estrecho de Sicilia hacia el Mediterráneo Occidental y, por último, emerge al Océano Atlántico a través de el Estrecho de Gibraltar. El lugar preferido de formación de la LIW es la región del Giro de Rodas, aunque existen observaciones de la formación de aguas intermedias en otras áreas del Mar Levantino (véase la revisión de Lascaratos et al. (1999)).

Como se ha mencionado anteriormente, una parte importante de la circu-

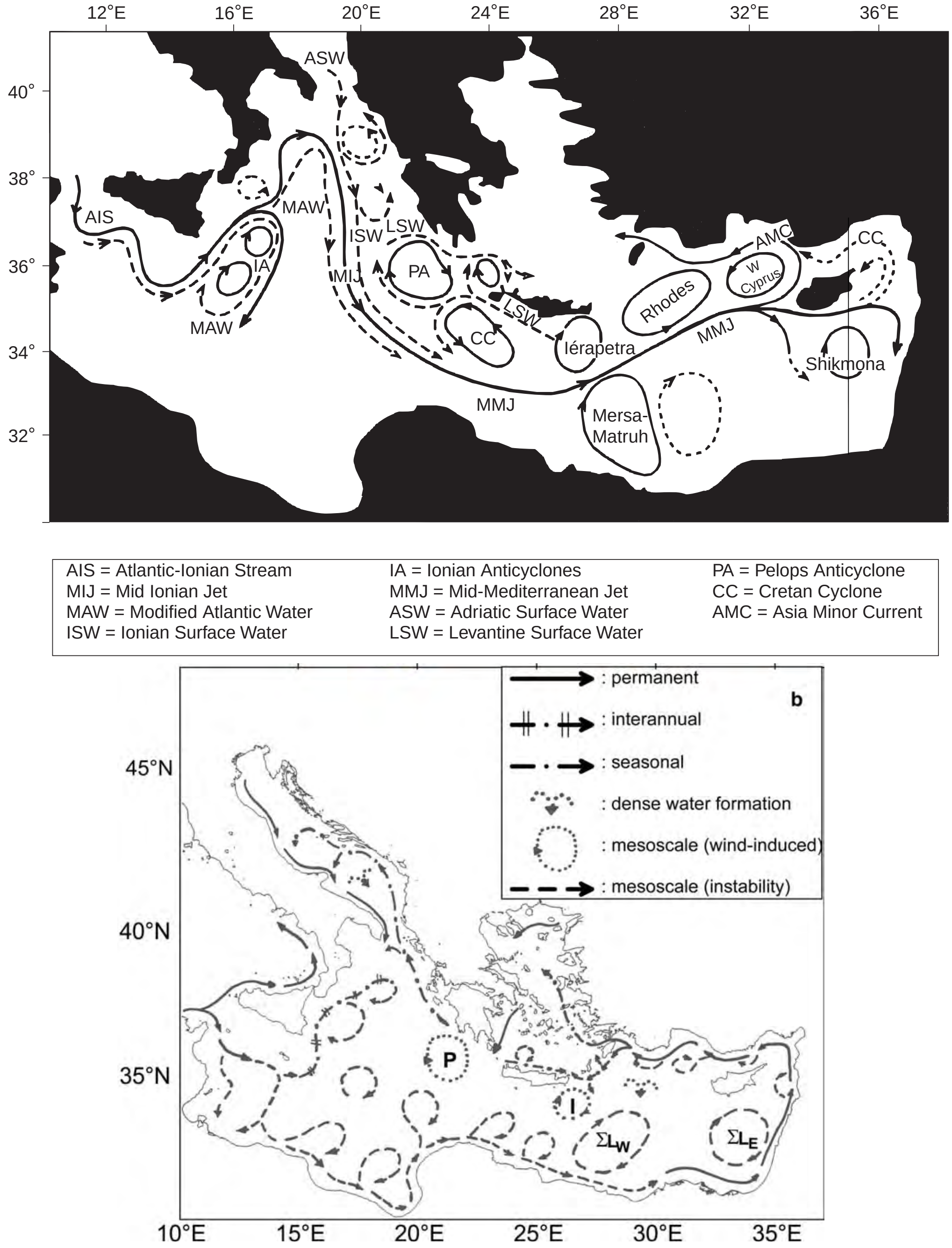

Figure C.7: Dos variaciones de la circulación en el Mediterráneo Oriental. Robinson and Golnaraghi (1994) (arriba), Hamad et al. (2005) (abajo) lación del Mediterráneo proviene de remolinos y characteristicas de mesoescala. La circulación de mesoescala es turbulenta y muestra una gran variabilidad espacial y temporal. No todas las áreas del Mediterráneo exhiben una cantidad similar de actividad de mesoescala. Mientras que algunas regiones muestran una alta actividad como son el Mar de Alborán, a lo largo de la Corriente Argelina y también la cuenca Levantina por debajo del Arco de Creta, otras regiones como la cuenca Liguro-Provençal, los mares Tirreno y Adriático tienen una actividad de mesoescala baja (Pujol and Larnicol, 2005).

Los remolinos de mesoescala se forman a través de inestabilidades a lo largo del las corrientes costeras, como la Corriente Argelina, y eventualmente pueden desprenderse de las corrientes convirtiéndose en remolinos oceánicos e interactuar con la corriente misma. Los remolinos se pueden formar con un movimiento tanto ciclónico y anticiclónico, siendo los primeros más pequeños y de corta duración (días o semanas), y los segundos más grandes y capaces de durar meses o incluso más de un año. Los grandes remolinos anticiclónicos pueden tener efectos significativos en la circulación en amplias zonas y durante largos períodos de tiempo. Pueden alcanzar un tamaño (desde varias decenas a unos pocos cientos de kilómetros) y profundidad considerables, y pueden interactuar con las corrientes costeras o incluso bloquear la circulación por completo, especialmente en la proximidad de estrechos y canales (Millot, 1999). Esto pone de relieve la importancia de los estudios de la variabilidad de mesoescala en la comprensión de la circulación superficial del Mar Mediterráneo.

Dado que la escala horizontal de remolinos de mesoescala está relacionada con el radio de deformación de Rossby, que en el Mar Mediterráneo es de $\sim$10-14 kilometros, el estudio adecuado de los remolinos de mesoescala requiere un muestreo muy fino o modelado de alta resolución.

Formación de Aguas Profundas

El Mediterráneo tiene una intensa circulación termohalina, siendo una de las pocas regiones en el mundo donde se produce convección profunda en mar abierto (Herrmann et al., 2008b) y por lo tanto uno de los pocos lugares capaces de redistribuir agua a grandes profundidades (Schroeder et al., 2010). La formación de aguas profundas es importante tanto para el Mediterráneo como para el océano global. Es el principal mecanismo que permite el intercambio de oxígeno y nutrientes entre la superficie y las capas más profundas. Las aguas profundas también pueden actuar como marcadores climáticos ya que una vez que se hunden hacia las capas más profundas, mantienen las propiedades que fueron determinadas por las condiciones atmosféricas prevalecientes en su lugar de formación, lo que permite estudios de climas pasados siempre que las escalas de tiempo de renovación lo permitan (que pueden ser décadas o siglos en el Mediterráneo) (Lascaratos et al., 1999). La figura C.8 muestra una representación esquemática de la circulación termohalina en el Mar Mediterráneo.

El proceso de convección profunda consiste en tres fases, comenzando con el pre-acondicionamiento, donde el área de convección profunda se prepara para la mezcla vertical. En el Golfo de León, el agente de pre-acondicionamiento es la circulación ciclónica en su centro, que eleva las isopicnas y expone las aguas más densas y menos estratificadas a la atmósfera, lo que facilita el proceso de mezcla. Además, una región puede mantener la señal de los eventos de convección de un año, pre-acondicionando el evento de convección profunda en el año siguiente. Una vez que la estratificación de la columna de agua ha sido lo suficientemente degradada por el pre-acondicionamiento, la segunda fase es la convección y mezcla profunda, que puede ser iniciada por un único o múltiples fenómenos atmosféricos intensos. La tercera y última etapa es la reestratificación de la columna de agua una vez que la turbulencia se ha disipado

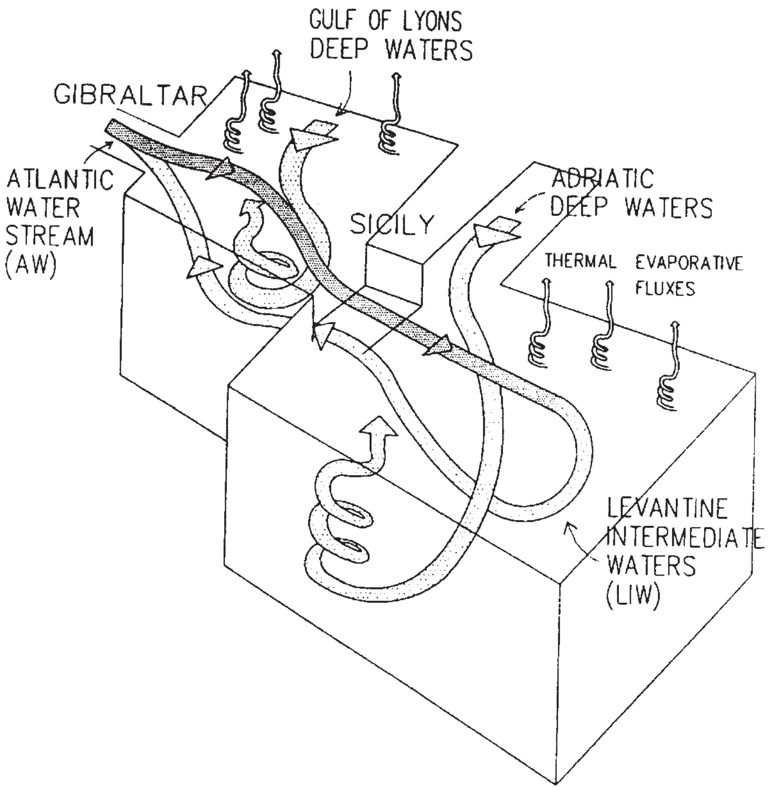

Figure C.8: Representación esquemática de la circulación termohalina en el Mediterráneo de Lascaratos et al. (1999).

y los gradientes de densidad restablecidos (Juza, 2011).

El Mediterráneo Nor-Occidental es una de las principales localizaciones de formación de aguas profundas del Mar Mediterráneo. Los principales impulsores de la convección profunda en el Mediterráneo Nor-Occidental son atmosféricos, principalmente los fuertes vientos del norte y la importante pérdida de calor durante los mese de invierno junto con el giro ciclónico en el centro del Golfo de León. Estas condiciones atmosféricas (Tramontana, Mistral, la ciclogénesis del Golfo de Génova, etc) son causadas por la orografía local de la costa del Mediterráneo Nor-Occidental (Alpes, Pirineos, Valle del Ródano), que canalizan los vientos fuertes y fríos hacia la zona (Herrmann and Somot, 2008). En esta región, los vientos secos y fríos inician la mezcla violenta de las aguas Atlánticas superficiales (AW) con las cálidas y saladas aguas Levantinas Intermedias subyacentes (la LIW), que al seguir enfriándose conduce a la formación de aguas profundas del Mediterráneo Occidental (WMDW) (MEDOC Group, 1970; Schroeder et al., 2010), que se hunden hasta el fondo de la región a ~2000 metros. Durante los inviernos suaves, la convección se sigue produciendo, pero la pérdida de flotabilidad no es suficiente para producir aguas profundas y por tanto forma aguas intermedias, las llamadas aguas intermedias occidentales (WIW) (Font et al., 1988). Teniendo en cuenta que estos eventos son una consecuencia directa del forzamiento atmosférico, muestran una variabilidad interanual considerable.

La cuenca del Mediterráneo Oriental (EMED) también contiene ciertas áreas donde la se forman aguas profundas. En esta cuenca, las aguas profundas son formadas en su mayoría en el Mar Adriático sur, con pequeñas contribuciones de la parte norte (Lascaratos et al., 1999). La formación de estas aguas profundas sigue un procedimiento similar a las del Mediterráneo Nor-Occidental, que consta de fuertes vientos y la pérdida de calor en superficie combinado con un giro ciclónico permanente en el Mar Adriático sur. Estas aguas profundas del Adriático (ADW) llenan las partes más profundas del Jónico y el Mar Levantino. Esta era la imagen tradicional de la formación de aguas profundas en el Mediterráneo Oriental (EMDW) hasta el descubrimiento del "East Mediterranean Transient" (EMT) durante la década de los 1990 (Roether et al., 1996). A principios de la década de los 1990, se observó un cambio en la ubicación de la formación de aguas profundas, pasando de la típica zona al sur del Mar Adriático al Mar Egeo. Esto fue causado por varios procesos de pre-acondicionamiento y, finalmente, provocado por el invierno 1992-1993, que fue un invierno excepcional en términos de pérdida de calor y la fuerza del viento. A continuación, las aguas profundas formadas en el Egeo, se desbordaron hacia la cuenca Levantina y el Jónico por los estrechos del Arco de Creta, elevando la antígua EMDW y creando una anomalía cálida, salada y densa en las características hidrográficas de las capas profundas del Mediterraneo Oriental y una anomalía fría y menos salada en las capas intermedias (Roether et al., 2007; Beuvier et al., 2010). También se observó en el Giro permanente de Rodas la presencia de agua Levantina profunda (LDW) (Sur et al., 1992).

Modelos Numéricos

El Mediterráneo es una región muy interesante para los modelos oceánicos. Como se ha mencionado anteriormente, muchos de los procesos dinámicos de los océanos ocurren en el Mediterráneo, por lo que es una región muy adecuada, pero difícil para los estudios de modelización. Sin embargo, no deja de tener sus desafíos. La topografía del Mediterráneo es extremadamente compleja (figura

Figure C.9: Imagen satélite del Mar Mediterráneo con su topografía de fondo, y el detalle de varios canales y estrechos (fuente: Google Earth).

La dinámica del Mediterráneo está dominada por la variabilidad de mesoescala, por lo tanto, los modelos que se pretendan estudiar los procesos que no sean únicamente de gran escala deben tener la resolución suficiente para resolver la mesoescala. También hay procesos dinámicos tales como la convección profunda que son vitales para el Mediterráneo y la oceanografía global y en general son difíciles de modelar debido a su dependencia de los fenómenos atmosféricos cortos e intensos, así como en las pequeñas inestabilidades baroclinas de mesoescala (Herrmann et al., 2008a).

Varios estudios se han centrado en el Mar Mediterráneo utilizando modelos regionales de alta resolución de $1/8^o$ y $1/16^o$ como por ejemplo DIECAST (Fernández et al., 2005), OPAMED8 (Somot et al., 2006), EU-MFSTEP (Tonani et al., 2008), NEMOMED8 (Sevault et al., 2009) y MED16 (Béranger et al., 2010) por nombrar algunos. La simulación DieCAST de 1.8^o utilizada en Fernández et al. (2005) no es un análisis retrospectivo, sino que se trata de una simulación para evaluar la circulación y la variabilidad del transporte en el mar Mediterráneo. Está forzado por una climatología de vientos mensuales promedio y aplica relajación hacia una climatología mensual de temperatura superficial y salinidad. La simulación OPAMED8 de $1/8^o$ por Somot et al. (2006) es un escenario del Mar Mediterráneo bajo condiciones IPCC-A2 de cambio climático y forzado por un modelo atmosférico climático regional (ARPEGE) a lo largo del período 1960-2099 con una jerarquía de tres modelos diferentes. Su objetivo es obtener una forzamiento atmosférico de alta resolución para ejecutar la simulación OPAMED8 (basado en el modelo de OPA (Madec et al., 1998) del mar Mediterráneo bajo un escenario de cambio climático transitorio. La simulación EU-MFSTEP de $1/16^o$ por Tonani et al. (2008) es un modelo de muy alta resolución en base al código OPA (Madec et al., 1998) utilizado para predicciones operacionales diarias del Mar Mediterráneo. Está disponible desde 1997. NEMOMED8, de $1/8^o$ por Sevault et al. (2009) es una simulación centrada en el estudio de la dinámica detrás de ciertas características y variabilidad del Mar Mediterráneo. También se ha utilizado en los estudios recientes realizados por Beuvier et al. (2010) y Herrmann et al. (2010) centrados en la EMT y los eventos de convección produnda de 2005-2006 en el Mediterráneo Nor-Occidental respectivamente. MED16 (Béranger et al., 2010) es un experimento de modelización para evaluar el rendimiento de la resolución del forzamiento atmosférico en la convección oceánica invernal en el Mediterráneo mediante la ejecución de dos simulaciones de 4 años de 1998 -2002 (con 11 años de iniciación (spin-up)), una utilizando ERA40 y la otra con ECMWF (que contiene campos de superficie analizados con el doble de resolución que ERA40). Además, algunos estudios recientes, como el Hu et al. (2009) y Schaeffer et al. (2011) han utilizado simulaciones cortas, de muy alta resolución ($\sim$1 km) para estudiar áreas y procesos muy específicos en el Mediterráneo (en concreto, remolinos de mesoescala en el Golfo de León).

A lo largo de esta tesis estudiamos el comportamiento de una variedad de modelos oceánicos en el Mar Mediterráneo; desde modelos globales de resolución media ($1/4^o$), hasta modelos regionales de $1/8^o$ y, finalmente, una primera iteración de una simulación global de $1/12^o$.

Motivación y Objetivos

Las motivaciones y objetivos generales de esta tesis son el estudio de la variabilidad del Mediterráneo (con atención especial en el Mediterráneo Occidental) a través del análisis y la validación de cinco simulaciones numéricas oceánicas (análisis retrospectivos) mediante la comparación con diferentes fuentes de observaciones (incluyendo de datos *in situ* y de teledetección).

Tratamos de realizar un análisis exhaustivo de las principales características y variables que representan el Mar Mediterráneo; la circulación, las masas de agua y la dinámica, y los comparamos con datos reales, y sugerimos dónde las simulaciones tienen margen de mejora. En los capítulos 5 y 6 usamos simulaciones de resolución media de $1/4^o$ con el objetivo de mejorar nuestra comprensión de la variabilidad interanual a largo plazo y a escala de cuenca. En el capítulo 7, usamos dos simulaciones de más alta resolución de $1/8^o$ y $1/12^o$ para evaluar las mejoras obtenidas por la mayor resolución, así como estudios más detallados de sub-cuenca y mesoescala.

Los estudios de modelización exigen una gran cantidad de trabajo en su programación, ejecución, diagnósticos, etc. Parte de los objetivos de esta tesis surgen de un convenio de colaboración con LEGI (Laboratoire des Ecoulements Géophysiques et Industriales) y MERCATOR-OCEAN para validar sus simulaciones oceánicas en la zona del Mar Mediterráneo.

El capítulo 5 es una primera aproximación en el análisis y la validación en el Mar Mediterráneo de una simulación oceánica global, la simulación ORCA025-G70. Esta simulación fue elegida porque era, en ese momento, una de las simulaciones de mayor resolución disponible a nivel global. Era moderna y había sido validada en varias regiones de los océanos del mundo. Sin embargo, no se había prestado especial atención a su comportamiento en el

Mediterráneo. Modelos regionales de mayor resolución ya estaban disponibles para el Mediterráneo, pero nadie había analizado un modelo global en esta zona. La resolución de $1/4^o$ no es suficiente para reproducir la dinámica de mesoescala, pero es adecuada para la circulación a gran escala que es el foco principal de este capítulo (sobre todo a escala de cuenca). En concreto, el alcance de este capítulo es evaluar si ORCA-G70 es capaz de reproducir correctamente el estado del mar con respecto a ciertas variables clave. Variabilidad y tendencias a escala de cuenca en temperatura y salinidad promedio a distintas capas de profundidad mediante la comparación de la simulación con la base de datos MEDAR de temperatura y salinidad. Análisis de la serie temporal de altura del nivel del mar y estérica en cuanto a su amplitud y la fase de ciclo estacional, variabilidad interanual, tendencias, así como la distribución espacial de las tendencias, la varianza y la amplitud anual. Esto se hace mediante la comparación de la simulación con datos de altimetría. Por último se comprueba si el transporte a través de las dos entradas principales de agua en el mar Mediterráneo (las aguas del Atlántico por el Estrecho de Gibraltar, y de entrada de agua dulce desde el Mar Negro) son correctas y si el balance de agua se mantiene a través de ellos mediante la comparación con las publicaciones disponibles.

Capítulo 6. Tras los resultados positivos e interesantes obtenidos en el análisis de ORCA-G70, el objetivo de este capítulo es el de ampliar el trabajo realizado en el capítulo 5 añadiendo más simulaciones con diferentes configuraciones para el análisis y evaluar de qué manera sus diferentes características (misma resolución de $1/4^o$) afecta su capacidad para reproducir las características de circulación en el Mediterráneo Occidental. Además de ORCA-G70, se analizan ORCA-G85 (una simulación con un forzamiento atmosférico mejorado, mayor resolución vertical y relajación de salinidad en superficie más débil), y GLORYS1V1 (una simulación más corta con asimilación de datos).

La inclusión de GLORYS1V1 tiene como objetivo verificar si los productos de reanálisis que incluyen asimilación de datos ayudan a mejorar la descripción y la comprensión de la variabilidad oceánica en el Mediterráneo Occidental. Se pondrá de relieve qué grado de mejoría se puede esperar de un reanálisis del océano en esa región con respecto a una simulación libre. Además del análisis a nivel de cuenca realizado en el capítulo 5, nos centramos en algunos aspectos específicos de la circulación en el Mediterráneo Occidental tales como la formación de aguas profundas en el Golfo de León y el transporte a través de los canales del Mar Balear, y evaluamos cómo las diferencias en las configuraciones de modelo afectan a su rendimiento. Finalmente, se analiza la circulación geostrófica promedio a gran escala en el Mediterráneo Occidental mediante la descomposición en sus componentes principales utilizando Funciones Empíricas Ortogonales (EOF).

Capítulo 7. En este último estudio, vamos un paso más allá y analizamos dos simulaciones de alta resolución, uno global (ORCA12, $1/12^o$ de resolución) y uno regional (NEMOMED8, $1/8\ ^o$ de resolución) . Con estas simulaciones de alta resolución, el objetivo es estudiar la variabilidad de mesoescala de la circulación del Mediterráneo Occidental. Para mantener la coherencia con capítulos anteriores también realizamos los análisis básicos de temperatura y salinidad a escala de cuenca, así como de la capacidad de formación de aguas profundas de estas simulaciones de alta resolución, ya que, en las conclusiones de los capítulos anteriores, la resolución (tanto de la simulación y el forzamiento atmosférico) es una de las limitaciones a la hora de reproducir los eventos de convección profunda en el Golfo de León. Sin embargo, la mayor parte de este capítulo está dedicado a investigar las características dinámicas del Mediterráneo Occidental, y para ello nos centramos en la circulación geostrófica de las simulaciones calculada a partir de la altura del nivel del mar y la comparamos con la circulación geostrófica calculada a partir de mediciones de altimetría. Para evaluar la variabilidad de mesoescala, se analiza la energía cinética de Eddy (EKE). Por último, tratamos de analizar e identificar los componentes principales de la circulación de mesoescala del Mediterráneo Occidental mediante la utilización de Funciones Empíricas Ortogonales en tres regiones principales: el Mar de Alborán, la cuenca Argelina y la cuenca del Mediterráneo Nor-Occidental.

Metodología

En esta tesis se han utilizado una variedad de métodos estadísticos para analizar los diferentes conjuntos de datos. En este capítulo se describen las metodologías y adjuntan las referencias a los capítulos en los que se han utilizado.

Estadística General

A lo largo de los trabajos presentados en esta tesis se utilizan una serie de métodos estándar de análisis estadístico para analizar las diversas variables y bases de datos. Estos son los utilizados principalmente:

Medias En algunos casos usamos medias temporales, creando mapas bi-dimensionales, y en otros casos usamos medias espaciales, creando series temporales de mares, cuencas o regiones más pequeñas.

Varianza es una medida de la cantidad de variación de una variable en particular. Usamos la varianza para evaluar la variabilidad espacial de ciertas variables (por ejemplo, altura del nivel del mar) mediante el cálculo de la varianza durante un período determinado para cada punto de la malla del conjunto de datos y creando un mapa bi-dimensional de varianza. Esto se utiliza en el capítulo 5.

Tendencias son útiles para describir el comportamiento a largo plazo de un conjunto de datos o de series temporales. Dado que los datos utilizados en esta tesis doctoral son de una frecuencia bastante baja, compuesta de promedios mensuales o anuales de datos dispuestos en una malla, calculamos las tendencias mediante regresión lineal simple (por mínimos cuadrados) a un nivel de confianza del 95 %:

$$\hat{a} = \frac{\sum_{i=1}^{n} y_i(t_i - \bar{t})}{\sum_{i=1}^{n}(t_i - \bar{t})^2} \tag{C.1}$$

$$d = \pm\frac{\hat{s}}{\sqrt{\sum_{i=1}^{n}(t_i - \bar{t})^2}} T_{n-2}(1 - \alpha/2) \tag{C.2}$$

donde $\hat{a}$ es la estimación de la pendiente, d es el intervalo de confianza al nivel α, $\hat{s}$ es la estimación de la desviación estándar, y T_{n-2} es la inversa de la función de probabilidad cumulativa t-student con n-2 grados de libertad (Vargas-Yáñez et al., 2005). La tendencia se puede calcular ya sea con la señal completa o con la señal menos el ciclo estacional. El paso final es ajustar una línea recta al conjunto de datos utilizando la función $f = \hat{a}x + \hat{b}$.

El Coeficiente de Correlación es una medida de la relación estadística entre dos conjuntos de datos dependientes. Las correlaciones se han calculado utilizando la siguiente fórmula:

$$r = \frac{\sum_m \sum_n (A_{mn} - \overline{A})(B_{mn} - \overline{B})}{\sqrt{(\sum_m \sum_n (A_{mn} - \overline{A})^2)(\sum_m \sum_n (B_{mn} - \overline{B})^2}} \tag{C.3}$$

donde $\overline{A}$ la matriz media de A, y $\overline{B}$ es la matrix media de B.

Ciclo Anual (o estacional). A lo largo de esta tesis hemos utilizado dos métodos diferentes para calcular el ciclo anual (o estacional), en el capítulo 5 obtenemos el ciclo anual ajustando dos funciones armónicas usando un método de mínimos cuadrados para determinar si la amplitud de los patrones espaciales a lo largo de los ciclos anuales del modelo y las observaciones coinciden.

$$y(t) = A_a \cos\left(\frac{2\pi}{365.25}t - \phi_a\right) + A_{sa} \cos\left(\frac{2\pi}{182.63}t - \phi_{sa}\right) \tag{C.4}$$

donde A_a y ϕ_a son la amplitud y la fase del ciclo anual, y A_{sa} y ϕ_{sa} son la amplitud y la fase del ciclo semi-anual (Pascual et al., 2008).

En la mayoría de los casos en que se quiere estudiar la variabilidad interanual de una señal determinada, el ciclo estacional, que suele ser la señal dominante, tiene una amplitud mucho mayor que todas las demás señales, lo que dificulta la interpretación de la variabilidad interanual de las demás señales. Por lo tanto, eliminamos el ciclo estacional restándolo de la señal total. La eliminación del ciclo estacional para el análisis de series temporales se lleva a cabo mediante la eliminación de una climatología mensual de los datos de series temporales. La climatología se crea mediante el cálculo de la media de todos los meses del año (es decir, media de todos los eneros, febreros, etc.)

Funciones Empíricas Ortogonales (EOFs)

Las EOFs se utilizan para identificar y cuantificar la variabilidad espacial y temporal de forma consistente mediante reducción de las dimensiones de los grandes conjuntos de datos a unos pocos modos de variabilidad significativos ortogonales (no correlativos), y para estimar la cantidad de varianza asociada a cada modo de variabilidad en términos porcentuales.

A pesar de la reducción dimensional de las bases de datos realizadas por el método de EOF, los patrones espaciales y sus coeficientes de dilatación (componentes principales (PC), es decir, la evolución en el tiempo de los modos espaciales) no son siempre fáciles de interpretar, sobre todo en referencia a los PC de los modos secundarios de variabilidad, a menudo complicada por señales no periódicas. Es importante tener en cuenta que los modos de variabilidad contienen información sobre el conjunto de datos que no necesariamente está relacionada con las características físicas (Olita et al., 2011).

En los capítulos 6 y 7 utilizamos EOFs para descomponer la señal de la compleja circulación oceánica en sus componentes principales de variabilidad espacial $F_k(x, y)$ y sus componentes temporales asociados temporales $a_k(t)$ haciéndolos más fácil de analizar y describir por separado.

La señal $O(x, y, t)$ se descompone utilizando la siguiente formulación:

$$O(x, y, t) = \sqrt{n-1} \sum_{k=1}^{n} F_k(x, y) a_k(t) \tag{C.5}$$

where $\mid a_k \mid = 1$ and $\mid F_k \mid \neq 1$

Transporte de Masas de Agua

El transporte a través de estrechos y canales se calcula mediante la integración de las velocidades zonales proporcionadas por las simulaciones, ya sea en dirección Norte-Sur, Este-Oeste, o transectos diagonales. Los valores positivos son considerados para el transporte hacia el Este (por ejemplo, entrada del Atlántico al Mar Mediterráneo) o el Norte, y los valores negativos se consideraron transportes hacia el oeste (la salida por ejemplo, de aguas Mediterráneas hacia el Océano Atlántico) o hacia el Sur. En el caso de los transectos diagonales, que en este estudio sólo se refiere al canal de Mallorca, los valores positivos se consideran los flujos con una componente dominantes hacia el norte y los negativos se consideran los flujos de componente dominante hacia el sur.

Diagramas Hovmöller

En esta tesis utilizamos diagramas Hovmöller para mostrar la evolución temporal de perfiles verticales de temperatura y salinidad. Los ejes X e Y son tiempo y profundidad respectivamente, con el valor de temperatura o salinidad representado por los gradientes de color. Estos son utilizados en los capítulos 6 y 7 para estudiar la evolución temporal de los eventos de convección profunda en el Golfo de León.

Energía Cinética Eddy (EKE) La Energía Cinética Eddy es una medida del grado de variabilidad y puede identificar las regiones con fenómenos muy variables, tales como los remolinos, meandros en las corrientes, frentes o filamentos. Se calcula a partir de la anomalía del nivel del mar (eta') mediante la asunción de geostrofía:

$$EKE = \frac{1}{2}[U_g^{'2} + V_g^{'2}] \tag{C.6}$$

$$U_g^{'} = -\frac{g}{f}\frac{\partial \eta^{'}}{\partial y} \tag{C.7}$$

$$V_g^{'} = \frac{g}{f}\frac{\partial \eta^{'}}{\partial x} \tag{C.8}$$

donde $U_g^{'}$ y $V_g^{'}$ son las anomalías de las velocidades geostróficas zonales y meridionales. f es el parámetro de Coriolis, g es la aceleración por gravedad y las derivadas $\frac{\partial \eta^{'}}{\partial y}$ y $\frac{\partial \eta^{'}}{\partial x}$ son calculadas por diferencias finitas donde x e y son las distancias en longitud y latitud respectivamente (Pascual et al., 2007).

Resumen del Capítulo 5

El capítulo 5 se ha centrado en el estudio de la variabilidad interanual y estacional en el Mar Mediterráneo mediante el análisis de la simulación ORCA-R025 G70, y comparándola con altimetría y la base de datos MEDAR de temperatura y salinidad.

En la comparación entre los resultados de ORCA G70 con la base de datos MEDAR hemos encontrado que los valores medios de temperatura superficial y los de la capa superficial (0-150 m) durante el período de 1962-2001 son reproducidos con bastante precisión (correlaciones de 0,7). Sin embargo, la relajación en salinidad superficial que se aplica al modelo elimina la mayor parte de la variabilidad interanual (correlación de 0,36).

Las temperaturas medias para esta capa son ligeramente superiores en el modelo (0.08 a 0,16^{o}C), probablemente relacionada con una subestimación de perdida de calor total en el forzamiento atmosférico (ERA40) ($\sim$3,88 W/m^2 para ORCA en el Mediterráneo, en comparación con el valor medio bien establecido mediante observacines de $\sim$5 W/m^2 inferido del transporte de calor en Gibraltar. Esto significa que el Mediterráneo está ganando calor. Sin embargo, este resultado se encuentra dentro del rango de otros estudios observacionales y de modelado. Ruiz et al. (2008) reúne una tabla de los diferentes estudios de flujo de calor y da un rango de valores entre -11 W/m^2 y 29 W/m^2).

Las capas Intermedias (150-600 m) y profundas (de 600 m hasta el fondo) muestran una clara tendencia positiva que no se observa en MEDAR. Esto es posiblemente debido a la resolución del forzamiento atmosférico que impide la formación de aguas profundas, lo que resulta en que las aguas frías y densas, no llegan a las profundidades del océano que con el tiempo se calienta mediante difusión. Nuestros resultados han demostrado que la salinidad media en superficie de toda la cuenca del Mediterráneo es significativamente más baja en G70 que en MEDAR (~0,3 psu), que se replica en las capas intermedias y profundas en menor grado y podría ser consecuencia de una relajación de salinidad superficial demasiado débil, sin suficiente evaporación para compensar la subestimación de ERA40 en el flujo de pérdida de agua.

La evaluación de G70 con respecto al nivel del mar (tanto en términos de altura absoluta de la superficie del mar (SSH) como su componente estérico) ha revelado que el modelo reproduce la variabilidad interanual a gran escala razonablemente bien, así como el ciclo estacional cuando se compara con datos de altimetría. Sin embargo, el modelo presenta una tendencia positiva de SSH poco realista (~15 mm/año). Teniendo en cuenta que el transporte de agua entrando al Mediterráneo se encuentra dentro del rango de valores obtenidos por otros estudios observacionales (aunque el transporte a través de los estrechos del Mar Negro puede mostrar un error significativo y contribuir a la tendencia del nivel del mar), la tendencia positiva observada en SSH del modelo está probablemente relacionada con un desequilibrio en el balance hídrico de la simulación.

Como es de esperar con un model de $1/4^o$ de resolución, el modelo es incapaz de reproducir correctamente las características de mesoescala. Esto es especialmente notable en el Mar de Alborán y la Corriente Argelina, donde el modelo es no reproduce los giros y remolinos que se forman en estas regiones. Además de la mesoescala y las tendencias del nivel del mar, esta simulación global oceánica se comporta bien en el Mar Mediterráneo, teniendo en cuenta su limitada resolución para las características dinámicas de este mar semicerrado. A pesar de algunos puntos clave, como la relajación de salinidad en superficie y el forzamiento atmosférico) que, una vez identificados, se pueden mejorar, la simulación oceánica G70 puede proporcionar una herramienta muy prometedora para el estudio del ciclo estacional y la variabilidad interanual del

Mediterráneo.

Resumen del Capítulo 6

En este capítulo analizamos el rendimiento de tres simulaciones numéricas globales, G70, G85 y GLORYS (esta última con asimilación de datos) continuando el trabajo del capítulo 5 (que se basa en Vidal-Vijande et al. (2011)), pero esta vez centrándonos en el Mediterráneo Occidental. Las tres simulaciones se basan en el mismo código NEMO de $1/4^o$ (Madec, 2008) configurado en una malla ORCA. G70 y G85 son análisis retrospectivos de los últimos cincuenta años desarrollados por el Grupo DRAKKAR (Barnier et al., 2007), se diferencian en la resolución vertical (G70 cuenta con 46 niveles verticales y G85 tiene 75), un forzamiento atmosférico ligeramente distinto basado en ERA40 (G70 usa DFS3 y G85 usa el mejorado DFS4) y en la intensidad de la relajación en salinidad superficial, que en G85 es seis veces más débil que en G70. El término relajación en salinidad se aplica para corregir la deriva en el balance de agua dulce de las simulaciones, y añade agua dulce o incrementa la evaporación cuando y donde sea necesario basándose en una climatología. GLORYS tiene una configuración similar a G70, pero incluye asimilación de datos y se ejecuta durante el período de 2002 a 2008.

La variabilidad de la temperatura promedio se reproducen bien en las capas superficiales e intermedias, aunque G70 en las capas intermedias y profundas muestra tendencias que son más positivas que las obtenidas de las bases de datos observacionales. La mejor continuidad del forzamiento atmosférico DFS4 junto con una mayor resolución vertical, mejora en gran medida estas tendencias en G85. El efecto combinado de un forzamiento atmosférico más consistente (la interfaz entre el ERA40 y ECMWF en 2002), los flujos corregidos y un estrés de viento más realista ($\sim$10% más fuerte, (Brodeau et al., 2010) junto con la mayor resolución vertical que mejora la coeficiente de mezcla vertical resultan en una notable mejora en las tendencias de las capas intermedia y profundas.

La salinidad es la variable más problemática. Ni la variabilidad interanual, ni las tendencias coinciden con las observaciones. La relajación en salinidad superficial elimina la variabilidad interanual y el grado de relajación afecta directamente a la tendencia en salinidad. Esto es evidente con G85 que muestra una tendencias negativas muy fuertes en capas superficiales y especialmente en las intermedias. La salinidad se ve directamente afectada por el forzamiento atmosférico y el equilibrio de agua dulce de las simulaciones. Seguir trabajando para mejorar la calidad y la resolución de forzamiento atmosférico probablemente mejore los resultados de la salinidad.

Los acontecimientos excepcionales de convección profunda de 2004-2005 y 2005-2006 (Schroeder et al., 2006, 2008a, 2010; Herrmann et al., 2010; Font et al., 2007; Smith et al., 2008)) en del Mediterráneo Noroccidental se analizaron en detalle utilizando las simulaciones G85 y GLORYS (G70 acaba en 2004), así como su propagación hacia los canales del Mar Balear. Estos canales son de vital importancia ya que es donde ocurre una gran parte de los intercambios Norte-Sur de agua y calor en el Mediterráneo Occidental. Estos dos inviernos excepcionales se han caracterizado por una evaporación y pérdida de calor extremas en el área del Golfo de León, lo que causó los eventos de convección profunda muy intensos y también modificó las propiedades de las aguas intermedias Levantinas (LIW). En G85, la fuerte convección y la modificación de LIW son claramente visibles, con la convección del invierno 2005-2006 llegando penetrar por debajo de la LIW hasta las capas profundas. Sin embargo, la baja resolución del modelo y, especialmente, del forzamiento atmosférico hace que los eventos de convección más débiles no penetren en la LIW. Esto provoca que las capas intermedias se calienten ya que evidenciado por los años 2004-2006, la mezcla invernal de estas aguas más frías juega un papel vital en el mantenimiento de la temperatura de la LIW y que se parezca a las observaciones.

GLORYS muestra el evento de convección fuerte en el invierno 2005-2006, y debido a la disponibilidad de resolución temporal diaria la convección queda muy claramente marcada y aislada. Esto está respaldado por los resultados EN3 que también muestran la convección profunda en ambos inviernos, con 2005-2006 como la más fuerte. Estos resultados muestran que mientras las condiciones de forzamiento sean lo suficientemente fuertes, estas simulaciones son capaces de producir aguas profundas a pesar de la baja resolución forzamiento atmosférico. Sin embargo, durante condiciones de convección normales estos modelos no son capaces de hacer que la convección llegue a las aguas profundas. Esto es debido a la baja resolución espacial, tanto de la modelo y como del forzamiento atmosférico, que tiene que ser de al menos 50 kilómetros a fin de permitir la simulación de la convección del Mediterráneo (Li et al., 2006; Herrmann and Somot, 2008; Béranger et al., 2010).

En cuanto el nivel del mar, todos los modelos reproducen correctamente el ciclo estacional y la variabilidad interanual, pero ya que las simulaciones sin asimilación (G70 y G85) no mantienen el equilibrio de agua dulce y subestiman la evaporación (Herrmann et al., 2008b), muestran exageradas tendencias positivas. G70 muestra una tendencia de 14,96$\pm$1,46 mm/año y G85 con una relajación de salinidad más débil muestra una tendencia incluso más positiva (20,27$\pm$1,37 mm/año), lo que indica que en la actualidad estas simulaciones requieren el término relajación a fin de mantener tendencias dentro de niveles aceptables. GLORYS tiene su balance de agua artificialmente ajustado a cada paso de tiempo por lo tanto, no sufre este problema.

Hemos encontrado que todas las simulaciones recrean la circulación superficial promedio de forma correcta dentro de sus límites de resolución, lo que les impide resolver la mesoescala, aunque a través del análisis de patrones mediante Funciones Empíricas Ortogonales, algunas de las características más grandes de mesoescala son visibles. El transporte a través del Estrecho de

Gibraltar está dentro de los valores establecidos mediante observaciones Candela (2001); Tsimplis and Bryden (2000); García Lafuente et al. (2002), que muestran un flujo correcto de entrada (G70: 1,078 Sv, G85: 1,006 Sv), de salida (G70 : 1,008 Sv, G85: 0,955 Sv) y neto (G70, G85: 0.067: 0.050 Sv). Sólo GLORYS parece mostrar un intercambio más intenso (1,296 Sv de entrada y 1,243 Sv de salida), pero el flujo neto es correcto (0,052 Sv). Los canales de Ibiza y Mallorca juegan un papel vital en el Mediterráneo Occidental, ya que es a través de estos canales que se produce una gran parte del intercambio Norte-Sur de calor y el agua. Todas las simulaciones muestran la variabilidad estacional correcta en el Canal de Ibiza, con el transporte predominante hacia el sur en invierno y hacia el norte en verano. G70 tiene valores correctos medios, pero no reproduce los eventos de 1996-1998 de transporte elevados hacia el sur. Estos eventos son reproducidos por G85 y coinciden con las observaciones de Pinot et al. (2002) durante el Experimento CANALES. Es importante señalar que de según G85, estos años son excepcionales. GLORYS produce un flujo muy intenso hacia el sur (1,5 a 2,5 Sv), muy por encima de las otras simulaciones. Las observaciones no están disponibles para los años de GLORYS por lo que no se pueden comparar directamente, sin embargo, los datos de observación disponibles de años anteriores muestran transportes más débiles (0,6 a 1,3 Sv). Este estudio contribuye a la mejora de la jerarquía de simulaciones ORCA y señala las fortalezas y debilidades de estas simulaciones en el mar Mediterráneo.

Resumen del Capítulo 7

Hemos analizado dos simulaciones numéricas de alta resolución, NEMOMED8 ($1/8^o$) y ORCA-12 ($1/12^o$), y las hemos comparado con datos observacionales (EN3 para la temperatura y la salinidad y altimetría para la circulación promedio y análisis dinámico). A través de estas comparaciones, varios aspectos de las características dinámicas de la circulación del Mediterráneo Occidental han sido estudiados.

A diferencia de los capítulos anteriores en los que las simulaciones numéricas utilizadas tenían una resolución demasiado baja para producir la variabilidad de mesoescala del Mediterráneo, NM8 y O12, tienen en teoría una resolución suficiente para producirla, aunque tal vez no resolverla por completo. Aparte de la diferencia de resolución, NM8 y O12 son simulaciones muy diferentes. NM8 es una simulación madura, evolucionada a partir de OPAMED8 (Somot et al., 2006), y personalizada al Mediterráneo. El forzamiento atmosférico utilizado, ARPERA es un reanálisis dinámica de más alta resolución de los campos ECMWF/ERA-40, también probado y optimizado para el Mediterráneo, y, finalmente, no hay relajación en salinidad. Por el contrario, O12 es la primera iteración (de muchas por venir) de las simulaciones globales ORCA a $1/12^o$. Utiliza el forzamiento atmosférico ERA-Interim que también es un reanálisis de mayor resouciión de los campos ECMWF/ERA-40, aunque no está específicamente optimizado para el Mediterráneo. En general esta simulación sea quizás prematura, pero no obstante es una simulación interesante para analizar por primera vez.

Como NM8 es una simulación más madura y puesta a punto, tiende a funcionar mejor que O12 en prácticamente todos los análisis. Dada la complejidad de los modelos numéricos, la resolución por sí sola no es suficiente para obtener los mejores los resultados.

En el análisis de la temperatura y la salinidad (sección 7.2), el rendimiento de la temperatura superficial es bueno en ambas simulaciones, como lo ha sido en todos los capítulos anteriores, debido principalmente a que capa superficial está fuertemente influenciada por el forzamiento atmosférico que se basa en observaciones reales similares. La salinidad sigue siendo un parámetro difícil para estas simulaciones, aunque NM8 muestra resultados significativamente mejores en la superficie y las capas intermedias que las simulaciones ORCA (tanto O12 como las anteriores G70 y G85) a pesar de no usar relajación en salinidad. Este es un buen resultado y una notable mejora.

Otro aspecto interesante que se ha estudiado en el capítulo 6 es la formación de aguas profundas en el Golfo de León. Las conclusiones de los análisis realizados en el capítulo 6 indican que para que las simulaciones numéricas puedan reproducir de forma fiable los eventos de convección profunda, son necesarias mejoras en la resolución tanto de la simulación como del forzamiento atmosférico (así como la corrección de las subestimaciones conocidas en el forzamiento atmosférico). Los resultados obtenidos en este capítulo son interesantes porque, aunque estas conclusiones son válidas para NM8, no lo son para O12. En ambos casos, tanto las simulación como el forzamiento atmosférico son de mayor resolución, pero es la optimización de este último la que marca la diferencia. NM8 reproduce los eventos de convección profunda y la estructura vertical de la columna de agua en el Golfo de León de forma muy parecida a las observaciones. Hay que decir que este fue uno de los principales objetivos de esta simulación (amplios estudios sobre convección profunda usando NM8 en Herrmann et al. (2010)). Por otro lado, O12 genera una capa intermedia excesivamente cálida y estable lo que previene que la convección penetre más allá de esta capa.

El esquema de la circulación geostrófica promedio del Mediterráneo Occidental también se ha analizado y comparado con altimetría. Las simulaciones muestran un patrón de circulación general correcto, pero ambas simulaciones tienen ciertas discrepancias con respecto a la altimetría en áreas específicas del Mediterráneo Occidental. Ambas simulaciones producen un campo de circulación en general más suave que la altimetría, con O12 siendo aún más suave que NM8, un resultado que es sorprendente dada la mayor resolución de O12. NM8 no reproduce el Giro Oeste de Alborán (WAG) y tiene una Corriente Argelina (AC) menos definida. La Corriente del Norte se reproduce bastante bien, pero la recirculación que suele ocurrir al oeste de Mallorca, es más débil, y en su mayor parte ocurriendo más al norte. O12 recrea el WAG, ni el EAG en sus localizaciones normales, sino que produce un WAG desplazado (Flexas et al., 2006). En esta simulación, la Corriente Argelina no está bien definida y ajustada a la costa, sino que se representa como un amplio gradiente que fusiona la Corriente Argelina con la actividad anticiclónica de mesoescala de la Cuenca Argelina. La Corriente del Norte está representada como una circulación ciclónica en el Golfo de León, sin protuberancia hacia el Mar Balear debido a la obstrucción por un remolino anticiclónico permanente.

Otra forma de evaluar la circulación oceánica es analizar la energía cinética de remolinos geostróficos (EKEg), que se calcula a partir de anomalías del nivel del mar y da una medida de la actividad de mesoescala. En este sentido, los tres conjuntos de datos (altimetría, NM8 y O12) coinciden en las regiones de máxima EKEg, principalmente el Mar de Alborán y la cuenca Argelina. La altimetría y NM8 tienen niveles similares de EKEg y reproducen tanto el WAG como la variabilidad del EAG, así como las regiones de EKEg altos a lo largo de la trayectoria de la Corriente Argelina. O12 muestra unos niveles de EKEg que son menos de la mitad de los de altimetría y NM8. Esto es debido a la baja variabilidad del régimen de circulación, que es eliminado en el cálculo de las anomalías dejando unos valores más bajos de EKEg.

El análisis de la circulación media es adecuado como una visión general sobre si las simulaciones están produciendo una circulación correcta, sin embargo, es demasiado amplia para profundizar en los diferentes procesos que generan esta circulación, ya que todas las señales están mezcladas. Por esta razón, separamos los componentes principales de la circulación y los analizamos utilizando funciones empíricas ortogonales (EOF) sobre de la señal completa de circulación media y también sobre la anomalía espacial. La separación de la circulación en sus componentes principales hace que sea posible analizarlos por separado y por tanto con mayor éxito.

El primer y segundo modo EOF-F representa en casi todos los casos principalmente a la circulación promedio modulada por una variabilidad temporal relativamente débil (estacional e interanual), y produce patrones similares a los observados en la sección 7.5, sin embargo en el caso de las simulaciones en la Cuenca Argelina, esta técnica es particularmente útil en la separación de la Corriente Argelina de la variabilidad de mesoescala de la cuenca (esto se ve muy claramente en NM8).

Los modos de anomalía EOF-A han resultado ser especialmente interesantes, ya que muestran la parte de la variabilidad que es difícil de ver en la circulación promedio. Tanto en el primer como en el segundo modo EOF-A, NM8 ha demostrado un rendimiento excepcional al comparar con altimetría en todas las regiones, mostrando unos patrones espaciales muy similares y con la fase temporal apropiada (aunque la variabilidad interanual no es coincide, lo cual es de esperar ya que la simulación no asimila datos y sería muy difícil que reprodujera la variabilidad interanual de mesoescala real). Una característica interesante que ha aparecido y no era visible en la circulación promedio es el Frente Nor-Balear. Este frente es visible en el primer modo EOF-A en los tres conjuntos de datos (aunque un poco más débil en O12).

En conclusión, el análisis de estas dos simulaciones numéricas de alta resolución proporciona una oportunidad interesante para estudiar la dinámica de la variabilidad del Mediterráneo Occidental y también las características y comportamientos de los dos simulaciones muy diferentes. NEMOMED8 se confirma como una simulación madura y sólida, constantemente produciendo buenos resultados cuando se valida con datos observacionales. A pesar de sus buenos resultados, NM8 tiene todavía margen de mejora. Algunas características de la circulación claves como el WAG no se reproducen correctamente y su resolución aún no es suficiente para resolver con exactitud la mesoescala y submesoescala. Una simulación de $1/16^o$ o $1/32^o$ con un rendimiento similar sería una herramienta muy interesante para estudios de la variabilidad del Mediterráneo.

ORCA12.L46-MAL95, como la primera iteración de una simulación global de $1/12^o$ es un impulso hacia adelante interesante, con la capacidad de resolver con mayor detalle las características físicas del océano. También tiene la resolución suficiente para convertirse en una herramienta útil para estudios de variabilidad en el Mar Mediterráneo. Sin embargo, esta primera versión está todavía en sus primeras etapas de desarrollo y debe ser ajustado para producir resultados mejores y más realistas. En el Mediterráneo Occidental, y aunque los esquemas de circulación a escala de cuenca son correctos, la circulación de mesoescala más fina y la ubicación de ciertos giros (WAG, EAG) y corrientes (Corriente Baleares, Corriente del Norte) sigue necesitando mejorar.

Conclusiones Generales y Perspectivas

Esta tesis se ha centrado en explorar los diferentes aspectos de la variabilidad del Mar Mediterráneo a través de la validación de una serie de modelos numéricos oceánicos. Hemos realizado un análisis exhaustivo de las principales características y variables que definen su circulación, las características de las masas de agua y su dinámica. Para ello, hemos combinado el estudio de las simulaciones numéricas con un número de diferentes fuentes de datos de observación. Mediante el uso de varios modelos con diferentes configuraciones y características, hemos sido capaces de explorar lo las configuraciones de los modelos que ofrecen los mejores resultados en las diferentes áreas y en qué necesitan mejorar. A través de los diversos métodos estadísticos utilizados en la validación con las observaciones, hemos aprendido las fortalezas y debilidades tanto de los modelos y como de las observaciones. Mientras que extensas bases de datos de observación son ideales para el estudio del estado del océano, la realidad es que en muchas regiones del océano global (incluyendo el Mar Mediterráneo) todavía existen muchas lagunas tanto temporales como espaciales. Las simulaciones numéricas por otro lado ofrecen una imagen completa del estado del océano, y con las simulaciones recientes que abarcan el último medio siglo, los estudios de escala climática comienzan a ser posibles. Esto, en teoría, hace que los modelos sean una herramienta perfecta para estudiar todo tipo de procesos oceánicos, siempre y cuando la resolución del modelo es suficiente para resolverlos.

Sin embargo, debido a las limitaciones computacionales (y también, de nuestra comprensión de la física detrás de algunos de los procesos que gobiernan la dinámica de los océanos), los modelos numéricos todavía se basan en la simplificación y parametrización de los procesos que no pueden resolver. Para las simulaciones como las que aquí estudiamos, cuyo objetivo es producir resultados realistas, y que dependen de forzamientos externos basados en observaciones, son también la calidad y la resolución de estas observaciones las que se convierten en un factor limitante. Simplemente no somos capaces de alimentar a los modelos con datos lo suficientemente buenos como para simular a la perfección el estado de los océanos y sus tendencias medio y largo plazo.

Mientras que nuestros resultados muestran que en muchos casos, las simulaciones son adecuadas para los estudios sobre los patrones de circulación, la variabilidad interanual y los ciclos estacionales, los mismos resultados evidencian que las tendencias climáticas siguen siendo un área en la que los modelos necesitan mejorar su solidez antes de usar estos resultados para hacer declaraciones sobre la evolución futura del océano y el clima. Por ejemplo, las tendencias del nivel del mar generalmente no se mantienen dentro de los valores de observación cuando se las permite desarrollarse libremente (cómo podemos hacer declaraciones sobre las tendencias futuras si los modelos no pueden reproducir las tendencias conocidas del pasado?). Lo mismo ocurre con la temperatura en algunas de las simulaciones. La salinidad, que es una variable clave en la circulación termohalina de los océanos, es generalmente una variable problemática para los modelos oceánicos, que en muchos casos requieren una fuerte relajación hacia una climatología con el fin de evitar una deriva significante.

Estas limitaciones hacen que la validación de las simulaciones con datos reales sea un proceso vital para se puedan considerar lo suficientemente fiables para el estudio de determinados procesos, sobre todo cuando se trata de tendencias climáticas.

En este capítulo se resumen las conclusiones más importantes remarcadas a lo largo de esta tesis y sugerimos algunas ideas para el trabajo futuro.

Temperatura Hemos analizado l evolución de la temperatura promedio a escala de cuenca de todas las simulaciones (G70, G85, GLORYS, O12 y NM8) en varias capas de profundidad. En las capas superficiales, todas las simulaciones consiguen buenos resultados. Esto no es sorprendente, ya que al estar todos ellos forzados por forzamientos atmosféricos realistas (y similares), las temperaturas en superficie se comparan bien con las observaciones. Esto confirma que los modelos tienen una buena física de interacción entre la atmósfera y el océano. En las capas intermedias y profundas, el rendimiento no es tan bueno y las diferencias están marcadas por la calidad del forzamiento atmosférico. Con las simulaciones G70 y G85, que se diferencian por el forzamiento atmosférico (G70 usa DFS3 y G85 usa DFS4) y la resolución vertical, G85 muestra una mejora en las tendencias tanto en las capas intermedias como profundas, debido a la mejor continuidad temporal de DFS4 (la interfaz entre ERA40 y ECMWF, los flujos corregidos, y un estrés de viento más realista). Un problema que muestran las simulaciones de $1/4^o$ es una desviación de las temperaturas medias, sobre todo en las capas intermedias que tienden a ser considerablemente más calientes que las observaciones. La mayor resolución de O12 y NM8, que se basan en mejores forzamientos atmosféricos de mayor resolución, muestran buenos resultados de tendencias y la variabilidad en todas las profundidades.

Salinidad Como ya se ha mencionado anteriormente, la salinidad es generalmente una variable problemática para las simulaciones numéricas. Esto se debe principalmente a los desequilibrios en los flujos de agua dulce del forzamiento atmosférico, derivado de la falta de observaciones de calidad sobre la precipitación / evaporación en el océano abierto, y también en la menor cantidad de observaciones de salinidad disponibles para la validación (sin embargo las nuevas tecnologías como el reciente satélite SMOS mejorará las observaciones superficiales de salinidad). Estos desequilibrios requieren que muchos de los modelos apliquen una fuerte relajación hacia climatología afectando negativamente a la variabilidad. En consecuencia, los modelos en los que se aplica la relajación tienen muy mala correlación con las observaciones. A menos que los flujos de agua dulce estén en equilibrio, esta relajación es necesaria como lo demuestran los resultados de G85, que utiliza una relajación más debil resultando en una deriva negativa de salinidad muy fuerte (lo cual también afecta al nivel del mar en la dirección opuesta). Por otro lado, NM8, que es una simulación regional madura y especialmente adaptada al Mar Mediterráneo, con un balance de agua equilibrado, no es necesario aplicar relajación en salinidad para reproducir la variabilidad interanual de la salinidad razonablemente bien.

Convección profunda en el Golfo de León Hemos centrado una parte de este estudio en la capacidad de las simulaciones para reproducir eventos de formación de aguas profundas en el Golfo de León. Estos eventos son de vital importancia para la renovación de las aguas en las llanuras abisales y forman parte de la circulación termohalina del Mediterráneo. La convección profunda por lo general ocurre durante eventos cortos de vientos fuertes, fríos y localizados en areas relativamente pequeñas del Golfo de León. Estas condiciones, en principio, requieren que cualquier modelo destinado a la reproducción de estos eventos tienen una resolución espacial suficiente como para hacerlo (tanto en el modelo, así como el forzamiento atmosférico). Esto se evidencia por los resultados de NM8, muy similar a las observaciones donde se reproducen los eventos intensos de 2004-2006, así como los eventos más débiles. O12 es también capaz de reproducir los eventos más débiles pero debido a una capa intermedia demasiado calientey estable, éstas no llegan a alcanzar el océano profundo. En las simulaciones de $1/4^o$, G85 sólo es capaz de reproducir los eventos excepcionalmente intensos de 2004-2006. Su resolución en términos de malla y forzamiento atmosférico (ERA40 $\sim$150 kilometros) es insuficiente para los eventos más débiles.

Nivel del Mar Esta es una de las variables climáticas clave. Todas las simulaciones reproducen correctamente el ciclo estacional y la variabilidad interanual, sin embargo en el caso de las simulaciones globales, la tendencia no es realista. Esto es debido al desequilibrio de agua dulce mencionado anteriormente, lo que provoca una deriva positiva significativa (empeorando si la relajación en salinidad aplicada es menor).

Circulación Superficial y Transporte Lo que las simulaciones pueden y no pueden reproducir en términos de circulación depende en gran medida en su resolución espacial. Como es de esperar las simulaciones de $1/4^o$ sólo pueden reproducir la circulación a gran escala del Mediterráneo Occidental, que en realidad hacen razonablemente bien. Esto incluye el transporte a través del Estrecho de Gibraltar y los Canales del Mar Balear. Los modelos de mayor resolución, NM8 y O12 tienen el poder resolutivo para reproducir la mayor parte de la variabilidad de mesoescala del Mediterráneo Occidental. Se han utilizado Funciones Empíricas Ortogonales para analizar en profundidad las características de la circulación promedio del Mediterráneo Occidental, y esta metodología proporciona unas perspectivas muy interesantes sobre las señales que los modelos pueden reproducir. En este sentido, y al comparar a la circulación geostrófica inferida a partir de altimetría, NM8 muestra un rendimiento excepcionalmente bueno, con una variabilidad de mesoescala muy similar a las observaciones a pesar de algunas discrepancias en lugares específicos (por ejemplo, ausencia de la WAG en el Mar de Alborán). O12 por otro lado, y a pesar de su mayor resolución, muestra que es una simulación de primera generación a esta resolución. Su circulación general es correcta, pero los campos son muy suaves, con poca variabilidad. La comparación entre NM8 y O12 muestra que, dada la complejidad de los modelos oceánicos, la resolución por sí sola no es suficiente para obtener el mejor rendimiento.

En general este estudio nos ha permitido investigar aspectos muy interesantes de cómo los modelos funcionan simulando el océano real, donde rinden bien y donde existe margen de mejora. Una de las claras conclusiones de esta tesis es que, independientemente de la resolución del modelo, un factor importante cuando se trata de crear un análisis retrospectivo realista es la calidad del forzamiento atmosférico. Otros factores también son importantes, tales como una mejor representación del Estrecho de Gibraltar (como en NEMOMED8), mejor batimetría y también la falta de necesidad de utilizar relajación. Más trabajo debe llevarse a cabo en la estimación y corrección de las subestimaciones y las desviaciones que existen en los datos actuales de forzamiento atmosférico. "Downscales" dinámicos como el ARPERA (ajustados para el Mediterráneo) que se utiliza en NM8 parecen estar dando resultados muy positivos.

También es evidente, que la cantidad de observaciones es aún limitada, sobre todo para variables tales como la salinidad, y también para muchas áreas del océano profundo. Esto hace que la validación del modelo para ciertas variables y regiones sea mucho más difícil puesto que la fiabilidad de los reanálisis de datos disponibles se reduce.

Cuando se trabaja con modelos numéricos, la cantidad de variables analizadas en el estudio es sorprendente. Uno por lo tanto, debe elegir bien el foco de su estudio a fin de realizar un análisis en profundidad. Debido a esto, siempre hay margen de mejora y estudio.

El trabajo futuro debe incluir una mejor cuantificación y análisis de los parámetros en el forzamiento atmosférico que son la fuente de los desequilibrios en las simulaciones (incluyendo flujos de agua y de calor). En cuanto a la circulación de los océanos y las características dinámicas, esta tesis ha proporcionado una visión general de las características de la circulación media, pero con la disponibilidad de mejores simulaciones de mayor resolución, se puede ir mucho más en el detalle de la cuantificación y análisis de procesos específicos. Si bien se ha mencionado brevemente, la asimilación de datos en modelos numéricos puede proporcionar una excelente herramienta para comprender mejor los procesos dinámicos. Para ello, también es necesario incluir nuevas observaciones proporcionadas por las distintas plataformas que se han vuelto muy activos en los últimos años: boyas ARGO, planeadores submarinos, datos del satélite SMOS de salinidad superficial, SWOT (altímetro de nueva generación), etc. Todas estas fuentes de datos contribuirán a mejorar el conocimiento actual de los océanos y los procesos que los afectan, y sólo puede conducir a nuevos avances y la mejora en el modelado y comprensión de los océanos.

Appendix D

List of Acronyms

AW	Atlantic Water
AC	Algerian Current
ADW	Adriatic Deep Water
DFS3 & DFS4	DRAKKAR Forcing Set 3/4
DH	Dynamic Height
EAG	Eastern Alboran Gyre
EMDW	Eastern Mediterranean Deep Water
EMED	Eastern Mediterranean
EMT	Eastern Mediterranean Transient
EN3	EN3_v2a
EOFs	Empirical Orthogonal Functions
G70	ORCA-R025 G70
G85	ORCA-R025 L75.G85
GLORYS	GLORIS1V1
LIW	Levantine Intermediate Water
MDT	Mean Dynamic Topography
MEDATLAS	Mediterranean Hydrographic Atlas
MFS	Mediterranean Forcasting System
MSL	Mean Sea Level
NAO	North Atlantic Oscillation

NDHF	Net Downward Heat Flux
NEMO	Nucleus for European Models of the Ocean
NM8	NEMOMED8
NC	Northern Current
NUWF	Net Upward Water Flux
O12	ORCA12.L46-MAL95
SH	Steric Height
SLA	Sea Level Anomaly
SSH	Sea Surface Height
SST	Sea Surface Temperature
WAG	Western Alboran Gyre
WIW	Western Mediterranean Intermediate Water
WMDW	Western Mediterranean Deep Water
WMED	Western Mediterranean

List of Figures

Bibliography

Alvarez, A., J. Tintoré, G. Holloway, M. Eby, and J. M. Beckers, 1994: Effect of topographic stress on circulation in the western mediterranean. *J. Geophys. Res. C*, **99 (C8)**, 16,053–16,064.

Astraldi, M., F. Conversano, G. Civitarese, G. P. Gasparini, M. R. d'Alcalà, and A. Vetrano, 2002: Water mass properties and chemical signatures in the central mediterranean region. *J. Mar. Syst.*, **33-34**, 155 – 177.

Astraldi, M., et al., 1999: The role of straits and channels in understanding the characteristics of mediterranean circulation. *Prog. Oceanogr.*, **44 (1-3)**, 65 – 108.

Ayoub, N., P.-Y. Le Traon, and P. De Mey, 1998: A description of the mediterranean surface circulation from combined ers-1 and topex/poseidon altimetric data. *J. Mar. Syst.*, **18 (1-3)**, 3–40.

Baldacci, A., G. Corsini, R. Grasso, G. Manzella, J. T. Allen, P. Cipollini, T. H. Guymer, and H. M. Snaith, 2001: A study of the alboran sea mesoscale system by means of empirical orthogonal function decomposition of satellite data. *J. Mar. Syst.*, **29 (1-4)**, 293 – 311.

Barnier, B., 1998: *Ocean Modelling and Parameterization*, chap. Forcing the Ocean, 45–80. Kluwer Academic Publishing.

Barnier, B., et al., 2006: Impact of partial steps and momentum advection schemes in a global ocean circulation model at eddy-permitting resolution. *Ocean Dynamics*, **56**, 543–567.

Barnier, B., et al., 2007: Eddy-permitting ocean circulation hindcasts of past decades. *CLIVAR Exchanges*, Vol. 12, 8–14.

Beranger, K., L. Mortier, and M. Crepon, 2005: Seasonal variability of water transport through the straits of gibraltar, sicily and corsica, derived from a high-resolution model of the mediterranean circulation. *Prog. Oceanogr.*, **66 (2-4)**, 341–364.

Béranger, K., et al., 2010: Impact of the spatial distribution of the atmospheric forcing on water mass formation in the mediterranean sea. *J. Geophys. Res.*, **115 (C12041)**, 1–22.

Bethoux, J., B. Gentili, and D. Tailliez, 1998: Warming and freshwater budget change in the mediterranean since the 1940s, their possible relation to the greenhouse effect. *Geophys. Res. Lett.*, **25**, 1023–1026.

Bethoux, J. P. and B. Gentili, 1996: The mediterranean sea, coastal and deep-sea signatures of climatic and environmental changes. *J. Mar. Syst.*, **7 (2-4)**, 383 – 394.

Bethoux, J. P. and B. Gentili, 1999: Functioning of the mediterranean sea: past and present changes related to freshwater input and climate changes. *J. Mar. Syst.*, **20 (1-4)**, 33 – 47.

Beuvier, J., F. Sevault, and S. Somot, 2008: Modélisation de la variabilité interannuelle de la mer méditerranée sur la période 1960-2000 a láide de nemomed8. Note Cent. 105, Groupe de Meteorol. de Grande Echelle et Clim., Cent. Natl. de Rech. Meteorol., Toulouse, France.

Beuvier, J., et al., 2010: Modeling the mediterranean sea interannual variability during 1961-2000: Focus on the eastern mediterranean transient. *J. Geophys. Res.*, **115 (C8)**, C08 017.

Bouffard, J., L. Roblou, F. Birol, A. Pascual, L. Fenoglio-Marc, M. Cancet, R. Morrow, and Y. Ménard, 2009: *Coastal Satellite Altimetry*, chap. Assessment of improved coastal altimetry strategies over the North Western Mediterranean Sea. Springer Verlag.

Bouzinac, C., J. Font, and J. Johannessen, 2003: Annual cycles of sea level and sea surface temperature in the western mediterranean sea. *J. Geophys. Res. C*, **108**.

Brachet, S., P. Y. Le Traon, and C. Le Provost, 2004: Mesoscale variability from a high-resolution model and from altimeter data in the north atlantic ocean. *J. Geophys. Res. C*, **109**.

Brodeau, L., B. Barnier, A.-M. Treguier, T. Penduff, and S. Gulev, 2010: An era40-based atmospheric forcing for global ocean circulation models. *Ocean Modelling*, **31 (3-4)**, 88 – 104.

Candela, J., 2001: *Ocean Circulation and Climate*, chap. Mediterranean Water and Global Circulation, 419–429. 5.7, Academic Press.

Carrère, L. and F. Lyard, 2003: Modeling the barotropic response of the global ocean to atmospheric wind and pressure forcing - comparisons with observations. *Geophys. Res. Lett.*, **30**.

Cazenave, A., C. Cabanes, K. Dominh, and S. Mangiarotti, 2001: Recent sea level change in the mediterranean sea revealed by topex/poseidon satellite altimetry. *Geophys. Res. Lett.*, **28**.

Chelton, D. B., J. C. Ries, B. J. Haines, L.-L. Fu, and P. S. Callahan, 2001: Chapter 1 satellite altimetry. *Satellite Altimetry and Earth Sciences A Handbook of Techniques and Applications*, L.-L. Fu and A. Cazenave, Eds., Academic Press, International Geophysics, Vol. 69, 1 – ii.

CIESM Initiative Group, 2002: Long-term sustained observing system for climatic variability studies in the mediterranean. *Third EuroGOOS Conference, Athens.*

CLIPPER Project Team, 1999: Modélisation à haute résolution de la circulation dans l'océan atlantique forcée et couplée océanatmosphère. Sci. Tech. Rep CLIPPERR399, Lab. des Ecoulements Géophys. et Ind., Grenoble, France.

Dee, D. P., et al., 2011: The era-interim reanalysis: configuration and performance of the data assimilation system. *Quarterly Journal of the Royal Meteorological Society*, **137 (656)**, 553–597.

Demirov, E. and N. Pinardi, 2002: Simulation of the mediterranean sea circulation from 1979 to 1993: Part i. the interannual variability. *J. Mar. Syst.*, **33-34**, 23–50.

Déqué, M. and J. Piedelievre, 1995: High-resolution climate simulation over europe. *Climate Dynamics*, **11 (6)**, 321–339.

Dobricic, S., 2005: New mean dynamic topography of the mediterranean calculated from assimilation system diagnostics. *Geophys. Res. Lett.*, **32 (L11606)**.

Fernández, V., D. E. Dietrich, R. L. Haney, and J. Tintoré, 2005: Mesoscale, seasonal and interannual variability in the mediterranean sea using a numerical ocean model. *Prog. Oceanogr.*, **66**, 321–340.

Ferry, N., L. Parent, G. Garric, B. Barnier, N. C. Jourdain, and M.-O. Team, 2010: Mercator global eddy permitting ocean reanalysis glorys1v1: Description and results. *Mercator Newsletter*, **(36)**, 15–27.

Flexas, M., D. Gomis, S. Ruiz, A. Pascual, and P. León, 2006: In situ and satellite observations of the eastward migration of the western alboran sea gyre. *Prog. Oceanogr.*, **70 (2-4)**, 486 – 509.

Font, J., P. Puig, J. Salat, A. Palanques, and M. Emelianov, 2007: Sequence of hydrographic changes in nw mediterranean deep water due to the exceptional winter of 2005. *Scientia Marina*, **71 (2)**.

Font, J., J. Salat, and J. Tintoré, 1988: Permanent features of the circulation in the catalan sea. *Oceanol. Acta*, **18**, 207–219.

Gaillard, F., E. Autret, V. Thierry, and G. P., 2008: Quality control of large argo datasets. *J. Atmos. Ocean Tech.*, **(26)**, 337–351.

Gaillard, F. and R. Charraudeau, 2008: New climatology and statistics over the global ocean. *MERSEA del. 5.4.7. June 2008.*

García Lafuente, J., J. Delgado, and F. Criado, 2002: Inflow interruption by meteorological forcing in the strait of gibraltar. *Geophys. Res. Lett.*, **29 (19)**, 1914.

García-Lafuente, J., J. Delgado, J. M. Vargas, M. Vargas, F. Plaza, and T. Sarhan, 2002: Low-frequency variability of the exchanged flows through the strait of gibraltar during canigo. *Deep-Sea Res.*, **II (49)**, 4051–4067.

Gill, A., 1982: *Atmosphere-Ocean Dynamics.* Academic Press.

Gomis, D., M. N. Tsimplis, B. Martín-Míguez, A. W. Ratsimandresy, J. García-Lafuente, and S. A. Josey, 2006: Mediterranean sea level and barotropic flow through the strait of gibraltar for the period 1958 – 2001 and reconstructed since 1659. *J. Geophys. Res.*, **111 (C11005)**.

Goosse, H., 1997: Modelling the large scale behaviour of the coupled ocean-ice system. Ph.D. thesis, Universite Catholique de Louvain, Louvain-la-Neuve, Belgium.

Hamad, N., C. Millot, and I. Taupier-Letage, 2005: A new hypothesis about the surface circulation in the eastern basin of the mediterranean sea. *Prog. Oceanogr.*, **66**, 287–298.

Herrmann, M., C. Estournel, M. Déqué, P. Marsaleix, F. Sevault, and S. Somot, 2008a: Dense water formation in the gulf of lions shelf: Impact of atmospheric interannual variability and climate change. *Continental Shelf Research*, **28 (15)**, 2092 – 2112, sediment Dynamics in the Gulf of Lions; the Impact of Extreme Events.

Herrmann, M., F. Sevault, J. Beuvier, and S. Somot, 2010: What induced the exceptional 2005 convection event in the northwestern mediterranean basin? answers from a modeling study. *J. Geophys. Res.*, **115 (C12)**.

Herrmann, M., S. Somot, F. Sevault, C. Estournel, and M. Déqué, 2008b: Modeling the deep convection in the northwestern mediterranean sea using an eddy-permitting and an eddy-resolving model: Case study of winter 1986–1987. *J. Geophys. Res. C*, **113 (C04011)**.

Herrmann, M. J. and S. Somot, 2008: Relevance of era40 dynamical downscaling for modeling deep convection in the mediterranean sea. *Geophys. Res. Lett.*, **35 (4)**.

Hu, Z. Y., A. M. Doglioli, A. A. Petrenko, P. Marsaleix, and I. Dekeyser, 2009: Numerical simulations of eddies in the gulf of lion. *Ocean Modelling*, **28 (4)**, 203–208.

Ikeda, M. and F. Dobson, 1995: *Oceanographic Applications of Remote Sensing*. CRC-Press.

Ingleby, B. and M. Huddleston, 2007: Quality control of ocean temperature and salinity profiles – historical and real-time data. *Journal of Marine Systems*, **65 (1-4)**, 158 – 175, marine Environmental Monitoring and Prediction - Selected papers from the 36th International Liège Colloquium on Ocean Dynamics, 36th International Liège Colloquium on Ocean Dynamics.

Ishii, M. and M. Kimoto, 2009: Reevaluation of historical ocean heat content variations with time-varying xbt and mbt depth bias corrections. *Journal of Oceanography*, **65**, 287–299.

Iudicone, D., R. Santoreli, S. Marullo, and P. Gerosa, 1998: Sea level variability and surface eddy statistics in the mediterranean sea from topex/poseidon data. *J. Geophys. Res.*, **103 (C2)**, 2995–3011.

Juza, M., 2011: Modélisation numérique et observations de l'océan global : développement des interfaces, évaluation de simulations et de réseaux d'observations, investigations dynamiques. Ph.D. thesis, Université de Grenoble.

Kantha, L. H. and C. Clayson, 2000: *Numerical models of Oceans and Oceanic Processes*. Academic Press. USA.

Krahmann, G. and F. Schott, 1998: Longterm increases in western mediterranean salinities and temperatures: Anthropogenic and climatic sources. *Geophys. Res. Lett.*, **25 (22)**, 4209–4212.

Large, W. and S. Yeager, 2004: Diurnal to decadal global forcing for ocean and sea-ice models. Tech. rep., NCAR Technical Note, 22 pp.

Larnicol, G., N. Ayoub, and P. Y. Le Traon, 2002: Major changes in mediterranean sea level variability from 7 years of topex/poseidon and ers-1/2 data. *J. Mar. Syst.*, **33-34**, 63 – 89.

Larnicol, G., P.-Y. Le Traon, N. Ayoub, and P. De Mey, 1995: Mean sea level and surface circulation variability of the mediterranean sea from 2 years of topex/poseidon altimetry. *J. Geophys. Res. C*, **100 (C12)**, 25,163–25,177.

Lascaratos, A., W. Roether, K. Nittis, and B. Klein, 1999: Recent changes in deep water formationand spreading in the eastern mediterranean sea - a review. *Prog. Oceanogr.*, **44**, 5–36.

Le Traon, P.-Y., Y. Faugere, F. Hernandez, J. Dorandeu, F. Mertz, and M. Ablain, 2003: Can we merge geosat follow-on with topex/poseidon and ers-2 for an improved description of the ocean circulation? *J. Atmos. Ocean Technol.*, **20 (6)**, 889–895.

Le Traon, P.-Y., F. Nadal, and N. Ducet, 1998: An improved mapping method of multisatellite altimeter data. *J. Atmos. Ocean Technol.*, **15 (2)**, 522–534.

Leaman, K. and F. Schott, 1991: Hydrographic structure of the convection regime in the gulf of lions - 1987. *J. Phys. Oceanogr.*, **21 (4)**, 575–598.

Li, L., A. Bozec, S. Somot, K. Béranger, P. Bouruet-Aubertot, F. Sevault, and M. Crépon, 2006: Chapter 7 regional atmospheric, marine processes and climate modelling. *Mediterranean*, P. M.-R. P. Lionello and R. Boscolo, Eds., Elsevier, Developments in Earth and Environmental Sciences, Vol. 4, 373 – 397.

Lopez García, M., C. Millot, J. Font, and E. García-Ladona, 1994: Surface circulation variability in the balearic basin. *J. Geophys. Res.*, **99 (C2)**, 3285–3296.

López-Jurado, J., C. Gonzalez-Pola, and P. Velez-Belchi, 2005: Observation of an abrupt disruption of the long-term warming trend at the balearic sea, western mediterranean sea, in summer 2005. *Geophys. Res. Lett.*, **32 (24)**.

Madec, G., 2008: *NEMO Ocean Engine. Note du Pole de modélisation.* Laboratoire d'Oceanographie et du Climat: Experimentation et Approches Numeriques, 27th ed.

Madec, G., P. Delecluse, M. Imbard, and C. Levy, 1998: *OPA 8.1, Ocean general circulation model, reference manual.* Université P. et M. Curie, B102 T15-E5, 4 place Jussieu, Paris cedex 5,, IPSL/LODYC, France, Note du Pôle de modélisation.

MEDAR-Group, 2002: Mediterranean and black sea database of temperature, salinity and biochemical parameters and climatological atlas [4 cd-roms].

MEDOC Group, 1970: Observation of formation of deep water in the mediterranean sea in 1969. *Nature*, **227**, 1037–1040.

Millot, C., 1999: Circulation in the western mediterranean sea. *J. Mar. Syst.*, **20**, 423–442.

Molcard, A., N. Pinardi, M. Iskandarani, and D. Haidvogel, 2002: Wind driven general circulation of the mediterranean sea simulated with a spectral element ocean model. *Dynamics of Atmospheres and Oceans*, **35**, 97–130.

Molines, J., B. Barnier, T. Penduff, L. Brodeau, A. Treguier, S. Theetten, and G. Madec, 2007: Definition of the interannual experiment orca025-g70, 1958-2004. Report LEGI-DRA-2-11-2006i, LEGI.

Olita, A., A. Ribotti, R. Sorgente, L. Fazioli, and A. Perilli, 2011: Sla-chlorophyll-a variability and covariability in the algero-provencal basin (1997-2007) through combined use of eof and wavelet analysis of satellite data. *Ocean Dynamics*, **61 (1)**, 89–102.

Özsoy, E. and U. Unluata, 1998: *The Sea*, Vol. 11, chap. The Black Sea. Wiley, New York.

Pascual, A., C. Boone, G. Larnicol, and P.-Y. Le Traon, 2009: On the quality of real-time altimeter gridded fields: comparison with in situ data. *J. Atmos. Ocean Technol.*

Pascual, A., B. Buongiorno Nardelli, G. Larnicol, M. Emelianov, and D. Gomis, 2002: A case of an intense anticyclonic eddy in the balearic sea (western mediterranean). *J. Geophys. Res. C*, **107**.

Pascual, A., M. Marcos, and D. Gomis, 2008: Comparing the sea level response to pressure and wind forcing of two barotropic models: Validation with tide gauge and altimetry data. *J. Geophys. Res. C*, **113 (C07011)**.

Pascual, A., M.-I. Pujol, G. Larnicol, P.-Y. Le Traon, and M.-H. Rio, 2007: Mesoscale mapping capabilities of multisatellite altimeter missions: First results with real data in the mediterranean sea. *J. Mar. Syst.*, **65 (1-4)**, 190 – 211.

Penduff, T., B. Barnier, A.-M. Treguier, and P. Y. L. Traon, 2006: Synergy between ocean observations and numerical simulations: Clipper heritage and drakkar perspectives. ESA.

Penduff, T., M. Juza, and B. Barnier, 2007: Assessing the realism of ocean simulations against hydrography and altimetry. *CLIVAR Exchanges*, **12 (3(42))**, 11–12.

Peneva, E., E. Stanev, V. Belokopytov, and P. Y. Le Traon, 2001: Water transport in the bosphorus straits estimated from hydro-meteorological and altimeter data: seasonal to decadal variability. *J. Mar. Syst.*, **31 (1-3)**, 21–33.

Pickard, G. and W. Emery, 1990: *Descriptive Physical Oceanography: An Introduction*. 5th ed., Pergamon Press.

Pinot, J. M., J. L. López-Jurado, and M. Riera, 2002: The canales experiment (1996-1998). interannual, seasonal, and mesoscale variability of the circulation in the balearic channels. *Prog. Oceanogr.*, **55 (3-4)**, 335 – 370.

Pinot, J.-M., J. Tintoré, and D. Gomis, 1995: Multivariate analysis of the surface circulation in the balearic sea. *Prog. Oceanogr.*, **36 (4)**, 343 – 344.

Poulain, P.-M. and E. Zambianchi, 2007: Surface circulation in the central mediterranean sea as deduced from lagrangian drifters in the 1990s. *Continental Shelf Research*, **27 (7)**, 981 – 1001.

Puillat, I., I. Taupier-Letage, and C. Millot, 2002: Algerian eddies lifetime can near 3 years. *J. Mar. Syst.*, **31 (4)**, 245–259.

Pujol, M.-I. and G. Larnicol, 2005: Mediterranean sea eddy kinetic energy variability from 11 years of altimetric data. *J. Mar. Syst.*, **(58)**, 121–142.

Reynaud, T., H. Legrand, and B. Barnier, 1998: A new analysis of hydrographic data in the atlantic and its application to an inverse modeling study. Silver Spring, Md.

Rio, M.-H., P.-M. Poulain, A. Pascual, E. Mauri, G. Larnicol, and R. Santoleri, 2007: A mean dynamic topography of the mediterranean sea computed from altimetric data, in-situ measurements and a general circulation model. *J. Mar. Syst.*, **65 (1-4)**, 484 – 508.

Rixen, M., et al., 2005: The western mediterranean deep water: A proxy for climate change. *Geophys. Res. Lett.*, **32 (L12608)**.

Robinson, A. and M. Golnaraghi, 1994: *Ocean Processes in Climate Dynamics: Global and Mediterranean examples*, chap. The physical and dynamical oceanography of the Mediterranean Sea. Kluwer Academic Publishing.

Robinson, A., W. Leslie, A. Theocharis, and A. Lascaratos, 2001: *Encyclopedia of Ocean Sciences*, chap. Mediterranean Sea Circulation, 1689–1706. Academic Press Ltd., London.

Roether, W., B. Klein, B. Bruno Manca, A. Theochratis, and S. Kioroglou, 2007: Transient eastern mediterranean deep waters in response to the massive dense-water output of the aegean sea in the 1990s. *Prog. Oceanogr.*, **74**, 540–571.

Roether, W., B. Manca, B. Klein, D. Bregant, D. Georgopoulos, V. Beitzel, V. Kovacevic, and A. Luchetta, 1996: Recent changes in eastern mediterranean deep waters. *Science*, **271 (5247)**, 333–335.

Roullet, G. and G. Madec, 2000: Salt conservation, free surface, and varying levels: A new formulation for ocean general circulation models. *J. Geophys. Res.*, **105**, 23 927–23 942.

Ruiz, S., J. Font, M. Emelianov, J. Isern-Fontanet, C. Millot, J. Salas, and I. Taupier-Letage, 2002: Deep structure of an open sea eddy in the algerian basin. *J. Mar. Syst.*, **33-34**, 179–195.

Ruiz, S., D. Gomis, M. G. Sotillo, and S. A. Josey, 2008: Characterization of surface heat fluxes in the mediterranean sea from a 44-year high-resolution atmospheric data set. *Global Planet. Change*, **63 (2-3, Sp. Iss. SI)**, 258–274.

Ruiz, S., A. Pascual, B. Garau, Y. Faugere, A. Alvarez, and J. Tintoré, 2009: Mesoscale dynamics of the balearic front, integrating glider, ship and satellite data. *J. Mar. Syst.*

Salat, J. and J. Pascual, 2006: Principales tendencias climatológicas en el mediterráneo noroccidental, a partir de más de 30 años de observaciones oceanográficas en la costa catalana. *Clima, Sociedad y Medio Ambiente*, **A (5)**, 284–290.

Sánchez-Román, A., G. Sannino, J. García-Lafuente, A. Carillo, and F. Criado-Aldeanueva, 2009: Transport estimates at the western section of the strait of gibraltar: A combined experimental and numerical modeling study. *J. Geophys. Res.*, **114 (C06002)**.

Schaeffer, A., P. Garreau, A. Molcard, P. Fraunié, and Y. Seity, 2011: Influence of high-resolution wind forcing on hydrodynamic modeling of the gulf of lions. *Ocean Dynamics*, **61**, 1823–1844.

Schroeder, K., G. P. Gasparini, M. Tangherlini, and M. Astraldi, 2006: Deep and intermediate water in the western mediterranean under the influence of the eastern mediterranean transient. *Geophys. Res. Lett.*, **33 (21)**.

Schroeder, K., S. A. Josey, M. Herrmann, L. Grignon, G. P. Gasparini, and H. L. Bryden, 2010: Abrupt warming and salting of the western mediterranean deep water after 2005: Atmospheric forcings and lateral advection. *J. Geophys. Res.*, **115 (C8)**.

Schroeder, K., A. Ribotti, M. Borghini, R. Sorgente, A. Perilli, and G. P. Gasparini, 2008a: An extensive western mediterranean deep water renewal between 2004 and 2006. *Geophys. Res. Lett.*, **35 (18)**.

Schroeder, K., V. Taillandier, A. Vetrano, and G. Gasparini, 2008b: The circulation of the western mediterranean sea in spring 2005 as inferred from observations and from model outputs. *Deep Sea Research Part I: Oceanographic Research Papers*, **55 (8)**, 947 – 965.

Sevault, F., S. Somot, and J. Beuvier, 2009: *A regional version of the NEMO Ocean Engine on the Mediterranean Sea : NEMOMED8 user's guide*. Note de centre GMGEC, CNRM.

Simmons, A. and J. Gibson, 2000: The era-40 project plan. Tech. Rep. 1, European Centre for Medium Range Weather Forecast, Reading, UK.

Smith, R., H. Bryden, and K. Stansfield, 2008: Observations of new western mediterranean deep water formation using argo floats 2004-2006. *Ocean Science*, **(4)**, 133–149.

Somot, S., 2005: Modélisation climatique du bassin méditerranéen variabilité et scénarios de changement climatique. Ph.D. thesis, Univ. Paul Sabatier, Toulouse.

Somot, S., F. Sevault, and M. Déqué, 2006: Transient climate change scenario simulation of the mediterranean sea for the twenty-first century using a high-resolution ocean circulation model. *Climate Dynamics*, **27 (7)**, 851–879.

Soto-Navarro, J., F. Criado-Aldeanueva, J. GarcÌa-Lafuente, and A. Snchez-Romn, 2010: Estimation of the atlantic inflow through the strait of gibraltar from climatological and in situ data. *J. Geophys. Res.*, **115 (C10)**.

Sparnocchia, S., G. Manzella, and P. La Violette, 1994: The interanual and seasonal variability of maw and liw core properties in the western mediterranean sea. *Coast. Estuar Stud.*, 177–194.

Sur, H., E. Ozoy, and U. Unluata, 1992: Simultaneous deep and intermediate depth convection in the northern levantine sea, winter 1992. *Oceanol. Acta*, **16**, 33–43.

Tintore, J., 2009: Oceanbit - an international coastal observing and forecasting system based in the balearic islands.

Tintoré, J., P. La Violette, I. Blade, and A. Cruzado, 1988: A study of an intense density front in the eastern alboran sea: the almería-oran front. *J. Phys. Oceanogr.*, **18 (10)**, 1384–1397.

Tonani, M., N. Pinardi, S. Dobricic, I. Pujol, and C. Fratianni, 2008: A high-resolution free-surface model of the mediterranean sea. *Ocean Science*, **4 (1)**, 1–14.

Tsimplis, M. N. and T. F. Baker, 2000: Sea level drop in the mediterranean sea: An indicator of deep water salinity and temperature changes? *Geophys. Res. Lett.*, **27 (12)**, 1731–1734.

Tsimplis, M. N. and H. L. Bryden, 2000: Estimation of the transports through the strait of gibraltar. *Deep-Sea Res.*, **47 (I)**, 2219–2242.

Tsimplis, M. N. and S. A. Josey, 2001: Forcing of the mediterranean sea by atmospheric oscillations over the north atlantic. *Geophys. Res. Lett.*, **28 (5)**, 2136.

Tsimplis, M. N., M. Marcos, S. Somot, and B. Barnier, 2008: Sea level forcing in the mediterranean sea between 1960 and 2000. *Global Planet. Change*, **63 (4)**, 325 – 332.

Tsimplis, M. N. and M. Rixen, 2002: Sea level in the mediterranean sea: The contribution of temperature and salinity changes. *Geophys. Res. Lett.*, **29 (23)**, 2136.

Unluata, U., T. Oguz, M. Latif, and E. Özsoy, 1990: *The Physical Oceanography of Sea Straits*, chap. On the physical oceanography of the Turkish Straits, 25–60. Kluwer Academic Publishing.

Uppala, S. M., et al., 2005: The era-40 re-analysis. *Quarterly Journal of the Royal Meteorological Society*, **131 (612)**, 2961–3012.

Vargas-Yáñez, M., F. Moya, E. Tel, M. C. García-Martínez, E. Guerber, and M. Bourgeon, 2009: Warming and salting in the western mediterranean during the second half of the 20th century: inconsistencies, unknowns and the effect of data processing. *Scientia Marina*, **73 (1)**, 7–28.

Vargas-Yáñez, M., F. Plaza, J. Garca-Lafuente, T. Sarhan, J. M. Vargas, and P. Vélez-Belchi, 2002: About the seasonal variability of the alboran sea circulation. *J. Mar. Syst.*, **35 (3-4)**, 229–248.

Vargas-Yáñez, M., J. Salat, M. Luz Fernández de Puelles, J. L. López-Jurado, J. Pascual, T. Ramírez, D. Cortés, and I. Franco, 2005: Trends and time variability in the northern continental shelf of the western mediterranean. *J. Geophys. Res. C*, **110**.

Vidal-Vijande, E., A. Pascual, B. Barnier, J.-M. Molines, and J. Tintoré, 2011: Analysis of a 44-year hindcast for the mediterranean sea: comparison with altimetry and in situ observations. *Scientia Marina*, **75 (1)**.

Vignudelli, S., P. Cipollini, L. Roblou, F. Lyard, G. P. Gasparini, G. Manzella, and M. Astraldi, 2005: Improved satellite altimetry in coastal systems: Case study of the corsica channel (mediterranean sea). *Geophys. Res. Lett.*, **32**.

Viúdez, A., J. M. Pinot, and R. L. Haney, 1998: On the upper layer circulation in the alboran sea. *J. Geophys. Res. C*, **103**, 21 653–21 666.

Viúdez, A. and J. Tintoré, 1995: Time and space variability in the eastern alboran sea from march to may 1990. *J. Geophys. Res.*, **100 (C5)**, 8571–8586.

Volkov, D. L., G. Larnicol, and J. Dorandeu, 2007: Improving the quality of satellite altimetry data over continental shelves. *J. Geophys. Res. C*, **112**.

Woolfe, D., A. Shaw, and M. N. Tsimplis, 2003: The influence of the north atlantic oscillation on sea-level variability in the north atlantic region. *J. Atmos. Ocean Sci.*, **9 (4)**, 145–167.

Wu, P. and K. Haines, 1996: Modeling the dispersal of levantine intermediate water and its role in mediterranean deep water formation. *J. Geophys. Res.*, **101 (C3)**, 6591–6607.

Wüst, G., 1961: On the vertical circulation of the mediterranean sea. *J. Geophys. Res.*, **66 (10)**, 3261–3271.

Curriculum Vitae
Enrique Vidal Vijande

Datos Personales

Dirección	C./ Josep Boria, 6 - 7ºB 07014 Palma de Mallorca España	**Fecha de Nacimiento**	07 Septiembre 1983
		Lugar de Nacimiento	Palma de Mallorca
		Nacionalidad	Española
Email	enrique@solvisuals.com	**Teléfono Móvil**	+34 669 373 966

Perfil

· Master de Oceanografía (MOcean) por el National Oceanographic Centre, Southampton
· Licenciado en Ciencias del Mar y D.E.A. en Oceanografía por la ULPGC
· 5 idiomas (Español, Inglés, Francés, Alemán, Catalán)
· Experiencia en el uso de equipo oceanográfico, campañas, toma y proceso de datos.
· Fotógrafo Documental y Reportaje especializado en actividades y divulgación científica

Formación

2011 (Ene-Jun)	:	Analista de datos de satélite & teledetección en SOCIB.
2007 - 2010	:	Beca predoctoral (realización de Tesis) I3P (4 años) en IMEDEA (CSIC-UIB)
2009 (Abril)	:	Obtención del Diploma de Estudios Avanzados (sobresaliente) bajo el Programa de Doctorado en Oceanografía de la ULPGC / CMIMA
2008 (verano)	:	Asistencia al 1er MedCLIVAR-ESF Summer School (Rhodas, Grecia)
2007 - 2009	:	Realización de Cursos de Doctorado en Oceanografía (ULPGC-CMIMA)
2006 (Jul - Dic)	:	Beca en IMEDEA (CSIC-UIB) - Proyecto “CABRERA” como técnico de instrumentación y muestreo.
2006 (Junio)	:	Curso : Advanced Oil Spill Modelling using GNOME (NOAA ORR HAZMAT)
2001 - 2005	:	Master de Oceanografía (MOcean = licenciatura + master), National Oceanography Centre, Universidad de Southampton, Reino Unido *Homologado en España a “Licenciado en Ciencias del Mar”*

Publicaciones Científicas

Vidal-Vijande, E., A. Pascual, B. Barnier, J.M. Molines and J.Tintoré. - 2011. Multiparametric Analysis and Validation in the Western Mediterranean of three global OGCM Hindcasts. *Scientia Marina - Special EOF Edition*. *In Press*

Pascual, A., Bouffard, J., Ruiz, S., Nardelli, B., Vidal-Vijande, E., Escudier, R., Sayol, J.M., Orfila,A. - 2012. Recent advances on mesoscale variability in the Western Mediterranean Sea: Complementary between satellite altimetry and other sensors. *Marine Geodesy*, *submitted.*

Schunter, C., Carreras-Carbonell, J., Macpherson, E., Tintoré, J., Vidal, E., Pascual, A. - 2011. Matching genetics with oceanography: directional gene flow in a Mediterranean fish species. *Molecular Ecology, Vol: 20, 5167.*

Vidal-Vijande, E., A. Pascual, B. Barnier, J.M. Molines and J.Tintoré. - 2011. Analysis of a 44-Year Hindcast for the Mediterranean Sea : Comparison with Altimetry and In Situ Observations. *Scientia Marina **75**(1),* 71-86. ISSN 0214-8358 doi: 10.3989/scimar.2011.75n1071

ESTANCIAS

2009 (Oct - Dic)	:	Estancia de Investigación en CNR, Roma, Italia (Dr. Bruno Buongiorno Nardelli)
2008 (Oct - Dic)	:	Estancia de Investigación en LEGI, Grenoble, Francia (Prof. Bernard Barnier)

CONGRESOS

2011 (Mayo)	:	Presentación Oral: Multiparametric Analysis and Validation in the Mediterranean of 4 eddy-permitting global OGCM hindcasts of past decades, Vidal-Vijande, E, Pascual, A, Somot, S, Barnier, B, Molines, J.M, Tintoré, J, Congreso: *HYdrological cycle in the Mediterranean EXperiment* , Menorca, España
2010 (Oct)	:	Presentación Oral: Multiparametric Analysis and Validation in the Mediterranean of 4 Eddy Permitting Global OGCMs of Past Decades, Vidal-Vijande, E, Pascual, A, Barnier, B, Molines, J-M, Tintoré, J, Congreso: *1er Encuentro Oceanografía Física Española*, Barcelona, España
2009 (Nov)	:	A Multi-sensor Approach Towards Coastal Ocean Processes Monitoring, Pascual, A., Bouffard, J., Escudier, R., Ruiz, S., Garau, B., Martínez-Ledesma, M., Vidal-Vijande, E., Faugere, Y., Larnicol, G., Vizoso, G., Tintore, J., Congreso: *Eveyone's Gliding Observatories meeting & glider school*, Larnaca, Cyprus
2009 (Sept)	:	Póster: Analysis of a 44 - Year Hindcast for the Mediterranean Sea : Comparison with altimetry and in situ observations. Vidal-Vijande, E, Pascual, A, Barnier, B, Molines, J-M, Rixen, M, Tintoré, J. Congreso: *OceanObs'09*, Venecia, Italia
2008 (Nov)	:	Póster: Analysis of a 44 - Year Hindcast for the Mediterranean Sea : Comparison with altimetry and in situ observations. Vidal-Vijande, E, Pascual, A, Barnier, B, Molines, J-M, Rixen, M, Tintoré, J. Congreso: *OSTST & GODAE Final Symposium*, Nice, Francia
2008 (Mayo)	:	Póster: Analysis of a 44 - Year Hindcast for the Mediterranean Sea : Comparison with altimetry and in situ observations. Vidal-Vijande, E, Pascual, A, Barnier, B, Molines, J-M, Rixen, M, Tintoré, J. Congreso: *International Symposium on the Effects of Climate Change on the Worlds Oceans*, Gijón, España

2006 (Jun)	:	Asistencia a las Jornadas Internacionales Sobre Gestión de Emergencias por Contaminación de Aguas Marinas, Proyecto SOSMER, Palma, España

CAMPAÑAS Y TRABAJO DE CAMPO

2011 (Junio)	:	Campaña SOCIB BlueFin Tuna - estudio sobre supervivencia larvaria del atún rojo.
2006 - 2010	:	Múltiples campañas de recogida y lanzamiento de Gliders y boyas Argo
2009 (Mayo)	:	Oceanógrafo físico y técnico de instrumentación en la campaña SINOCOP (IMEDEA CSIC-UIB) departamento TMOOS.
2007 (Julio)	:	Oceanógrafo físico en la campaña ECOOP Sur de Mallorca (BOE García del Cid).
2006 (Oct - Dic)	:	Oceanógrafo físico en la campaña Antártica JR161, British Antarctic Survey (BAS), (a bordo del RRS James Clark Ross). Contrato 2 meses.
2006 (Jun - Oct)	:	Múltiples campañas de colocación y recogida de instrumentación sumergida (boyas, correntímetros, mareógrafos y fondeos)
2006 (Mayo)	:	Oceanógrafo físico en la campaña D304 del NERC, Reino Unido (a bordo del RRS Discovery). (Voluntario)
2005 (Nov)	:	Oceanógrafo físico en la campaña CD177 del NERC, Reino Unido (a bordo del RRS Charles Darwin). (Voluntario)

DIVULGACIÓN CIENTÍFICA

Producción de un video-reportaje de la Feria de la Ciencia 2011 para la Direcció General de R+D+i de les Illes Balears. [producción de SOL Visuals]
Producción del Vídeo de Presentación de CSIC Baleares para la Delegación Institucional CSIC Baleares. [producción de SOL Visuals]
Co-Organización de la Exposición Fotográfico-Científica CSIC Baleares para la Delegación Institucional CSIC Baleares. [producción de SOL Visuals]
Producción de 15 entrevistas mini-reportaje sobre doctorandos para la Direcció General de R+D+i de les Illes Balears. [producción de SOL Visuals]
Producción, diseño y renovación del espacio de exposición del Centro Oceanográfico de Baleares del IEO para la Semana de la Ciencia 2010. [producción de SOL Visuals]
Producción de un video-reportaje de la Feria de la Ciencia 2010 para la Direcció General de R+D+i de les Illes Balears. [producción de SOL Visuals]

APTITUDES

Idiomas	:	Español (lengua materna) Inglés (Bilingüe, escrito y hablado) Catalán (nivel medio, hablado) Francés (Nivel medio, escrito y hablado) Alemán (Nivel medio-bajo, escrito y hablado)

Conocimientos Informáticos : Mac OSX, Windows, Linux, Office, Matlab, GNOME, Photoshop, Lightroom, In-Design, Premier-Pro, AVID Media Composer, Final Cut Pro

Títulos : Patrón de Yate
Yachtmaster Theory (RYA)
Diesel Maintenance Course (RYA)
Advanced Open Water Diver (PADI)
STCW95 Curso de Supervivencia Personal en el Mar
Permiso de Conducir B

REFERENCIAS

SOCIB (www.socib.es)
Director : Prof. Joaquín Tintoré Subirana

IMEDEA (www.imedea.uib.es)
Directora de Tesis : Dra. Ananda Pascual

BAS (British Antarctic Survey) (www.antarctica.co.uk)
JR161 Investigador Principal : Dr. Rachel Shreeve

NOC (National Oceanography Centre, Southampton) (www.noc.soton.ac.uk)
Tutor personal : Prof. Harry L. Bryden

OTROS TRABAJOS

Trabajo Voluntario

2003 : Atlantic Whale Foundation", Tenerife. Experiencia obtenida: Observación, identificación y clasificación fotográfica de delfines y ballenas.

Trabajo Remunerado

2000 - 2006 (veranos) : Patrón de embarcaciones en una compañía de alquiler de barcos (www.nautinort.com)
Rescates de emergencia.
Mantenimiento e invernaje de embarcaciones.

Aficiones

Fotografía, aikido, navegación a motor y vela, buceo, waterpolo, esquí, volley playa, escalada, dibujo

CURRÍCULUM FOTOGRÁFICO

Premios de Fotografía

2009 : Primer premio del certamen (para Mallorca) : “Fotografía Científica”, Baleares

2009 : Segundo premio del certamen : “Opticaigua 2009: El Ciclo del Agua” (Emaya)

2008 : Accésit del certamen : “El Placer de Leer” (Ayuntamiento de Salamanca)

2008 : Primer premio del certamen : “El Hombre y el Medio Ambiente” (Consellería de Medio Ambiente de las Islas Baleares)

2007 : Semifinalista del certamen : “Shell Wildlife Photographer of the Year 2006” (BBC Wildlife)

2007 : Segundo Premio del Certamen : “Panoramio” (Google & Panoramio)

2006 : Ganador del Certamen : “Fotobook “

Exposiciones de Fotografía

2011 : Exposición con Tomeu Canyellas : Mallorca, L’Illa de les Mil Cares (Fundació Barceló, Palma).

2011 : Exposición con Tomeu Canyellas : The Mallorca Collection (Puro Hotel, Palma)

2009 : Exposición Colectiva : Feria de la Ciencia (Baleares) 2009 : Fotografía Científica

2009 : Exposición Colectiva : Opticaigua 2009 (Emaya)

2008 : Exposición Colectiva : Centro Reina Sofía / Renfe sobre Violencia Contra la Mujer.

2008 : Exposición Colectiva Itinerante - “El Placer de Leer” (Ayuntamiento de Salamanca)

2008 : Exposición en la Feria de Arte : Station Studio en Binissalem

2008 : Exposición Colectiva : El Hombre y el Medio Ambiente (Consellería de Medio Ambiente Baleares)

2007 : Exposición Individual - Salón Náutico de Barcelona

Contribuciones Fotográficas a Publicaciones

2011 : Plan de Implementación: Sistema de Observación Costero de las Islas Baleares (SOCIB)

2010 : Folleto Corporativo del Instituto Mediterráneo de Estudios Avanzados (IMEDEA)

2009 : Plan Estratégico del Dpto. de Tecnologías Marinas, Oceanografía Operacional y Sostenibilidad (TMOOS, IMEDEA)

2009 : Pla de Ciència, Tecnologia i Innovació de les Illes Balears 2009-2012

2009 : Catálogo del Certamen Nacional de Fotografía “FOTOCIENCIA”

2008 : Sistema de Indicadores para la Gestión Integrada de la Zona Costera (GIZC) de las Illes Balears